Novel methods and models to validate H2 storage in solid state materials

A thesis presented
by

Testi Matteo

to
The Department of Physics
in partial fulfilment of the requirements
for the degree of
Doctor of Philosophy
in the subject of

Physics

PhD Thesis
submitted the 4^{th} February 2017
and defended the 17^{th} February 2017

under suggestion of:
Head of ARES unit Crema Luigi(FBK), main supervisor

Novel methods and models to validate H2 storage in solid state materials.

PhD Thesis

Printed by
Font: LaTeX 2ε

University of Trento
Fondation Bruno Kessler
Applied Researh on Energy Systems - ARES

Via Sommarive, 19
IT-Trento, Povo
Italy
Phone: (+39) 0461 314886
www.unitn.it
www.fbk.eu

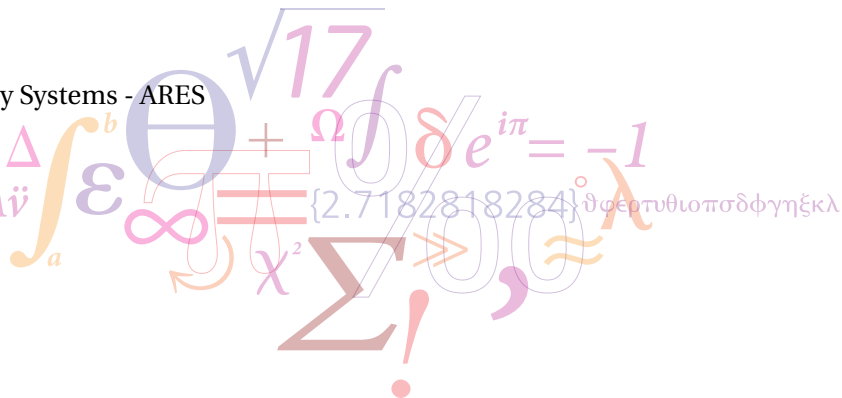

Examination Committee members

Marcelo Baricco
Full professor and Vice rector of Politecnico di Torino.
Department of Chemistry, Politecnico di Torino.

Paolo Tosi
Associate Professor.
Department of Physics. University of Trento.

Stefania Specchia
Associate Professor.
Department of Applied and Technological Science. Politecnico di Torino.

Acknowledgements

The realization of this work has been an enriching journey that could not have been achieved alone. First of all, I should like to thank my tutor, dott. Luigi Crema for the opportunity to work and participate in one of the most interesting current energy topics. I would like to thank all researchers and technicians of ARES unit, and in general of FBK, for the support that have given me in these years. I wish to thank in particular A. Vaccari and A. Paris for the useful discussion about kinetic modelling; M. Roccabruna, R. Bartali, G. Coser, G. Speranza, N. Laidani, A. Zanetti, M Frizzi and A. Saltori for the support to the experimental point of view, and all other ARES's members: F. Alberti, S. Amicabile, M.Malfatti, G.Cicolini, M. Cozzini and S. Dalpez and A.Bertaso. I want to thank also M. Bielewski and P. Moretto from JRC (*Europese Commission - Joint Research Centre*) of Petten for the suggestions about the validation of characterizing instrument hereby reported. Moreover, I want to thank P. Parilla from NREL for the useful discussion about the theoretical approach on itself volumetric instrument. Lastly, I want to thank A. Bianchin and E. Forlin for the characterization data of hydrogen storage prototype reported in this work. Thank you.

Abstract

Hydrogen storage, Differential Volumetric Instrument, Material Modelling, Nb_3O_5 .

In this work an improved methodology for the study of hydrogen storage material (HSM) is presented, for the characterization of smaller samples of HSM at increased accuracy. It includes: the realization of innovative differential instrument; a novel approach to the detailed micro kinetic modelling; increase the comprehension of absorption and desorption mechanisms; support research efforts in this topic. As side results, a *macro* and *lumped* model for the design of generic hydrogen storage tank are developed and validated.
The study of a novel IDA (Isochoric Differential apparatus) is presented, describing all the steps from the initial theoretical approach, to the detailed design and the definition of an experimental proceeding. It includes the necessary technical improvements to increase the measure uncertainty compared to the classical *SIevert*. Novel *micro* kinetic modelling for HSM is explained as variation of classic nucleation and growth model (JMAK model). The nuclei's growth is assumed to be limited by surface or even by radius of powder's particles. Micro modelling is applied on Mg-based material, introducing high accurate kinetic measures obtained by IDA. This leads to extrapolate information about kinetic parameters and kinetic mechanisms of hydrogen sorption. The obtained *micro* modelling is used as core for the development of a model at a higher scale (*macro*) which keeps in consideration also heat and hydrogen diffusion in porous materials typical in hydrogen storage tank. Experimental data collected by a prototipal realization of hydrogen storage tank are used to validate macro modelling. Moreover, a lumped model is developed with the scope to built a numerical tool able to give preliminary indications on proper design/layout of hydrogen storage tank, based on hydrogen flow, temperature or pressure requirements. Lumped modelling is finally compared with results by the numerical simulation of validated macro model. Finally, micro kinetic model is applied on high accuracy sorption data (by IDA) on innovative catalysed Mg-material. Material is produced by a novel approach, where catalyst, Nb_2O_5, is deposited by PVD techniques at extremely low concentration on the surface of powder to exploit its higher catalyst proprieties.

Publications

Conference paper

- L.Crema, **M.Testi**, F.Alberti, "EDEN: novel power-to-power system for enhanced hydrogen storage in solid state", EFC2015 - European Fuel Cell Technology & Applications Piero Lunghi Conference, December 16-18, 2015, Naples, Italy.

- L. Crema, **M. Testi**, F. Alberti, A. Bianchin, E. Forlin, D. Platzek, S. Ortega and J. C. Ruiz Morales, “Novel hydrogen based power to power system: integration between reversible SOFC-SOE and a new hydrogen storage tank”, PLENARY SESSION at HYCELTEC 2015 - V Iberian Symposium on Hydrogen, Fuel Cells and Advanced Batteries, July 5-8, 2015, Tenerife, Spain.

- D. Platzek, P. Matteazzi, A. Bianchin, L. Crema, S. Ortega, E. Forlin, G. Noriega, **M. Testi**, M. Bielewski, F. Alberti, J.C. Ruiz-Morales, N. Laidani, R. Bartali, "NEW CONCEPT FOR THERMAL MANAGEMENT IN A HYDROGEN TANK", 9th Int. Symposium Hydrogen & Energy, January 25-30, 2015, Emmetten, Switzerland.

- **M.Testi**, F.Alberti, A.Bianchin, E.Forlin and L.Crema, “DEVELOPMENT OF A EXPERIMENTALLY VALIDATED MODEL FOR SOLID STATE HYDROGEN STORAGE DESIGN OF MATERIAL AND TANK”, Proceedings of EFC2013 - Fifth European Fuel Cell Technology & Applications Conference - Piero Lunghi Conference, December 11-13, 2013, Rome, Italy

Poster

- R. Bartali, N. Laidani, G.Gottardi, V. Micheli, **M. Testi**, L. Crema, A. Bianchin and E. Forlin, "Nb2O5 deposition on Mg by plasma technique for hydrogen storage applications", NANOENERGY 2015 - International Conference on Nanotechnology, Nanomaterials & Thin Films for Energy Applications, June 1-3, 2015, Manchester, United Kingdom..

- L. Crema, **M. Testi**, F. Alberti, A. Bianchin, E. Forlin, D. Platzek, S. Ortega and J. C. Ruiz Morales, “Novel hydrogen based power to power system: integration between reversible SOFC-SOE and a new hydrogen storage tank”, PLENARY SESSION at HYCELTEC 2015 - V Iberian Symposium on Hydrogen, Fuel Cells and Advanced Batteries, July 5-8, 2015, Tenerife, Spain.

- **M.Testi**, F.Alberti, A.Bianchin, E.Forlin and L.Crema, "Development of a simulation toll for design of magnesium H2 storage tank", FCH-JU projects on hydrogen storage Joint Workshop, October 2013, Tenerife, Spain.
- **M.Testi**, L.Crema. "Design of DPA for evaluation of H2 uptake and reaction kinetics with improved performance", FCH-JU projects on hydrogen storage Joint Workshop, October 2013, Tenerife, Spain

Patent

- Author: Ruben Bartali, Laidani N., **Testi M.**, Pucker G., Gottardi G., Speranza G., Crema L. Victor Micheli, Gianni Coser, Gloria Gottardi, Michele Fedrizzi, Eki Setijadi. *Materiale composito a base di grafene per la generazione d'idrogeno e calore in ambiente acquoso e processo per la sua produzione*, owner: FBK, Submitted data: 15/10/2016,nr.102016000104397.

White book

E. Setijadi, R. Bartali, **M. Testi**, L. Crema, G. Speranza, "Decoration of graphene flakes with magnesium nanoparticles: wet chemical processing", White book Flagship Graphene. [under review]

Contents

Nomenclature

Abbreviations

JMAK	*Johnson-Mehl-Avrami-Kolomogoov* model
AAD	Average Absolute Deviation
CH	Chemical Order model
COP21	Conference Of the Party, 21^{th} session
CV	Contracting Volume model
D	Diffusion model
DSC	Differential Scanning Calorimetry
ECU	Electronic Control Unit
EDEN	High **E**nergy **DEN**sity Mg-based metal hydrides storage system
EoS	Equation of state
FBK	Bruno Kessler Foundation
FCEV	Fuel Cell electric Vehicle
FEM	Finite Elements Method
HSM	Hydrogen Storage Material
IDA	Isochoric Differential Apparatus
MBWR	Modified Benedict-Webb-Rubin equation
ME	Mixed Empirical model
MS	Mass Spectroscopy
NG	Nucleation adn Growth model
RKS	Redlich-Kwong-Soave equation
TDS	Thermal Desorption Spectroscopy
TGA	ThermoGravimetric Analysis

Greek letters

α	Nucleation coefficient
β	Volume expansion ratio
χ	Uncertainty

Nomenclature

ϵ	Porosity
η	Merit of figure about volumetric instrument resolution. (1^{st} Chapter)
κ	Thermal conductivity
λ	Avrami Nucleation constant rate
λ_a	Ratio of chamber and Expansion sample volume
λ_b	Ratio of chamber and Expansion reference volume
μ	Time variable
ρ	Density
τ	Time variable
θ	Reacted fraction

Roman letters

ΔP	Differential Pressure
$\dot{N}$	Nucleation rate
$\hat{x}$	Growth direction of nuclei, radial
$\hat{y}$	Growth direction of nuclei, superficial 1
$\hat{z}$	Growth direction of nuclei, superficial 2
$\overrightarrow{v}$	Velocity of gas
C_s	Specific heat
k	Constant rate
n	JMAK coefficient
N_0	Total number of available nucleation site
R_0	Radius of particle
t	Time
$V(t)$	Reacted fraction volume formed at time t
V_a	Expansion volume of sample's side
V_{ex}	Extended Total Volume of particles
V_{tot}	Total Volume of particles
Z	Compressibility factor
n	Moles (1^{st} Chapter)
G	Growth rate of nuclei
I	Nucleation constant rate
R	Universal gas constant
S	Heat Source

Subscripts

$conn$	Refereed to connections and pipes.
eff	Effective term
ex	Extended
Mg	Reference to Magnesium.
MgH_2	Reference to magnesium hydride.
0	Initial state
a	Refereed to sample side
b	Refereed to reference side
cl	Closing valve state
el	Ellipsoid
eq	Equilibrium state
f	Final state
in	Intial state (refereed to gas loading in volumetric procedure)
iso	Isothermal condition
max	Maximum allowed value
t	State at time t
w	Working condition

Superscripts

i	Cycle *i*
i-	Cycle *i-1*

1 Introduction

1.1 Energy scenario

Nowadays, the growth of world population, the increasing energy demand combined with the acclaimed climate changes require proper and timely responses. A new system in acquired since the current model is overall considerably under environmental and even from the economic point of view. This vision is confirmed by the milestone COP21 Paris agreement on December 2015, where many countries recognise the common importance of energy technology and innovation in meeting climate objectives, as reduction of CO_2 emission and leverage of energy efficiency. [1] In the last decades, several actions have been taken to gradually substitute the actual energy production based on fossil fuel more environmentally friendly sources. In this context,renewable energies globally grew by 5 % in 2015, supported by public policies there are driven by energy security, environmental and climatic issues. In the same year (2015), renewable generation, driven by on shore wind and solar photovoltaic plants, achieved the 23 % of total electricity generation, mainly distributed in China (23 %), European Union (17 %) and United State (11 %)[2, 3].
However, the aleatory nature of renewable sources, combined with their relatively rapid introduction on the electric network, can have periods of surplus and deficit, which may be different from region to region. Moreover, variable generation as a result of weather changes can lead a rapid transition in output supply which instantaneously unbalances electricity grid. This is limiting renewable sources in within the electric market, posing several limitations and complications to the penetration of further renewable plants in the electrical grid. In this context, energy storage is generally accepted as one of the technological solutions to combine unpredictable renewable sources with the energy demand. Moreover, an innovative and more performing storage system should allow the management of actual renewable production, as well as pushing forward the development of smart cities and communities. The most common storage technologies can be divided in: electrochemical batteries (lead-acid,

lithium, flow batteries, et.), mechanical storage technologies(pump hydro, compressed air, etc) and hydrogen storage.[4]
Hydrogen storage is considered one of the most prominent for many reasons: it has a large amount of chemical energy per unit mass (142 MJ/kg compared to 50 MJ/kg of gasoline), low-carbon footprint with the potential to strongly reduce energy-related CO_2 emissions, higher flexibility as energy carrier and the possibility to be produced from a large variety of feedstocks. These include fossil fuels (as natural gas and coal) as well as renewable resources, via proper production processes as steam reforming, photo-catalyst or thermally activated conversions. Furthermore, hydrogen can be directly generated from electricity and water, stored in large amounts over long periods and re-transformed again to electricity (via power-to-power system, P2P). Moreover, it can be mixed with the natural gas into gas grid (Hydro-Methane) or converted to synthetic methane (via power-to-gas, P2G) or even directly used as fuel for fuel cell electric vehicles (FCEV) in the automotive sector (via power-to-fuel process). In summary, hydrogen has the potentiality to connect different energy grids and thus increase the operational flexibility of future low-carbon energy systems. [5]
Despite of great potentialities, the performance of hydrogen storage systems is the real bottleneck for the realization of a self-sustainable hydrogen utilization. This is directly correlated to the extremely low gas density at standard condition (0.08 g/l). For this reason, researches are concentrating a lot of efforts on this topic since many times. US Department of Energy (DOE) in agreement with automotive industry has released several storage capacity's targets for the hydrogen storage system [6] which are the most diffused criteria to compare the performance of hydrogen storage system. For 2020, gravimetric density target is 1.8 kWh/kg (correspondent to hydrogen gravimetric density of 5.5 % w/w) with a ultimate target of 2.5 kWh/kg (7.5 % w/w hydrogen /hydrogen stored system). Similarly even volumetric density target is fixed (2020: 0.04 kg/l and ultimate: 0.07 kg/l) with proper target values for minimum lifetime, refilling time and working parameter such as pressure and temperature. [7–9]
Three main methods exist to store hydrogen gas at elevate volumetric and gravimetric density: compressed vessel, cryogenic liquid tank and solid state material. Benchmarking actual fuels (e.g. methane, natural gas), compressed hydrogen storage is standardized at pressure of 70 MPa at the current state of art. However, Gray [10] demonstrated as 2020 DOE's target can be achieved only with hydrogen pressure at 255 MPa, without considering vessel weight. Moreover it has to be considered that compression step at 70 MPa consumed a equivalent energy amount equivalent to 15 % of stored hydrogen, with an increment of energy consumption at higher pressures. Secondly, liquid hydrogen storage consists of hydrogen in liquid state, cooling down it at 20.3 K or below critical temperature (32.9 K). Hydrogen liquefaction process consumes the 30 % of stored chemical energy in the chemical bond of $H-H$, hydrogen. Moreover, heat leaks result in the continuous evaporation of liquid H_2 and so the pressurization of liquid storage tank, which has to be vented at regular interval. This

means a continuous losses of stored hydrogen (evaluated around 0.5 % daily by Broom [7], de Witt and Faaij [11]).
The last approach regards the hydrogen storage in solid state material. Nowadays, HSMs (hydrogen storage material) report, in many cases, the best performance about gravimetric and volumetric density (higher than compress and liquid storage). There are many other types of potential hydrogen storage materials, including metal hydrides, complex hydrides and microporous materials, and many others are under investigations. HSMs can be categorized by operating temperature and pressure or by mechanism through which they adsorb (on the surface) or absorb (in the bulk of materials) hydrogen, fig. 1.1.
Speaking about metal hydride materials, some commercial applications based on

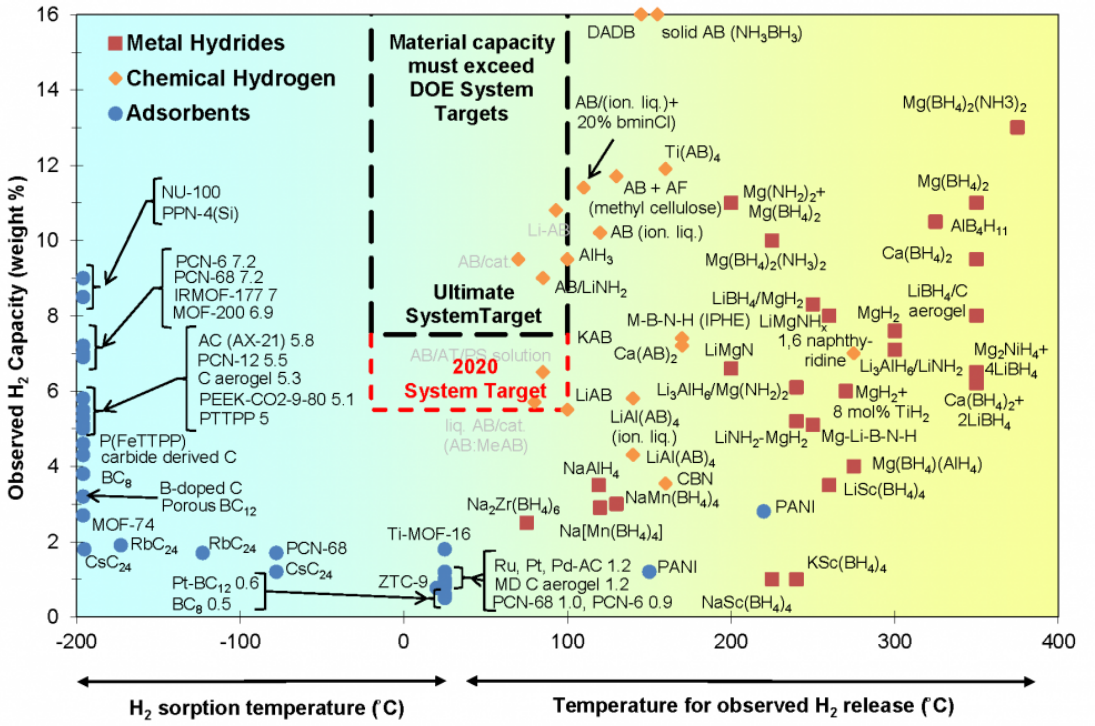

Figure 1.1: Gravimetric capacity and typically working temperature for several HSMs [12].

Mg or $LaNi_5$ [13, 14] already exist. However they don't still reaching DOE's target, and present much of a problematic: elevate enthalpies of reaction and subsequent low working hydrogen pressure as well as low kinetic of reaction. So, notwithstanding the advantage exposed about hydrogen storage approach, many issues still obstacle their full commercial diffusion and reducing industrial performance and not fully penetration in energy sector.
For these reason, the researches for new hydrogen storage materials are currently receiving a great deal of attention from the scientific community. The ultimate aim is to

develop a material that properly replies to the requirements of real hydrogen storage system in particular for automotive sector, where it needs to store large amounts of hydrogen in a light, safe and compact complete storage system.

Finally, public funding program plays a relevant role in this context. European innovation initiative proposed within before by Seventh Framework Programme and now in Horizon 2020, financially support several funding activities addressed to transfer of the scientific results to the industrial application through proper prototyping step and innovation actions, in order to rapidly commercialize and spread hydrogen technologies. The final purpose of European commission is the approach of the real hydrogen economy.

1.2 State of art and Motivation

Hydrogen storage materials (HSMs) have been study have been for a several number of years. Palladium was the first material described as able to absorb considerable amount of hydrogen gas by Graham [15] in the 19th century. Only around since the mid-1900s, many other HSMs were investigated by Sievert [16–18], which even realized one of the first volumetric instrument, still used today for the characterization of HSM and gas sorption in general. In the same period, Avrami published its theoretical approach for the kinetics modelling on phase transformation, based on nucleation and growth mechanism, widely applied on HSM's study.[19–21]. During the 50s, the more interest around nuclear topic contributed to discover the first inter-metallic hydride, $ZrNiH_3$, during the investigation of hydrogen embrittlement of nuclear reactor walls [22]. From this point, researches on HSM were grown as number of published papers, pushed forward by the new available characterizing techniques and the more and more interest about hydrogen storage topics. Novel material were identified, including the reversible AB_2, AB_5 (the most known material is $LaNi_5$) structure materials. Moreover, research on HSM focused on lightweight hydride as Mg and Ca and their alloys with metal transition element which are capable to destabilize hydride structure of alkaline element as well increase the kinetics of sorption reaction. In the 90s, high energy ball milling was introduced into HSM preparative in order to improve kinetics hydrogen sorption rate via increment of structural defects. [23] In the 2000s, a new type of hydrogen storage material, *complex or chemical hydride*, started to attract scientific interest. These material (i.e. $NaBH_4$) were able to release big quantity of hydrogen at relative mild conditions but desorption reaction was irreversible, with some little exception.[8] In the same period, the addition of catalysts was a route introduced by several work in order to improve kinetics of HSM. In particular, numerous studies were performed on Mg-material where absorption and desorption reactions were speed up by the presence of different metal oxide, including V_2O_5,

Cr_2O_3, Fe_2O_3, MnO_4, La_2O_3 and Al_2O_3.[24–27] In contrast with chemisorption phenomena occurred in hydride material, a parallel branch of research has focused on the develop of material that stored hydrogen through physisoprtion phenomena on the surface of itself materials. From these study, many material were identified as potential storage materials (as CNT-Carbon Nano tube, MWCT-Multi Wall Carbon Nano Tube). Some of these work claimed extraordinary hydrogen gravimetric density on nano-structured carbon (from 10 to 65 % wt of hydrogen sorption).[28, 29] However, these experimental results and their interpretation were strongly criticized.
From the incorrect data sorption interpretation and their poor reproducibility in some work, many researchers have raised questions as to the effective accuracy of used characterizing instrument and applied experimental procedure [30, 31]. Moreover, new frontier of hydrogen storage research is addressing to the synthesize of nano-structured material to exploit superior surface's characteristic of HSM, as reported by Liu et al. [32], Jia et al. [33], Bérubé et al. [34] for magnesium hydride material. Synthesize routes of such materials generally produce only few tens of mg or less, typical for lab scale, requiring an improvement in the characterization apparatus to approach sufficiently accuracy in sorption results.
Secondly, main kinetics modellings for the description of sorption phenomena on metal hydride materials have been developed several year ago, and are widely applied without relevant improvement or further study. In this contest, JMKA model interprets hydrogen sorption reaction in terms of nucleation and growth processes. It is the most diffuse kinetics model used to describe absorption and desorption data in metal hydride-hydrogen system. However, only few works have introduced some improvement on the original theory, including only different nucleation's approaches [35, 36].
Parallel to the develop of more and more performant HSM, in the last year, considerable effort was focused on the modelling and realization of efficient hydrogen storage tanks and its application in more complete storage system. Although many peer review papers reports different layout innovation and design solution, there is a little number of works that report full sorption study from sample characterization to final tank modelling, as done by Chaise et al. [37].

1.3 Objectives

The aim of this work is to develop a reliable and validated methodology to study of hydrogen storage materials and investigate its kinetics sorption processes. In particular, this thesis evolved covering different aspects from the kinetics characterization of sample to the kinetics modelling of HSM for potential application in real hydrogen storage tank. Such methodology has been initially applied on magnesium based mate-

rials produced within EDEN European project [38]: firstly, characterizing the kinetics performance of Mg material with high accurate measuring instrument; secondly, identifying and understanding the main kinetics mechanisms occurring in absorption and desorption reaction of storing material and thirdly, developing proper kinetics modelling at microscopic and macroscopic scale for the highly reliable physical representation and optimization of proper hydrogen storage tank based on Magnesium. Finally, a novel catalysed Mg-material with reduced catalyst contain is presented and analysed with such improved methodology.
The different steps carried out throughout this project can be listed as follows:

- Development and validation of an innovative highly accurate instrument for the kinetic and thermodynamic characterization of hydrogen sorption phenomena in potential HSM.
- Development of properly kinetic model for a depth comprehension of hydrogen sorption mechanism.
- Kinetic modelling of Mg-based material, based on characterization data performed by developed instrument.
- Dynamic validation of macro modelling on hydrogen storage tank based on kinetic modelling of Mg material. The ultimate purpose is the development of a modelling tool for the optimization of hydrogen storage tank's design.
- Application of novel characterization technique and kinetic modelling approach on an innovative catalysed Mg-material, produced with reduced content of catalyst.

1.4 Thesis Outline

This thesis is divided in 5 main chapters covering the aspects outlined in the above section. A brief overview of each chapter is provided hereunder:

Chapter 2 describes any step involved into development and realization of novel characterizing instrument (Isochoric Differential Apparatus, IDA) to analyse HSM and potentially for any gas sorption reaction on solid state materials. Apparatus has been realized inside Bruno Kessler Foundation facility, included proper electronic control unit (ECU) and managing software with automatic procedure of calibration and measurements. Instrument has been validated with two well known reference material: Palladium for mild conditions analysis (293-400 K and hydrogen pressure of 0.001-0.4 MPa) and pure magnesium for

high temperature characterization (573-633 K and hydrogen pressure of 0.001-1 MPa).

Chapter 3 reports the development of proper micro kinetic model based on actual kinetic models for gas-solid reactions. A novel approach on classic nucleation and growth model (JMKA) has been applied to describe hydrogen absorption reaction in magnesium at high temperature conditions. Next, hydrogen storage tank modeling has been developed on Mg sample nd dynamically validated against experimental data by H_2 storage tank prototype. Moreover, a lumped parameters model is introduced as easy tools to preliminary estimate goodness of layout or design of tank.

Chapter 4 reports the study on a novel magnesium based material, catalysed with extremely low quantity of Nb_2O_5. Kinetic characterization are performed by IDA and kinetics analysis utilizes kinetic micro model develop in chapter 3.

Chapter 5 summarizes the main findings of this contribution, analysing the main objectives stated at the beginning of this work. Furthermore suggestions are given for future work.

2 Design and development of a novel instrument to assess physical properties of hydrogen storage materials

Abstract

The quantification of Hydrogen sorption in solid state is a crucial step in the assessment of storage materials and their possible applications. Unfortunately, volumetric instruments, one of the most applied methods to characterize sorption proprieties of storage materials, are in many cases affected by several problems, including low accuracy, long times for material properties characterization. This is due to several factors such as temperature uncertainty, misleading calibration proceeding. Here, we present a novel instrument designed to characterize kinetics and thermodynamics proprieties of storage materials, based on volumetric Sievert, here defined Isochoric Differential Apparatus (IDA). The characterization ranges from low to high temperature and pressure levels. IDA integrates a layout designed with two parallel connected Sieverts branches. Pressure values are sampled from a differential transducer. The differential layout can improve measurement accuracy due to the drastic limitation of all transient phenomena and non-linear effects occurring during the gas expansion. A physical model to measure the sorbed gas is reported, including real gas behaviour at non-isothermal condition. A detailed error analysis of the kinetic and thermodynamic models has been carried out. Moreover, a comparison on the uncertainty obtained by IDA and standard Sieverts' layouts is reported. The specific contribution of single variables on error propagation in final measures is estimated. Palladium and Magnesium are utilized as benchmark materials, to test the differential apparatus at ambient and high temperature values ($> 300^{\cdot}C$). For both materials, the kinetic and the thermodynamic behaviours have been acquired by the differential layout with an accuracy of an order of magnitude higher than standard methods.

2.1 Introduction

One of the ultimate goal to approach the hydrogen economy reality, is the realization and the development of proper hydrogen storage system that matches or excesses the international target (actually from US DOE [6] or IEA [5]). Besides conventional storage methods, i.e. high pressure gas and liquid state, solid storage is one the hottest fields in science research. For this reason, over the last decades, investigations on innovative materials for hydrogen storage applications have attracted a high number of researchers and it has been supported by considerable amount of budget and efforts. The approaching to hydrogen storage goals drives researchers to develop and produce highly nano-structured materials with tight control of chemistry to increase and tune their kinetics and thermodynamics proprieties. Most of the innovative materials for hydrogen storage can be produced through new synthesis processes, at a small capacity of production (from few milligrams). The sample materials have to be further divided/partitioned to have a full characterization by the use of different techniques. For these reasons, kinetics and thermodynamics gas sorption characterization are carried out on a significantly small amount of sample (50-500 mg). The minimal mass of available sample needs proper measuring instruments to approach extremely low detection limit.

In this context, gas sorption measurements are affected by several sources of errors with relevant reduction of measurements' accuracy, as demonstrated by the initially unsatisfactory characterizations performed on carbon structures, poor reproducibility and repeatability of storage measures and discrepancies from benchmarked analyses.[30, 39–46] In his exhaustive works, D. Broom resumed main error causes which contributes to wrong characterizations in several characterization approaches [47, 48]. Besides, a Round Robin test [30] has revealed that also methodology and sample histories (degassing, cycling, and instrument calibration) affect final uncertainty of measurements. This is corroborated also by another Round Robin *investigation*, conducted with less number of active participants respect to previous one. Hurst et al [49] concluded that predominant uncertainties on sorption measures are caused by systematic errors. The systematic errors include:: inaccurate calibration operations, inadequate data analysis models, error associated with non uniform temperature fluctuations and small sample mass.

Therefore, all the processes to characterize hydrogen sorption have to be highly accurate and and show, even at the extremes of the measure range, a high accuracy (high pressure, 10 MPa, and low temperature, 77 K). So, an improvement of accuracy along the characterization of the process is necessary to have reliable results in hydrogen sorption measures. In this context, several scientific papers concentrated considerable efforts on the improvement of accuracy in characterization techniques, focusing on: methodology, more accurate mathematical or data analysis models and technical improvements on instrumentations.[44, 50–55]

Scope of this chapter is to illustrate the realization of a novel instrument for the study of HSM. The research activities involved in: the identification of more appropriate characterization approach, based on the feature's comparison of actual method to study HSM. Secondly, the realization of the instrument layout and the development of proper mathematical model for moles estimation in sorption measurements. The final activities regards the validation of instrument by the characterization of a reference sample.

2.1.1 Choice of characterizing techniques

Amount of hydrogen released or uptake during a gas-solid reaction can be revealed by different approaches. Few techniques can selectively detect hydrogen sorption phenomena (i.e. desorption mass spectroscopy [56] or neutron scattering [57]). Nuclear techniques based on neutron scattering is the solely able to directly determine hydrogen, light-atom positions and their dynamics, in crystal structures of host materials.[58] Moreover, the different cross-section between hydrogen isotopes (i.e deuterium) can be used to provide additional insight into the structure of materials and their interaction with hydrogen. Finally, the absorption of neutrons is low in most materials in comparison with other sources such as X rays and electrons. It means that nuclear scattering method can be available for in situ measurements and integrated with other techniques. Main investigations with nuclear methods included: defects of structures and vacancies in host lattice, hydrogen mobility and diffusion profiles and finally size/shape morphology and surfaces of nanoparticles and nanopores [59]. Unfortunately, such techniques generally require expensive instruments and tools, with a complicate sample preparation, moreover neutron scattering approach can only be performed at major national and international facilities because a neutron source is required (either a nuclear reactor or a spallation source, which requires a particle accelerator). For these reason, they will not be taken in consideration in this work.
Unlike nuclear scattering, indirect characterization methods to study hydrogen sorption are more affordable, and offer a interesting trade off between accuracy and economic/technical efforts.They can be considered indirect because are not selective, because they typically involve measurements of gas pressure, calibrated volumes, gas flow or sample mass in a gas handing system, generally consisting of: hydrogen sink, gas manifolds and sample cells. Indirect approaches can be divided in: thermogravimetric, gravimetric and volumetric methods.
In the next paragraphs, the three main characterization approach will be exposed. At the end, a brief summary of advantages and disadvantage of every approach will be reported, with a discussion to support the decision/reasons to the type of instrument to realize.

Thermogravimetric method In thermogravimetric technique, hydrogen desorption from a sample is measured during a temperature programmed ramp and it involves exclusively non-isothermal measures on only desorption phenomena. It is analogous to classic thermo-gravimetric analysis (TGA), Differential Scanning Calorimetry (DSC), which finds wide applications in the study of materials' science.[60, 61]
TGA apparatus includes a micro-balance system where sample can be mounted. The measure run at atmospheric pressure under a carrier gas, although even high and low pressure system are available in commerce. The micro balance monitors the mass variations as a function of temperature, but it is possible to work at constant temperature in the case of analysis of material with slow kinetics on hydrogen desorption.
A mass spectrometer (quadrupole analyser) can been added to a TGA instrument in order to identify the nature of the decomposition or desorption products, making TGA technique more direct and reliable to detect H2 sorption. The characterization method is indeed more complicated respect to volumetric or pure gravimetric system, requiring more performant vacuum pump (below 10^{-2} Pa), as well as a additional calibration procedure for the mass spectrometer. This technique is known as TGA-MS.[62]
TDS techniques, known also as Temperature-Programmed Desorption, TPD, is not a pure gravimetric approach (it can not require a micro balance), however it is inserted in this category because TDS measurements occur at a controlled temperature ramp. TDS refers to a wide range of experimental methods which involves the hydrogen desorption into a volumetric-type instrument, where a calibrated vessel initially at vacuum is used. The hydrogen gas is desorbed by sample into the vessel. The pressure increment is correlated to the amount of desorbed hydrogen during the temperature ramp program. However, TDS techniques is generally integrated with mass spectroscopy to investigate more in depth and quantify desorption reactions, allowing to distinguish the nature of sorbed molecules.
A note about DSC. Differential Scanning Calorimetry (DSC) is a thermal analysis technique applied to investigate the thermodynamic properties of a material. It measures the heat flow necessary to maintain a sample material and a reference material at the same temperature during a temperature programmed ramp in vacuum or in a inert carrier flux. Although it is a powerful tool for the characterisation of thermodynamics and kinetics proprieties, it has to be coupled with quantitative techniques, because it is not able to detect the hydrogen sorbed amount, but exclusively the heat flow to or from the sorbed reaction.[48, 63]

Gravimetric method In last years, gravimetric method has been applied successfully to investigate gas sorption phenomena, including for HSM [47, 64–67].
The amount of gas sorbed by sample is indirectly estimated by its weight variation. "Indirectly" because this technique doesn't distinguish what is the nature of sorbed

gas. Gravimetric systems typically involve in the same components: an accurate balance (uncertainty on the order of μg), a vacuum system for sample degassing and chamber evacuation, a gas supply system to tune the hydrogen pressure during the characterization in the balance chamber and finally a proper system to thermostat the sample at working temperature. The measurement occurs at isothermal conditions. The pressure can be maintained constant using a dynamic control or also in static mode, providing additional gas during absorption or bleeding the evolved gas during desorption step, without modification of the thermodynamic driving force.
Core of instrument is the micro balance system. Although it has a high accuracy (μg), it is affected by several problematic , that can increase its uncertainty. Buoyancy phenomenon is the most important problem that can strongly alter the accuracy and reliability of measurements. More, buoyancy is heightened by several factors as: thermal gradient, volume dilatations of sample and not ideal thermal contact between sample and temperature transducer. For these reasons, gravimetric approach adopts a series of mathematical algorithm to compensate such factors, which include a calibration of balance before the measure step.[9, 48, 58, 63]
As for all gravimetric techniques, the control of sample temperature can be a error source because the temperature sensor can not be in direct contact with the plan of balance. Moreover, gravimetric approach are not suitable for air sensitive material, without installing particular auxiliary components, to avoid sample air contact during sample loading in the instrument. Gravimetric method generally follows a static approach as measure procedure where aliquots of gas are added or removed from sample chamber in order to adjust pressure in the sample's chamber. It is possible to conduct measurements in dynamics approach with the application of a proper mass flow meter.

Volumetric method Similar to gravimetric method, the volumetric approach is an indirect method to quantify gas sorption phenomena and it is widely used in HSM study. It relies on the variations of pressure due to the amount of hydrogen molecules in the gas versus the solid state (both on the surface or in the bulk sample), where sorbed state molecules don't contribute to the gas pressure.
Sorption proprieties of material and gas sorptions are determinated by temperature-volume-pressure correlation in a proper instrument by real equation of the gas, or other analogous mathematical model (compressibility factor correction, van der Waals, Redlich–Kwong [64], Soave–Redlich–Kwong, Peng–Robinson EOS, etc.)[30, 68]).
Volume of instrument is particularly relevant for such methodology. So the procedure of volume's calibration is fundamental to the final accuracy of volumetric instrument.[9]
The volumetric approach is also called manometric, due to the relevant role of pressure in the estimation of gas sorbed moles. The layout apparatus is called Sievert. The

name is given by the German chemistwho conceived the first concept of volumetric approach for sorption measurements[16]. The basic layout is shown in fig. 2.1: Classic

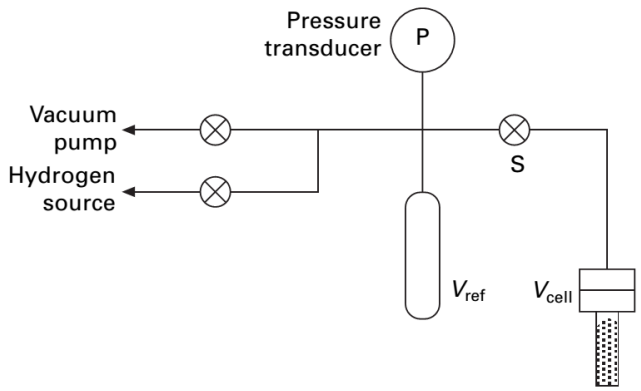

Figure 2.1: Classic design of SIEVERT instrument. V_{ref} is calibrated reference volume while V_{cell} is the sample holder. **S** is the main valve of apparatus. Picture from [9].

Sievert apparatus is composed of two connected volumes, called "chamber volume" and "expansion volume" (respectively V_{cell} and V_{ref} in fig. 2.1). Chamber volume contains the sample at working temperature, while the second volume is used as "calibrated" volume, kept at isothermal condition, to calculate variation of gas-moles due to sorption phenomena. Estimations of hydrogen sorption in a volumetric apparatus require teh developing of a suitable model to estimate sorbed moles of gas from pressure data, considering temperature of sample and calibrated volumes. Mathematical model takes in consideration: layout of system, a proper EoS (Equation of State) and the procedure adopted in the characterization operation. Generally speaking, accuracy and resolution in volumetric techniques is correlated to the size of expansion volume and the accuracy of used pressure sensor. The main problems of a volumetric instruments are due to the possible gas leakage and the temperature fluctuation, which can strongly affect the sorption's measures. Otherwise, volumetric approach is intrinsically adequate to study air sensitive material with a slightly modification of sample chamber. Also, volumetric method generally follows a static approach where aliquots of gas are added or removed by the sample chamber, and the measurements collect the pressure data until reaching the equilibrium . However, it is possible also in this case, to conduct measurements in dynamics approach with the installation of a proper mass flow meter and relative pressure regulator.

This work is focused on the realization of experimental instrument based on volumetric approach. Volumetric method has been chosen as the most appropriate

techniques for the study of HSM. In order to support such choice, some evaluation points are proposed to resume the main features of any previous exposed techniques. The main ones are :

- accuracy of measures,
- range of characterization,
- gas selectivity,
- cost of system,
- reliability and maintenance,
- versatility, as the possibility to couple other techniques and characterization, or tune its performance based on the type/size of investigated sample,
- simplicity, intended as the easiness to use the instrument, including calibration operation and characterization's procedure.
- suitability for air sensitive materials,

Table 2.1 wants to resumes the main strengths and shortcomings of available techniques for the study of HSM about the evaluation points.

	Volumetric	Gravimetric	Thermogravimetric
Accuracy	√	√	√+
Gas selectivity	-	-	√
Investigation range	√	√	-
Cost	√	-	-
Reliability	√	√	√
Versatility	√	-	-
Simplicity	√	-	-
Air-sensitive sample	√	-	-

Table 2.1: Comparison resuming table of evaluation points for the different approach for the study of HSM.

Techniques including mass spectrometers (as TDS, or some gravimetric instrument associated with a MS) achieve higher accuracy respect to the other ones. They find application for the characterization of very small sample and when nature of sorbed gas is relevant. However, instruments are usually delicate, expensive, require complicate calibration procedure, trained operators and the range of investigated pressure range

is limited (at vacuum and only about desorption process). Generally, thermogravimetric method are applied as complementary analysis, charactering other aspect of HSM that gravimetric and volumetric techniques are not able to study.
Also techniques based on a micro balances measurements achieve high accuracy and sensibility ($\pm 0.1 \mu$g of sorbed mass)[48], but it is strongly affected at high pressures by the increasing significance of the buoyancy corrections, which also increase with decreasing sample density. Moreover, the mass sample is limited by size of balance's pan.
Volumetric method can challenge other techniques thank to its great versatility. In principle, it can be equipped with multiple volume size in order to use the proper volume for the optimal compromise between sample size and required uncertainty. It is more suitable to characterize materials with high sorption kinetics because the measures are more rapidly than gravimetric. Indeed, the delicate micro balance needs to be handle more carefully, in terms of pressurisation rates and change of working temperature. Volumetric techniques can perform other type of study, as BET analysis [69, 70], and it can analysis air sensitive sample because the sample holder can be easily disassembled by instrument and loaded with investigated sample inside a glove box atmosphere. Other techniques can also treat air sensitive materials but operating with auxiliary components that make more complicate the overall procedure of sample loading. Furthermore, a generic volumetric instrument include cheaper components, respect to gravimetric and thermogravimetrics one, where the micro balance system impacts on the cost of instrument as well as on the maintenance.
Among the characterization methods, volumetric approach shows both greater simplicity and room for improvement compared with other indirect techniques (gravimetric and thermogravimetric one). As reported by [65] and [64], volumetric and gravimetric approaches have approximately the same degree of accuracy. Besides, relatively easy calibrations, intrinsic suitable procedures for air/moisture sensitive samples and an easy implementation, as well as handling, are reasons to prefer volumetric technique.

2.1.2 Volumetric method: instrument and actual procedure

Volumetric approach is performed with a characteristic instrument layout, reported in fig. 2.1. The procedure can be applied in principle to any type of gas. Assuming to perform a static measure, the hydrogen sorption characterization is made stepwise measuring uptake or release of hydrogen in a discrete ramp of pressure at equilibrium state. Considering the same layout, a pressure $P_{f,j-1}$ of hydrogen is present into apparatus at the end of a generic j-1 th step. The connecting valve, S, is closed to isolate the sample cell, which has an empty volume V_{cell}. In next step j, a new initial pressure $P_{o,j}$ is established in the reference volume, V_{ref}. Once achieving thermal

equilibrium, S is opened and the new value $P_{f,j}$ is measured. The magnitude of sorption phenomena in the j-th step, is then calculated by the change in the pressure measured when S is opened. [7, 50, 71, 72]. Considering layout in fig. 2.1, the previous described procedure and the real equation of gas, $n = \frac{PV}{RTZ}$, with n amount of moles of gas and Z, compressibility factor, it is possible to estimate amount of sorbed moles from eq. 2.1:

$$\Delta n_{tot} = \sum_{j=1}^{m} \left[\frac{P_{f,j-1} V_{cell}}{Z_{P_{f,j-1},T} RT} + \frac{P_{o,j} V_{ref}}{Z_{P_{f,j},T} RT} - \frac{P_{f,j}(V_{ref} + V_{cell})}{Z_{P_{f,j},T} RT} \right] \tag{2.1}$$

P is pressure, o and f index identify respectively initial and final state of measure. Z(P,T,gas) is the gas compressibility factor, which depends by temperature, pressure and nature of gas. In the left side of eq. 2.1, first term represents the amount of moles, sorbed during j-step of measurements.
As it is noted in 2.1, sorbed moles are estimated by the variation of pressure in a isochoric apparatus. Temperature can be assumed a constant of process, supporting technical improvement of apparatus (chillers) or more realistic assumption of the model. Otherwise, the value of reference and chamber volumes has to be extrapolated by a black experiment, and their uncertainties have an direct impact in errors associated to final gas sorbed amount. So, the estimation of volume size in a volumetric instrument is the most critical parameter to achieve high accurate measures. Equation 2.1 only applies isothermal measurement, as systems thermostat and completely immersed in a water bath. However, the most of characterizations are performed at temperatures which it would be impractical to thermostat the entire apparatus. Numerous approaches exist to treat cases of not isothermal conditions in a volumetric instrument. Literature specifically for the improvement of volumetric methodology is focused about two main contributes : mathematical model or technical enhancements.
Technical improvements in volumetric layout aim to reduces the numerous error sources, that affect the uncertainty of sorption measures obtained. Among them: gas leakages, volumes uncertainty, thermal gradients, achieving pseudo-thermodynamic equilibrium ([50]), dead valves volume and hop spot caused by valves heating (when equipped with electrical actuators) [54, 73], thermal transpiration issue at low pressure measurements ([74]) and gas physisorbed on/from chamber walls [75]. Some other work want to enhance the procedures, as the estimation volume uncertainty introduced by sample density ([72, 73, 76, 77]), the evaluation of ideal gas approximation ([44, 50, 52, 72, 78, 79]), the optimal compromise between mass sample and reference and chamber volume size ([50, 77]) and the procedure for the calibration ([71]). Other studies reported as ratio of volume's sizes (reference and chamber) and even ratio between sample and chamber size can be optimized to exploit the best performance of instrument ([50, 72, 77].

About mathematical model, the efforts are focused to develop proper model to describe no isothermal condition, or no gas ideality in the sorption characterization. In particular, [9] resumes the main different approaches for the estimation of critical value of V_{cell} for not isothermal study:

- *Equivalent Volume model.*
  In *equivalent volume model*, V_{cell}^{eq} of eq. 2.1 is estimated as an equivalent volume at the reference temperature.[77] Generally, it is estimated before every measurements for any working temperature, performing a null test measurement, and evaluating the equivalent volume from a simple gas expansion. With such consideration:

  $$V_{cell}^{eq} = V_{iso} + \int_0^x \frac{A(x)}{T(x)} T_{ref} = V_{iso} + V_{n-iso} \tag{2.2}$$

  the equivalent volume is composed by an isothermal contribution V_{iso} (the value of volume estimated at the same temperature of rest of instrument), and a not linear contributions, V_{n-iso}, (which includes the volume of chamber involved in thermal gradient). Compressibility factor is assumed to be constant at the pressure and temperature of isothermal side. A(x) is the section profile of sample holder long the its overall height (x), while T(x) is the temperature profile (gradient). Equivalent model is simply to apply, however it require a extremely accurate temperature control during whole characterization operation, with proper thermal insulation of pipes. Equivalent volumes (V_{cell}) is estimated by a null measurement test ($\Delta n_{tot} = 0$). A working temperature scanning can give a complete characterization of V_{eq} for overall investigated temperature range.

- *Divided Volume model*
  In *Divided volume model*, V_{cell} is assumed as physically divide in two volume section, V_a and V_b at two temperature, respectively T_a for the part of volume at contact with sample and T_b for volume included in the conduits and not a reference temperature (section 2.1.2). Volume constraint is $V_{cell}^{eq} = V_a + V_b$. The V_a and V_b are estimated by scanning of T_a during a null measurements. Divided model seems to be more robust of previous model. It requires a constant reference temperature during calibration step and a well defined boundary between V_a and V_b, independent from working pressure and temperature. Such model has been more depth by [53].

Otherwise, other work uses different approaches as Checchetto et al. [51], which applied a correction temperature on to calibrated volume value as well, similar to Gross et al. [63]. Considering technical improvement on volumetric instrument, recently,

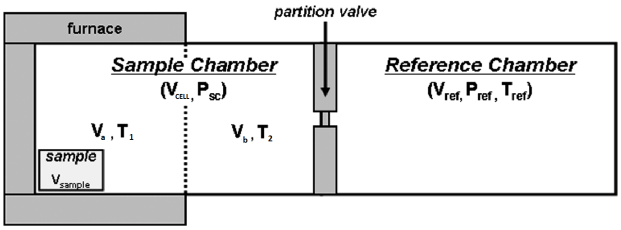

Figure 2.2: Representation of divided volume model. Sample chamber is divided in two sub-volume, considered at two different temperature. From [53].

some papers reported the realization of a volumetric instrument with a differential layout. [39, 40, 79–82] for the characterization of physisorption phenomena in carbon structures. Differential apparatus includes the coupling of two volumetrically identical classic apparatus: the first is called “sample” and the second is the “reference” branch. An example of the difference between classic *Sievert* and differential layout can be seen in fig.2.3. Differential layout promises several advantages over the traditional

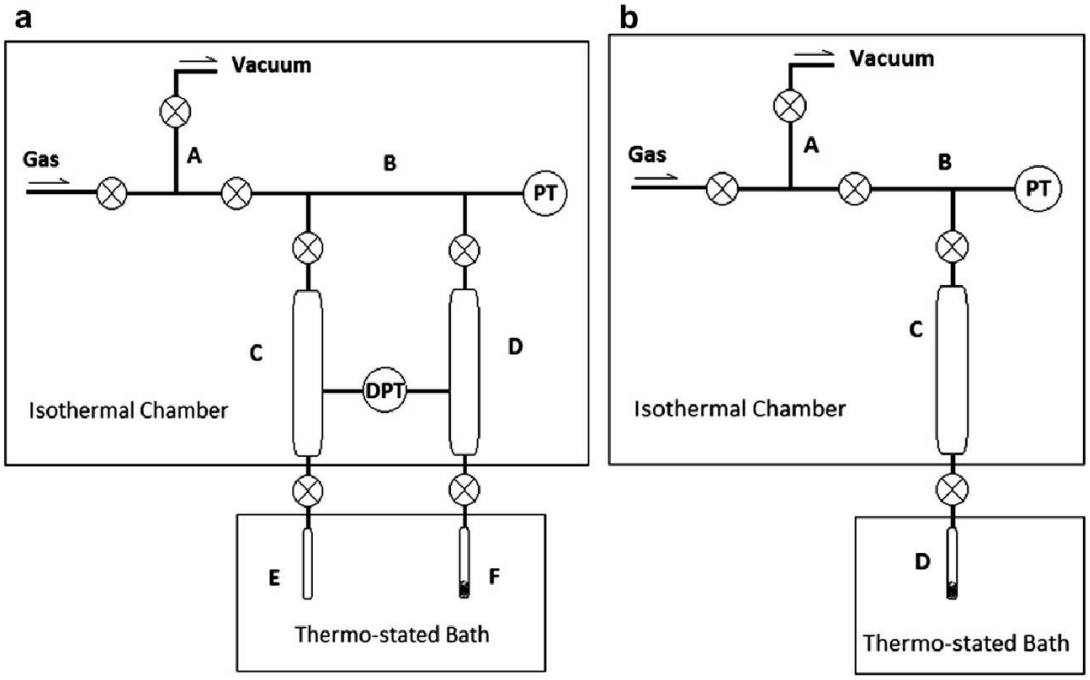

Figure 2.3: a. Differential layout of volumetric apparatus develop in this work. b. Classical layout in standard volumetric instrument (Sievert). (Picture form [80])

"Sievert" instrument.

- The differential layout allows for a great tolerance to temperature fluctuations,

because both volumes (sample and reference) are equals in size and experience the same temperature trends.

- The differential pressure transducer is more accurate than absolute sensor. The scale and accuracy of the differential transducer is more than ten-fold smaller than the absolute one.
- The differential layout reduces artefacts caused by gas non-idealities, as both compartments experience these effects equally.

At the moment of writing, differential apparatus are validated and applied to analyse hydrogen physisorption at elevate pressure for: Zeolite pellets at 298 K ([81]), Carbon Nano Fibers at 298K([40]), high surface super-activated carbon powder at 298 K ([79]) and activacted carbon at 273-293 and 313 K ([80]). Differential layout has not been tested at temperature far to room temperature (cryogenic or high temperature), but it has shown an incredible level of accuracy (around 0.05% w for 100 mg of carbon sample [79]). Mathematical formulation for the estimation of sorbed moles in differential approach is similar to the classic volumetric system and it was partially defined in previous cited articles. Even in this instrument, estimation of volumes is a critical operation, recital also there are more volumes to calibrate (one for every side, reference and sample).
Relied on the previous description and considering the strengths of differential layout, the differential apparatus results as a well compromise between versatility (sample mass, gas amount span, range of characterization), cost (basically, spare parts are pipes, volumes and pressure sensors) and room to improvement the accuracy of measures.

2.1.3 Objectives

The Approaching to highly accurate measurements in hydrogen storage application requires the design and the construction of proper instrument as well as ehancement of working methodology. In this context, some papers have recently reported the realization of a modified volumetric apparatus with differential layout and reduced uncertainty of measures. In this work, we design, realize and investigate the performance of differential volumetric apparatus, from room temperature (Pd material), to higher temperature, (Mg sample). A proper physical model is developed, including the real gas equation of state and non-isothermal conditions. The contribution of every variable (temperatures, volumes, etc...) on final uncertainty is exposed in a rigorous analysis.
Hereby work aimed to explore the performance of a Volumetric Instrument with a differential pressure layout, defined as “Isochoric differential apparatus” (IDA). A proper data analysis model has been developed for differential layout. Error analysis

was carried out using mathematical equation resulted by a such model to calculate rigorously the modification of relative uncertainty of every significant parameter calculated on the total error, considering all parameters involved in kinetic and thermodynamic analysis. In addiction it has been elucidated how the relative uncertainty of every working parameter involved in the sorption processes changed depending on Sieverts instrument configuration. Although a differential instrument allows better performances for hydrogen sorption measurements at room temperature compared to classic one, the hydrogen sorption measurements were not documented in literature at working temperature typically used for metal hydride (greater than room temperature). This work want to cover this lack in literature, demonstrating that differential layout performs kinetics and thermodynamics study with higher accuracy compared to classic instrument layout also for high temperature characterizations. Palladium and magnesium are chosen are reference material because they are extensively studied in last years, with a robust collection of kinetics and thermodynamics data.

In the next section of document, instrument layout with differential approach is introduced, with a detailed technical description. In the material and methodology part, experiment procedures are exposed with the description of analysed reference sample material (palladium and magnesium) to benchmark the performance of instrument. Results section collects characterization results, performed on benchmark materials. Then, in the discussion section, results are discussed with an uncertainty analysis carried out to show the principal error sources in the sorption process measurements, still comparing differential instrument with the classic "Sievert" volumetric layout.

2.2 Experimental Apparatus

In this section, a complete description of home-made volumetric apparatus is reported. It includes the detailed hardware description of instrument, the development of a rigorous mathematical model for the calculation of sorbed moles based on volumetric approach and the explanation of the experimental procedure for the characterization of H2 sorption. Theoretical model section contains the description of governing equation for the volumetric system, included the main assumptions hypothesized in the model, each of them are fully justified and explained in the context of this work. Then, a detailed explanation of volume calibration carried out in this work is included in a proper section. The calibration operation is a basilar operation in volumetric approach and it has been well thorough in order to reduce uncertainty in estimations of apparatus' volume. Developed software that it implements automatic procedure of characterization, is exposed in proper ECU (Electronic control unit) section. Last section includes a list and the descriptions of all procedures per-

formed in this work, including: degassing and activation operations, Kinetics and thermodynamics characterizations and finally cycling analysis.

2.2.1 Isochoric Differential Apparatus: hardware description

Isochoric differential apparatus (IDA) described in this work is a homemade system, based on the design of instrument realized by Zielinski [81], Blackman [40, 82], Qajar [80], Adams [83] and Browining [84]. IDA is a volumetric apparatus, that determines the amount of gas adsorbed by a sample based on a differential pressure variation between a reference and a sorption branch, containing sample. Basically, differential layout is the coupling of two classic Sievert instrument (fig. 2.3), where main pressure reading is supplied by proper differential pressure transducer. The set-up has two volumetrically balanced limbs each comprising multiple reservoir volumes and sample/reference cells/chambers to expand the range of pressure characterization in static mode, and the investigated sample size. Eventually volumetric discrepancies are taken in consideration in the mathematical model for the estimation of hydrogen sorbed mass. IDA includes two identical Sieverts apparatus (fig. 2.1), identified by two

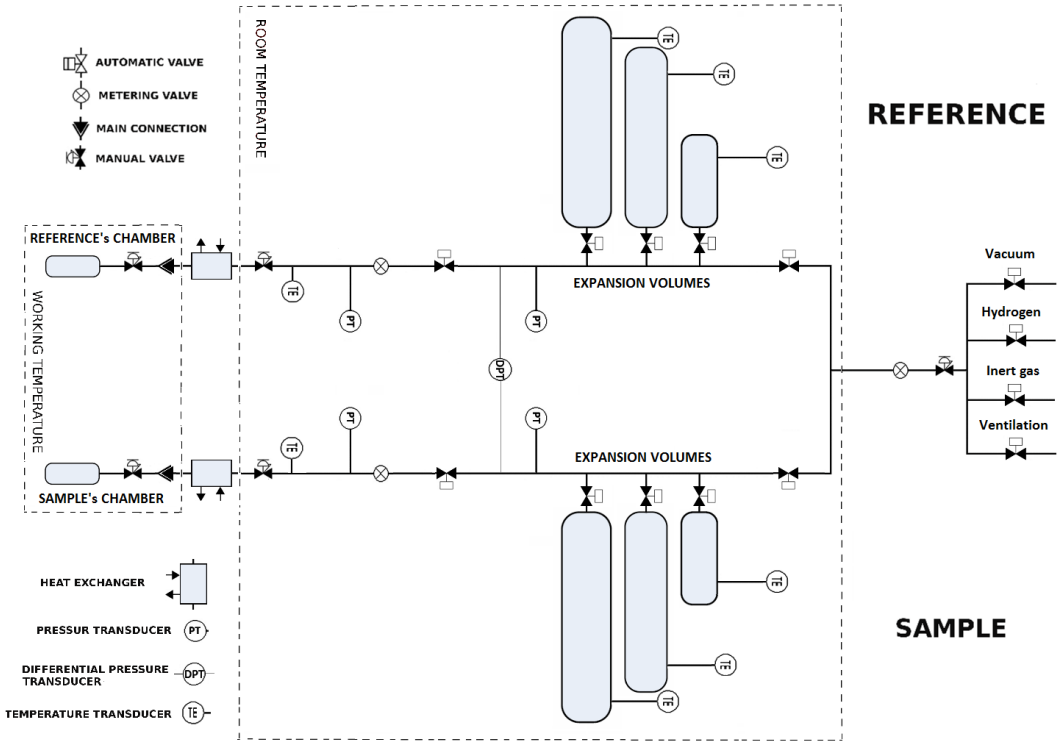

Figure 2.4: Scheme of differential apparatus realized in FBK facility.

mirrored sections called “Sample” and “Reference” (fig. 2.4). Each section is divided in

two volumes: an "expansion" well-calibrated volume at isothermal condition (inserted in a thermostat metallic box) and a "chamber" volume at working temperature with a proper heating and thermostat system.
In the next part of document, hardware of volumetric instrument is described in-depth.

Expansion Volumes Expansion volume size are crucial parameters in the volumetric apparatus as described by [71, 72]. In particular, Emre et al. [50] underlines the main guidelines that should rules the optimal ratio between sample size, chamber and expansion volume size in volumetric instrument.
Firstly, chamber and expansion volumes have to be larger than sample volume (approximately to a magnitude of 2). This minimizes the impact on the uncertainty by sample density variation during sorption investigation. Secondly the ideal ratio between chamber and expansion volumes has to be approximately 1, which is the optimal ratio between two volumes in order to minimize uncertainty in the volume calibration by gas expansion operation.
Furthermore, Emre et al. [50] introduces a useful figure of merit (η) to evaluate the maximum required volume for every sample size. η is estimated by eq.

$$\eta = \frac{s_k}{\epsilon_{\Delta P}} \tag{2.3}$$

s_k represents the variation of pressure in the isochoric instrument volume caused by complete sorption process of studied HSM. It is evaluate by applying real gas equation (eq.2.4), including an estimation of the total sorbed moles (n_{tot}) and the sum of every volume scale on their temperature (T_k).The sum in j-terms takes in consideration multiple sorption step.

$$s_k = \frac{n_{tot} R}{(\Sigma_j \frac{V_j}{Z(P,T_j)T_j})} \tag{2.4}$$

So, figure of merit η can be expressed by the ratio of s_k and accuracy of used pressure sensor ($\epsilon_{\Delta P}$). About [50], η has to be greater of 100 for obtaining data of high quality. Evidently, smaller is the volume, higher is the accuracy in the measurement. So, it is possible to evaluate the maximum requires volume size, estimating the maximum gas sorbed by sample and the accuracy of pressure transducer.
Unfortunately, a characterization performed with too small volume sizes, can easily overcome the differential pressure span, risking to damage the sensor, as well as not respected the isobaric condition in case of kinetics test. So, it needs to take in consideration also a lower limit for the volume size relied to the maximum span of differential sensor.
Equipping instrument with a unique volumes restricts the quantity and the type of

investigated materials about the previous described limit. Otherwise, equipping multiple volumes, it should be possible to combine them to improve gas detection of instrument. This solution allows both to enhanced feasibility of instrument and to make it able to perform thermodynamic and kinetics investigation maintaining a good compromise between high accuracy and range of measurements. In differential layout, every installed reservoir is replicated in the reference brunch, every one control by an appropriate automatic valves.
IDA has been equipped with four reservoirs with different size. The installing vessels are double ends, one side plugs to the process connection, while opposite end connection is equipped with Pt-100 sensor for the temperature data collection. The volume's sizes are approximately 100, 200 and 1000 cm^3, with an additional XXS volumes size of 40 cm^3, composed by the empty volume of the connections and pipes. Considering an average sorption quantity equals to $2 \cdot 10^{-3}$ mole (equals to the hydrogen amount sorbed by 50 mg magnesium, or 250 mg of Palladium), the merit's figure, eq.2.3, introduced by Emre et al. [50] is greater than 100, in agreement with the guidelines presented by Demirocak et Al.

Chamber volumes

As for expansions volume, the sample chambers and their holders (for both sample and reference side of IDA) are fundamental components in a volumetric apparatus, and they have been carefully designed to achieve accurate and reliable measures of gas sorption. The layout of chambers have to keep in consideration several constrains:

- a proper volume size, in accordance with the rest of instrument dimension and the useful volume for sample.
- the management of air-sensitive samples.
- a proper thermal control system.
- an excellent homogeneity of temperature in the zone of sample.
- a constant temperature gradient, long the wall of chamber, during all measurements (for not isothermal characterization)

IDA is equipped with two chamber (for reference and sample side, fig. 2.4). A inner sample holder in stainless steel 316L is in included in any chamber, fig. 2.5, with a empty volume's size approximately less than 10 cm^3 (considering also conduits). Chamber have been tested at pressure of 30 Bar in helium for possible leakage. Gas Sealing is guaranteed by two concentric o-rings, the first one in ™Kalrez, which has a

great resistance at high temperature, and second one in ™Viton which has less thermal resistance features but lower hydrogen permeability. More in detail, chambers are

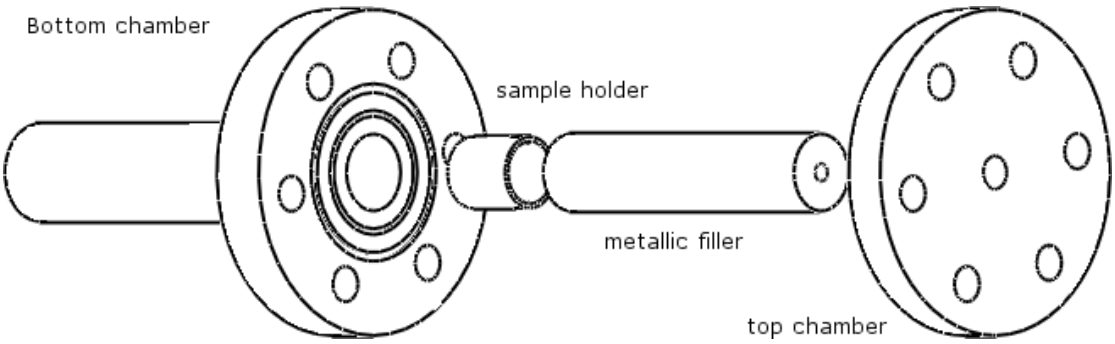

Figure 2.5: Chamber assembly.

composed by: bottom element,sample holder, filler metallic element to fill as more as possible the empty volume of chambers (fig. 2.6), and finally, the top element directly connected to the pipe.
IDA's chambers are designed for the study of gas sorption proprieties of a sample at

Figure 2.6: Bottom chamber for reference and sample side, with relative fillers and sample holder. A long unique fillers has been cut in two piece to facilitate the drilling of bottom piece.

temperature between RT and over than 400°. However, it can perform study also at cryogenic temperature, submerging the bottom side of chambers in a liquid nitrogen bath, or adding a suitable cryogenic system. In any case, the heating system includes a heater band wrapped on the base of sample and reference chambers, managed directly by PID algorithm, based on proper ECU (electronic Control Unit) and developed software. About thermal proprieties, the considerable mass of steel gets an apprecia-

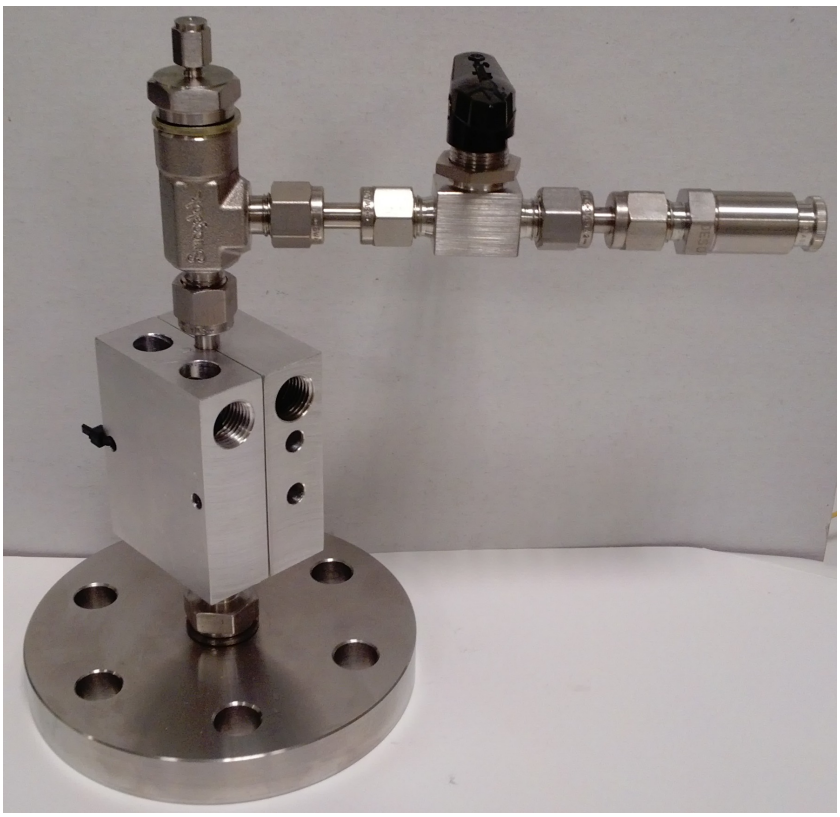

Figure 2.7: Top side of chamber for reference and sample line. It is possible to note the thermocouple's connection, the manual valves for the loading procedure of air sensitive sample and teh small aluminium heat exchanger to thermostat stainless steel tube.

ble thermal inertia to the chambers, which strongly contribute to the homogeneity and stability of temperature during the analysis (in case of sample with considerable enthalpy of reaction).
A proper thermal modelling was developed on ™COMSOL software to drive the design of sample and reference chambers, including thermal diffusion phenomena and the relative constraint about sample holder (size of heating component, position of cooling support, et.). The main goals of chamber's design are: approaching a sufficient well thermal homogeneity in the proximity of sample and to restrict the thermal gradient's domain in a constant portion of space for different pressure and temperature conditions. Moreover, it is necessary to ensure a suitable cooling at the top chamber side, in order to prevent overheating of plastic o-ring. Several numerical simulations were performed to optimize chamber's geometry. Boundary conditions applied on numerical simulation, reflects a typical experimental set up for high temperature HSM (working temperature 633 K and hydrogen pressure of 1 MPa). Finally, suitable geometry was identified with proper dimensioning of any components (height of chamber, position of cooler exchangers, etc., as reported in fig. 2.12). Simulated tem-

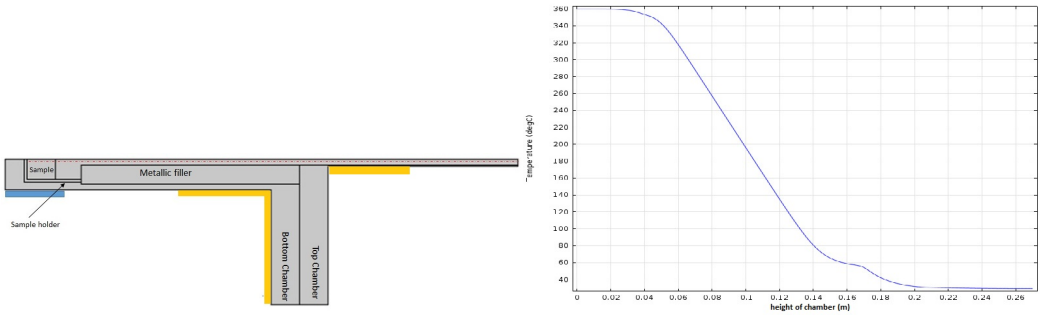

(a) Chamber layout.

(b) Temperature profile simulated at different Pressure (0.1-0.5-1 MPa).

Figure 2.8: In (a), design of chamber volume simulated in ™COMSOL multyphysics software is reported, blue square represents the heating band used to heat the sample, otherwise yellow squares are the cooler devices. In (b) numerical simulation of temperature is shown, the temperature data are collected long red line in fig. (a), for numerical simulation performed at 0.1-0.5-1 MPa of hydrogen pressure.

perature profile long the height of volume chamber, fig. 2.8(b), supports chosen layout. Temperature in the proximity of sample (0-2 cm) can be considered uniform and constant, while temperature at the o-ring position approaches relative low value (less than 60° at 0.15 cm in the plot fig. 2.8(a)). Finally, hydrogen pressure doesn't impact on temperature profile of chamber's volume, as reported in fig.fig. 2.8(b), because thermal conductivity of hydrogen gas is basically constant in the considered pressure range [85].

Taking in consideration the characterization on air sensitive material, chamber's volumes are equipped with two manual valves. One of that is visible inf fig. 2.7. They allows an easily disassembly of chambers, and the sample charging and sealing inside a glove box, under controlled atmosphere (e.g. Argon or Nitrogen). Moreover, two ™VCR connections allow a simply release of chambers from main body of instrument, without undermining the sealing's performance.

Valves and pipes IDA adopts diaphragm pneumatic valves. They were chosen to respect explosive normative and to avoid local hot spots, typical for the long opening time of solenoid valves [54]. Valves system includes a secondary distribution air station to feed pragmatical signal to the actuator. Air distribution station is placed outside of instrument's box and it is based on electrical valves, controlled directly by ECU (electronic control unit) of apparatus.
Fittings and connections were purchased by Swagelok Company, which ensure speci-

fied leak rate of system components lower than 10^{-9} STD cm3/s. All components are made in stainless steel (SS 316L), resistant to hydrogen embrittlement, as suggest by several works.[43, 52, 54, 55]
IDA have been tested towards leakages using a helium mass spectrometer, verifying the presence of gas leaks on all connections and fittings. Pressure of leakage test was 70 Bar.

Sensor High accuracy of IDA is guarantee by using high accurate differential pressure transducers (Siemens Delta bar PMD75, 0 ± 3 Bar, certified accuracy at full scale: ± 0.15 mBar), coupled by 4 absolute pressure transducer Swagelok "PTI-E" series with span 0-10MPa(a), calibrated with internal procedure (± 5 mBar). Absolute sensors are necessary to collect absolute pressure at working conditions and to compensate no perfect volumetric symmetry between the two branch of differential layout.
Apparatus is equipped with two types of temperature sensors: the first ones are PT-100 1/10 Din (with an accuracy of ± 0,04 K at room temperature). PT-100s are directly inserted in each volume for a quick and accurate measurement of gas temperature of expansion volume. The second ones are K-type thermocouples, inserted in different parts of the instrument. An additional K-thermocouple is placed in direct contact with the sample, while in the reference one, it is in contact with the chamber background.

Gas Inlet Management A proper gas inlet distributor has been realized. The available utilities for IDA are:

- Vacuum.
  A Scroll Pump (*BOC Edwards XDS10 XDS-10 Oil-Free Dry Scroll Vacuum Pump Rebuilt Refurbished*) guarantees vacuum-pressure up to 10^{-2}mBar. The scroll design (free oil) avoids eventual back-flow of oil-based contaminants.

- Hydrogen.
  The Purity of hydrogen is 99,99999%

- Nitrogen.
  The Purity of nitrogen is 99,99999%

A proper ventilation pipe has been installed to ventilate the apparatus. A system of check valves has been installed to avoid possible air back flow in the pipes, more, the ventilation operation stops at 1.3 Bar as additional safety condition. Finally, when hydrogen is ventilated to the atmosphere, it is mixed with a flow of nitrogen to reduce the concentration of explosive gas at the pipe's outcome.

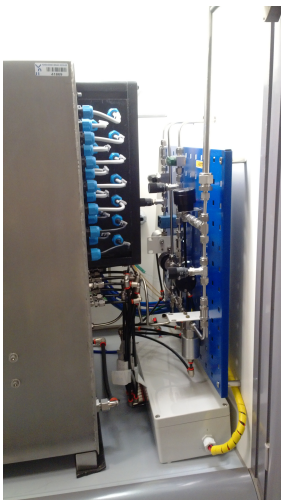

Figure 2.9: Inlet gas system.

Electronic Control Unit: ECU

In fig. 2.10, it is shown ECU's architecture for the management of overall IDA unit. ECU is based on National Instrument platform, NI-DAQ with proper acquisition data modules for acquiring PT-100s, thermocouples and 4-20 mA signals data.

ECU includes: proper power supply to electrically power the transducers, DAQ-

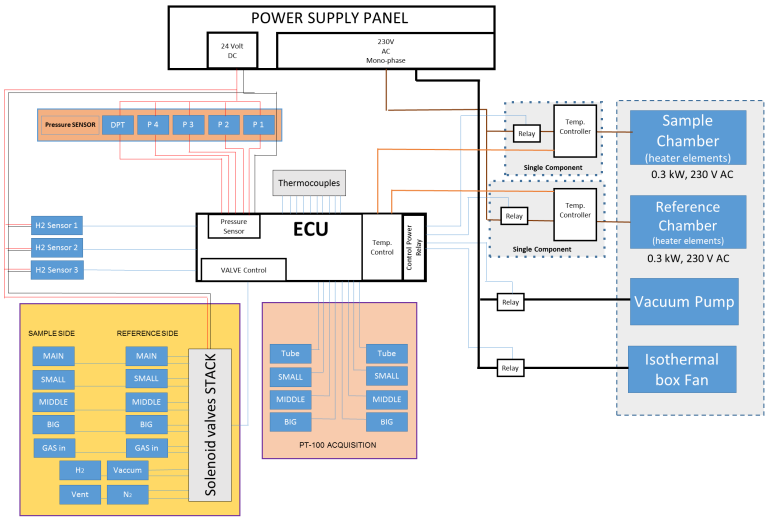

Figure 2.10: Scheme of ECU developed to manage IDA system.

platform for data collection, PID controller for the thermal management of chamber's volumes and proper relays to control all devices and valves. ECU was fully assembled

and programmed on ™Labview software in FBK facilities.

2.2.2 Thermal management

Volumetric approach is extremely sensitive to temperature variations, as explain in the introduction of this chapter. Furthermore, a successfully volumetric layout has to support the assumption of the temperature model chose to describe not isothermal conditions. It means to separate and keep constant the temperature in overall instrument, during both calibration and characterization operations. For these reasons, IDA is divided in two well separated thermal section: isothermal and not isothermal zone.

Isothermal Zone Isothermal zone is contained in a proper thermostat metallic box, which includes expansions volumes of respective sample and reference side, and almost the whole pipes and connections. A small portion of isothermal zone is placed outside of the box and include the little part of pipe which is in proximity of chambers (fig. 2.4).
Isothermal condition is guaranteed by different auxiliaries and precautions. Firstly,

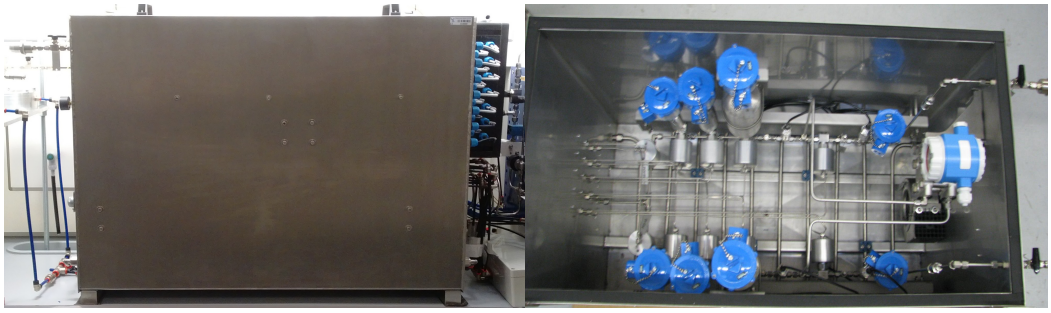

(a) External view. (b) Internal view.

Figure 2.11: Photo of external and internal view of isothermal zone of IDA contained into the metallic box. In (b), Picture of inner side of isothermal box. It is shown the two branch *sample* and *reference*, with the respective pressure sensors and expansion volumes.

a closed loop water circulation fed by a chiller (with an accuracy of 0,03 K) fluxes in a proper serpentine on the bottom of inner side of box. Secondly an air fan keeps a constant air circulation in the inner volume of the box. Electric engine of air fan is installed outside of instrument to avoid local heating raised by the motor's body. Finally, a thick external thermal insulation guarantees a good thermic insulation respect to the environment of the lab.
For achieving improved temperature homogeneity, air flow inside box is manipulated

by several air flow diverters. Different geometry and position of diverters are tested, in order to achieve the optimal thermal homogeneity (maximum temperature gap about 0.3 K).

Not-Isothermal Zone Non isothermal zone includes all volumes of instrument affected by thermal gradient. Thus, it incorporates whole volume of sample and reference chambers and a part of proximate conduits. The main targets for a successfully chamber design is to maintain the thermal gradient in a precise and constant zone of the chamber, for every working conditions. For these reasons, IDA adopts two heat exchanger fed by the same chiller used to thermostat isothermal box. The first one is the itself support of the chamber and it thermostats the bottom flange of chambers, avoiding possible thermal damage of o-ring which guarantee the gas sealing. Finally, a second heat exchanger is installed on the pipes directly connected to the chambers. Its roles is to thermostat that pipe's section, and the hot hydrogen which rapidly outcomes from chamber, particularly during high temperature desorption process.
These precautions support the assumption that every volumes of apparatus have a specific and constant temperature over every type of characterizations. Some thermocouples attached on pipe in the proximity of chambers, check the effective compliance of such assumption. Thermal transpiration issue ([74]) is intrinsically resolved with IDA, because it affects both sample line and reference line, and so doesn't impact on differential pressure measurement.

2.2.3 Theoretical Approach

The classical theoretical approach for volumetric method, epitomized in equation 2.1, presents several strong assumption (eg, neglecting inner volume of valves,...) and some difficult aspects about procedures (eg, it needs to calibrate only chamber volume at every variation of working conditions). In this work, the more appropriate approach of Parilla [86] has been adopted. Such approach allows to reducing reliance on unknown pressure in chambers and minimizing the error introduced by valve' volumes.[79]
Considering a classical volumetric instrument layout (2.1), the mass balance equation during a sorption investigation can be written as eq.2.5:

$$n_i = n_{in} - n_{eq} = (n_0^i - n_{cl}^{i-1}) - (n_{eq}^i - n_{eq}^{i-1}) \tag{2.5}$$

The amount of gas sorbed by the sample (n_i) is calculated as the difference between gas mass charging in the only expansion volume (n_{in}, as difference between gas mass

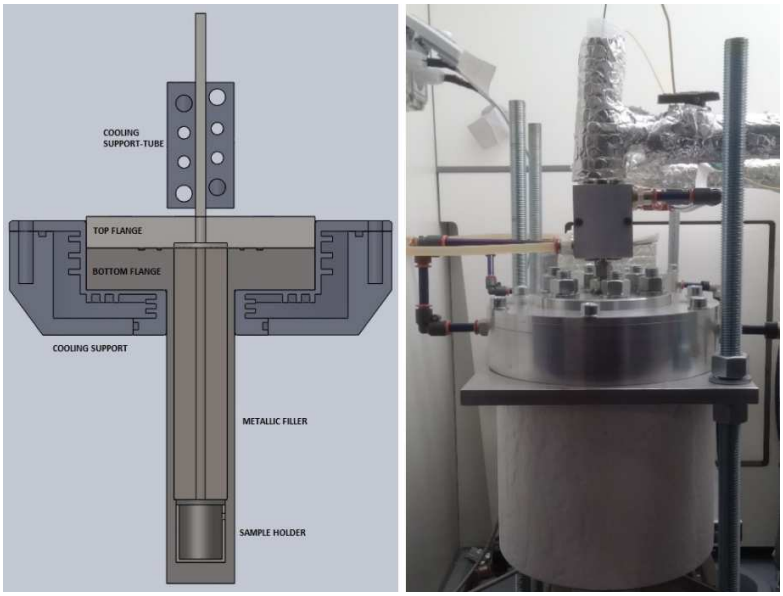

Figure 2.12: Scheme of chamber volume (left figure). Picture of chamber volume assmebled with its holder and connected to isothermal box of IDA

present after charging step, n_0^i, and before gas charging step,n_{cl}^{i-1}) and variation of gas mass in overall apparatus at equilibrium condition (n_{eq} ,as difference between gas mass in all apparatus volumes before step of characterization, n_{eq}^i, and after expansion gas step,n_{eq}^{i-1}). Fig. 2.13 represents the sequential step of measurements following Parilla's approach.[86] The measure starts from a state of equilibrium (*eq.*), defined with cycle indexes *(i-1)*. In the same cycle, the following step is indicated with *cl*-pedix, where the main valves are closed. At this point, the main characterization step starts. In the next cycle (*i*), the expansion volume is filled with pressurized H_2, indicated with a the index (*0*). When opening the main valves, the gas sorption phenomena starts. Measurement stops when the system achieve the state of equilibrium (*eq*). This method calculates the magnitude of sorption process measuring and calibrating only the volume related the expansion of the gas and the overall volume of the instrument. Other methods require the calibration of connected dead volumes, such as those on the valves, which are difficult to estimate. Hydrogen uptake or release (n) can be calculated through real gas law, including the compressibility factor (Z factor). Z depends on the typology of the gas, on its Pressure (P) and Temperature (T) and it can be easily deduced by NIST database [87].

$$n_{real} = \frac{P \cdot V}{R \cdot T \cdot Z(P,T,gas)} \tag{2.6}$$

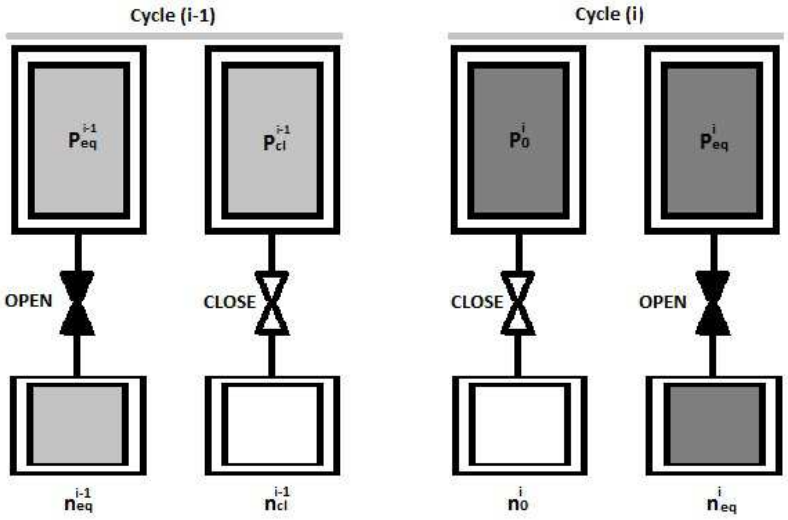

Figure 2.13: Description of a single measure. 0-mark means initial cycle condition, cl-mark means condition after achievement of equilibrium state and after the closing of valves. Eq-mark means equilibrium condition with all open valves.

If gas moles (n_{real}) are expressed through the equation 2.6, Eq. 2.5 can be rewritten as:

$$n_i = \left[\left(\frac{P_0^i}{Z_0^i} - \frac{P_{cl}^{i-1}}{Z_{cl}^{i-1}}\right) - \left(\frac{P_{eq}^i}{Z_{eq}^i} - \frac{P_{eq}^{i-1}}{Z_{eq}^{i-1}}\right)\lambda\right]\frac{V_A}{RT_{ISO}} \tag{2.7}$$

V_A is the expansion volume of chamber side at isothermal condition. The parameter λ represents the ratio between the total volume of the apparatus V_{TOT} (including chamber and expansion volume) and only expansion one ($\lambda = V_{tot}/V_A$). V_A and λ terms are carefully calibrated before each hydrogen measurement using an inert gas (e.g. helium or nitrogen), with the sample at the working temperature and the rest of apparatus at thermal equilibrium. The approximation of the ideal gas law can introduce a systematic error on the measure of stored hydrogen in the sorption process.

In differential layout, the hydrogen uptake in the sample is calculated through differential pressure measures between the two identical volumetric sections. In this case, the mathematical formulation changes with respect to eq. 2.7, introducing the so called "reference section" – (index B) in a linear system:

$$\begin{cases} n_{i,a} = \left[\left(\frac{P_{0,a}^i}{Z_{0,a}^i} - \frac{P_{cl,a}^{i-1}}{Z_{cl,a}^{i-1}}\right) - \left(\frac{P_{eq,a}^i}{Z_{eq,a}^i} - \frac{P_{eq,a}^{i-1}}{Z_{eq,a}^{i-1}}\right)\lambda_a\right]\frac{V_a}{R \cdot T_{iso}} \\ n_{i,b} = \left[\left(\frac{P_{0,b}^i}{Z_{0,b}^i} - \frac{P_{cl,b}^{i-1}}{Z_{cl,b}^{i-1}}\right) - \left(\frac{P_{eq,b}^i}{Z_{eq,b}^i} - \frac{P_{eq,b}^{i-1}}{Z_{eq,b}^{i-1}}\right)\lambda_b\right]\frac{V_b}{R \cdot T_{ISO}} \end{cases} \tag{2.8}$$

$n_{i,b}$ is equals to 0 for reference side. T_{ISO} indicate the temperature of isothermal zone of apparatus. Merging the common terms in the equation 2.8 and adopting the definition of differential pressure $\Delta P = P_A - P_B$,

$$\begin{aligned} n_i = \Big[&\Big(\frac{\Delta P_0^i}{Z_{0,a}^i} - \frac{\Delta P_{cl}^{i-1}}{Z_{cl,a}^{i-1}}\Big) - \Big(\frac{\Delta P_{eq}^i}{Z_{eq,a}^i} - \frac{\Delta P_{eq}^{i-1}}{Z_{eq,a}^{i-1}}\Big) \\ &+ P_{0,b}^i\Big(\frac{1}{Z_{0,a}^i} - \frac{\beta}{Z_{0,b}^i}\Big) - P_{cl,b}^{i-1}\Big(\frac{1}{Z_{cl,a}^{i-1}} - \frac{\beta}{Z_{cl,b}^{i-1}}\Big) \\ &+ P_{eq,b}^{i-1}\Big(\frac{\lambda_a}{Z_{eq,a}^{i-1}} - \frac{\beta\lambda_b}{Z_{eq,b}^{i-1}}\Big) - P_{eq,b}^i\Big(\frac{\lambda_a}{Z_{eq,a}^i} - \frac{\beta\lambda_b}{Z_{eq,b}^i}\Big)\Big] \frac{V_a}{R \cdot T_{ISO}} \end{aligned} \tag{2.9}$$

Where β represents the volume ratio between sample and reference expansion volumes ($\beta = V_b/V_a$), while λ_a and λ_b are volume ratios between overall volume and expansion volume, respectively for sample and reference sections ($\lambda_a = V_{tot,a}/V_a; \lambda_B = V_{tot,b}/V_b$). Finally, four terms of eq-2.9 have to be calibrated in order to perform a proper measure with a differential volumetric instrument: λ_a, λ_b, β and V_a. In next section, calibration approach will be explain to complete the overview about theory of differential apparatus.

Compressibility factors

Compressibility factor is generally estimated by EoS (Equation of state). Among them, Redlich-Kwong-Soave (RKS) [88], standardised equation [89] or more general MBWR equation [90] are the most widely used mathematical formulation of EoS. In this work, MBWR (Modified Benedict-Webb-Rubin) equation 2.10 was used to calculate the compressibility factor,

$$P = \rho RT + \sum_{j=1}^{19} G(j)\rho^{k_j} R^{m_j} + \sum_{j=20}^{32} G(j)\rho^{k_j} R^{m_j} e^{\gamma\rho^2} \tag{2.10}$$

P is the pressure, T is temperature, R the constant of gas and ρ the density of gas. $G(j)$, k_j, m_j are the 32-terms of MBWR equation. The utilized parameters are obtained by the literature [90]. The estimation of Z-factor is performed through iterative calculations (secant method) as reported by [52], rewritting eq. 2.10 as:

$$f(\rho) = \rho RT + \sum_{j=1}^{1} 9G(j)\rho^{k_j} R^{m_j} + \sum_{j=20}^{32} G(j)\rho^{k_j} R^{m_j} e^{\gamma\rho^2} - P \tag{2.11}$$

with the iteration formula ,

$$\rho_{k+1} = \rho_k - \frac{f(\rho_k)(\rho_k - \rho_{k-1})}{f(\rho_k) - f(\rho_{k-1})} \tag{2.12}$$

The real gas density is estimated by iterative loop calculation up to a sufficient tolerance. Final compressibility factor is evaluate as the ratio between real calculated density and the ideal one. As initial values for the stating of iterative process is: 0 and the ideal gas density, P/(RT). The values of the compressibility factor are in good agreement with data obtained by NIST. In the range of pressures and temperatures considered in the paper, the compressibility factor is close to one, while its error is approximately 0.02%, as reported also by [87].

Volume calibration

Volume calibration is the operation to obtain an estimation of λ_a and λ_b, before doing any further measures. On the contrary, the β and V_a terms are measured at every change in the instrument configuration (transducer replacing, modification of connections or pipe, et.). The calibration procedure can be divided in two separate case. The first regards the estimation of the expansion volumes in the instrument (V_a and V_b, and related β value) at isothermal conditions. This is called "*basic calibration*". The second operation is the estimation of λ_a and λ_b at working conditions (called "*working calibration*").

Basic Calibration The adopted methodology for "basic calibration" has been specifically designed to avoid any significant change in the configuration and to get a better estimation of the expansion volume at isothermal conditions.
Initially, two external volumes (V_1 and V_2), were calibrated through water filling, following the NIST procedures [91].
V_1 and V_2 volumes are carefully thermal insulated and cleaned. Once calibrated, they are installed in IDA, replacing the reference and sample chambers. The basic calibration procedure involved initially the gas filling of the expansion volume (V_a and V_b) at fixed pressure (P_0). Following, the gas expands on the external volume (V_1 or V_2) at P_f, previously maintained in vacuum. Several gas expansion at isothermal condition was performed, and initial and final pressure data are collected at thermal equilibrium. The inert gas used in basic calibration is nitrogen.
The described procedure allows the definition of the following system of equations for each internal expansion volume V_a^i, where i-terms indicates the different size volume in IDA (*Super, Small, Mid and Big*) and a-pedix, the branch of apparatus (sample or

reference one):

$$\begin{cases} \frac{P_{0,1}V_a^i}{Z_{0,1}^a} = \frac{P_{f,1}}{Z_{f,1}^a}(V_a^i + V_{conn} + V_1) \\ \frac{P_{0,2}V_a^i}{Z_{0,2}^a} = \frac{P_{f,2}}{Z_{f,2}^a}(V_a^i + V_{conn} + V_2) \end{cases} \tag{2.13}$$

P is the pressure measured at the thermal equilibrium and f and 0 pedixs indicate initial and final state. T the isothermal temperature of overall instrument, Z is the compressibility factor (depending exclusively by pressure) while V_conn is constant volume between the expansion volumes and the external ones. In order to maintain the most costant as possible the V_{conn}-terms, external volumes are installed using the same connections and pipes.
Basic calibration has been performed several times, in order to have a sufficient number of data (approximately 30) to apply statistical method for the estimation of errors (both causal and systematic ones).

Working Calibration Respect to the previous calibration, in working calibration, λ_a, λ_b are estimated at every change of sample materials or working temperature. Such calibration is similar to the basic one, performing steps of gas charging in expansion volume and gas expansion into the chamber previously maintained in vacuum. In this case, the aim is to estimate the ratio between the expansion and the overall volumes for each section of the instrument (sample and reference ones) with the sample material at working conditions. Nitrogen was used as inert gas in the calibration procedure, to preserve the properties of air sensitive samples. A model similar to the equivalent volume approach of Gray et Al was applied [9] to evaluate V_{tot} (and so, λ_a and λ_b). Such approach measures a fictitious or equivalent volume V_{tot} corresponding like the overall instrument volume is at isothermal condition, considering portion of volume involved in thermal gradient as an equivalent volume at constant temperature. Formulation for λ_i is derived by real equation of gas (eq.2.6), as:

$$\lambda_n = \frac{V_{tot}(P, T[x])}{V_n} = \frac{P_0}{P_f}\frac{Z(T_{iso}, P_f)}{Z(T_{iso}, P_0)} \tag{2.14}$$

So, it is possible to express V_{tot} by eq. 2.15: an isothermal contribution, which includes the volume of the apparatus at the same temperature of the reference volume, and a non–isothermal contribution.Last one depends on the compressibility factor and the temperature gradient T[x] along the chamber volumes, (where x is spatial coordinate which identify the characteristic lengths of chamber):

$$V_{tot}(P,T[x]) = V_{iso} + \int_0^X \frac{Z(P,T_{iso})\,T_{iso}}{Z(P,T[x])\,T[x]} A(x)\,dx \tag{2.15}$$

Not-isothermal volume is resumed in the mathematical integration on the portion of volume affected by the thermal gradient (A(x) is the section profile of sample volumes). Under rigorous point of view, V_{tot} (and so, λ_a and λ_b) values depend on pressure as well as on the utilized gas (eq.4), while V_{tot} is considered constant. Such approximation is justified and validated in the next sections.

Assumption

The physical model hereby described includes several assumptions principally on the volume calibration (and so on the calculation of sorbed gas), which could increase the error on the measurements. For this reason, these assumptions must be carefully considered and justified.
The estimation of the volume can be affected by gas physisorption phenomena, which involve the surface of the storage material and the itself wall of instrument. This contribution can be considered negligible because metal hydride materials, hereby studied, have a low specific surface with respect to other materials with bigger physisorption phenomenon. Sorption process is studied at higher temperature (T>300 K) and at lower pressure (≤ 1.5 MPa). At these conditions, physisorption phenomena are reduced. Moreover, the method used in this work realizing the measures with a differential layout, allowed the drastic reduction of uncertainty caused by gas physisorption on the walls, because it occurred with approximately similar contribution on both parts of IDA (sample and reference sections), provided of identical volumes. Uncertainties caused by variations on the thermal gradient during the analysis are neglected because it is considered limited to a specific portion of chambers' volume by proper adopted technical choices. This assumption is strengthened by the presence of two coolers on the both the chamber volumes. Furthermore, geometry of the chambers presents a considerable ratio between length and radius of pipes and chambers (and so a more intimal contact between metallic wall and gas), a considerable thermic inertia and proper thermal insulation which contribute to the local thermal equilibrium approximation.
Uncertainty due to the use of two different gasses in the procedures of calibration (nitrogen) and characterization (hydrogen) has been carefully studied. Such uncertainty impacts on the estimation of V_{tot} and consequently,λ_a and λ_b. The errors is focused in the evaluation of at non-isothermal volume, as expressed in 2.2, because the compressibility factor depend also by nature of gas. This equation shows the dependence of the total volume on gas used, represented by the compressibility factors

Z. However, It is possible to estimate the uncertainty caused by such approximation. Assuming a constant temperature gradient in chambers' volume at a defined working temperature, and rearranging the eq.2.2, it is possible to express the error in the V_{tot} estimation as:

$$\chi^{g}_{V_{tot}} = |V^{H_2}_{tot} - V^{N_2}_{tot}| = \int_0^X \frac{T_{iso}}{T[x]} A(x)\Big(\frac{Z^{H_2}_{T_{iso}}}{Z^{H_2}_{T(x),P}} - \frac{Z^{N_2}_{T_{iso}}}{Z^{N_2}_{T(x),P}}\Big)dx \tag{2.16}$$

From eq. 2.16 it is possible to estimate the maximum error associated to the utilization of different gases during the calibration steps. Considering a worst possible case (overall volume sample chamber equals to 10 cm3, calibrating pressure of 3 bar and a homogeneity distributed working temperature of 400°C in all not-isothermal volumes), the integral formulation of eq. 2.16 can be simplified to a product of terms, obtaining the maximum hypothetical error of +0,02 cm^3, defined as the maximum uncertainty for the use of two different gas for the estimation of not-isothermal volume. In real conditions, chamber's volumes have a thermal gradient and not a homogeneity distributed high temperature,so the volume error is smaller than the value estimated.

Similar to the previous case, V_{tot} and consequently,λ_a and λ_b, are considered independent to the pressure. This is an important source of systematic error because the Z factor is pressure-dependent. The error can also be estimated again by eq. 2.16. obtaining the variation of compressibility factor from calibration of the maximum and minimum hydrogen's pressures.

$$\chi^{p}_{V_{tot}} = |V^{P_w}_{tot} - V^{P_c}_{tot}| = \int_0^X \frac{T_{iso}}{T[x]} A(x)\Big(\frac{Z(T_{iso},P_w)}{Z(T(x),P_w)} - \frac{Z(T_{iso},P_c)}{Z(T(x),P_c)}dx\Big) \tag{2.17}$$

Using eq. 2.17, the maximum hypothetical error (applying the same previous hypothetical condition) for a calibration step performed at 0,3 MPa, is +0,03 cm^3 for a hydrogen storage analysis run at 1,5MPa, while it is -0,01 cm^3 for an hydrogen storage analysis run at 0,1 MPa.
Systematic error due to different gases from hydrogen and/or applying a different working pressure from the one used in the calibration steps has been taken in consideration. However, their impact in final uncertainty is not relevant and can be neglected in error estimation for the range of pressure and temperature considered.

2.2.4 Uncertainty analysis

In previous section, the justifications for the model's assumptions are exposed to evaluate possible systematic causes in final uncertainty. However, error associated to gas sorption measurements have to take in considerations even many other factors.

As described above, Gas moles sorption is calculated as function of several parameters (temperature, pressure, volume,et...) from eq. 2.9. Every single variables is affected by a characteristic uncertainty. Assuming a normal distribution of data (with no systematic errors), such uncertainty is generally associated to the standard deviations of the variable population, which correspond to the casual errors on measures . About physical measurements, as temperature or pressure, uncertainty on data is typical expressed by accuracy of transducers, reported on data sheet of device. So, uncertainty on final sorbed moles can be calculated through the classic error propagation theory. Neglecting variable correlations or assuming independent variables, a common formula among engineers and experimental scientists is applied to calculate error propagation. Based on eq. 2.9, mathematical formulation for the error propagation is:

$$\chi_n = \sqrt{\sum_{k=1}^{n} \left(\frac{\delta n}{\delta x_k}\Big|_a \chi_{x_k}\right)^2} \tag{2.18}$$

ϵ_n is the final uncertainty on gas moles measures. It is calculated as the error propagation of every variable x_k with error ϵ_{x_k}, involved in the measurement. Any single uncertainty's contribution include two terms: first one is the proper errors of considered variable, while the second one involves how such parameters impact on the amount of sorbed mole. Last term is mathematically resumed as the derivation of the main equation respect with the considered value. In tab.2.2, the main physical variable estimation with relative errors are reported.

Table 2.2: Resuming table of variable and associated absolute and relative uncertainty. Errors for β, λ and V_a are purely indicative and it represents an average values considering the experimental conditions.

Variable	χ_{abs}	$\chi_{\%}$
Differential Pressure	1.5E-4 [bar]	0.01 [%]
Absolute Pressure	1.5E-4 [bar]	0.01 [%]
Temperature	0.5 [bar]	0.08 [%]
Expansion Volume [V_a]	6E-5 - 1.8E-3 [liters]	0.01 [%]
β	1E-4 [1]	0.03 [%]
λ	1E-4 [1]	0.6 [%]
Z-factor	2E-4 [1]	0.02 [%]

For the sake of clarify, in next part of this document, uncertainty on measures are exclusively obtained by 2.18.

2.2.5 Software

Generally speaking, characterizations of potential hydrogen storage material can take a considerable amount of time. Considering thermodynamics study (e.g. PCT) that requires the achievement of a pseudo-equilibrium of sample-hydrogen system, a typical analysis can take several hours.
For this reason, a proper automatic control is necessary to speed up processes of characterization, reducing time delay of all manual operations that a operator should be run manually (stability check, gas loaded, etc). Automatic control monitors overall system, guaranteed a low level safety procedure when an emergency occurs (hydrogen leakage, chemical hood fault, etc.).
The realization of a suitable electronic unit and relative management software could be seemed a fancy frill for the development of final measuring apparatus, but it is generally the main cost in a commercial instrument.
Software was realized in ™Labview environment. The architecture of software include several parallel cycle loop, to optimize the time cycle, which run respectively:

- Data collecting loop. It includes other three parallel loop cycles to collect at the optimal speed every signal from instrument (pressure transducer, temperature transducer and digital relays).
- Safety loop. Collected data are elaborated in safety loop to ensure the respect of previous set parameter, and in case to turn off and to secure instrument and laboratory. The case of alarm are discussed below.
- Program loop. It includes all instruction to autonomously operate the different characterizations (thermodynamics and kinetics one)
- GUI loop. A proper loop which visualize collected data. It include the manual control on the instrument and the setting of main parameters.

Data collection loop is composed by three sub loop to acquire at most optimal time the conditioned signal data. IDA collecting times are: 0.4 s for highly accuracy pressure sensor data, 1.5 for highly accurate thermocouple signal and 10 ms for relays signal.
Safety loop is a mandatory component of software. IDA operates with high pressure hydrogen gas, in presence of high temperature points (chambers). It is a strong risk of interference as well as the inflammable nature of hydrogen. IDA software autonomously activates safety procedure for 4 main reason: hydrogen gas in air outside of instrument, malfunction of fume hood where apparatus is placed, excess of temperature in the chambers and finally excess of gas pressure in the instrument. Safety procedure is basically the same for all emergency signal. Any active procedure is stopped, all valves are closed to compartmentalize the instrument's volume and

chamber's heaters are turn off, waiting operator action.
Program loop collects all instruction for the performing of a correct operation of measurements. Initially, it has been developed a procedure to pressurize or evacuate at fixed pre-setting pressure a selected volume of apparatus. Then, every single operation (self calibration, kinetics or thermodynamics characterizations) has been realized repeating the basic operation, with proper constraints, setting by operator.
Generally, automatic procedures require proper algorithm to determine the ending and the starting of any procedure step. They regard: the stability of physical signal (as temperature and pressure), the evaluation of correct pressure for every operation, the evaluation of compressibility factors and a estimation of uncertainty on the gas sorption.

Stability Algorithm In thermodynamics measurements, equilibrium time is fundamental for a correct characterization of HSM. The requirements to forwards to next steps of measures have to take in consideration the achieving of equilibrium in the sorption process and also the thermal equilibrium of the apparatus ([50]). IDA software include a proper stability algorithm to evaluate equilibrium state of system, monitoring the pressure (and so the profile of gas sorption), and the temperature of instrument.
Algorithm collects the data of: differential pressure, the temperatures of volume involved in the measures and finally, the temperature of chambers, in a specific period of time selected by operator (default value is 300 s). The collected data are elaborated to give, firstly, their statistical dispersion (difference between maximum and minimum values) and secondly, the average absolute deviations (**AAD**) of every single arrays of data. The requirements for the approaching of equilibrium state of system are applied on the data.

- For differential pressure value, equilibrium state is considered achieved when AAD value is less than differential pressure uncertainty.

- For temperature values of the expansion volume and chambers, thermal equilibrium is achieved when average temperature in the selected time is close to the initial temperature (inside of the interval of the double of its uncertainty) and the AAD of temperature data is less than pt-100 uncertainty.

Once the equilibrium requirements are satisfied, software starts the procedure for the subsequent step. Such conditions allow to obtain accurate and reproducible data.

Pressure setting IDA software implements a proper algorithm to calculate initial pressure to set in expansion volume for any measures (both thermodynamics or kinetics). Algorithm can be set in two way: or imposing a volume for the characterization (software estimates the pressure from the calibration data) or set an estimation of HSM proprieties (as gas storage capacity and investigated mass). In last way, software is able to evaluate the optimal volume to use as a compromise between complete storage characterization and uncertainty.
IDA is not equipped with a tunable pressure regulator so, the gas charging or discharging operations have to be carefully controlled to approach the selected value by means to a dynamic approach. Gas inlet system is equipped with a metering valves to reduce the flow of hydrogen incoming or out coming. Software controls such operations, acting on the main valves of gas supply. When pressure of gas is in proximity of selected pressure value, an proper algorithm stops the gas charging or evacuation at an fixed pressure before the target (which depend by pressure itself and type of selected volume) with sufficient delay to approach the set value. In this way, the control of pressure is sufficiently high to be reproducible.

Compressibility factor estimation An additional algorithm for the calculation of Z factor of gas is implemented in IDA software. As mentioned by [52], Z factor can be calculated by iterative formula based on MBWR equation of state, as reported in previous section. The data are fully in agreement with compressibility data factor of NIST, evaluated through ™Refprop software.

Uncertainty estimation A proper algorithm based on eq. 2.18 and eq. 2.9 has been developed for the estimation of uncertainty in gas sorption moles during the characterization. Algorithm has been developed in ™Labview and associated with ™EES (Equation Engineering Solver) sketch for the evaluation of single contribute of every variable to final uncertainty.
Finally, last loop cycle in IDA software permits the visualization of data (fig. 2.14(c)), a basic elaboration of sorbed moles during the characterization (fig. 2.14(b)) and the manual setting of parameter as well as the manual control of instrument (fig. 2.14(a).

2.3 Experimental section

2.3.1 Objective of section

A complete study on the sorption properties of the material utilized for hydrogen storage included several steps: degassing, activation procedure and, finally, kinetics and PCT characterization. These operations were fully automatized in a software

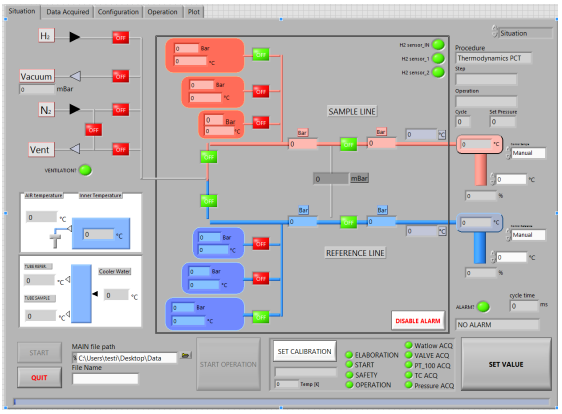

(a) Manual control interface

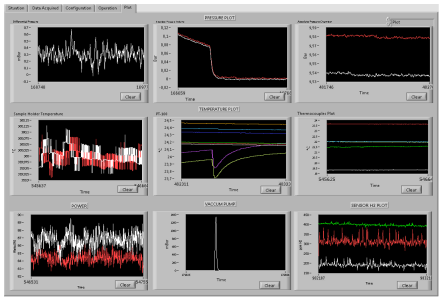

(b) Visualization Data interface

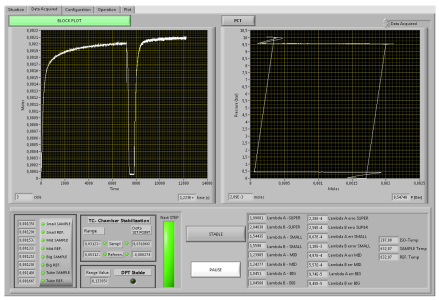

(c) Sorption analysis Interface

Figure 2.14: Software interface of IDA.

specifically developed to control the IDA equipment. In the next section, a description of any characterizing procedure is described. Next, an example of full calibration of instrument is reported, considering the initial basic and final calibration. At the end a performed null measurement (without sample) will give a partial confirmation of the reliability and robustness of apparatus. Finally, in order to fully validate the volumetric approach, hereby followed, palladium and magnesium sample have been analysed.

The Palladium-Hydrogen system has been extensively studied, [92–100], also for validation of characterizing instrument [65] . Based-Pd material owns a fast kinetic of sorption process and allows ignoring the effect of poisoning with O_2 and moisture. For these reasons Pd has been chosen as reference material to calibrate the IDA instrument. However, palladium measure are performed at relative low temperature (maximum 400 K) and low pressure (maximum 2-3 Bar).

For these reason, in order to validate IDA also for high temperature and higher pressure studies, magnesium sample has been chosen as second reference material. MagnesiumH_2 system is well known [101–105]. Moreover, the highly chemical reactivity respect to air/oxygen/moisture of magnesium allows to fully test the air sensitive procedure in IDA. Characterization on magnesium sample has occurred at

relatively high pressure for metal hydride system (0.5-1 MPa) and at higher temperature (633 K) respect to Palladium study.
In the next discussion part, any gas sorption characterization performed with IDA, is compared with an analogous Sievert instrument, in order to confront performance on measurements and their uncertainties between these two type of layouts. The sample section of IDA fig. 2.4 was isolated to be used as a classic Sievert apparatus. Eq. 2.7 is applied to calculate the sorbed moles and the uncertainty propagation.
The scope of such analysis is to investigate the performance of an classic instrument layout respect to the new differential one, but with same characteristic design and management as: volume's sizes, temperature management and procedure.

2.3.2 Procedure

IDA implements: null measurement test, degassing operation, Activation procedure, kinetics characterization and thermodynamic characterization (PCT). In this section, the procedure applied for the analysing of reference materials are described.

Null measurement Null measurements are basically a series of kinetics analysis performed on empty chambers to check the effective null sorption both for uptaking and releasing process. Generally can be performed with or without loaded sample, although last option requires inert gas (e.g. nitrogen). Assuming no physi-sortpion phenomena, it is possible to evaluate goodness of mathematical model, hereby developed.
Considering null sorption, $n_i = 0$ in eq. 2.9, null tests are used to check and validate parameters estimated from previous calibration operations. In the experimental section, a null measurements is performed with hydrogen gas and no sample charged in the chamber, in order to validate theoretical approach.

Degassing Degassing operation is required to clean the material surface, removing contaminants from the samples (e.g. solvents, not reacted precursors) and physisorbed on the chamber's walls. The degassing procedure was carried out in vacuum at a temperature of 360°C for a variable time. It is considered complete when the inside pressure of the instrument approach the limit pressure of the vacuum pump (in the range 1-5 Pa).

Activation Activation procedure is required to achieve the real kinetics performance of the analysed sample, especially to study reversible cycling of hydrogen storage. Indeed, the activation mechanisms involve several phenomena: the surface segregation of the metallic particles, the phenomena of cracking of the oxidized surface layer or

simply the rupture of material grains caused by changing abruptly its volume with the consequent exposition to gas of the new clean surfaces [93, 95]. So, through a series of complete hydride and de-hydriding reaction, sample asymptotically approach its maximum kinetics proprieties.
In this work, the activation procedure was carried out with a series of fully absorption and desorption processes at high temperature (633 K) and with high driving force (1 MPa hydrogen pressure for absorption step and vacuum (1-10 Pa) for desorption analysis). The procedure is autonomously performed by IDA. Activation procedure can be considered as a cycling characterization, which operates in the same way.

Kinetics Characterization The kinetics measurements represented the time evolution in the sorption process, with a transient described by an asymptotical evolution from zero, at the beginning of the process, to a maximum value, corresponding to the maximum sorbed capacity of the tested material. That procedure is generally performed at constant pressure and temperature; nevertheless, for an isochoric apparatus it is difficult to maintain a perfect isobaric condition. For this reason, some solutions are indicated in bibliography: Mac Gray proposed a layout of the experimental apparatus with a variable volume, which changes in order to maintain the same pressure during the experiment [9]. Checchetto et Al [51] introduced an interesting automatic procedure to fill or evacuate small amount of gas contained in the apparatus in order to maintain the value of pressure within a limited range. Another option is to reduce the variation of the pressure at the end of measurement, applying a big volume for kinetics measurements. IDA can be managed on both of two last described procedures.

PCT Characterization PCT measurements were carried out through sequential gas expansion steps (called also multi-micro-kinetics) in order to obtain the value of hydrogen concentration in the sample at different pressures and at thermodynamic equilibrium. Generally, PCT is plotted with H_2 concentration in metal in x-axis (or sorbed moles) and H2 pressure in y-axis.Van't Hoff equation (eq.2.19) can be applied to estimated enthalpy and entropy of hydriding or de-hydriding reaction, which is compared with literature data to validate instrument and method applied.

$$ln(\frac{P_{eq}}{P_0}) = \frac{\Delta H}{RT} - \frac{\Delta S}{R} \tag{2.19}$$

P_{eq} is the equilibrium pressure, characteristic of the gas sorption reaction with specific ΔH and ΔS. P_0 is the pressure reference (0.1 MPa). This procedure has a great disadvantage: the error of every expansion step is accumulated resulting in a bigger final error. For this reason, some works reported in bibliography adopted an extreme solution: to restore the sample at initial conditions after every step of gas expansion,

hydrogen is completely filled or evacuated [106] . In this work, cumulative micro kinetics study on IDA were performed to obtain PCT plot. The cumulative error is restrained due to the high accuracy of apparatus and low uncertainty on each kinetic step.

2.3.3 Validation 0: Not isothermal Calibration and null measurements

In this section, the basic and an example of working calibration were reported. Next,a null measurement was performed with hydrogen gas to demonstrate robustness, reliability and reproducibility of differential measures in gas sorption analysis. The two extreme volume size (the smallest and the biggest one) were taken in consideration for null measurements.

Basic calibration

As described in previous section, the basic calibration estimates the size of expansion volumes of IDA, installed inside isothermal box. The developed procedure allows to calibrate expansion volume with high accuracy, as well as taking in consideration the small but not negligible dead volumes of valves.
Two external volume's sizes (V_1 and V_2) were previously calibrated by gravimetric method ([107]), respectively (137.2 ± 0.1 cm^3 and 475.7 ± 0.12 cm^3). The solution of the equation 2.13 allowed the calculation of the volumes of internal vessels, by volumetric approach, excluding dead volumes (e.g. from valve connections and pipes) which are very difficult to individually estimate (V_{conn}). External volumes were connected to the instrument with same fitting fitting in order to keep constant the V_{conn}. The pressure values were collected through differential pressure transducers, maintaining the complementary section in dynamic vacuum conditions, with a successfully approach introduced by [106], which increases accuracy of pressure data. Calibrated values of V_a were reported in tab. 2.3 with relative errors. Value of V_b (expansion volumes of reference side) can be derived by definition of $\beta = V_a / V_b$. Uncertainty on

Volume	V_a $[cm^3]$	χ_{V_a} $[cm^3]$	$\chi_{\%}$	β [1]	χ_β [1]
SUPER	47.06	0.08	0.23	0.962	0.002
SMALL	86.29	0.14	0.15	0.982	0.003
MID	196.40	0.34	0.28	0.991	0.003
BIG	1043.5	1.8	0.21	0.997	0.002

Table 2.3: Estimation of V_a volume and β in IDA from *"basic calibration"*.

values (χ) in table 2.3 took in consideration: errors propagations of uncertainty of any single parameters in eq. 2.13 (as error on estimation of external volumes, uncertainty

on temperature and on pressure data) and the statistical deviation of the data population value. In last case, it assumed a normal distribution of the casually distributed value. The deviation from the mean value of the normal data population of 2σ (95% of data) was assumed as value's uncertainty.

Example of Working calibration

While basic calibration is performed at every structural changing of instrument, it is necessary to calibrate λ_a and λ_b after every sample loading or different working temperature.
In order to perform a null test measurement, a typical working calibration was conducted as example of the followed procedure. The basic rule for this operation is that: instrument must maintain the same temperature condition both during calibration and characterization operation. Firstly, a degassing procedure is followed in order to remove possible gas contaminants that can affect calibration measurements. Contemporaneously, it is a good practice to run the self-tuning of PID algorithm at the working conditions, in order to stabilize as more as possible the thermal condition of the chambers. IDA software can set self-tuning from GUI.
Working Calibration involved with a series of gas expansion, between the expansion volumes of IDA and the respective chambers. Value of λ_a and λ_b were derived by eq. 2.14. Final data pressure after every expansion step was collected when system approached thermal equilibrium. In this example, working calibration performed with working temperature at 633 K, isothermal temperature at 297.5 K with a calibration pressure of 3 Bar.
Calibrated values was reported in tab. 2.4. The estimation of λ-terms completes the

Side	Volume	λ[1]	χ_λ[1]
Sample	Super	2.0038	0.0002
	Small	1.5475	0.0008
	Middle	1.2404	0.0005
	Big	1.04537	0.00009
Reference	Super	2.0529	0.0002
	Small	1.562	0.001
	Middle	1.2439	0.0008
	Big	1.0459	0.0001

Table 2.4: Estimation of λ parameter both for sample and reference side of IDA. ϵ_λ are obtained substituting eq.2.14 in eq.2.18.

calibration of IDA for a specific temperature.

Hydrogen Null test

Hydrogen null test was performed on IDA without loading sample in order to preliminary verify mathematical model and experimental set up. Null measurement run, using respectively the two extreme volume size equipped in IDA: the smallest one (called *super*) and the biggest one (called *big*). The reason of the using of these volumes was because they reflected the ultimate strengths and weak points correlated to the size of expansion volume in a volumetric instrument.
Super volume allow to exploit the maximum moles resolution in a gas sorption characterization, unfortunately its investigation range is limited to the differential pressure span. Otherwise, *Big* volume can study a wide spectrum of mass sample, with a considerable gas storage capacity, regrettably its moles resolution is low. Obviously, also the measurement's accuracy is correlated to the volume size, in similar way of moles resolution. Characterizing gas was hydrogen, in pursuance to simulate a real measurement and evaluate calibrated parameters, previously estimated. Null test run at high working temperature (633 K) and in the typical investigated range of pressure of metal hydride materials (0-1 MPa). The scope of these test was to validate the theoretical approach on differential apparatus and the assumption made.

Super volume First null measurements performed on the "*SUPER*" volume (47.06 cm^3) included a null measurement of PCT study at 633 k and in a range of pressure of 0.1-0.9 MPa. Elaborated data were compared with the reciprocal Sievert. From fig. 2.15 is possible to quickly note as differential layout reported a lower uncertainty on the measurement respect to the classic volumetric layout. So the cumulative errors grew less, allowing a sufficient accuracy for the whole step of PCT plot.
About calibration, it was possible to confirm a relative good agreement of data with a null test. However, there was a drift in the points, which tended to distance from 0-value. This trend can be cause by a relative tiny systematic error of calibrated data, which was cumulate in every step. Nevertheless, error bars of points included 0-value, physically confirming the goodness of previous calibration operation for the *super* volumes.
Second null measurements performed on the "*SUPER*" volume (47.06cm^3) included the simulation of kinetics measurement at 633 K and 0.5 MPa. Fig.2.16 compared a null kinetics test performed at 0.5 MPa. also in this case, differential layout showed a higher accuracy respect to classic "Sievert" apparatus. Also in these case, the two scale's plot differed for an order of magnitude.
However, during the null measurement there was an accidentally and involuntary strong variation of temperature in the isothermal section of instrument. It is interesting to note as temperature fluctuation impacted on the both layouts. In the differential design, there was a slight oscillation in the asymptotic trend of values. Instead, classic

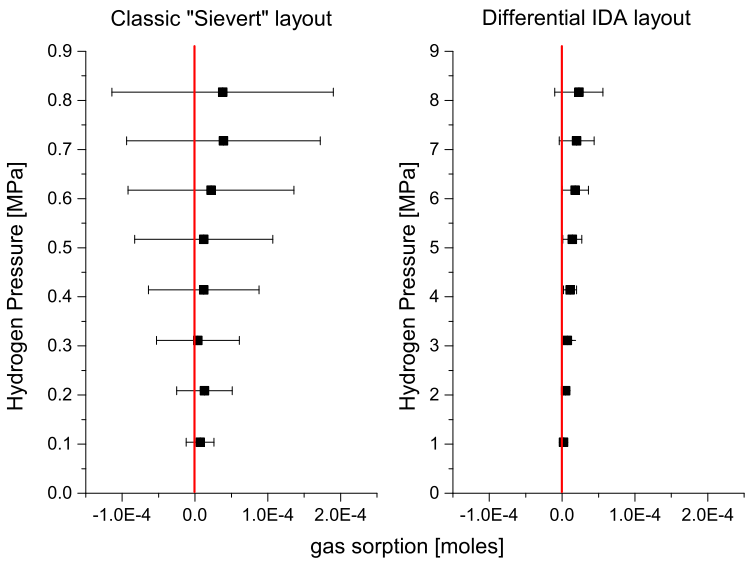

Figure 2.15: PCT Null measurement performed with *Super* volume. The two plot compares the null test obtained with differential layout (*right*) and the complementary "Sievert" layout. The red line is only a "eye guide" for the 0-value. The sorption mole scale is the same for the two plots.

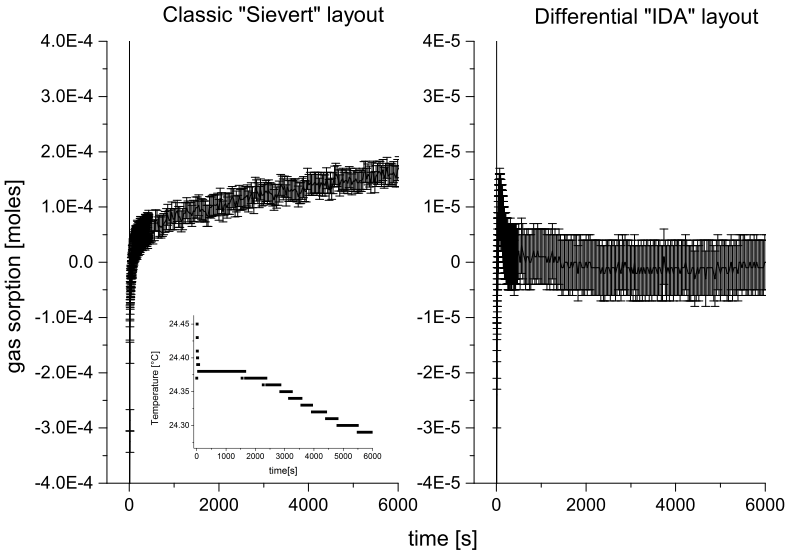

Figure 2.16: Kinetic null test performed with *Super* volume. The two plot compares the null test obtained with differential layout (*right*) and the complementary "Sievert" layout. The inserted plot is the isothermal temperature of apparatus. The sorption mole scale for IDA layout an order of magnitude less than "Sievert" one.

design showed a important raising tendency in the measurement of gas sorption moles. It was possible to attribute this affection at the temperature oscillation. Indeed, a suddenly cooling of the isothermal box (inset plot in fig. 2.16) could causes a fake gas uptake (for the no compensated pressure reductions), as it was reported in the plot.
In the first seconds of both null test, there was a strong oscillation of gas sorbed value. This was due to the absence of sample in the chamber which guarantees the contact between thermocouple sensor and chamber's wall. For this reason, a quick gas expansion, in particular from vacuum conditions, caused a significant variation of the local temperature of chambers, sufficient to impact on the equivalent volume estimation and giving a fake sorption signals. This phenomenon was temporary, and tended to decrease in few minutes when the PID control of heating system compensated the temperature bias. In the real characterization operation, the presence of a sample in chamber, drastically minimized this issue.

BIG volume As for the previous case, a null measurements performed with "*BIG*" volume (1043.5 cm^3) of IDA was reported. Working temperature was 633 k and the investigated range of pressure was 0.1-0.7 MPa. Elaborated data was compared with the equivalent Sievert system. Also with *Big* size volume, differential layout showed a

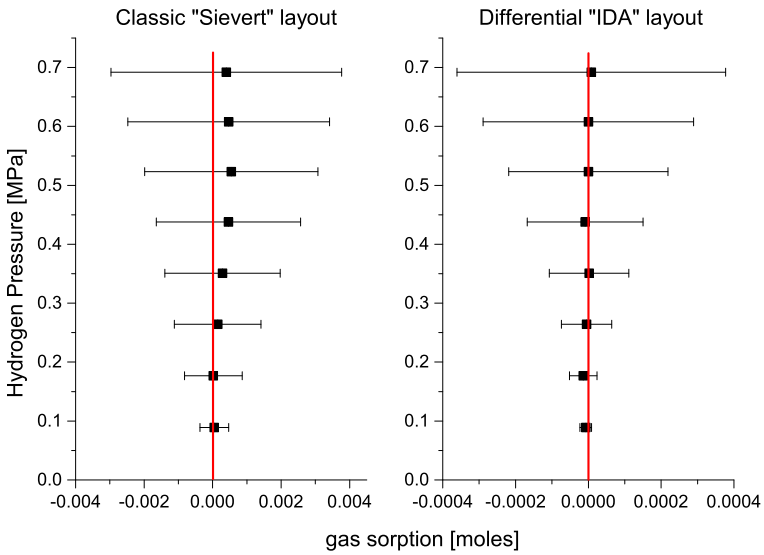

Figure 2.17: PCT null test performed with *Big* volume. The two plot compares the null test obtained with differential layout (*right*) and the complementary "Sievert" layout.

intrinsically higher accuracy than the classic layout. Null measurement confirmed also in this case, the goodness of calibrated parameter and the preliminary corrobora-

tion of mathematical model of gas sorption estimation.
Basing on the uncertainty results of fig. 2.15 and 2.17, it was clear how a well PCT analysis must is compensated by the possibility to characterize bigger sample, and to perform kinetics characterization in static mode, with only small variation of pressure (kinetics driving force).
Second null measurements on *Big* volume considered a kinetics measurements at 633 K and 0.5 MPa.
A temperature's fluctuation in the isothermal zone occurred during null measure-

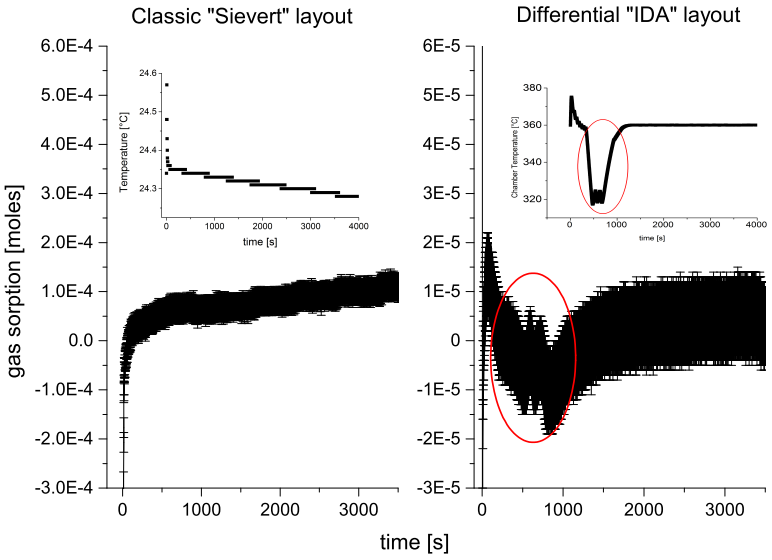

Figure 2.18: Kinetic null test performed with *Big* volume. The two plot compares the null test obtained with differential layout (*right*) and the complementary "Sievert" layout. The inserted plots are: the isothermal temperature of apparatus (left inset plot) and chambers temperature (right inset plot). The sorption mole scale for IDA layout is an order of magnitude less than "Sievert" one.

ments (temperature left plot in fig. 2.18). It was interesting to note as even for *big* expansion volume, differential measurement was not affected by this variation. At the contrary a classic analysis showed a continuous drift of the final data, caused by cooling gas in expansion volume.
Unfortunately, a wrong command in PID heating of reference chamber, changed for few minutes the temperature set-point (visualized in temperature right plot in fig. 2.18). It caused an artificial variation in the gas sorption quantity calculated by differential layout (red cycle in the cited figure). When such interference disappeared, estimated values approached again the real one. Last test preliminary confirmed mathematical models developed for IDA and goodness of working and basic calibration procedures.

2.3.4 Validation 1: Palladium sample

First round of measurements with reference sample were performed with high purity palladium (>99.999%) purchased by Sigma-Aldrich (CAS 7440-05-3) using a sample of (215,3 ± 0.1) mg. Palladium has been chosen because its sorption reaction occurs at conditions not so far from standard one (300-400 k, in a range of pressure between 0-0.5 MPa). Consequently, it is suitable for initial testing IDA at mild conditions.
Procedure for the analysis included: a overnight (12h) degassing operation at high temperature, a working calibration step at the proper temperature and next, the characterization operations.
Absorption and desorption PCT characterizations were performed at respectively 400 K, 343 K, 323 K and 303 K in a range of pressure between 0 and 0,45 MPa. Extrapolated data by PCT study were compared with data in literature to check the reliability of instrument and goodness of theoretical model applied for the sorbed moles estimation. Two single PCT plot for absorption and desorption curve obtained by IDA and "classic" layout were compared to analyse the differences in performance between the two volumetric approach.
Kinetics absorptions and desorption measures were collected to complete the study on Pd sample. Also in this case, kinetics results of IDA were compared with the identical study performed with a identical classic "Sievert" layout to observe the difference in terms of measure's accuracy. Finally an uncertainty analysis was performed on the results of PCTs and kinetics study of Pd sample, to individuate sources of errors.
About activation step, for the palladium sample, three full cycles of activation procedure were sufficient to ensure its maximum gas sorption capacity and kinetics and continue on subsequent study. For sake of clarity, uncertainties, resumed in the next plots as error bars, were calculated by uncertainty propagation theory (Taylor expansion) , reported in eq. 2.18. Middle volume of IDA was used. Such volume size allowed to estimate with sufficiently accuracy the hydrogen sorption reaction, but at the same time, it conserved almost constant driving force of process.

PCT study

Thermodynamics study of Palladium sample included a series of PCT characterization, with the aims to extrapolate pressure equilibrium values of absorption and desorption phenomenon at fixed temperature.
Fig. 2.19 reported absorption PCT analysis. δP approach was applied for the thermodynamic study. Unfortunately, Pd sample has a very low equilibrium pressure at room temperature (in a range between $10^{-3} - 10^{-2}$ MPa), and the management of gas loading step in expansion volume of IDA was not so efficient for those low pressure studies. So, minimum amount of hydrogen added at any step of PCT characterization was not sufficiently small to resolve plateau region of Pd sample with a suitable number of

points. Fig. 2.19 reported the Pressure-Composition study on Pd sample for a series

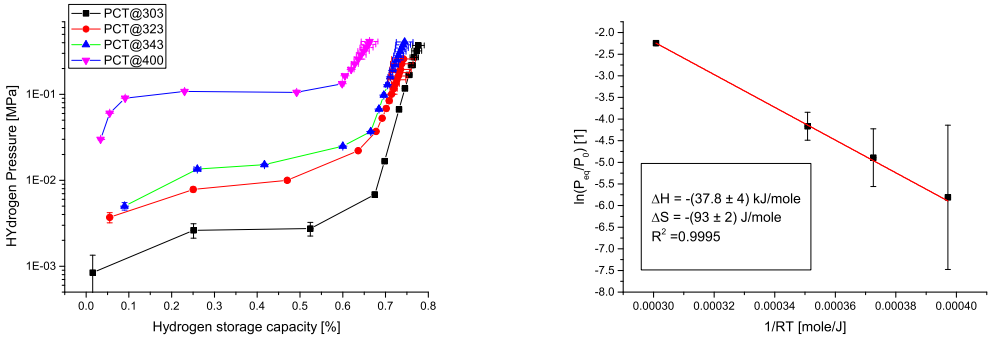

(a) PCT H_2 ABS measures at 303-323-343-400 K.

(b) Van't Hoff plot

Figure 2.19: Pressure Composition Temperature study for Pd sample. X-axis value of (a) are the weight percentage of hydrogen in the palladium.

of absorption isothermal measures (303, 323, 343 and 400 K). Equilibrium pressure, or plateau equilibrium in PCT plot, were extrapolated by the middle point of any curve reported in fig. 2.19(a). Equilibrium pressure data were plotted in well known Van't Hoff plot ($ln(P_{eq})$ *vs* $1/T$), in fig. 2.19(b) to estimate thermodynamic parameter of absorption reaction from Van't Hoff relation (eq. (2.19)). Linear regression model was applied on van't hoff plot, fig. 2.19(b), to evaluate linear coefficient and intercept of Van't Hoff plots. Linear model fitted very well the experimental data ($R^2 > 0.999$). For the palladium sample, considering R costant of gas (8.314 J/(K mol)), absorption enthalpy were evaluated equals to 37.8 ± 4 kJ/mole. With the same approach, absorption entropy of reaction was evaluated equals to 93 ± 2 J/(K moles). Uncertainty on thermodynamics data were evaluated by the linear regression model by ™Origin 9 Pro software.

Second PCT study was performed to study thermodynamics proprieties of hydrogen desorption process in Pd sample, fig. 2.20. Respect to absorption study, the control on gas loading in the chamber was more efficient for low pressure values. Indeed, in this case the step's pressure for any points of fig. 2.20(a) were only limited by expansion volume's size and initial pressure, which could be at minimum the limit vacuum pressure of vacuum pump.

As for previous case, equilibrium pressure of desorption plot in fig. 2.20(a), were elaborated and plotted as Van't Hoff plot, fig. 2.20(b). Equilibrium pressure values were estimated from the middle point in the plateau region of PCT measures. Linear regression model was applied with a robust result ($R^2 > 0.999$). Enthalpy for desorption process were estimated equals to 39.9 ± 1.2 kJ/mole, while entropy of desorption reaction was 93 ± 4 (J/(K moles)).

In tab 2.5, previous results were summarized with reference value found in literature

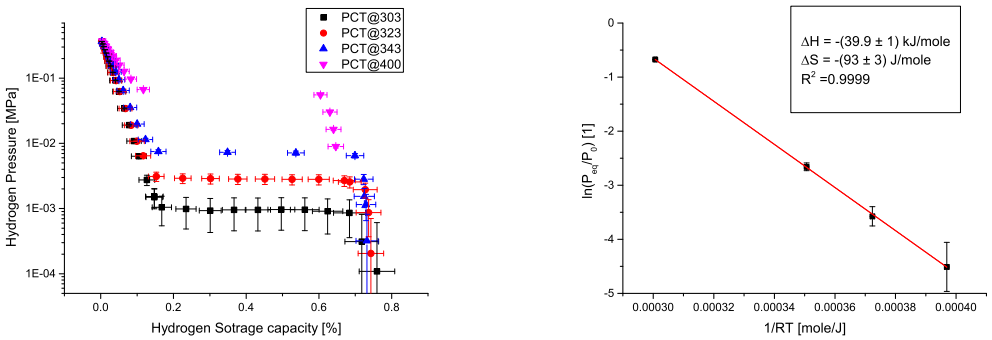

(a) PCT H_2 DESmeasures at 303-323-343-400 K.

(b) Van't Hoff plot

Figure 2.20: Pressure Composition Temperature study for Pd sample. X-axis value of (a) are the weight percentage of hydrogen in the palladium.

for thermodynamics proprieties of Pd-Pd-H_2 system.

Ref.	Reaction	ΔH [kJ/moles]	ΔS [kJ/(K moles)]
This work	ABS	37.8 ± 1.2	93 ± 2
	DES	39.9 ± 4	93 ± 3
[99]	ABS	37.4 ± 0.3	92.5 ± 0.5
	DES	39.0 ± 0.58	92.5 ± 1.3
[100]	ABS	39.5 ± 0.2	-
	DES	41.6± 0.4	91.2 ± 0.8
[108]	ABS	38.1 ± 0.3	93.2
	DES	38.56± 0.3	93.2

Table 2.5: Resuming table of thermodynamics data for Pd material, reported in literature

Value of reaction enthalpy and entropy energy obtained by IDA are within the range of reference data in literature, confirming the goodness and reliability of instrument and its measurements. The sample uncertainty on the final value of ΔH and ΔS are probably due to consistent uncertainty in pressure data acquisition. Indeed for low temperature study, Pd-H system showed an equilibrium pressure extremely low (approximately 1000 Pa at 303 K)[92], too close to the instrumental errors of pressure transducer (± 5000 Pa) and so, increasing relative uncertainty on the pressure data. Finally, a comparison between differential and classic "Sievert" layout was reported. Two PCT, absorption and desorption on Pd sample were compared in fig. 2.21. Comparison plot regarded two Pressure-Composition Isotherm study performed at 400 K

on Pd sample. In absorption PCT investigation reported, in fig. 2.21(a), uncertainty

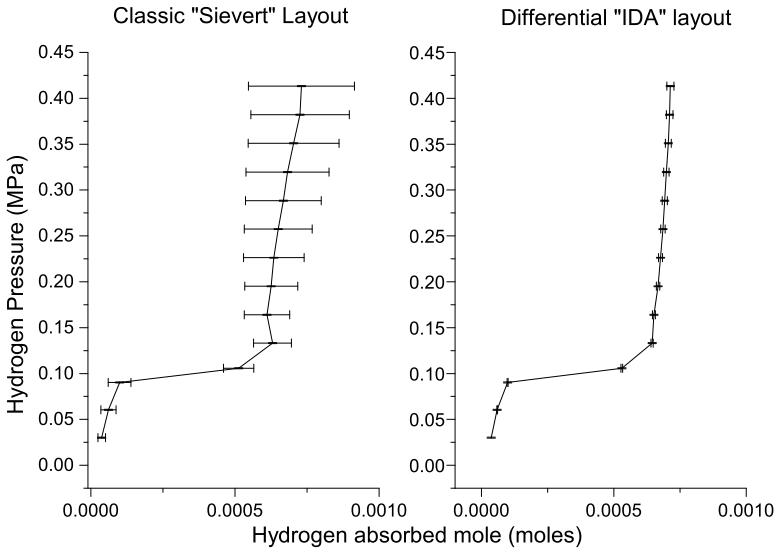

(a) Absorption PCT study.

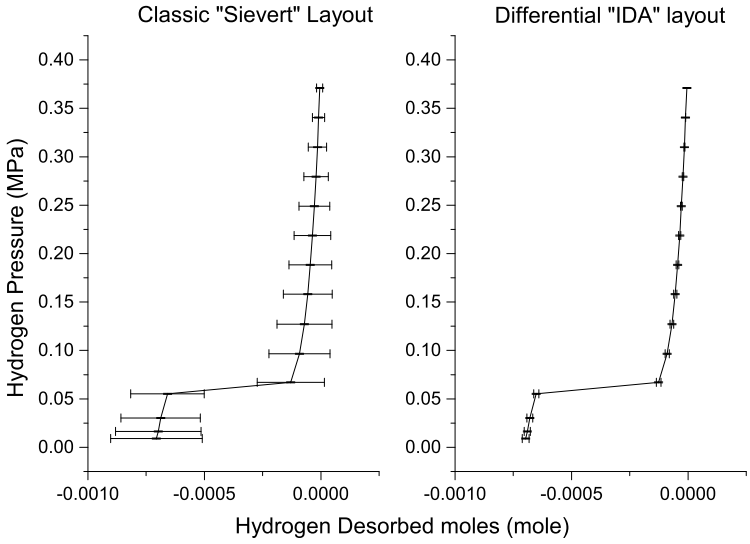

(b) Desorption PCT study.

Figure 2.21: Comparison of results and uncertainties obtained by a classic "Sievert" layout and the differential "IDA" layout.

on absorbed moles achieved a value of $1.9 \cdot 10^{-4}$ moles at the end of thermodynamic study performed with classical layout, while differential one approached value of $1.3 \cdot 10^{-5}$ for the identical number of steps. In similar way, final moles uncertainties for desorption study (fig. 2.21(b)) achieved $1.9 \cdot 10^{-4}$ and $2.4 \cdot 10^{-5}$ moles for the classic

and differential layout instrument, respectively. IDA showed a considerable higher accuracy respect to the equivalent "Sievert layout" (10-fold decreasing) for the range of investigated conditions. Such superior performance was particularly evident in PCT measurements where cumulative errors strongly impact on the final uncertainty experimental data. Uncertainties, hereby reported were estimated by error propagation theory, through eq. 2.18.

Kinetics study

Kinetics study on Palladium sample were directly compared with data collected by an equivalent "Sievert" instrument to empathize the main difference between the two type of approaches. Four absorption measures were conducted on Pd sample at 303 K

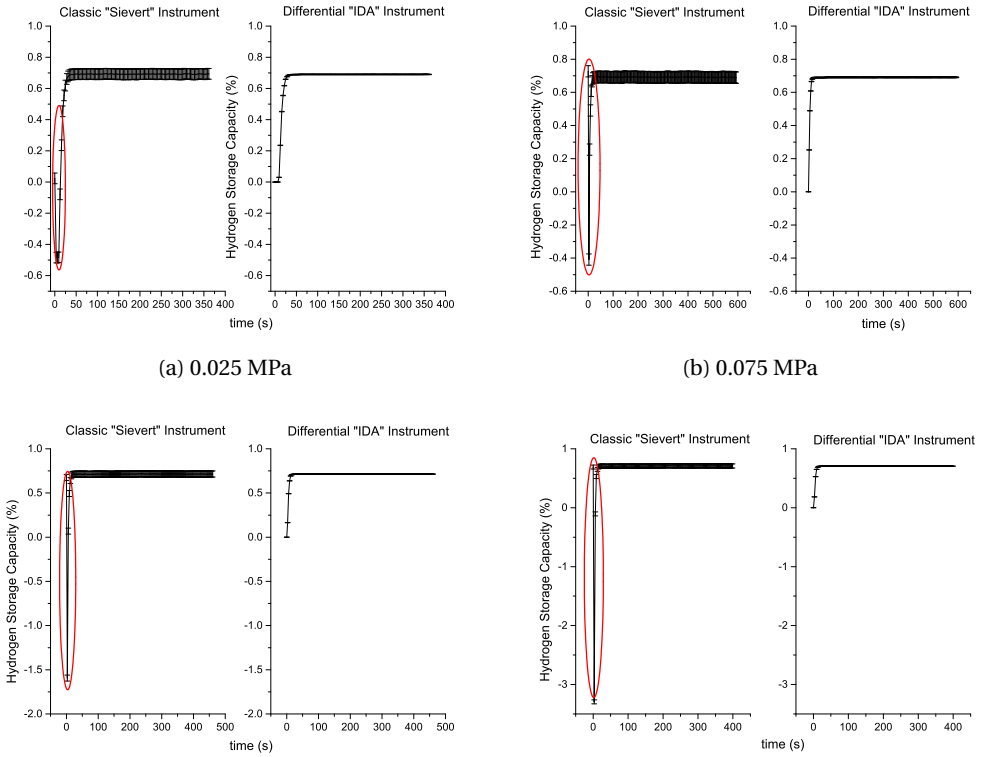

(a) 0.025 MPa

(b) 0.075 MPa

(c) 0.1 MPa

(d) 0.2 MPa

Figure 2.22: Absorption kinetics profile of Pd sample at 303 K and different of hydrogen gas pressures. The different scale allows to underline the behaviour in the first moments of hydrogen sorption reaction with Palladium for the two type of instrumenting layouts.

and at different hydrogen pressure 0.025, 0.075, 0.1 and 0.2 MPa. Kinetics plot were reported with proper mole's uncertainties in fig. 2.22. Classical layout estimates a total H_2 absorption equals to $8.0 \cdot 10^{-4}$ mole, with an uncertainty of $\pm 7 \cdot 10^{-5}$ moles. In term

of gravimetric capacity, it achieved (0.74 ± 0.08)%, at 0.2 MPa and 303 K. At the same experimental conditions, differential layout estimated absorption hydrogen about $7.58 \cdot 10^{-4}$ mole with a uncertainty of $(1 \cdot 10^{-5})$ mole. The correspondent gravimetric capacity was (0.701 ± 0.009)%. The little discrepancies on the result can be attributed to the higher accuracy of differential data respect to absolute ones. Gravimetric hydrogen capacity of Pd sample is agree with literature data [92].
Also here, the superior performance of differential layout can be appreciated with lower uncertainties correlated to the amount of hydrogen amount absorbed on Pd sample, corresponding averagely to 10-fold respect to classical design. Moreover, differential layout allowed to identify the first points of kinetics measures occurred in the first seconds of study, that otherwise should be hidden by suddenly gas expansion into the sample chamber . Differential layout intrinsically reduces and partially neglects such behaviour, because it simultaneously compares the phenomenon between two identically volume at the same conditions. On the contrary, such non linear effect was visible in classic layout (red circle in fig. 2.22) and can hide initial stage of H_2 sorption reaction, especially for HSM with elevate sorption kinetics as Palladium.

Uncertainty analysis

In this section an analysis on measurements uncertainty for the characterization of Pd sample was reported. An identical characterization performed on Differential and "Sievert" layout was analysed, the aims was to estimate the single contributions from any error's sources on final measure's uncertainty. The kinetics measurements at the maximum pressure span and at 303 K was considered (fig, 2.22 (*d*)). However error's analysis focuses on the last point of measures, when hydrogen-Palladium system was considered at equilibrium state. For classic *Sievert* layout, results of analysis was shown in tab. 2.6 derived by eq. 2.7, while differential layout analysis was reported in tab. 2.7 and derived by 2.9, through uncertainty propagations theory (eq. 2.18). ™EES software was used to elaborate contribution of any error's source to the final uncertainty. Values and their uncertainties in these tables were obtained by proper working calibration procedure with Pd sample already loaded in the sample chamber, however with a previous version of layout of volumetric instrument (different expansion volume sizes respect to the actual layout reported in tab.2.3). Uncertainties on measured variables were reported in 2.2.
The most contribution on final moles uncertainty in classic *Sievert* layout was principally due to errors of pressure data (compressively more than 99 %) derived by specific used absolute pressure transducers. Errors on temperature, compressibility factors not had appreciable impacts on final uncertainty (less than 0.4%). Surprisingly, volume calibrations had a small impact on sorption mole error (around 0.3%). Analyse of error's contributions underlined as for considered *Sievert* layout, pressure

Table 2.6: Errors estimation and contribution on total sorbed moles uncertainty (for Classical *Sievert* apparatus). Null value for error's contribution means an impact inferior than 0.01%.

Symbol	Unit	Value	Error	Contribution [%]
P_0^i	Bar	2.440	0.005	20.11
P_{eq}^i	Bar	1.925	0.005	29.48
P_{cl}^{i-1}	Bar	0	0.005	20.17
P_{eq}^{i-1}	Bar	0	0.005	29.55
V_a	dm^3	0.1829	0.0003	0.03
T_{iso}	K	303	0.5	0.03
λ_a	1	1.2105	0.0003	0.27
Z_0^i	1	1.001	0.0002	0.19
Z_{eq}^i	1	1.001	0.0002	0.17
Z_{cl}^{i-1}	1	1	0.0002	0
Z_{eq}^{i-1}	1	1	0.0002	0
H_2 Sorption	mole	$8.0 \cdot 10^{-4}$	$7 \cdot 10^{-5}$	100
m_{Pd}	g	0.2153	0.0001	0
H_2 grav. capacity	% w/w	0.74	0.08	100

transducers performance were the main bottlenecks for increasing the accuracy of sorption measures. At the contrary, uncertainty's analysis on differential layout, tab. 2.7, showed different results.

In differential approach, contributions on final moles uncertainty is mainly distributed among more sources of errors. Temperature uncertainty concurs at little more respect to previous case (around 1.8%) while, pressure contributions have to be distinguished between the differential terms (from differential pressure transducer) and absolute terms (from absolute pressure transducers). Differential pressure uncertainties accounts for the 6 % on the final uncertainty, while absolute pressure errors for less than 0.25 %, overall. At the contrary of *Sievert* layout, compressibility factor's errors impact more strongly on the final sorbed mole's errors, accounted for more than 50 %, preceded only by volume's uncertainties derived by calibration procedure, which contribute for the almost 40 % of total uncertainty. The reason for the difference error's contributions between the two considered layouts was caused by the better performance of differential one. The higher accuracy achieved by IDA (in particular with the enhancement of pressure data accuracy), highlight the contribution from the other error's sources, which impact more strongly on the finale mole's uncertainty than classic instrument.

This lead to state that: assuming a classic *Sievert* layout and a differential one with the same volumes size and equipped transducers, bottlenecks of *Sievert* instrument's performance are the accuracy limit of its hardware (in this case absolute pressure

Table 2.7: Errors estimation and contribution on total sorbed moles uncertainty for *IDA*.Null value for error's contribution means an impact inferior than 0.01%.

Symbol	Unit	Value	Error	Contribution [%]
ΔP_0^i	mBar	-0.3	0.15	1.25
ΔP_{eq}^i	mBar	-83.5	0.15	1.84
ΔP_{cl}^{i-1}	mBar	-0.1	0.15	1.26
ΔP_{eq}^{i-1}	mBar	-0.1	0.15	1.84
$P_{0,b}^i$	Bar	2.440	0.005	0.12
$P_{eq,b}^i$	Bar	2.007	0.005	0.06
$P_{cl,b}^{i-1}$	Bar	0	0.005	0.12
$P_{eq,b}^{i-1}$	Bar	0	0.005	0.06
V_a	dm^3	0.1829	0.0003	1.83
T_{iso}	K	303	0.5	1.86
λ_a	1	1.2105	0.0003	18.56
λ_b	1	1.2155	0.0003	19.82
$Z_{0,a}^i$	1	1.001	0.0002	13.22
$Z_{eq,a}^i$	1	1.001	0.0002	12.06
$Z_{cl,a}^{i-1}$	1	1	0.0002	0
$Z_{eq,a}^{i-1}$	1	1	0.0002	0
$Z_{0,b}^i$	1	1.001	0.0002	12.91
$Z_{eq,b}^i$	1	1.001	0.0002	12.97
$Z_{cl,b}^{i-1}$	1	1	0.0002	0
$Z_{eq,b}^{i-1}$	1	1	0.0002	0
H_2 Sorption	mole	$7.58 \cdot 10^{-4}$	$1 \cdot 10^{-5}$	99.85
m_{Pd}	g	0.2153	0.0001	0.15
H_2 grav. capacity	% w/w	0.701	0.009	100

transducers). At the contrary, IDA fully exploited any installed transducers, and its performance's bottleneck involves volume's calibration procedure and gas coefficient's estimation (in particular for compressibility factors estimation). Moreover, in order to increase the accuracy of measurements should be appropriate to equipped new more accurate absolute pressure transducer on the classic instrumental layout, or to use a smaller expansion volume to reduce the relative errors on pressure data at the same experimental condition. Nevertheless, kinetics study should be performed as more as possible constant pressure in order to investigate kinetics processes at constant driving force. Using small volumes in the volumetric apparatus, means to have a considerable pressure gap during the kinetics investigation, which it moves away from the driving force requirements.
Those results exclusively regard characterizations occurs at relative mild condition of

temperature and pressure. With Palladium characterization, this work has demonstrated as IDA and more in general differential layout can be a powerful instrument to characterize with high accuracy HSM at mild conditions. The next section of this experimental discussion want to extend the application of IDA also for the study of HSM at high temperature, confirming its performance also for this range of investigations.

2.3.5 Validation 2: Magnesium sample

IDA performance was tested on Mg material at higher temperature (> 573K). A small amount (49.0 ± 0.1 mg) of Magnesium powder, purchased by Sigma Aldrich with purity of 99% has been selected as testing material. Analogously to previous Pd study, Magnesium powder characterization includes: an overnight degassing step (12h), a proper volume calibration at working conditions and finally thermodynamics (PCT) and kinetics measurements.For magnesium sample, fully activation of material takes 10 cycle of complete absortpion and desorption processes at 633 K and 1 MPa and 0.03 MPa, respectively.
PCT absorption and desorption studies were performed at 553-593-613-633 K in a reange of pressure between 0.01 to 1 MPa. Enthalpies and Entropies of sorption reactions were extrapolated by Van't Hoff relation (previously introduced eq.2.19), and compare with reference data in literature data. Two single PCT plot for absorption and desorption curve obtained by IDA and "classic" layout are compared to analyse the differences in performance between the two volumetric approach in high temperature study.
At the same way, kinetics absorptions and desorption measures were collected to complete the study on Mg sample and to compare the performances of differential and classic layout instrument. Kinetics absorption and desorption measurements are performed at temperature of 633K and pressure of 1MPa and .
Finally an uncertainty analysis concluded this section about Mg characterization, analogously to the previous one. Based on high theoretical H_2 storage capacity of magnesium, BIG volume of IDA was used for next magnesium characterization. Such volume size allowed to estimate with sufficiently accuracy the hydrogen sorption reaction, but at the same time, it conserved almost constant driving force of process and so the pressure.

PCT study

Similar to the Pd study, the PCT analysis on Mg sample aimed to estimated enthalpy and entropy of hydrogen absorption and desorption reaction through *Van't Hoff* analysis. First study, fig. 2.23, presented the absorption PCT analysis conducted on magnesium sample at different working temperature, while fig. 2.23(b) collected the

equilibrium pressure data in the well known *Van't Hoff* plot.
Enthalpy and entropy values were estimated by linear regression model. Enthalpy

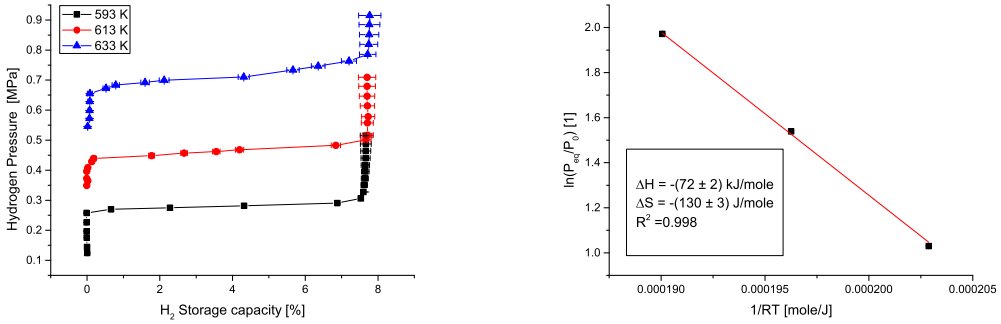

(a) PCT H_2 ABS measures at 593-613-633 K.

(b) Van't Hoff plot

Figure 2.23: Pressure Composition Temperature study for Mg sample. X-axis value of (a) are the weight percentage of hydrogen in the palladium.

and Enthalpy for H_2 absorption reaction were evaluated (-72 ± 2) kJ/mole and (-130 ± 3) J/(mole·K), respectively, with a well fit ($R^2 = 0.998$).
Absorption PCT study was conducted also at 553 K, however they were not reported here in fig. 2.23 because pressure data were collected at not pseudo-equilibrium state, due to not sufficiently equilibrium time.
Second study, fig. 2.24 presented the hydrogen desorption PCT analysis conducted on magnesium sample. Fig. 2.24(a) showed the single PCT measures performed at

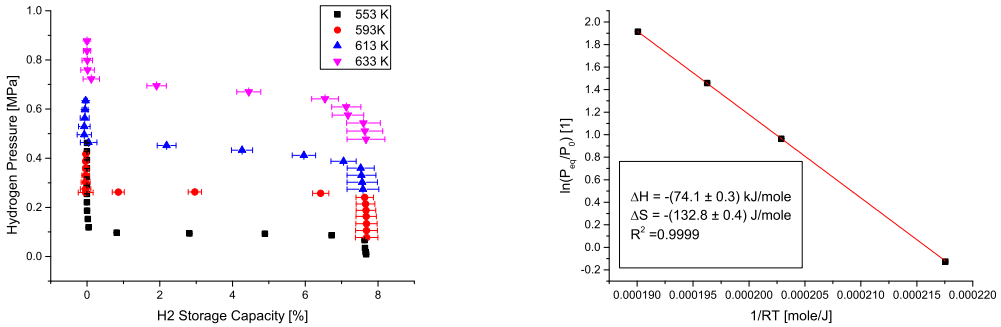

(a) PCT H_2 DES measures at 553-593-613-633 K.

(b) Van't Hoff plot

Figure 2.24: Pressure Composition Temperature study for Mg sample. X-axis value of (a) are the weight percentage of hydrogen in the palladium.

553-593-613-633 K, while fig. 2.24(b) reported *Van't Hoff* plot for hydrogen desorption

study. In this case, enthalpy and entropy of desorption reaction were estimated as (-74.1 ± 0.3) kJ/mole and (-132.8 ± 0.4) J/(mole·K), respectively. Also in this case, linear fitting was in agreement with empirical data (($R^2 = 0.9999$)). Thermodynamic data on Mg sample, hereby reported, are in agreement with literature data [101, 102, 102–105, 109].

Kinetics study

Kinetics measure about hydrogen absorption and desorption reaction on Magnesium sample were conducted at 633 K. The measures were collected both with differential approach and classic one (considering exclusively the sample branch of IDA as a *Sievert* instrument) in order to compare their performances. Absorption study was performed at 633 K and 1 MPa of hydrogen pressure. H_2 absorption monotonically increased during whole sorption process, achieving the saturation at approximately 5-6 h (comparable with similar kinetics study on pure Mg [110]), with an extremely low rate compared to Palladium study (2.22). From fig. 2.25(a), it was possible to directly compare performance of kinetics measures obtained from differential and classic layout. IDA showed a superior accuracy on moles detection ($1.7 \cdot 10^{-4}$ moles) respect to an equivalent *Sievert* instrument ($5 \cdot 10^{-4}$ moles) evaluated at the end of measure. Errors analysis, reported in next section of document, investigated the reason for such elevate uncertainty respect to Palladium study. Hydrogen capacity obtained by differential instrument is in line with literature data of (7.6 ± 0.8)%.[101–105] On the contrary, *Sievert* layout showed a relevant drift in the hydrogen storage capacity detected, approaching an unrealistic value of (10.6 ± 2.1)%. Such discrepancy can be attributed to the variation of temperature in the isothermal box caused by unexpected variation of external laboratory temperature, fig. 2.25(b). Classic volumetric measures are based on the elaboration of absolute pressure data, collected exclusively in the sample limb of instrument. For this reason, it is extremely sensible to temperature's variation of the volume and it'd require a proper temperature correction to compensate it. Moreover, the effect of temperature variation is further amplified by volume's size. On the contrary, differential layout is based on differential pressure data, measured between the two volumetric limbs of instrument and affected by the same temperature deviation. For this reason, differential pressure data are more temperature-independent respect to absolute one, as shown in fig. 2.25(c), so not requiring any additional temperature correction or calibration.
Second kinetics study regarded desorption reaction performed at 633 K and 0.045 MPa. The full saturation of H_2 desorption, fig. (a), was achieved approximately at 0.7 h (2500 s) equal to gravimetric capacity of 7.6 ± 0.8) %, calculated by IDA, while (7.8 ± 2.1) % for *Sievert* layout. Also here, storage capacity is in agreement with literature data.[104, 105] Desorption study occurred at stronger isothermal conditions, fig. 2.26(b) respect to absorption one. So, absolute pressure data were not shifted by

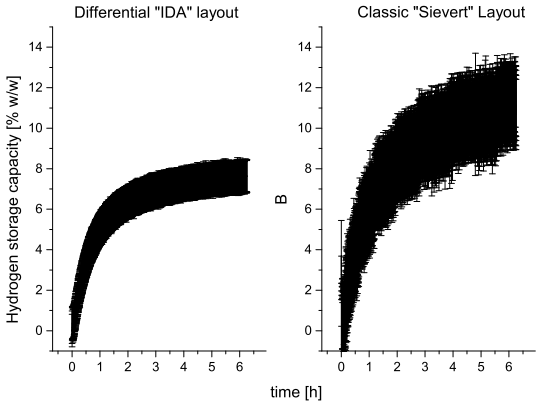

(a) Hydrogen storage capacity measures.

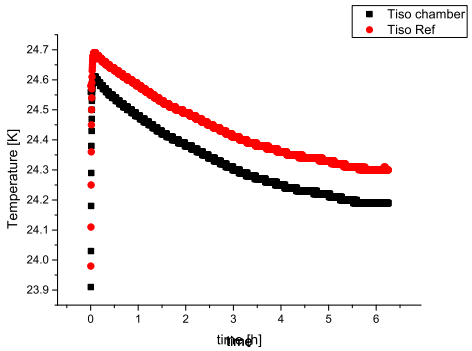

(b) Temperature.

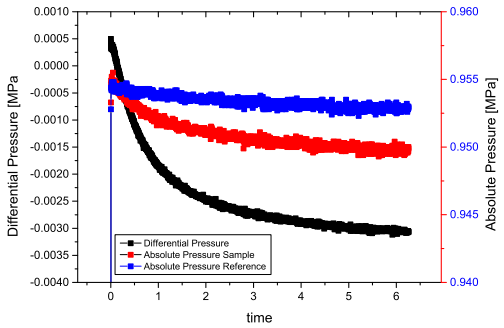

(c) Absolute and differential pressure.

Figure 2.25: H_2 absorption kinetics measure at 633 K. Comparison of results and uncertainties obtained by a classic "Sievert" layout and the differential "IDA" layout. The last two plots show the absolute pressure and temperature trend in the expansion volumes used in hereby reported characterization.

temperature effect, and *Sievert* instrument measured a value of storage capacity in agreement with value obtained by differential approach. However, sorption uncertainty obtained by classic layout was 3-fold respect to differential one, with a minor gain in terms of accuracy respect to mild characterization conducted with previous Pd sample.

Uncertainty analysis

In this section an analysis on measurements uncertainty for the high temperature characterization on magnesium sample was reported. An identical characterization performed on Differential and "Sievert" layout is analysed, the aims is to estimate the single contributions from any error's sources on final measure's uncertainty. Un-

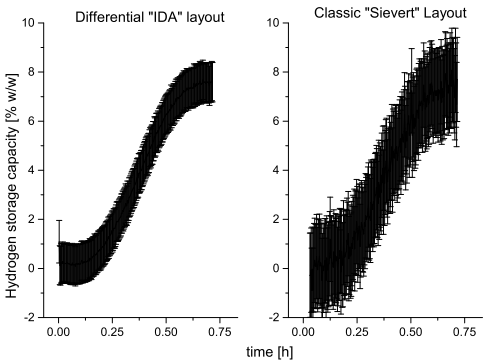

(a) Hydrogen storage capacity measures.

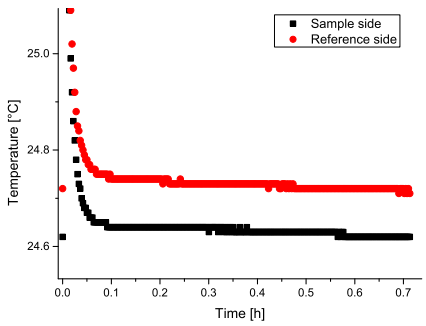

(b) Temperature.

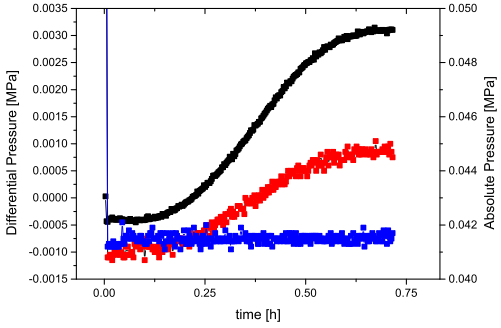

(c) Absolute and differential pressure data.

Figure 2.26: H_2 desorption kinetics measure at 633 K. Comparison of results and uncertainties obtained by a classic "Sievert" layout and the differential "IDA" layout. The last two plot report the absolute pressure (c) and temperature (b) in the expansion volumes used for the measures at isothermal condition.

certainty analysis was conducted on desorption kinetics analysis reported in fig. (a), which presented identical final uncertainty of complementary absorption study. Last point of measure was considered, when hydrogen-Magnesium system was considered at equilibrium state. For classic *Sievert* layout, results of analysis was shown in tab. 2.8 derived by eq. 2.7, while differential layout analysis was reported in tab. 2.9 and derived by eq. 2.9, through uncertainty propagations theory (eq. 2.18). Also here, ™EES software was used to elaborate contribution of any error's source to the final uncertainty. Values and their uncertainties in these tables were obtained by proper working calibration procedure with Mg sample already loaded in the sample chamber. Uncertainties on measured variables were reported in 2.2.

Classical layout estimated a total H_2 desorption equals to $1.9 \cdot 10^{-3}$ mole, with an uncertainty of $5.3 \cdot 10^{-4}$ moles. In term of gravimetric capacity, it achieves $(7.8 \pm 2.1)\%$, at 0.45 MPa and 303 K, in agreement with reference data. The most contribution

Table 2.8: Errors estimation and contribution on total sorbed moles uncertainty (for Classical *Sievert* apparatus). Null value for error's contribution means an impact inferior than 0.01%.

Symbol	Unit	Value	Error	Contribution [%]
P_0^i	Bar	0	0.005	22.28
P_{eq}^i	Bar	0.445	0.005	22.03
P_{cl}^{i-1}	Bar	9.505	0.005	24.33
P_{eq}^{i-1}	Bar	9.502	0.005	24.05
V_a	dm^3	1.041	0.00018	0
T_{iso}	K	298	0.5	0
λ_a	1	1.0443	$1 \cdot 10^{-4}$	0.7
Z_0^i	1	1	0.0002	0.01
Z_{eq}^i	1	1	0.0002	0
Z_{cl}^{i-1}	1	1.006	0.0002	3.15
Z_{eq}^{i-1}	1	1.006	0.0002	3.44
H_2 Sorption	mole	$1.9 \cdot 10^{-3}$	$5 \cdot 10^{-4}$	99.99
m_{Mg}	g	0.0490	0.0001	0.01
H_2 grav. capacity	% w/w	7.8	2.2	100

on final moles uncertainty in classic *Sievert* layout was principally due to errors of pressure data (more than 92 %) derived by specific used absolute pressure transducers ($\pm$ 0.005 Bar). Errors on temperature didn't impact on final uncertainty, however, compressibility factor terms had a strongly influence (more than 6.5 %). Volume calibrations had a small impact on sorption mole error (around 0.7%). Analyse of error's contributions underlined as even for high temperature measurements conducted by *Sievert* layout, pressure transducers performance were the main bottlenecks for increasing the accuracy of sorption measures. At the contrary, uncertainty's analysis on differential layout, tab. 2.9, showed different results as for the Palladium study.
Differential layout estimated a total H_2 desorption equals to $1.86 \cdot 10^{-3}$ mole, with an uncertainty of $2.1 \cdot 10^{-4}$ moles. In term of gravimetric capacity, it achieved (7.6 $\pm$ 0.8)%, at 0.45 MPa and 633 K, in agreement with reference data and with a better accuracy respect to *Sievert* apparatus (3-fold). As in previous case (Palladium), temperature and volume uncertainties gave bigger contribute (approximately 10 %) respect to classic layout, while errors on pressure data reach no more than 0.6 % (including both differential and pressure data uncertainties). Uncertainty on compressibility factor strongly affected final error of estimated sorbed mole (for a total of 90 %).

Respect to the previous Palladium study, magnesium investigation showed a considerable increment on uncertainty moles. The reason why this happens is due to

Table 2.9: Errors estimation and contribution on total sorbed moles uncertainty for *IDA*. Null value for error's contribution means an impact inferior than 0.01%.

Symbol	Unit	Value	Error	Contribution [%]
ΔP^{i}_{0}	mBar	-31.4	0.15	0.14
ΔP^{i}_{eq}	mBar	-31.4	0.15	0.15
ΔP^{i-1}_{cl}	mBar	1.0	0.15	0.13
ΔP^{i-1}_{eq}	mBar	31.0	0.15	0.15
$P^{i}_{0,b}$	Bar	0	0.005	0
$P^{i}_{eq,b}$	Bar	0.415	0.005	0
$P^{i-1}_{cl,b}$	Bar	9.536	0.005	0
$P^{i-1}_{eq,b}$	Bar	9.536	0.005	0
V_a	dm^3	1.041	0.0018	0.02
T_{iso}	K	298	0.5	0.02
λ_a	1	1.0443	0.0001	4.67
λ_b	1	1.0456	0.0001	4.98
$Z^{i}_{0,a}$	1	1	0.0002	0
$Z^{i}_{eq,a}$	1	1	0.0002	0.05
$Z^{i-1}_{cl,a}$	1	1.006	0.0002	21.35
$Z^{i-1}_{eq,a}$	1	1.006	0.0002	23.32
$Z^{i}_{0,b}$	1	1	0.0002	0
$Z^{i}_{eq,b}$	1	1	0.0002	0.05
$Z^{i-1}_{cl,b}$	1	1.006	0.0002	21.46
$Z^{i-1}_{eq,b}$	1	1.006	0.0002	23.47
H_2 Sorption	mole	$1.86 \cdot 10^{-3}$	$2.1 \cdot 10^{-4}$	99.97
m_{Pd}	g	0.0490	0.0001	0.03
H_2 grav. capacity	% w/w	7.6	0.8	100

the nature of error propagation estimation. The impact of any variable on final uncertainty depends also by the nature of mathematical formulation for total mass sorbed (eq. 2.7 and 2.9). Analysing the contribution derived by compressibility factor, correlated error's term depends by itself error of Z-factor's estimation, as well as the propagation factor, resumed in $\frac{\delta n}{\delta Z}$ of eq. 2.18. Last term is function of values of volume and pressure. This explained the discrepancy on uncertainty between Palladium and Magnesium investigation, where magnitude of hydrogen pressure and size of expansion volume were considerable bigger than Pd characterization. However it was important to highlight as kinetics measurement performed on magnesium sample involved in a small variation in driving force of desorption reaction. Indeed, pressure gap diverged for less than 0.003 MPa (fig. 2.26(c)) ensuring a reasonable constant driving force during desorption reaction, but a sufficient accuracy for the detection of

the amount of moles sorbed, at the same time.
Moreover, it is interesting to note how many works didn't consider uncertainty on compressibility factor [79, 80, 83]. If uncertainty of compressibility factor was considered neglected ,in this work final error on Mg sample (section 2.3.5) by IDA study approached 0.08 %, with the reduction of 90 % of total error.

2.4 Conclusion

The design and performance of a novel volumetric instrument for accurate hydrogen sorption measures was performed. A comparison between a classic Sievert layout and a differential instrument was made, resulting in the evaluation of uncertainty along the hydrogen sorption process. The differential design evidenced a higher accuracy with respect to a standard volumetric apparatus, under the same measure conditions. Moreover, differential design compensated nonlinear effects occurred during the initial step of gas expansions, making the study of the first step of sorption phenomena more detailed; that has a relevant importance for material provided of a high kinetic during the sorption process. Palladium and magnesium were utilized as benchmark materials, and the results are in good agreement with respect to a classic Sievert layout, considering an equivalent set up of the apparatus and neglecting the Z factor uncertainty. The IDA layout has been also performed at higher temperature using Mg as adsorbing material, confirming an equivalent reduction of error due to the experimental configuration. An higher accuracy of IDA was also demonstrated for cumulative errors typical of thermodynamics analysis and for tests at high temperature. We are convinced that IDA is able to analyze H2 sorption of small target material samples due to the higher accuracy of differential layout. Concluding, IDA has demonstrated the capacity to characterize very small mass sample or materials with low sorption capacity.

2.4.1 Future work

IDA includes the potentiality to perform BET measurements on specific area and porous distribution of sample. Next steps aim at realizing proper volume chambers to keep sample at 77 K, in a liquid nitrogen baths, and to test IDA for BET study, initially with reference materials. Secondly, investigation range of IDA will be expanded to study gas physisorption phenomena at high pressure conditions (10 MPa), in particular on graphene based material. At the moment, differential instrument is already equipped with high pressure transducer, however the requirements to approach reliable measurements at high pressure need additional effort, specifically to improve thermal management in whole apparatus (thermal insulation, pneumatic fan, etc.) and improve volume calibration procedures to minimize volume's uncertainty.

3 Mathematical modeling of kinetics in hydrogen storage materials

Abstract

The modeling of reaction kinetics are powerful tools to improve the description of reaction mechanism during absorption or desorption phenomena. The objectives is to direct research's activities towards a more performant hydrogen sorbing materials. In this chapter,several methods of mathematical modeling for HSM are investigated: 1. a micro scale model for the description of intimal sorption mechanism in the active material, 2. a macro scale model for the modeling of hydrogen storage tank based on active H_2 storage material and 3. a lumped model for preliminary analysis on optimized tank design.
A novel approach on micro scale kinetic models are introduced in order to improve the comprehension on hydrogen sorption phenomena on HSM Mg based material produced within EDEN project (European Union's Seventh Framework Programme FP7/2007-2013 for the Fuel Cells and Hydrogen Joint Technology Initiative) has been modelled and validated by experimental data in micro and macro scale model. Lumped approach has been preliminary validated against macro model results obtained by FEM. Finally, numerical simulation performed on validated macro modeling identifies an optimal tank's design used to built the storage system for EDEN project.

3.1 Introduction

The challenges of a novel society based on hydrogen and in particular the necessity to realize reliable and optimized hydrogen storage technologies requires considerable efforts from the research and engineering side. In this context, mathematical models and numerical simulations on sorption processes of HSM have received considerable attention over the past decades. The specific focus of mathematical modeling is to describe a real complex system in terms of relations. Once validated with real data, mathematical models are powerful tools to provide the behaviour of simulated system in different conditions or to study in-depth the processes inside a particular phenomenon.
Always more frequently, industry and applied researches requires robust and reliable tools to describe sorption proprieties of HSM. Although the topic is relatively new, journal papers with mathematical descriptions of HSM sorption phenomena rapidly growth in numbers in last decades [111–117]. In the same way, the industrial application of HSM had an increasing attention of scientific interest, in particular about the modeling and realization of performant hydrogen storage tank with different HSM[37, 118–123]
There are two main modelling approaches to hydrogen storage, with two specific objectives and targets. First, a kinetics sorption model at micro-scale level tries to represent the intimal sorption mechanism in hydrogen absorption or desorption process. This approach is clearly more directed towards the research side. A validated micro scale model can support the research in the topic, identifying the optimal direction where to develop an improved HSM. Micro scale model aims at an estimation of the uptake or release of hydrogen, through fitting experimental data with the optimal function.The micro model has two objectives: validate the mechanism of reaction; extrapolate the kinetics parameters for the sorption reaction. About microscopic modeling the description of H_2 sorption on HSM regards two mainly aspects of H_2 sorption reactions: thermodynamic and kinetics behaviour.
Thermodynamic models describes equilibrium state of HSM-hydrogen system, studying absorption/desorption capacities as well as pressure-temperature conditions for reversible reactions. Thermodynamic modelings approach the sorption problem in order to describe it with physically interpretable coefficients. More diffuse thermodynamic model are based on statistical description of the system, as the evaluation of partition function (in this case, hydrogen sorption process is treated as Gran or classic canonical ensemble)[124–126] or the estimation of chemical potential (μ)[35, 126–129]. More recently, more exhaustive thermodynamic model includes hydriding phase transition, with a in-depth physical explanation of the phenomena (in particular about hysteresis). In phase transition model, strain stress, generated by the decomposition or formations of hydride phase has a considerable roles in the equilibrium pressure of material.[130, 131] Scientific literature collect a large number of work focus on the

individuation of kinetics sorption mechanism and explanation of thermodynamic behaviour of HSM. Kinetics model will be depth in the next part of this thesis.
Secondly, the modeling supports the direct application of HSM, with the final scope to design and optimize high performers hydrogen storage tank based on HMS under engineering/industrial point of view. Here, micro scale models of HMS are applied in the development of a fully macro modeling of hydrogen storage tank, which have repeatedly appeals to numerical simulation for the develop of new more prominent layout, as well. The realization of a suitable metal hydride reactor for industrial and commercial hydrogen storage application, is very complex. Due to low thermal conductivity of hydride powder, kinetics performance of tank (regarding time of charging and discharging) is strongly affected by heat diffusion. [37, 118, 120, 121] Therefore, design and dimensioning of a hydrogen storage tank is an important development step in order to achieve and to exploit the best performance for any HSM. Mathematical modeling of tank design (macro model) includes the coupling of several physical behaviour in order to give reliable output solutions among: heat transfer, gas diffusion in porous media and the sorption kinetics model of hydrogen storage materials [37, 121, 132]. Although it is a modeling on a high level application, used HSM kinetics models are rigorous description of the hydrogen sorption processes. Numerical simulation performed by suitable software (i.e. COMSOL) can explain very well behaviour and performance of a hydrogen storage tank at different working condition, but it requires a well-knowledge of the sorption phenomena inside it (reaction, gas and thermal diffusion, et..) as well as a their correct and validated mathematical formulations. Last but not less important features, it is the time to perform the simulation, which depends by computing power and mesh's qualities. In this context, more rigorous models (as lumped one) can give approximated solutions for the hydrogen storage tank's development, if the real aims is to simply design a hydrogen storage tank or to have a quickly response about the goodness of the design developed.

3.1.1 Objective of chapter

Scope of this work is the developed and validation of a scientific approach for the study and modeling of a hydrogen storage application for a generic HSM, starting form the kinetic characterization of storage materials to the modeling of tank system. The main purpose is to realize a proper micro scale modeling for the explanation of hydrogen kinetics mechanism in a wide range of conditions of HSM, and next a proper macro scale model for the study and modeling for a hydrogen storage system. Micro scale modeling of sorption material has been applied as core for the realization of macro scale-model. Last objective is to present a lumped model developed by the previous ones. Such model allows to easily extrapolate modeling data for the optimization of hydrogen storage tank, knowing kinetics and thermodynamic proprieties of HSM and

its thermal and diffusive proprieties.
Next part of document is divided in three sections. The first one reports the development, application and validation of kinetics microscopic model on Mg based material, product within EDEN project. A set of mathematical expression for the description of sorption mechanism are derived. Validation include the extrapolation of kinetics parameters from characterization data obtained by IDA instrument. Estimated kinetics value are compared with literature data to confirm the goodness of micro model approaching. Micro scale model has been applied on a magnesium-graphite mixture produced by High energy ball milling in order to map kinetics sorption mechanism in a range of working temperature and pressure.
Second part of section includes the development and the dynamic validation of the macro modellinfor hydrogen storage tank based on the micro modeling of Mg material. After a brief introduction and the explanation of followed method, macro model has been validated by mean to numerical simulation performed by Comsol software. Results are compared against real prototype system to check the reliability of model.
Last part of section involves in the description of a new lumped model for the rapid estimation of main performance of a generic hydrogen storage layout. A complete description of theoretical model is reported, including theoretical assumptions and followed method for its validation.

3.2 Micro scale model

Kinetics modeling aims to describe the temporal behaviour of sorption phenomena in HSM, during hydriding or de-hydriding processes. It is a powerful approach for the in-depth understanding of kinetics sorption mechanism for HSM, and so for addressing the research activities to improve weakness aspect of investigated materials. Kinetics models express hydrogen uptake or release rate in terms of physical parameters (as constant rates, apparent activation energies, gas diffusion coefficient, et..) of investigated materials, under experimental conditions far from equilibrium. They can be applied to extrapolate useful kinetics parameters of a specific storage materials and to forecast kinetics behaviour in real system. The first objective of this section is the development and the validation of a successfully approach for the kinetic modeling of HSM. Modeling includes the description of hydrogen absorption and desorption phenomena in a specific range of temperature and pressure. The second objective is the application of developed kinetics model to Mg based material to characterize completely it and to extrapolate kinetics parameter useful for macro model implementation.

3.2.1 Methods

Kinetic models for HSM were developed starting from the state of art of solid state reaction modeling, which include the hydrogen sorption reaction of HSM [113, 117, 133, 134]. Based on definition of well known kinetics model, a complete set of mathematical tools corresponding to the different kinetics mechanism of gas sorption reaction are reported, enriched with the introduction of a new approach for the nucleation and growth models.

Set of model

The first scientific works on kinetics modeling for solid state kinetics reactions were developed in the first half of last century.[19–21, 135–139]. However, only in the last years, some reviews [113, 116, 134, 140] have contribute to present again the basics and the mathematical development of these kinetic models, adding some improvements, especially regarding HSM material and hydrogen sorption reactions.
In order to develop a proper kinetics model, it is basilar to figure and understand the mechanisms on the base of hydrogen sorption phenomena. The general approach assumes that gas absorption and desorption reactions on HSM occur as a series of consequent or parallel intermediate phenomena, each one described by its proper physical model. Generally, not all kinetic phenomena are taken in consideration in kinetics analysis but only those occur with considerable energetic barrier, which strongly impact on kinetic rate. Among there, the main ones are [111, 113, 141–143]:

- H_2 superficial physisorption.
- H_2 superficial dissociation and chemisorption on specific activated sites.
- H-atoms surface penetration.
- H-atoms bulk diffusion.
- phase transition.

Absorption and desorption processes don't follow identical of reversible series of step [113] as well as not the same ones, so it is a good practice to analyse them individually, discerning the limiting kinetic mechanism of each process. Further steps can be considered (as mass transport of H_2 gas from or to the material's surface) but they increase the complexity without guaranteeing the improved accuracy of the results. The main approach adopted in literature, assumes that kinetics sorption reaction are controlled by the slowest mechanism of the list, only some hybrid models admit contemporaneous contribution of multiple kinetics step [144, 145].

In homogeneous reactions, the aim of kinetics analysis is principally to extrapolate the rate constants of the involved physical phenomena. However, hydrogen sorption processes occur as a gas-solid reaction (heterogeneous kinetics). For these reason, kinetics modeling of HSM reaction keeps in consideration also the morphology of sorbing materials, which introduce a proper geometrical formulation of hydrogen absorption or desorption reactions. Starting from the kinetics models for solid state reactions, the generic time evolution for HSM reaction can be expressed by eq. 3.1:

$$\frac{d\theta}{dt} = kf(\theta), \qquad \int \frac{1}{f(\theta)} = g(\theta) = kt, \tag{3.1}$$

where k is the kinetics rate. θ is the reacted fraction rate of sorbing material, expressed as,

$$\theta = \frac{s_0 - s_t}{s_0 - s_f}, \tag{3.2}$$

where s can stand for weight, moles or volume of the reacted phase. 0-subscript indicates initial amount, f-subscript the final total amount, and t-subscript indicates the amount of reacted phase at time t. θ can vary from 0 to 1. g(θ) and f(θ) are the integral and differential mathematical functions of proper for the kinetics reaction model, respectively.
In the next paragraphs function models for HSM more widely applied are exposed.

Shrinking volume model, CV [113, 146–150] Shrinking models are very simple and intuitive for the description of sorption kinetics in HSM. It assumes that surface of HSM's particle are rapidly covered by the new phase (hydride or metal), with an extremely rapid process of nucleation and surface growth. Once covered by product phase, the interface between the two phase tends to penetrate homogeneously inside the particle. The reaction rate is controlled by interface speed towards the center of particle. The type of particle's geometry (spherical, cylindrical, et.) impacts on the mathematical representation of model.

Diffusive model,D [113, 149] In solid state reactions, diffusion phenomena play a relevant role, in particular at low temperature and for large powder's size. Diffusive models describe hydrogen absorption and desorption process as limited by diffusion, typically through the metal or hydride phase of HSM.
Diffusion is particularly relevant in solid state reaction, because molecules must permeate into the lattice where molecular motion is slowed and may depend on the presence of lattice defects.
Diffusive model are usually coupled with the geometrical shrinking approach, where

the decreasing interface velocity typically is given by diffusion. For this reason, in literature, a series of diffusive models exist, starting from the spherical shrinking model and including diffusive interface growth, density variations during sorption phenomena and pressure and temperature dependence of diffusivity coefficients.

Chemical order model, CH [134, 151] In chemical order models, kinetics rates of hydrogen sorption are function of the already formed reacted fraction elevated to a power representing the reaction order. It is possible to distinguish zero, first, second or higher order of reaction. Chemical order approaches find wide application in homogeneous reactions, nevertheless some authors consider them inappropriate for such application.[134]

Mathematical formulation for Shrinking, Diffusive and Chemical order models are exposed in the appendix 5.

Nucleation and growth model, NG [19–21, 140, 152] Nucleation and growth (NG) models are widely used for solid state reactions. They assume the combination of nucleation and growth processes as the basic mechanism of sorption reactions. Generally growth is assumed as to be isotropic (3D) and can occur with constant speed (interface controlled) or decreasing speed (diffusion controlled). On the other hand, the nucleation process can be considered under several aspects: as a instantaneous nucleation at the beginning of the reaction, as a constant rate of nuclei formation or as a auto-catalytic phenomenon (described by a power law). In order to take in consideration the overlapping of growth nuclei, it is necessary to introduce an impingement function which take in consideration the phenomena of ingestion and coalescence occurred on growth nuclei. These models, generally regarded as Johnson-Mehl-Avrami-Kolomogoov models (JMAK, who separately developed the basic mathematical relations), are expressed typically by:

$$\theta = 1 - exp[-(kt)^n], \tag{3.3}$$

where n-terms indicates the nucleation modes, dimensionality and rate-controlling step,. About the assumption on nucleation and growth process adopted by NG model, n-terms can assume values between 0.5 and 4, discriminating among different the growth mechanisms for hydrogen sorption (spheric 3D growth, plate 2D growth, 1 D growth or Diffusive growth and with instantaneous, constant or power law nucleation rate). k is the constant rate of nucleation and growth rates. It depends by the type of

initial physical assumption.

Mixed Empirical model, ME . In order to describe simultaneous multiple kinetics mechanism of sorption reaction, some authors proposed proper mathematical relations that represent all mechanism in a single general equation. Sestak and Berggren [145] introduced a combined form of different kinetic contributions:

$$\frac{d\theta}{dt} = k\theta^m(1-\theta)^n(-ln(1-\theta))^p, \tag{3.4}$$

where m, n p are constant and correspond to different kinetic mechanisms of the hydrogen sorption reaction. Shriniwasan [144] proposed similar approach, considering the reaction fraction as composed by different kinetics mechanism contributions, weighted by proper extrapolated coefficient. However, several works propose different mixed kinetics model to extrapolate kinetic parameters without rigorous assumptions on the reaction mechanism.[114]

These model give a remarkable description of hydrogen sorption process, but most of them introduce empirical parameters and approximations to force the model to fit results. On the other hand, kinetic sorption reactions can involves with different mechanisms. So, appling only one kinetic model can only partially fit the sorption curve's data. [144, 153].
JMAK model is diffusely applied in solid state reaction. Unfortunately, the same basic assumptions in NG theory doesn't allow to consider variation in n-index during sorption process, which is considered constant during whole process. Indeed, almost the totality of scientific literature extrapolate n coefficient of JMAK equation through a linear fitting of the so called Avrami plot ($ln(-ln(1-\theta))$ vs $ln(time)$), collecting an average or effective value of n_{eff} for the whole time range of sorption phenomena. Here, a kinetic model based on well-known JMAK equation has been developed to explain time variation of n-coefficient in classic Avrami model. Unfortunately, such model doesn't explain the behaviour of hydrogen sorption reaction for all range of temperature because the limited kinetics mechanism can be different from nucleation and growth approach. For this reason, other model integrates the lack of information (CV, contracting volume, D, diffusive, CH, pseudo chemical reaction order).

3.2.2 Limited Nucleation and growth model

In this section, we will derive a modified JMAK model, which involves in a different approach to represent growth rate of nuclei to the final scope to interpret the variation of n-terms (JMAK coefficient) during the time (eq. (3.3)).
Considering the reaction of H2 sorption in a HSM, we assume its phase transition as the process of nucleation and growth of a new phase domain in the parent one. In this approach, the formation of product phase can be assumed as function of several parameters as: the initial number of nuclei/seeds in the solid, the nucleation rate, the growth rate and the isotropy of this process. In particular, impingement has a relevant role in the develop of NG model. Generally speaking, if the NG model takes in consideration only nucleation and growth rate, any formed nucleus can overlap with the neighbours not tending to a limiting value, and thus having no physical meaning. For this reason impingement process is included in NG model to include the limited volume domain where particles can grow. Liu et Al [116] expose different approaches for impingement process, basically divided in two main way. Firstly, considering an hard impingement, which only includes the physical overlap of growing particle. It is the more suited approach for general applications on solid state reaction. Secondly, a soft impingement conditions is taken in consideration, assuming the overlap of diffusion fields surrounding the growing particles. Last approach is more complicate and find application only in some particular case.
About hard impingement, its theoretical formulation depends by some factors as: distributions of nucleus and isotropy of nucleus' growth. In case of random nuclei distributions on the parent domain and isotropic growth rate, the formation of new phase, after that time dt scan be written as [19–21, 113]:

$$\mathrm{d}V = (\frac{V_{tot} - V(t)}{V_{tot}})\mathrm{d}V_{ex} \tag{3.5}$$

If the time is increasing by $\mathrm{d}t$, $\mathrm{d}V$ represents the effective transformed volume while $\mathrm{d}V_{ex}$ is the extended volume rate. V_{tot} is the total available volume of crystal, V_t is the reacted fraction volume formed at time t. $\mathrm{d}V_{ex}$ represents the incrementing volume of product phase in parent one, that do not account for the overlap of growing particles. The physical meaning of eq. 3.5 considers that only a part of extended volume rate contributes to the increment of real volume weight over transfer term (1-V/$V_{[}tot$). Integrating eq. 3.5, mathematical formulation for reacted fraction is [140]:

$$\theta = 1 - exp(-\frac{V_{ex}(t)}{V_{tot}}) \tag{3.6}$$

where θ is the reacted volume fraction from eq. 3.2.
In NG model, the term $V_{ex}(t)$ in eq. 3.5 is the growth of new phase in the time t, excluding any impingement or overlapping phenomena between growth nuclei. It

is exclusively function of nucleation and growth rate and so, represent the core of NG model. The general formulation for the extended volume is defined as the sum of any nuclei's volume's at the time t. Assuming that nucleation and growth rate are independent, it is possible to formulate following mathematical relation for $V_{ex}(t)$:

$$V_{ex}(t) = \int_0^t \dot{N}(\tau) V(t-\tau) \tag{3.7}$$

Eq. 3.7 describes the extended volume on the base of previous assumptions. If the nucleation rate is $\dot{N}(\tau)$, the number of nuclei formed at time τ in the period dτ is $\dot{N}(\tau)d\tau$, consequently if the volume of any formed nuclei grows from τ to t as $V(t-\tau)$, the overall volume at the time t is expressed as the convolution $\dot{N}(\tau)\otimes$V(t-τ).
NG approach gives the possibility to apply different types of nucleation rate to fit the most suited description for hydrogen sorption phenomena (both absorption and desorption). On the other side, mathematical formulations for the estimation of volume growth rate of nuclei are mainly limited to a few case in literature (constant or diffusive rate)[19–21, 113, 140].

Various models on nucleation rate are reported in literature. [113, 116, 134, 140, 154]
Instantaneous nucleation is known also as Site saturation model. It assumes that the number of nuclei in the sample material remains constant during the overall transformation. In this case, $\dot{N}(\tau)$ takes the form of a delta function centred at time 0, eq.3.8

$$\dot{N}(\tau) = N_0 \delta(t-0). \tag{3.8}$$

Such model considers all possible nucleation sites active at the beginning of sorption reaction. If nucleation sites are very early saturated during the reaction, it could lead to an apparently instantaneous nucleation.
Continuous nucleation rate included several type of nucleation rate. In this case, $\dot{N}(\tau)$ is assumed as time dependent by eq. 3.9

$$\dot{N}(\tau) = \alpha I^{\alpha} t^{\alpha-1}, \tag{3.9}$$

where α is the nucleation coefficient, an empiric parameter which approaches non linear nucleation behaviour as the auto catalyst phenomenon and I represent the nucelation constant rate.
For α equals to 1, linear continuous nucleation is obtained [140],otherwise, $\alpha > 1$ indicates nucleation rate described by power law relations [134].
Avrami nucleation considers a finite number of sub-critical size available (N_0) in all sample domain.[19, 20, 134] Nuclei are formed by such sub-critical seeds at a specific

rate (λ). Avrami nucleation theory keeps also in consideration the reduction of parent phase volume, which is not more involved in the generation of new nuclei (phantom nuclei). The mathematical relation for Avrami nucleation model is described as follows:

$$\dot{N}(\tau) = \lambda N_0 exp(-\lambda t). \tag{3.10}$$

Avrami's approach includes a decreasing nucleation rate, which tends to an asymptotic maximum value (N_0).

Mixed nucelation models describe intermediate situation between the previous approach. Generally, they include the coupling of instantaneous and continuous nucleation, (eq. 3.8 for continuous nucleation rate and alternatively with Avrami approach 3.9). The mixed model composed by continuous and Avrami nucleation is not exposed because without physical meaning. [116],

$$\dot{N}(\tau) = N_0 \delta(\tau - 0) + \alpha k^{\alpha} t^{\alpha - 1} \tag{3.11}$$

or the Avrami model (3.9) with the presence of initial nuclei at t=0 (3.8),

$$\dot{N}(\tau) = N_0 \delta(\tau - 0) + \lambda N_0 exp(-\lambda \tau) \tag{3.12}$$

Previously cited models completes the description of the possibly approach to mathematically treat nucleation phenomenon. On the other hand, volume growth model considers V(t-τ)-term of eq. 3.7 as a linear or parabolic contribution. The main accepted mathematical formulation for volume growth is reported in eq.3.13,

$$V(t) = \left(\int_o^t G \mathrm{d}\tau \right)^{d/m}, \tag{3.13}$$

where G is the growth rate of nuclei forward a certain direction, while d and m are empirical parameters that take in consideration the dimensionality (d) and type of growth (m) respectively. Dimensionality of growth represents the shape of nucleus expansion: spherical 3D occurs with d=3, so plate 2D (d=2) or rod 1D (d=1), while m indicate if the growth is controlled by the formation of new interface (m=1) or controlled by diffusion (m=1/2). The diffusive approach is derived by definition of *characteristic diffusion length* ($\sqrt{4Dt}$, where D is the diffusion coefficient of hydrogen in the material) which represent the average hydrogen penetration in the material when the main transport process is diffusion. Combining the hard impingement assumption with the different type of nucleation rate and the growth rate reported in eq. 3.13, it is possible to obtain the main formulation of JMAK equation [113], reported in eq, 3.3.

This work wants to introduce a new approach to treat growth formulation of NG theory, including some limiting constrain on specific growth directions. Initial considerations are:

- nucleation phenomenon occurs exclusively on the surface [105, 115, 155, 156].
- the nucleation's site are the core of any growth grains of hydride in the magnesium surface.[115]
- any nucleus isotropically grows like an ellipsoids in 3D domains.[115, 156]

The concept at the base of such model is that some growth directions of grains are limited by some boundary conditions (for instance a finite superficial area), and the growth rate long such directions can decrease to zero before the culmination of sorption reaction. Assuming nucleus growth as a ellipsoid (*el*), the volume of any growth nucleus (V_{el}) can be estimated by eq. 3.14

$$V_{el} = \frac{4}{3}\pi(x \cdot y \cdot z) \tag{3.14}$$

where x, y, z are the semi-principal axes of ellipsoid nucleus. Assuming a superficial nucleation, we can define $\hat{x}$ as coincident with the radial direction of particles, while $\hat{y}$ and $\hat{z}$ are two perpendicular direction tangent to the particle surface. Introducing a growth rate $(\dot{x}(t), \dot{y}(t), \dot{z}(t))$, is it possible to express the volume growth of every nucleus from 3.14 as:

$$\begin{aligned} V_{el}(t) &= \int_0^t \dot{V}_{el}\mathrm{d}\tau \\ &= \int_0^t \frac{4}{3}\pi\Big[yz\dot{x}(\tau) + xz\dot{y}(\tau) + xy\dot{z}(\tau)\Big]\mathrm{d}\tau \\ &= \int_0^t \frac{4}{3}\pi\Big[\dot{x}(\tau)\Big(\int_0^\tau \dot{y}(\mu)\mathrm{d}\mu\Big)\Big(\int_0^\tau z(\mu)\mathrm{d}\mu\Big) + \\ &\qquad \dot{y}(\tau)\Big(\int_0^\tau \dot{x}(\mu)\mathrm{d}\mu\Big)\Big(\int_0^\tau \dot{z}(\mu)\mathrm{d}\mu\Big) + \\ &\qquad \dot{z}(\tau)\Big(\int_0^\tau \dot{z}(\mu)\mathrm{d}\mu\Big)\Big(\int_0^\tau \dot{y}(\mu)\,\mathrm{d}\mu)\Big)\Big]\mathrm{d}\tau \end{aligned} \tag{3.15}$$

where μ and τ are used as temporal variable for the integration. Eq. 3.15 allows to include also limited kinetics growth of nucleus, inserting a proper and well justified mathematical relations for $\dot{x}$, $\dot{y}$ and $\dot{z}$. Growth rates in eq.3.15 are considered identical for all three Cartesian direction ($\dot{x} = \dot{y} = \dot{z}$), in order to justify the assumption of random isotropic impingement relation (eq.3.5), previously accepted.
We consider that during sorption phenomena, nuclei formation only occurs on the surface of materials/particles. It is reasonable then to consider a spatial constraint in

the $\hat{y}$ and $\hat{z}$ growth, given that the particle surface is finite. The constraint must take in consideration the surface overlapping of any growth nucleus.
We assume that real increments on y (dy) and z (dz) of the product phase are affected by overlapping with neighbourhood grains. Assuming a random distribution of nuclei and isotropic impingement, we can write,

$$dy = (1 - \frac{y}{y_0})\mathrm{d}y_{ex} \qquad dz = (1 - \frac{z}{z_0})\mathrm{d}z_{ex} \tag{3.16}$$

where $\mathrm{d}y_{ex}$ and $\mathrm{d}z_{ex}$ are the incremental growth along y and z superficial direction of nucleus, without considering the overlap of nuclei on the surface. y_{max} and z_{max} are the maximum possible nucleus size along y and z direction. Assuming that excess growth occurs at the same constant velocity ($\mathrm{d}y_{ex} = k_y \mathrm{d}t$, $\mathrm{d}z_{ex} = k_z \mathrm{d}t$), k_y and k_z respectively, eq. (3.16) can be integrated in time to give:

$$y = y_0(1 - exp(-\frac{k_y}{y_{max}}t)) \qquad z = z_0(1 - exp(-\frac{k_z}{z_{max}}t)) \tag{3.17}$$

so the effective growth long y and z direction are:

$$\dot{y} = \frac{dy}{dt} = k_y exp(-\frac{k}{y_{max}}t) \qquad \dot{z} = \frac{dz}{dt} = k_z exp(-\frac{k_z}{z_{max}}t) \tag{3.18}$$

Now applying the assumption of isotropic growth, $k_y = k_z$, and random nucleation in spherical shape particles ($y_{max} = z_{max}$) we can rewrite the volume growth of ellipsoidal nucleus from eq. (3.15) as,

$$V(t)_{el} = \frac{4\pi}{3}\int_0^t \Big[\dot{x}\Big(\int_0^\tau \dot{y}\mathrm{d}\mu\Big)^2 + 2\dot{y}\int_0^\tau \dot{x}\mathrm{d}\mu \int_0^\tau \dot{y}\mathrm{d}\mu\Big] dt \tag{3.19}$$

Finally, taking in consideration the expansion surface velocity that includes the overlapping of growth nucleus, expressed by 3.18, and applying isotropic growth assumption on radial direction ($\dot{x} = k$), we can recombine eq. 3.19 to obtain estimation of excess growth volume at time t:

$$V(t)_{el} = \frac{4\pi}{3} y_{max}^2 kt\big[1 - exp(-\frac{k}{y_{max}}t)\big]^2) \tag{3.20}$$

Eq. 3.20 is the volume term, V(t), of eq. (3.7). This approach can be applied also on nucleus growth controlled by diffusion. In this case, $\dot{x}$, $\dot{y}$ and $\dot{z}$ growth rate are equals to $\sqrt{\frac{D}{t}}$ [140], where D is the diffusivity coefficient of hydrogen in the material.
Finally, it is possible to built a proper kinetics model introducing a suitable nucleation in the convolution equation eq. (3.7). Estimated V_{ex} term is inserted in eq. (3.6) to estimate the reacted fraction during sorption reaction.

The kinetics models hereby developed assumed a limitation growth only along superficial direction ($\dot{z}$ and $\dot{z}$). Assuming a spatial constraint along radial direction ($\hat{x}$), which is effectively spatial limited by the radius of HSM particle, radial growth of nuclei can be expressed analogously to $\dot{y}$ and $\dot{y}$ as:

$$\dot{x} = \frac{dx}{dt} = k_x exp(-\frac{k_x}{R_0} t), \tag{3.21}$$

where R is the radius of particles. So, assuming a isotropic growth ($k_x = k_y = k_z = k$) total volumes of every particles can be expressed by:

$$V(t)_{el} = \frac{4\pi}{3} y_{max}^2 R_0 \Big(1 - exp(-\frac{k}{y_{max}})\Big)^2 \Big(1 - exp(-\frac{k}{R_0})\Big) \tag{3.22}$$

where nuclei formed on the surface of particles grow with constant rate k, penetrating into bulk until the maximum depth of R, radius of particle.
Adopting eq. 3.22 as growth rate relation in eq. 3.7, the resulting $V_{ex}(t)$ directly represents the produced phase's volume, because impingement relation is already implemented into the mathematical formulation of nucleus's growth.

The approach hereby exposed, can be applied to other type of kinetics because it introduce geometric constraints that don't affect the basic assumptions of NG model as causal distribution of nucleus and isotropic growth of nuclei. NG model expressions for different nucleation and growth relation are collected in tab. 3.2.2. Such relations form the model's set available for the study of HSM. They take in consideration instantaneous, continuous and Avrami nucleation rate with diffusion, linear or limited model of growth. In order to extend the investigation range of kinetics sorption mechanism for HSM, shrinking-geometrical (CV) and diffusive model (D) are integrated in the model's set.

Kinetics analysis

The study of HSM kinetics proprieties aims to identify the limited mechanism of sorption processes and estimate the proper kinetics parameters (typically, the apparent energy of activation of the reaction [157, 158] and the driving force contribution). These parameters are useful for the comparison of different materials and for material modeling in a macro scale model. This is achieved determining and comparing best-fit models. Kinetic analysis can be applied on measures performed by several types of characterization techniques, conducted by different heating approachies: isothermal [134], linear heating (though Kissingher approach [159, 160]), modulated temperature (similar to scanning calorimetric techniques [114, 161]) and sample-controlled (characterization performed at constant sorption rate, SCTA technique [114, 162]).

Table 3.1: Set of kinetics model based on NG approach with different assumption on the nucleation and growth rate. g is the geometry factor.

Nucleation		Growth		Model		Parameter		
Name	Eq.	Name	Eq	Name	Final Eq.	a	b	c
JMAK equation				PureJMAK	$1-e^{[-(at)^n}$	-[a]		
Instant.	$N_0\delta(\tau-0)$	Lin.	$gk^3(t-\tau)^3$	N_0G_{3L}	$1-e^{-\frac{a}{2}t^3}$	$\frac{N_0gk^3}{V_{tot}}$		
		Dif.	$(\sqrt{4D(t-\tau)})^3$	N_0G_{3D}	$1-e^{-\frac{a}{2}t^{3/2}}$	$\frac{N_0gD^{3/2}}{V_{tot}}$		
		Lin-Lim[c]	$gy_{max}^2kt\left[1-e^{-\frac{k}{ymax}t)}\right]^2$	N_0GL_{2c+1}	$1-e^{-\frac{a}{2}(1-e^{-bt})^2t}$	$\frac{N_0gky_{max}^2}{V_{tot}}$	$\frac{k}{y_{max}}$	
		Dif-Lim[c]	$gy_0^2\sqrt{Dt}\left[1-e^{-\frac{2\sqrt{Dt}}{ymax}})\right]^2$	N_0GD_{2c+1}	$1-e^{-a\sqrt{t}(1-e^{-b\sqrt{t}})^2}$	$\frac{N_0g\sqrt{D}y_{max}^2}{V_{tot}}$	$\frac{2\sqrt{D}}{y_{max}}$	
Instant.	$N_0\delta(\tau-0)$	Lin.[b]	$g\left[1-e^{-\frac{k}{y_0}t}\right]^2\left[1-e^{-\frac{k}{R_0}t}\right]$	N_0G_{2A+1Al}	$a\left[1-e^{-bt}\right]^2\left[1-e^{-nt}\right]$	$\frac{gN_0}{V_{tot}}$	$\frac{k}{y_{max}}$	$\frac{k}{R_0}$
		Diff.[b]	$gy_{max}^2R\left[1-e^{-\frac{2\sqrt{Dt}}{ymax}}\right]^2\left[1-e^{-\frac{2\sqrt{Dt}}{R_0}}\right]$	N_0G_{2A+1Ad}	$a(1-e^{-b\sqrt{t}})^2(1-e^{-b\sqrt{t}})$	$\frac{N_0gy_{max}^2R_0}{V_{tot}}$	$\frac{2\sqrt{D}}{y_{max}}$	$\frac{2\sqrt{D}}{R_0}$
Linear $\alpha=1$	n	Lin.	$gk^3(t-\tau)^3$	N_1G_{3L}	$1-e^{\frac{a}{4}t^4}$	$\frac{ngk^3}{4V_{tot}}$		
		Dif.	$(\sqrt{4D(t-\tau)})^3$	N_1G_{3D}	$1-e^{-\frac{a}{2}t^{5/2}}$	$\frac{2ngD^{3/2}}{5V_{tot}}$		
Power $\alpha>1$	$\alpha I^\alpha t^{\alpha-1}$	Lin.	$gk^3(t-\tau)^3$	$N_\alpha G_{3L}$	$1-e^{-\frac{6a}{\alpha^4+6\alpha^3+11\alpha^2+6\alpha}t^{\alpha+3}}$	$\frac{\alpha I^\alpha k^3g}{V_{tot}}$		
		Dif.	$(\sqrt{4D(t-\tau)})^3$	$N_\alpha G_{3D}$	$1-e^{-\frac{3a\sqrt{\pi}\Gamma(a)}{4\Gamma(\alpha+5/2)}t^{\alpha+3/2}}$	$\frac{\alpha I^\alpha D^{3/2}g}{V_{tot}}$		
Avrami	$N_0\lambda e^{-\lambda t}$	Linear	$gk^3(t-\tau)^3$	N_AG_{3L}	$1-e^{-a\frac{\lambda^3t^3-3\lambda^2t^2+6\lambda t+6e^{-\lambda t}-6}{\lambda^4}}$	$\frac{N_0\lambda gK^3}{V_{tot}}$		
		Dif.	$(\sqrt{4D(t-\tau)})^3$	N_AG_{3D}	$1-e^{-a\frac{(4e^{\lambda t}t^{3/2}(-\lambda)^{3/2}+6\sqrt{\pi}e^{\lambda t}\sqrt{-n}-3\sqrt{\pi}erf(\sqrt{-\lambda t}))e^{-\lambda t}}{4\lambda^{5/2}}}$	$\frac{N_0\lambda gD^{3/2}}{V_{tot}}$		

[a] a-parameter for classic JMAK eq. depend by the type of nucleation and growth rate assumption.
[b] Impingement on the growth rate
[c] Limited growth rate applied only for instantaneous nucleation.

Table 3.2: Description of geometrical (CV), diffusive (D) and chemical order model applied for the study of HSM.

Model	Name	Equation = kt
Contracting volume *"Shrinking"* [a]	CV-2D	$1-(1-\theta)^{1/2}$
	CV-3D	$1-(1-\theta)^{1/3}$
Diffusive model [b]	D-Jander	$(1-(1-\theta)^{1/3})^2$
	D-GB	$1-\frac{2\theta}{3}-(1-\theta)^{2/3}$
	D-Valesi[c]	$\frac{z-[1+(z-1)\theta]^{2/3}-(z-1)(1-\theta)^{2/3}}{z-1}$

[a] for cylindrical particles
[b] for spherical particles
[c] z is the density ratio between product and reagent phase.

However, the main difference is in the approach used to identify the proper best fit kinetic model representing the reaction mechanism.
For isothermal characterization, direct fitting methods or the Sharp & Jones approach (linearization of reaction fraction curves with proper mathematical model formulation [163, 164]) are commonly used. Otherwise, isoconversional methods [113, 165] and model-free approachies [166] were widely applied on not-isothermal characterizations but with some justified apprehensions.[167] In this document, direct fitting and linearization method are applied to perform kinetic analysis of the investigated HSM. The followed approach includes:

- the identification of the main kinetic mechanism of sorption through direct non linear fitting or linearization approach;
- the estimation of kinetic parameter from the best fitted kinetics model;
- the validation of extrapolated data with literature database.

The first goal is achieved comparing the experimental fit to the mathematical set of models reported in the previous section (tab. 3.2.2 and tab. 3.2). The validity of a model is evaluated by the residual sum and the adjusted R-square value.
As soon as the most suited kinetic mechanism is identified, the next step corresponding to extrapolation of parameter of the model: the apparent activation energy (E_a^{app}) and the estimation of the driving force contribution (D(P)). Their values are generally derived by the characteristic k-values of the model applied, which is correlated to the growth velocity of the produced phase and to the nucleation phenomenon, when non instantaneous nucleation is considered. [112, 113]. According to Chou and Xu [111], E_a^{app} is the sum of the activation energy and of the enthalpy of single kinetic processes occuring during sorption reactions, such as physisorption, chemisorption, diffusion,

etc. [111]. K-terms of kinetic models are generally expressed as [111, 115, 141, 168–170]:

$$k(r,P,T) = G(r)D(P)A(T) = G(r)\cdot D(P)\cdot k_0 e^{-\frac{E_a}{RT}} \tag{3.23}$$

where G(r) is related to the sample geometry, D(P) represents the driving force of sorption phenomenon. Arrhenius relation A(T) is assumed as temperature contribution. In scientific literature, driving force contributions assume different mathematical forms[168, 170, 171]. Chou and Xu [111] identified the main $D(P,P_{eq})$ functions:
The relation between driving force contributions (D(P)) and the limiting kinetics

Table 3.3: Driving force mathematical relation from literature data.

Mechanism	H_2Sorption		Ref.
	Absorption	Desorption	
linear relation	$P-P_{eq}$	$P_{eq}-P$	[169, 172, 173]
Parabolic relation	$\sqrt{P}-\sqrt{P_{eq}}$	$\sqrt{P_{eq}}-\sqrt{P}$	[169, 172–174]
Normalized 1	$\frac{P}{P_{eq}}-1$	$1-\frac{P}{P_{eq}}$	[171]
Normalized 2	$1-\sqrt{\frac{P_{eq}}{P}}$	$1-\sqrt{(\frac{P}{P_{eq}})}$	[169, 171, 175]
Chemical reaction	$ln(\frac{P}{P_{eq}})$	$ln(\frac{P_{eq}}{P})$	[37, 169, 170, 176]
Empirical	$(\frac{P}{P_eq}-1)^2$	-	[168]

mechanism is not fully understand. According to Chou et Al. [111], the linear relation (P-P_{eq}) for absorption or (P_{eq}-P) for desorption can represent both physisorption and chemisorption phenomena while the parabolic relation represents bulk reaction or diffusion processes. Generally speaking, the linear contribution is directly correlated to superficial processes, while the parabolic relation regards principally phenomena occuring in the bulk.[111]. On the other hand, Fernandez and Snchez [168] adopted an empirical driving force equation which shows a considerable improvement in absorption data fitting $(1-(P_{eq}/P)^2)$, but without any explanation for such a dependence. For the desorption case, we report a driving force relation based on a normalized pressure approach proposed by Ron [171]. Other works proposed different driving force relations on the base of specific kinetics mechanism, as H_2 superficial dissociation $(\frac{P-P_{eq}}{a+bP_{eq}})$ and superficial chemisorption $(\frac{P-P_{eq}}{\sqrt{T}})$[173]. Although some works correlate specific driving force relations with peculiar kinetics mechanisms (for instance, NG model are associated with $D(P,P_{eq}=ln(P/P_{eq})$ [177]), this is not commonly accepted. The estimation of the driving force relation (*D(P)*) and of the activation energy E_a involves in the study and the elaboration of a series of kinetic characterizations performed at different temperature and hydrogen pressure.
The proper driving force relation is identified by the best linear fit of $k(P,T)$, as a

function of $D(P,P_{eq})$[37, 168]. Validity of the fit is evaluated by R^2 value. P_{eq}, the equilibrium pressure of reaction is evaluated by proper PCT study of investigated material.
The temperature contribution of eq. 3.23, $k_0 e^{\frac{-E_a}{RT}}$ is analysed. The apparent activation energy (E_a) and Arrhenius cofactor (k_0) can be easily extrapolated by the slope of the driving force as a function of $1/RT$ in a classic Arrhenius plot, where T is the working temperature of sorption characterization, and R is the universal of gas constant

3.2.3 Results

The scope of this section was the validation of a proper kinetics model for the description of absorption and desorption process in a specific magnesium sample. The identification of limit mechanism and kinetics fitting parameters involved the acquiring of a considerable number of kinetics isotherm measurements, and the application of appropriate kinetics analysis on the empirical data. The resulting model, once validated, was applied as input for the macro scale model, subsequently exposed.

Material

Magnesium based material produced by MBN Nanomaterialia S.p.A., within EDEN project (European Union's Seventh Framework Programme (FP7/2007-2013) for the Fuel Cells and Hydrogen Joint Technology Initiative), was investigated. Material was produced by High Energy Ball Milling process (patented by MBN) with a particle size inferior to 500μg(crystal size by XRD Scherrer Formula <35±2 nm), with a contain of 7% of graphite. BET measurement showed a surface area equals to 0.25 m^2/g just produced while it raised at 21.9 m^2/g after activation. The maximum quantity of hydrogen storage was estimated as 7.1 ± 0.4 % w/w.

Experimental procedure

An aliquot of Mg-based material (50.9 ± 0.1 mg) was characterized. Several absorption and desorption kinetics measurement was performed at 573, 593, 613, 633, 643 K. At least 3 measures were collected in absorption and desorption process for any investigated temperature.
The procedure for the storage storage and the sample chamber's loading were conducted inside a glove box under Argon atmosphere (oxygen and moisture < 0.5 ppm). Sample was degassed for 12 h at 633 K and dynamic vacuum (directly connected to vacuum pump at 1-5 Pa), until the approaching of limit vacuum pump. Sample was activated, with a series of complete absorption and desorption process (7 cycle), for

the achievement of the best kinetics performance. Next, the kinetics characterizations were performed at isothermal conditions, in a range of temperature between 643 K to 573 K.
Kinetic investigations were performed with IDA instrument, previously described, exploiting the advantages of such techniques respect to standard classic volumetric instrument (*Sievert*). In order to maintain as much as possible a constant pressure during the sorption phenomena, a proper expansion volume was used, compared to the mass of investigated sample. The variation of pressure involved during the characterization was at the maximum of 50 mBar, introducing a negligible error on the reaction's driving force. All experimental data were smoothed, applying an adja-

Table 3.4: Experimental condition for **ABS**orption and **DES**orption measurements.

Temp. [K]	Pressure[MPa]		Temp. [K]	Pressure[MPa]	
	ABS	DES		ABS	DES
643	1.3	0.5	633	1.09	0.6
	1.18	0.3		0.96	0.4
	1.08	0.2		0.87	0.2
613	0.98	0.2		0.74	0.15
	0.88	0.149		-	-
	0.79	0.101	593	0.96	0.151
	0.69	0.032		0.86	0.101
573	0.97	0.103		0.74	0.05
	0.87	0.045		0.64	-
	0.80	0.037			
	0.60	-			

cent average algorithm (weighted mobile average on 10 points), to reduce noise and disturbance in collected measurements.

Absorption characterization

Absorption characterization on Mg-sample was performed at different pressure and temperature conditions reported in tab. 3.4. The hydrogen uptake was estimated about 7.2 ± 0.1% (uncertainty calculated by 2.18) of IDA instrument, in agreement with data supplied by produced company. In the next plot, capacity of investigated material has been expressed as reacted fraction (from eq.3.2).
From plots in fig. 3.1, at highest driving force parameter, investigated material reaches fully hydride after 400s at 643K, 600s at 633 K, 800s at 613 K, approximately 1000 s at 593 K and finally at more than 1200 s at 573 K. Kinetics absorption rate increased with the temperature as well as working pressure. Generally, absorption reaction was rapid for pressure value far from equilibrium pressure of sample (elevate driving force). Indeed, despite of high temperature (633 K), kinetics curve collected at 0.74 MPa was

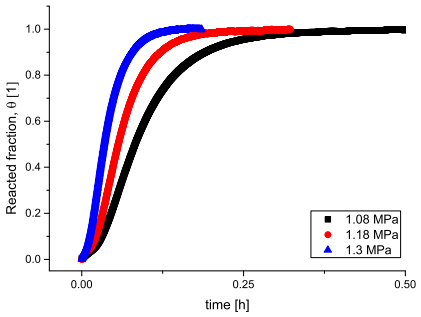

(a) H_2 *ABSorption at 643 K.*

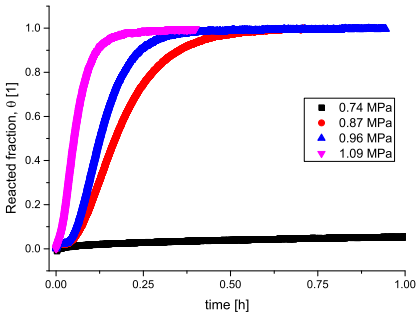

(b) H_2 *ABSorption at 633 K.*

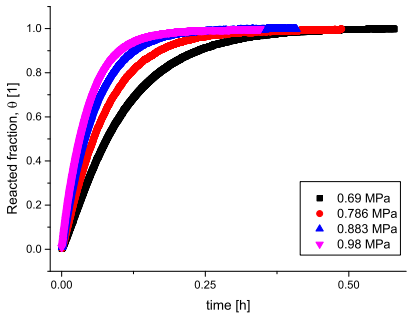

(c) H_2 *ABSorption at 613 K.*

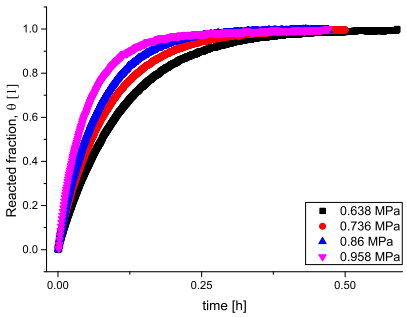

(d) H_2 *ABSorption at 593 K.*

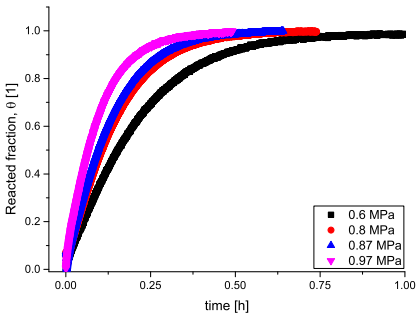

(e) H_2 *ABSorption at 573 K.*

Figure 3.1: Absorption characterization on Mg based.

considerable slower respect to the others isothermal measures, because it occurred at working pressure too close to the equilibrium pressure of material (0.71 MPa at 633 K). About mechanism of reaction, absorption curves in fig.3.1 showed different shapes. In the investigated range of pressure and temperature, temperature seemed to impact on the form of the sorption curve, on the other hand, pressure didn't affect the shape

of curve but only the kinetic rate. At high temperature measurements, a S-shape trend dominated (643-633 K) h, while at low temperature (613-593-573 K) absorption curves assumed monotonic behaviours and the inflection point, visible in the study at 633 and 643 K, was reduced and strongly smoothed at lower temperature (it was also slightly visible only in the first part of characterization at 613 K and almost neglected at 593 K). Changing in the involved kinetics mechanism of hydrogen absorption can explain these different behaviours.
In literature, hydrogen absorption reactions of Mg-MgH_2 system were usually fitted with nucleation and growth model (NG), especially with general formulation of JMAK equation (reported in eq. 3.3). For absorption process, n-term, which represents the dimensionality and the type of interface control of nucleation and growth processes, seems principally depends by working temperature at which reaction occurs. In particular, for low temperature hydrogen sorption reaction on Mg material (483K [144, 153]), Avrami coefficient took value between 0.5 and 1, ascribed to diffusive growth control. At higher temperature (more than 633 K [168, 178]) n-terms took values between 1 and 2, identifying possible 2D or 1D growth process with interface control (constant growth rate), based on classic interpretation of JMAK model. Lototsky et Al, [110] reported JMAK fit for numerous absorption characterizations conducted on Mg based material mixed with different carbon nano-structures. Here, n-terms took value between 1 and 4. Particle's sizes had an important role in the type of limited kinetics mechanism for absorption process too. Jeon et Al [179] showed as nano metric particles have an different n parameter (upper to 1), compared with similar studies at low temperature (473 K).
Basing on scientific literature which studied hydrogen sorption on Magnesium material [110, 178–181], absorption data in fig.3.1, were initially fitted with JMAK model reported in tab. 3.2.2. Fitted parameters of JMAK model were reported in tab. 3.5. NG model was applied between 0.01-0.98 of reacted fraction. Kinetics rate and JMAK coefficient (n) were directly extrapolated by non linear fitting, operated by ™Origin Pro program (based on *Levengerg Marquardt* iterative algorithm). Nucleation and growth model described quite well the experimental data ($R^2 \geq 0.99$). By a first look, n-terms took different values, principally depended by characterisations temperature. At low temperature, NG model seemed to confirm a hydriding kinetics mechanism involved in 1-dimensional growth of already formed superficial nuclei (instantaneous nucleation), with constant growth speed. This was compatible with the radial growth of superficial nuclei, which covered overall surface of particles in the first seconds of absorption reaction. However, at higher temperature (643-633 K and in part at 613 K) Avrami coefficient took values greater than 1 (1.2-1.7), identifying a kinetics mechanism which involved a higher growth's dimensionality and assuming an instantaneous nucleation (there was no reason to consider other type of nucleation). The relative poor goodness of fitting data for high temperature measures (adjusted R-Square < 0.999) revealed a possible variation of kinetics mechanism during the

Table 3.5: Value of JMAK coefficient and kinetics rate parameter extrapolated by JMAK model (Pure Avrami in tab.3.2.2), for different temperature and pressure experimental conditions.

Temp.[K]	Pres.[MPa]	JMAK coeff., n [1]	Kinetic rate [1/s]	Adj. R^2 [1]
643	1.06	1.55	$2.59 \cdot 10^{-3}$	0.9972
	1.18	1.68	$3.87 \cdot 10^{-3}$	0.9979
	1.30	1.60	$6.23 \cdot 10^{-3}$	0.9988
633	0.87	1.79	$1.3 \cdot 10^{-3}$	0.9978
	0.96	2.01	$1.81 \cdot 10^{-3}$	0.9972
	1.09	1.52	$4.05 \cdot 10^{-3}$	0.9976
613	0.69	1.11	$2.51 \cdot 10^{-3}$	0.9998
	0.79	1.07	$3.57 \cdot 10^{-3}$	0.9996
	0.88	1.02	$4.98 \cdot 10^{-3}$	0.9999
	0.98	1.02	$6.065 \cdot 10^{-3}$	0.9999
593	0.64	1.01	$2.55 \cdot 10^{-3}$	0.9998
	0.74	0.96	$3.3 \cdot 10^{-3}$	0.9996
	0.86	0.97	$4.03 \cdot 10^{-3}$	0.9999
	0.96	0.91	$5.49 \cdot 10^{-3}$	0.9999
573	0.60	1.05	$1.3 \cdot 10^{-3}$	0.9992
	0.80	1.10	$1.88 \cdot 10^{-3}$	0.9997
	0.87	1.06	$2.16 \cdot 10^{-3}$	0.9996
	0.97	01.01	$2.95 \cdot 10^{-3}$	0.9995

absorption process.
In order to investigate these discrepancies, the time profile of n-terms was estimated by experimental data. Experimental JMAK coefficients were obtained by rearrangement of JMAK equation in eq. 3.24.

$$\frac{d[ln(-ln(1-\theta))]}{dln(t)} = n(t) \tag{3.24}$$

Local n-terms from experimental data in fig. 3.1 were plotted in $n-\theta$ graph, in order to compare each other more efficaciously (fig. 3.2).
For absorption studies conducted at high temperature (643 K, 633 K an partially for 613 K, fig. 3.2), it is clear as n-values is not constant and doesn't coincide with n value extrapolated by non linear data fitting of JMAK equation reported in tab.3.5. In these measures, n-values starts from 0, quickly raising up to 2.25-2 and decreasing to 1 with proper rates. Such initial increment of n-values (from 0 to 2) can be caused by several factor as the raising of incubation time for the nuclei formations. On the contrary, at low temperature (593 K and 573 K), absorption mechanism is different. JMAK coefficient seems to appropriately reflect extrapolated n data, excluding reaction fraction

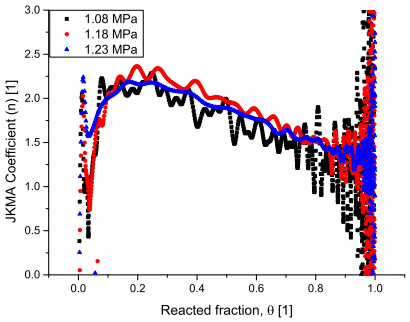

(a) *JMAK coefficient for measures at 643 K.*

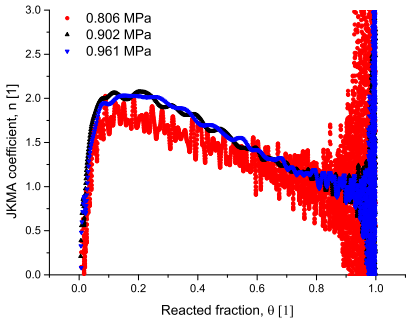

(b) *JMAK coefficient for measures at 633 K.*

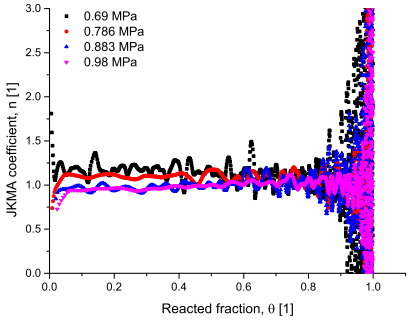

(c) *JMAK coefficient for measures at613 K.*

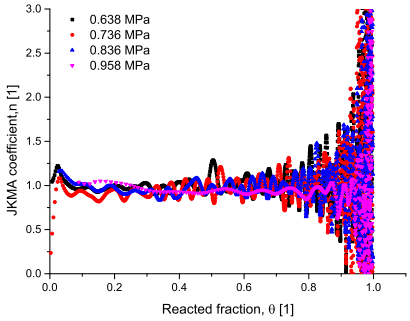

(d) *JMAK coefficient for measures at 593 K.*

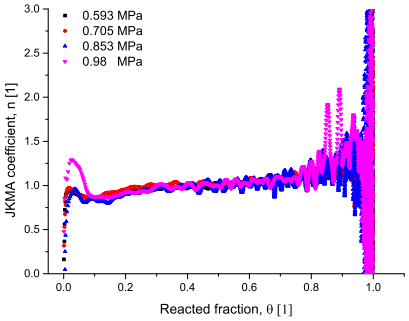

(e) *JMAK coefficient for measures at 573 K.*

Figure 3.2: Local JMAK coefficient calculated by eq. 3.24.

bigger to 0.75 at 573 K, where JMAK coefficients tend to slightly increase. For same isothermal measure, absorption pressures seems to regards exclusively the kinetics rate (as reported in fig. 3.1) but not the type of kinetics mechanism, in the range of pressure investigated.
From theoretical point of view, JMAK equation allows only integer values (n=1,2,3,4)

or half ones in case of diffusive control (n=0.5,1.5,..). moreover, it assumes a constant values during overall kinetics phenomenon.[112, 113, 182] In order to seek a explanation and possible interpretation about the variation of n coefficient during the high temperature absorption reactions, limited growth NG models are introduced.
Limited growth NG model ($N0 - GL_{2C+1}$ model, tab. 3.2.2) assumes that absorption reaction occurs with an instantaneous surface nucleation of a fixed number of nucleus on the surface of the magnesium's particles. It considers superficial growth of nuclei as restricted by finite superficial area and by overlapping of other growth nuclei. Finally, the penetration of hydride phase into the particle is classically treated by JMAK model, with proper impingement function or with a proper limited radial growth. Complete mathematical formulations are reported in tab. 3.2.2.
In this case, only linear growth models are considered. Diffusive model models are not applied for two main reasons. Firstly, diffusion controlled processes dominates at lower temperature than used ones for similar materials, as reported by Shriniwasan [153]. Secondly, JMAK coefficient for diffusion controlled growth should be around n = 0.5 for 1D growth, n=1 for 2D growth or n = 1.5 for 3 D growth in case of instantaneous nucleation. Approximating magnesium sample as composed by spherical particles, the hydride's growth proceeds from the surface of particles into their cores, along radial direction and in a pseudo one dimensional growth, as confirmed by SEM studies on similar Mg based materials [183, 184]. In this condition, a diffusion controlled kinetics should be revealed by JMAK coefficient equals to 0.5, however experimental JMAK coefficient, hereby reported, is always upper than 1. Secondly, a possible 2D diffusive controlled growth (n=1) is not justified, firstly because it requires pure plate-shape particles and secondly, because the suppression of one of growth direction is not justifiable in spherical geometry,.
The limited growth NG model (N0-G2A1D model) was applied to study high temperature hydrogen absorption measures. Data's fitting were reported in fig. 3.3, while fitting parameters in tab.3.6.

Table 3.6: Fitting parameter for limited growth NG model ($N_0 - GL_{2C+1}$ model) applied on high temperature characterization (643-633 K) reported in gig.3.1. The meaning of a and b values are explained in tab. 3.2.2.

Temperature [K]	Pressure [MPa]	a [1/s]	b [1/s]	Adj. R^2
633	0.87	$1.3 \cdot 10^{-3}$	$2.22 \cdot 10^{-3}$	0.9998
	0.96	$3.39 \cdot 10^{-3}$	$2.48 \cdot 10^{-3}$	0.9994
	1.09	$5.29 \cdot 10^{-3}$	$9.64 \cdot 10^{-3}$	0.9993
643	1.08	$3.44 \cdot 10^{-3}$	$5.93 \cdot 10^{-3}$	0.9998
	1.18	$5.79 \cdot 10^{-3}$	$6.47 \cdot 10^{-3}$	0.9999
	8.81	$5.29 \cdot 10^{-3}$	$10.7 \cdot 10^{-3}$	0.9998

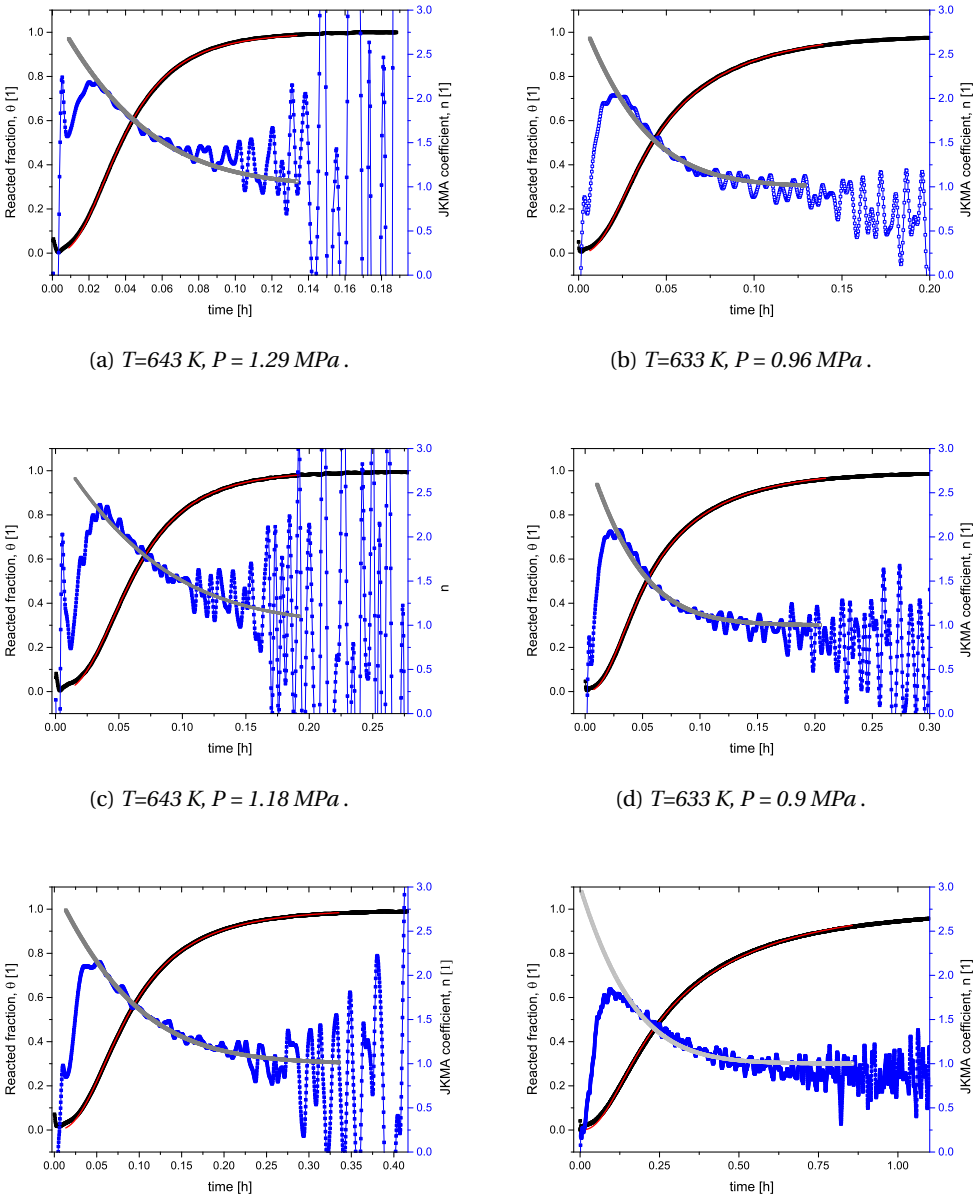

(a) *T=643 K, P = 1.29 MPa* .

(b) *T=633 K, P = 0.96 MPa* .

(c) *T=643 K, P = 1.18 MPa* .

(d) *T=633 K, P = 0.9 MPa* .

(e) *T=643 K, P = 1.08 MPa* .

(f) *T=633 K, P = 0.8 MPa* .

Figure 3.3: Data fitting of absorption experimental measures. Black curve is the reacted fraction, while red one is the non linear fitting with limited growth NG model. Blue curve is the experimental JMAK coefficient derived by experimental data from eq.3.24 while, grey curve is the JMAK coefficient calculated on the data fitting results.

Fig. 3.3 shows the non linear fitting of limited growth NG model on experimental data (fig. 3.1) collected at high temperature (643-633 K). In the same graph, the comparison of JMAK coefficient derived by empirical data and fitting model obtained by eq.

3.24 are plotted. Limited growth model didn't fit the first moments of measures (< 90 s), where n-values, estimated by fitting model, tended to 3 (which is the limit of the function of limited growth model for t=0). Initial increment of n-values can be attributed to several factor as noise fluctuation in the pressure data, due to the quick gas expansion in volumetric instrument, and the raising of incubation phenomenon regarding the nucleation process. However, mathematical relation for incubation time was extremely difficult to integrate mathematically in the nucleation and growth model (eq.3.7), because it require to introduce the terms $e^{-\frac{\tau}{t}}$ (t is the time of study and τ is the characteristic incubation time [185, 186]) in eq. 3.7.
Finally, limited growth NG model fitted with a considerable goodness ($R^2 \geq 0.999$) absorption data at high temperature, respect to classic *JMAK* equation, tab.3.6, in the range of temperature investigated. Moreover, the comparison of JMAK coefficient demonstrated that limited growth model not just fits the reacted fraction data but even gave a reasonably explanation of variation of n-values during the absorption reaction, tab.3.3.
This supports a possible interpretation of hydriding absorption mechanism on magnesium based material at high temperature. That could occur with following mechanism: firstly, an instantaneous nucleation of a finite number of nuclei involves on the surface of Mg's particles. Nucleation process probably includes a incubation phenomenon, which introduce a delay in the formation of nuclei. Secondly, any nucleus isotropically grows in 3-dimension like a hemisphere, penetrating into the Mg particle's bulk. Thirdly, surface of Mg particle is covered by the overlapping of growth nuclei with the progress of absorption reaction, resulting fully covered when empirical JMAK coefficient approach the unit. Finally, the phase transition's front proceeds to the core of magnesium particles, reacting with the remaining metallic phase.
The different kinetics mechanisms which were observed at distinct isothermal conditions could be explained by a divergent number of available nuclei at the beginning of absorption reaction. Indeed, number of nuclei and its formation rate depends by two opposite temperature contribution. Firstly, the high temperature tends to produce higher number of nuclei because energetic barrier of nucleation (correlated to the nucleation's activation energy) can be more easily overcome. On the contrary, at higher temperature, formed nucleus can be destabilized, and redissolved for simple thermal excitation.[186] So, it is reasonable to describe high temperature hydrogen absorption mechanism on Mg-sample as leading by the number of formed nuclei on the surface of particles, as supported by Tien et al. [180]. Few nuclei may grown a lot before to meet other nuclei's domains, proceeding with a more closest ideal 3D growth, limited only by geometrical constrain of particle (as finite superficial area and the radius). On the contrary, when experimental temperature decreases, the number of superficial nuclei raises for the previously cited reasons. Consequently, superficial area of sample's powder is rapidly covered, and hydriding reaction almost immediately proceeds to the core of particle with a 1-Dimensional growth model

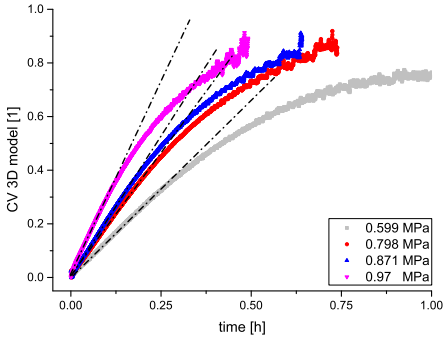

Figure 3.4: Hydrogen absorption data of fig.3.1 transformed using the function $1-(1-\theta)^3$ and plotted against t. Straight line are only guide for eyes.

tending to a contracting volume mechanism when number of nuclei is extremely high.

As additional support to such kinetics mechanism interpretation, some work identified CV (contracting or shrinking model) as the possible limiting mechanism of hydride phase in parent one. Barkhordarian and Revesz [187, 188] concluded that CV model (3D, spherical shrinking model) can quantitatively described Mg based material doped with Nb_2O_5, while Bösenberg et al. [189] identified contracting volume model as the principal kinetics mechanism for absorption phenomenon in Mg-Li sample. However, NG and CV model fitting can give similar results with consequently confusion about type of effective limiting kinetics mechanism, in particular for value of n close to the unit. Indeed, as reported by Pang and Li [113], geometrical and NG model can give overlapped results which are complicated to distinguish. Shrinking model tends to give effective-JMAK coefficient (by direct fitting data) equals to n = 1.1 for interface-controlled model (constant interface velocity), or n=0.6 for diffusion controlled geometric model (decreasing interface velocity: Jander, G-B or Valesi approach), when NG model is applied.

An additional investigation revealed as kinetics mechanism of hydrogen absorption on Mg sample at the lowest temperature characterization (573 K) can be even described by 3D geometrical-shrinking model. In fig. 3.4, the linearization of CV-3D model (Sharp & Jones approach) is reported for absorption data obtained at 573 K. Linear Straight black curve in fig.3.4 demonstrated that hydrogen absorption reaction on Mg can be effectively modelled by 3D contracting volume mechanism for the initial part of the overall absorption reaction. Furthermore, CV-3D mechanism can be noted by time variation of JMAK coefficient analysis in fig. 3.2(e). Here, n-value tended to increase from 1 to greater value at reacted fraction around 0.75-0.8. Such profile is characteristic for CV-3D mechanism [113]. Kinetics absorption measures conducted at 573 K were the only that appreciably manifests such mechanism.

On the base of previous discussions and results, it was possible to map (fig. 3.5) the kinetics absorption mechanisms occurred on Mg sample in a range of temperature between 573-643 K and pressure 0.6-1.3 MPa.

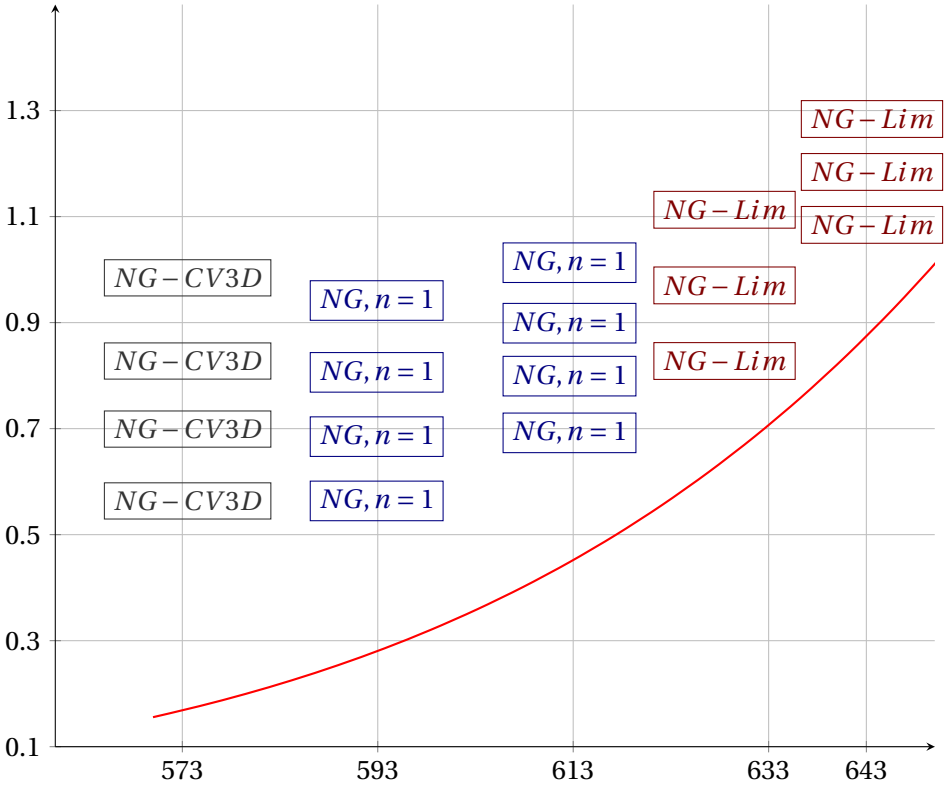

Figure 3.5: Map of kinetics mechanisms, involved in hydrogen absorption reaction on investigate Mg sample. Red curve represents the equilibrium pressure of material. NG-LIM: limited growth NG model. NG: nucleation and growth model (JMAK). CV-3D: Spherical Contracting Volume model.

Once to identify the kinetic mechanisms of absorption reaction, the next step of kinetic analysis sought to extrapolate the formulation of driving force from the kinetic constant obtained by previous kinetic mechanism analysis. For absorption case, kinetic parameters estimated by JMAK model (tab. 3.5) were used to next kinetic analysis. In high temperature data, kinetics rates were obtained by limited growth model. The estimation of driving force contribution meant to identify the mathematical relation with the best fit against experimental data, which was assumed as the thermodynamic contribution to the kinetic rate.[37, 168] Equilibrium pressure values were estimated by *Van't Hoff* relation, reported in the previous chapter about thermodynamic study on Mg sample. H_2 absorption reaction's enthalpy was evaluated equals to 72 [kJ/-mole], while entropy is about 130 $[J/mol \cdot K]$. Typical formulations for driving force contribution were collected in tab. 3.3, however just parabolic relation $(\sqrt{P} - \sqrt{P_{eq}})$

showed a reasonable goodness on data fitting ($R^2 > 0.995$) (as reported also by [109]). In fig. fig. 3.6(a), driving force relation based on linear relation was reported for all investigated temperature. The data at 633 K and 643 K were taken by limited growth NG model, while kinetics data at lower temperature measure, by pure JMAK model treatment, tab. 3.5. Consequently, *apparent* activation energy correlated to the growth

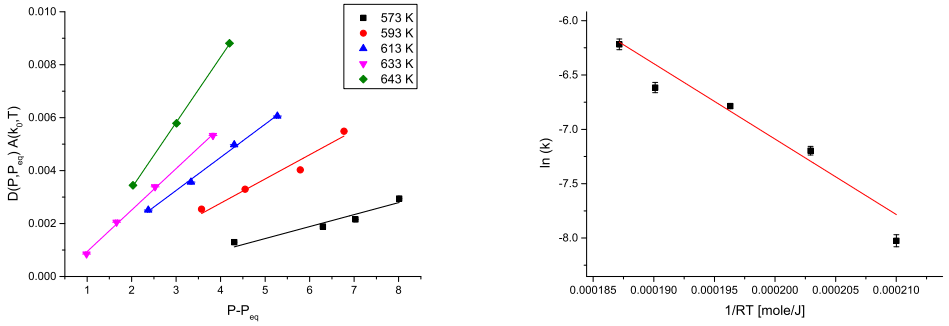

(a) *Pressure dependence.* (b) *Arrhenius plot.*

Figure 3.6: In (a), driving force fitting on experimental data are plotted and investigate with proper linear regression model. Fitting parameters are then study in Arrhenius type plot ((b)) to extrapolate information about apparent activation energy of sorption phenomenon.

process can be extrapolated by Arrhenius graph, fig. 3.6(b), plotting $ln[k(T)]$ versus $1/RT$; where k(T) is the angular coefficient of linear fitting extrapolated by previous driving force study. Apparent activation energy was estimated about (91 ± 8) kJ/mole for hydrogen absorption, while $ln(k_0)$ was equals to (12.5 ± 1.6) 1/s. Hereby extrapolated data is in agreement with literature reference for absorption process (apparent activation energy about 57-100 kJ/mole [109, 168, 190]).

Desorption characterization

Desorption characterizations on Mg-sample were performed at different pressure and temperature conditions, reported in tab. 3.4. Analogously to absorption study, gravimetric capacity of Mg sample was estimated as (7.2 ± 0.1) %, in agreement with data supply by produced company.

In kinetics studies conducted at high driving force (lower pressure), fully desorption conditions were achieved in 180 s at 643 K, 270 s at 633 K, 720s at 613 K, 1800 s at 593 K and more than 3 h at 573 K. Hydrogen desorption plots showed a common S-shape profile for all isothermal conditions. Pressure and temperature seem to impact on the kinetics rate of reaction. Furthermore, kinetic desorption measures performed close to equilibrium pressure of material (0.6 MPa at 633 K and 0.103 MPa at 573 K) showed identical S-profile respect to the other curves, contrary to the absorption reactions,

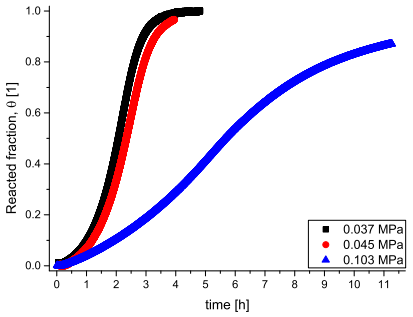

(a) H_2 *DESorption at 573 K.*

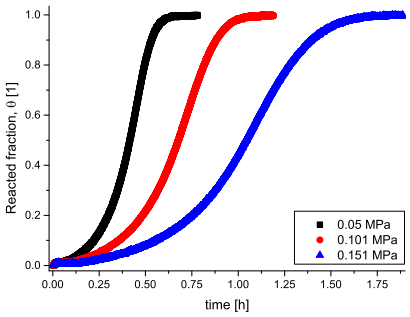

(b) H_2 *DESorption at 593 K.*

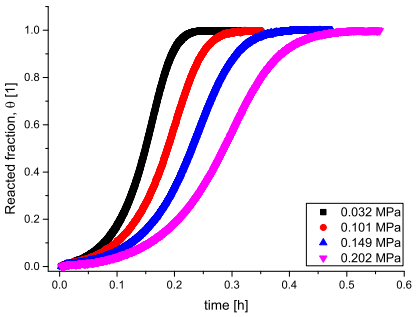

(c) H_2 *DESorption at 613 K.*

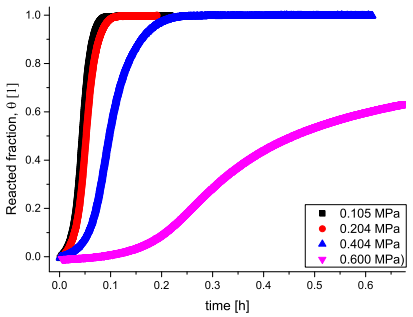

(d) H_2 *DESorption at 633 K.*

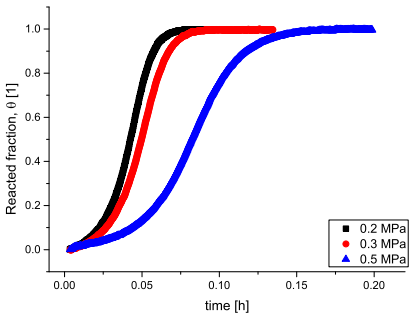

(e) H_2 *DESorption at 643 K.*

Figure 3.7: Desorption characterization on Mg based.

but with a considerable smaller kinetics rate.
The S-shape profile of curve supports the nucleation and growth model (JMAK or Avrami model with n>1) as possible interpretation of kinetics desorption reaction. [113] For this reason, JMAK model (tab.3.2.2) was initially applied on desorption data.
Fitting parameters (table 3.7) revealed that hydrogen desorption reaction on Mg sam-

Table 3.7: Value of JMAK coefficient and kinetics rate parameters extrapolated by JMAK model (Pure Avrami in tab.3.2.2) at different temperature and pressure experimental conditions for desorption reaction study, are reported.

Temp. [K]	Pres. [MPa]	JMAK coeff., n [1]	Kinetics rate [1/s]	Adj. R^2 [1]
643	0.2	3.61	$5.98 \cdot 10^{-3}$	0.9987
	0.3	3.61	$5.12 \cdot 10^{-3}$	0.9990
	0.5	3.32	$3.04 \cdot 10^{-3}$	0.9987
633	0.105	3.25	$4.40 \cdot 10^{-3}$	0.9990
	0.204	3.20	$3.75 \cdot 10^{-3}$	0.9990
	0.404	3.17	$42.46 \cdot 10^{-3}$	0.9990
613	0.032	3.77	$1.72 \cdot 10^{-3}$	0.9975
	0.101	3.73	$1.37 \cdot 10^{-3}$	0.9972
	0.149	3.70	$1.11 \cdot 10^{-3}$	0.9985
	0.202	3.71	$0.86 \cdot 10^{-3}$	0.9987
593	0.051	4.01	$6.25 \cdot 10^{-4}$	0.9966
	0.101	3.87	$3.81 \cdot 10^{-4}$	0.9967
	0.151	3.72	$2.45 \cdot 10^{-4}$	0.9980
573	0.037	3.21	$1.22 \cdot 10^{-4}$	0.9986
	0.045	3.24	$1.07 \cdot 10^{-4}$	0.9984
	0.103	1.77	$3.94 \cdot 10^{-5}$	0.9984

ple occurred through nucleation and growth mechanism, with high value of *n*-terms. [191–193] reported a JMAK coefficient n=4 for hydrogen desorption reaction on pure magnesium at 623 K, corresponding to a kinetics mechanism which involved in the continuous formation of stable Mg's nuclei in the hydride parent phase as rate limiting step in the H2 desorption kinetics. However, Fernandez and Snchez [168], Cabo et al. [190] extrapolated n-value around 2 by kinetics characterizations performed in range of temperature between 603-663 K, assuming kinetics step controlled by two-dimensional growth of random nuclei of Mg metal with constant interface velocity. Konstanchuk et al. [194] identified a n-value equals to 3 (instantaneous nucleation with 3D interface growth) however it raised some doubts on the instantaneous nucleation assumption. At the way, Liang et al. [172] extrapolated the same n-values (3) for the desorption study on catalysed Mg sample but he interpreted hydrogen desorption process as controlled by decreasing nucleation rate and two dimensional growth processes. Finally, Huot et al. [195] reported a n=3, for desorption study conducted on very similar material respect to investigated sample in this work.
According to fitted parameters reported in tab. 3.7, JMAK model interpreted desorption mechanism as due to a continuous nucleation rate with 3D growth of Mg-nuclei (n=4) or decreasing nucleation rate (3<n<4) in the investigated sample. Desorption

measure obtained at 573 K and at 0.103 MPa, presents a n-value equals to 1.77, in agreement with a 3D diffusion controlled growth, with a decreasing nucleation rate. However, some works noted that JMAK coefficient can change during the desorption reaction [178, 196]. For this reason, an additional investigation were conducted on all desorption measures (fig. 3.7), in order to estimate local JMAK exponents (estimated by eq. 3.24) against reacted fractions data.

Fig. 3.8 demonstrated as effectively JMAK coefficients was not constant for whole desorption reaction and for any investigated isothermal conditions. Local JMAK coefficient started to 0, increasing with proper slope which seems to slightly depends by temperature, up to approach at maximum n=4 or n=5 (for measurements at 613 and 593 K), then falling down to 0. In these case, JMAK coefficient is time increasing, approaching the maximum value for reacted fraction of approximately 0.5-0.7 (depended by pressure). n-terms reported in tab. 3.7 represent an average value during whole process. Local JMAK coefficients seemed to be more temperature independent compared to absorption reactions, impacting slightly in the first half of reacted fraction. On the contrary, pressure values seemed to affect on reaction mechanisms only at high reacted fraction value, while JMAK coefficient is almost pressure independent for $\theta < 0.5/0.6$.

The kinetics mechanism on hydrogen desorption phenomenon on Mg sample is not fully understood. Although nucleation and growth model gave a possible basic interpretations (continuous nucleation of Mg-seed in bulk materials following by 3D growth interface -controlled), the variations of local JMAK coefficient during the reaction weren't predicted and explained.

A possible explanation of initial local JMAK coefficient's increment may be attributed to incubation phenomenon, identified by Takeichi et al. [178] in desorption reaction on MgH_2 sample, which delays and hides the real kinetics mechanism. However, as already discussed, the mathematical treatment for incubation phenomenon is particularly difficult to integrate in nucleation and growth model.

Moreover, as reported by Mooij and Dam [197], hydrogen desorption reactions (on thin layer) didn't show any visual evidence for superficial nucleation of Mg in MgH_2 at any supersaturation state (although obtained at low pressure and temperature conditions), which instead occured in absorption reaction. This suggested that desorption phenomenon may even occurs even with a contemporaneous contracting volume mechanisms as supposed by [150] for small particles, and supported by SEM image ([153, 184]). Unfortunately, limited growth NG model, hereby develop, were not suitable to describe hydrogen desorption mechanism of reaction, because they described process of growth where growth's dimensionality and nucleation rate tended to decrease in the time because spatially limited. Instead, in desorption reaction, local n terms initially increased over the time. A proper mixed model were tested on

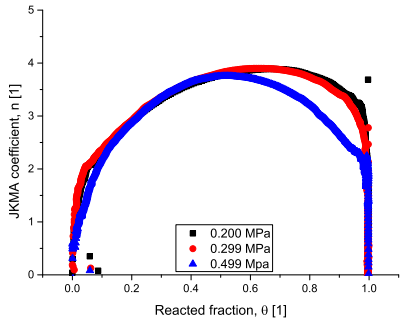

(a) *643 K.*

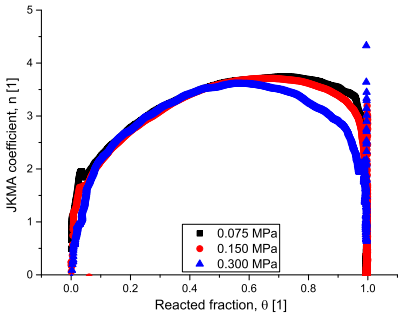

(b) *633 K.*

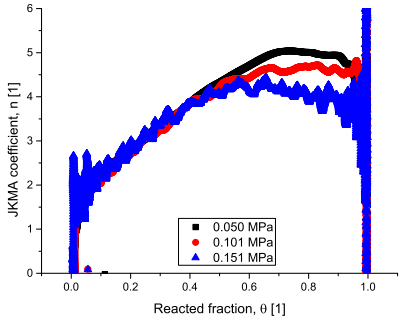

(c) *613 K.*

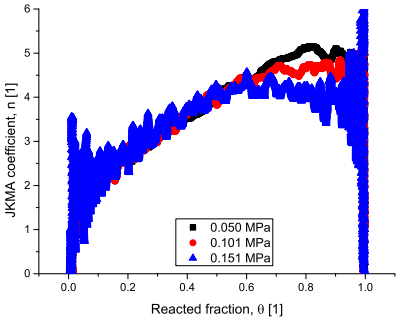

(d) *593 K.*

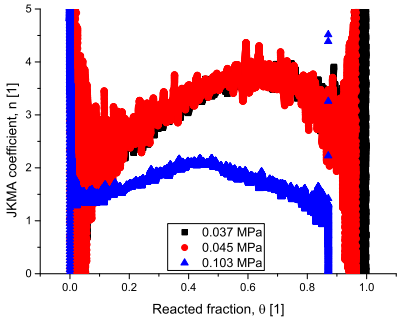

(e) *573 K.*

Figure 3.8: Local JMAK coefficient estimated by eq. 3.24 on desorption data in fig. 3.7. The discrepancy in term of curve profile of desorption measures at 573 K and 0.103 MPa (fig. 3.8(e)) could be ascribed by very low driving force (equilibrium pressure equals to 0.152 MPa)

desorption data, including NG parallel to a *shrinking* volume mechanism. However, the resulting fits were poor and not properly describe the physical phenomenon, for these reasons they weren't reported in this work.

Based on previous discussion, nucleation an growth model, known as JMAK method, is still the most suitable approach for the description and modeling of hydrogen desorption reaction on MgH_2 sample. In the investigated range of pressure (0-0.5 MPa) and temperature (573-673 K), hydrogen desorption reaction from investigated Mg-based material can be modeling with sufficient accuracy by JMAK model.
Kinetics constant k-terms obtained by JKMA model (tab. 3.7) were plotted with different mathematical relations to identify the more appropriate driving force contribution. Equilibrium pressure values were estimated by *Van't Hoff* relation, reported in the previous chapter about thermodynamic study on Mg sample, with H_2 desorption reaction's enthalpy equals to 74.1 [kJ/mole] and an entropy of 132.8 $[J/mol \cdot K]$. Even here, parabolic relation tab.3.3) showed the best linear fittings with a R^2 equals to 0.99 for the different isothermal characterizations. Driving force contribution is reported in fig. fig. 3.9(a). Scientific literature present spread values about apparent activation

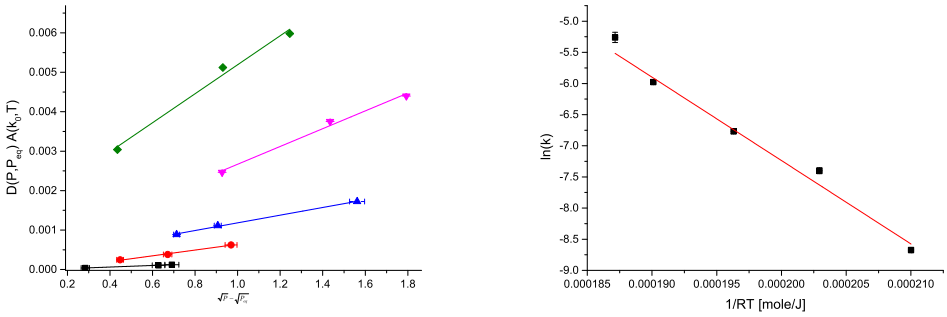

(a) *Pressure dependence.*

(b) *Arrhenius plot.*

Figure 3.9: In (a), driving force fitting on experimental data were plotted and investigate with proper linear regression model. Fitting parameters are then study in Arrhenius type plot ((b)) to extrapolate information about apparent activation energy of sorption phenomenon.

energy data: 141 kJ/mole for Bazzanella et al. [193], 120 kJ/mole for Huot et al. [195] while Jensen et al. [198] reports a considerable reviews on E_a value included in a range between 120-160 kJ/mole, some other work report value between 233 and 299 kJ/mole. In this work, Apparent energy of activation for desorption process has been extrapolated by proper Arrhenius's plot in fig. fig. 3.9(b). A value of (135 ± 7) kJ/mole was estimated with $ln(k_0)$ equals to (19.5 ± 1.4) [1/s], in agreement with literature data.

3.3 Macro scale model

In order to develop a successfully hydrogen storage tank based on magnesium hydride material, the elevate enthalpy of hydrogen sorption reaction on Mg/MgH_2 (72-75 kJ/mole) introduces a challenge in the designing of tank's inner layout respect to other metal hydride materials. Indeed, during hydrogen absorption absorption reaction, active materials tends to quickly approach the equilibrium temperature at the working pressure, stopping the storing process and limiting the efficiency. At the contrary, during H_2 desorption process, active material tends to rapidly cool down itself, drastically decreasing the reaction kinetics.
So, the bottleneck on the performance of stored reactor is the thermal diffusivity, and the capacity to quickly remove or supply elevate amount of heat power in Mg based material. In the light of these consideration, it is clear as design and dimensioning of a hydrogen storage tank has considerable role in order to achieve and to exploit the best performance from magnesium-based materials in industrial or commercial application.
In this contest, numerical simulations support the realization of a successfully hydrogen storage tank, maximizing the performance of storage material. However, an accurate and complete numerical simulation of hydrogen storage tank based on HSM, requires the development of a suitable mathematical model for the description of tank macro system, which considers: hydrogen sorption reaction of HSM and thermal and gas diffusion in the inner structure of tank. The ultimate scope of macro model and relative numerical simulation are the designing and optimization of a proper hydrogen storage tank where sorption kinetics performance approaches the intrinsic performance of materials applied.
Many investigators developed different approach on mathematical analysis about hydrogen storage tank, (LaNi5, [132, 199, 200] , activated carbon structure, [201]) and on Magnesium hydride [37, 118, 120, 121, 202]. Cited papers certify the useful of modeling, as successful numerical tool to explore different design of tank focusing on particular issues or components inside HSM's reactor with content costs and efforts.
Objective of this section of thesis is the development and validation of a macro model for the description and modeling of a hydrogen storage tank unit based on Mg material. Kinetics reaction of metal hydride is estimated on the base of physical micro modeling, hereby previously developed. Validation of macro model has been certified by the comparison of experimental data obtained by proper experimental set up.

3.3.1 Methods

Macro model includes the coupling of proper heat and gas diffusion model with the kinetics modeling of investigated metal hydride. In this case, micro scale model previously described, was used as core of macro scale model for the description of

hydrogen sorption processes. Physical parameters of materials (i.e. thermal and physical proprieties as thermal conductivity, gas permeability, et..) were obtained by proper characterization, while some others were directly extrapolated by experimental data. Finally, proper boundary conditions of the tank (shape of pelleted material, pressure conditions, heater positions, et..) completed the needed information for the numerical simulations.
COMSOL Multyphisics software, extended with Fluid Dynamic and Heat Transfer modules was used as modeling software.
Numerical results by macro modeling were validated against experimental data obtained by prototype of hydrogen storage tank based on Mg material. Dynamic solver of COMSOL software was applied to describe transient behaviour of magnesium-based material in pellet shape inside a tank, in particular about profile of pressure, temperature and reacted fraction, during the absorption and desorption reaction of hydrogen.

Assumption

Assumption in physical modeling are necessary to approach a consistent compromise between easily, accessibility and data fitting. The following approximation were well sustained by other scientific work on similar problems.

- Hydrogen was consider like ideal gas[37, 120, 203]. We assumed pressure-temperature relation as ideal state equation of gas ($\rho_{H_2} = (PV)/(PM_{H_2}T)$). In this condition, hydrogen compressibility factor (Z) was approximately to 1 (with a error of 0.1% at 10 bar calculated by revised standardized equation of Eric W. Lemmon [87, 89]).
- thermal equilibrium between gas and solid was assumed within the porous media of Mg-material.[204–206]
- Radiative heat transfer was neglected.[132]
- Thermo-physical proprieties of system were considered independent by temperature and hydrogen concentrations.[132]
- It was assumed that volume of Mg-pellet didn't change during absorption and desorption phenomena. This is a stronger assumption. Real variation of volume between magnesium and its hydride is approximately 20% (base on density data) but numerical model didn't consider any volume variation.
- As a consequence of hysteresis phenomenon (apparent different equilibrium pressure between absorption and desorption process), the enthalpy and entropy of sorption reaction was considered as an average value between the two value

extrapolated by thermodynamic investigation (ΔH^{abs}-ΔH^{des} and ΔS^{abs}-ΔS^{des}), reportd in the second chapter of this work.

Mathematical formulation

Mathematical model for the description of hydrogen storage tank included the specific kinetics modeling of hydrogen storing materials (resumed by the previously reported micro modeling) and the main physical variables as temperature and pressure inside the tank, described by proper thermal and gas diffusive model.
In real macro system, temperature and pressure can not be assumed as homogeneously distributed and constant over the time as assumed in previous chapter. For these reasons it was necessary to introduce the phenomena of thermal and gas diffusion. Heat and gas diffusion problem in porous material obeyed at known physical laws which can be analytically or numerically solved coupling them with the proper mathematical formulation of hydrogen sorption reaction obtained by micro scale model.

Temperature's distributions on the analysed domain was given by 3D heat equation,

$$\epsilon \rho_{H_2} C_{H_2} \frac{\delta T_{H_2}}{deltat} + (1-\epsilon)\rho_s C_s \frac{\delta T_s}{\delta t} + \epsilon \rho H_2 C_{H_2} \nabla (T_{H_2} \cdot \overrightarrow{v_{H_2}}) = \kappa_{eff} \nabla^2 T + S. \quad (3.25)$$

where κ_{eff} is the efficacy thermal conductivity of porous medium. It was estimated as linear combination of thermal conductivity of magnesium κ_{Mg} and magnesium hydride κ_{MgH_2} weighted on the porosity of materials (ϵ) and the thermal conductivity of hydrogen gas (κ_{H_2}) in eq.3.26.

$$\kappa_{eff} = (\kappa_{Mg} + (\kappa_{MgH_2} - \kappa_{Mg})\theta)(1-\epsilon) + \kappa_{H_2}\epsilon. \quad (3.26)$$

Analogously, thermal capacity and density of material were calculated in eq. 3.27:

$$C_s \rho_s = (1-\theta)\rho_{Mg} C_{Mg} + C_{MgH_2} \theta \rho_{MgH_2}. \quad (3.27)$$

S-term in eq. 3.25 represented the heat source derived by chemical reaction of hydrogen absorption or desorption. It was estimated by the enthalpy of reaction (ΔH) and reaction progress (θ).
Macro Model assumed no volume's changing during sorption reaction. So, the term $\rho^{app}_{MgH_2}$ was introduced as the apparent density of magnesium hydride like it maintained the same volume of original magnesium. In this way, S-term can be expressed

as:

$$S = \left[\frac{d\theta}{dt}\frac{\rho^{app}_{MgH_2} - \rho_{Mg}}{PM_{H_2}}(1-\epsilon)\Delta H\right]. \tag{3.28}$$

About Hydrogen pressure and gas diffusion in porous media, Darcy's law (eq.3.29) was used,

$$\overrightarrow{\nabla} P = -\frac{\eta}{k}\overrightarrow{v_{H_2}}. \tag{3.29}$$

In Darcy's law, flow of hydrogen was directly proportional with drop of pressure inside pellet. η is viscosity of hydrogen, while k_{H_2} is the gas permeability of magnesium pellet.
Assuming HSM composed by spherical particles, compressed in porous pellet-shape, k_{H_2} term can be estimated by Carman-Kozeny equation, 3.30,

$$k_{H_2} = \frac{\epsilon^3}{180(1-\epsilon)^2}d^2, \tag{3.30}$$

where d is the mean particle's size, while ϵ is the porosity of porous matrix.[207]
Variation of pressure inside porous material was associated to the variation of mass/-density of gas by ideal equation of gas,

$$P = \frac{\rho_{H_2}}{PM_{H_2}}RT. \tag{3.31}$$

Mass balance was introduced with,

$$\epsilon\frac{d\rho_{H_2}}{dt} + \nabla(\rho_{H_2}\overrightarrow{v_{H_2}}) = \left[\frac{d\theta}{dt}(\rho^{app}_{MgH_2} - \rho_{Mg})\right]. \tag{3.32}$$

Mass balance in eq. 3.32 included both hydrogen flow from sorption reaction and external source. θ is the reacted fraction (1 for fully hydride material and 0 for pure Mg).
Micro kinetics model developed in last section was applied and reported in tab. 3.8. JMAK model was applied, considering the range of temperature and pressure involved in typical hydrogen storage tank-bed of Magnesium (573-613 K and 0.1-1 MPa). For hydrogen absorption phenomena, JMAK coefficient was considered equals to 1, while a mean value of n = 3.5 was retained suitable for desorption reaction. Kinetics constants rate were estimated by eq.3.23, where $D(P, P_{eq})$ and relative parameters were the results of previous kinetics analysis on Mg material. For absorption process, a parabolic relation was assumed to describe driving force contribution. A parabolic function was used even for desorption phenomenon. *Driving force* relations and temperature contribution (Arrhenius equation) are resumed in tab. 3.9.

Table 3.8: Mathematical relation for kinetics absorption and desorption reaction derived by Micro model analysis. f(θ)= kt is reported (eq. 3.1)

Reaction	f(θ)	n
Absorption	$n(1-\theta)[-ln(1-\theta)]^{1-1/n}$	1
Desortpion		3.5

E_a^{abs} and E_a^{des} are respectively the activation energy of absorption and desorption

Table 3.9: Temperature and pressure contribution on constant rate for absorption and desorption processes.

Process	Driving force relation	Temperature contribution
Absorption	$\sqrt{P}-\sqrt{P_{eq}}$	$A_0^{abs}e^{\frac{-E_A^{abs}}{RT}}$
Desortpion	$\sqrt{P_{eq}}-\sqrt{P}$	$A_0^{des}e^{\frac{-E_A^{des}}{RT}}$

reaction, followed by proper cofactor terms, A_0^{abs} and A_0^{des}, estimated by micro model analysis. P_{eq} was evaluated by *Van't Hoff* relation. Enthalpy and Entropy of reaction was considered an average value between thermodynamic parameters of absorption and desorption reaction, calculated in second chapter of this work. Parameters are resumed in tab. 3.10.

Numerical software

COMSOL Multiphysics was utilized as environment software in order to successfully develop a numerical tool of magnesium-based tank. COMSOL was a powerful software to simulate different physical/chemical phenomena at small/medium scale with multiple options on the complexity and accuracy of physical laws through Finite Element Method (FEM). Software can simulate physical behaviour of a selected-built space domain, both if system is complex and it is time-dependent. Choose of suitable mesh is the most important step in order to have a high accuracy of numerical simulation. Typically, mesh is automatic chosen by type of utilized physical module, but if geometry of system results very complex, mesh creation can be customized. In numerical simulation, incorrect initial value can cause mathematical artefacts with following errors in simulation. For this reason, some precaution were necessary:

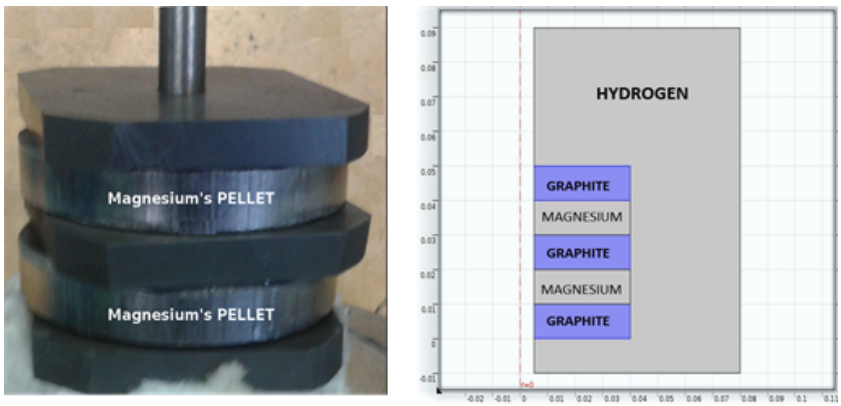

Figure 3.10: To the left, picture of real system including graphite fins and pelleted Mg-based material. Magnesium and graphite pellets are stacked in a sandwich configuration. The vertical metal bar is the heater element. On the right, the simulated 2D symmetrical geometry is reported.

Geometry and constraints

A Prototype of hydrogen storage tank were realized in MATRES-MBN nanomaterialia [208] facilities within of the EDEN project. Experimental set up of modelled system is reported in fig. 3.10. It included two Mg-based pellets in a sandwich configuration, alternate by three graphite square disks to improve thermal diffusions. Pellets were composed by magnesium powder produced by high energy ball milling, addicted with 7% of graphite to improve thermal proprieties of material. Active material was characterized in the previous part of document. Mg-material was properly compacted in pellets. Sizes and physical parameters of graphite and Mg pellet are reported in tab. 3.10. An appropriate heater elements was placed in the central part of every elements of prototype (graphite fin and Mg-pellet properly pierced). A thermocouple was placed between central graphite fin and adjacent magnesium pellets.
An identical 2D symmetrical geometry was realized by proper builder included in ™Comsol software, and reported in fig. 3.10. Simulated geometry replicated identical size and design of experimental set-up, included the empty space of tank for a correct estimation of external pressure. Analogously to the real system, a heater element was simulated in the center of Mg-pellets as a fixed temperature conditions on the left boundary of material's domain in the simulated design reported fig. 3.10. We assumed hydrogen gas diffusion exclusively occurred through the lateral right boundary of magnesium pellets.
Physical parameters of hydrogen gas (as thermal proprieties) were already included in the ™Comsol software.

Macro model here introduced, kept in consideration tank's thermal losses to the environment, which strongly affected temperature of material's bed inside tank. In this

case, thermal losses were estimated approximately in 300 W. This value was extrapolated by stationary study on tank when material was fully hydrided or de-hydrided, and temperature gradient inside tank was only due to thermal losses. Thermal dissipation was easily estimated considering thermal conductivity of graphite fin, and the position of thermocouple sensors. Experimental parameters of pellets (as thermal conductivity and capacity) were estimated by proper thermal and gas diffusion characterization on single pellet. Tab. 3.10 resumes all physical parameters used in this work.

Table 3.10: Main parameter involved for the numerical simulation of experimental set up system in fig.3.10. Micro model parameter were estimated by previous kinetics analysis conducted on Mg sample.

	Parameters	Symbol	Unit	Value
Micro model Parameter	Enthalpy	ΔH	[kJ/moles]	73.1
	Entropy	ΔS	[kJ/(moles*K)]	131.4
	Activation Energy	E_a^{abs}	[kJ/moles]	91
		E_a^{des}	[kJ/moles]	135
	Cofactor	A_0^{abs}	[1/s]	$exp(12.5)$
		A_0^{des}	[1/s]	$exp(19.5)$
	JMAK coefficient	n^{abs}	[1]	1
		n^{des}	[1]	3.5
	H_2 gravimetric capacity	%	[1]w/w	7.1
Experimental parameters	Thermal conductivity [a]	λ_{Mg}	[W/m·K]	16[f]
		λ_{MgH_2}	[W/m·K]	6[f]
	Thermal Capacity [a]	C_{Mg}	[J/kg·K]	1147[e]
		C_{MgH_2}	[J/kg·K]	2075[e]
	Density [a]	ρ_{Mg}	[kg/dm^3]	1.738
		ρ_{MgH_2}	[kg/dm^3]]	1.45
		$\rho_{MgH_2^{app}}$	[kg/dm^3]]	1.767
	Gas Permeability [b]	k_{H_2}	[m^2]	1E-14
	Porosity	ϵ[c]	[1]	0.5
	Pellet Radius	r	[m]	35E-3
	Pellet Height	h	[m]	10E-3
	Graphite Height	h_{fin}	[m]	10E-3
	Pellet Mass[d]	m_{Mg}	[g]	124.1
	Tank's volume	V_{tank}	[kg/dm^3]]	2.518

[a] graphite and hydrogen thermal and physical proprieties are estimated by ™Comsol's database.
[b] Estimated by Carman-Kozeny equation 3.30.
[c] Ratio between empty and total pellet volumes.
[d] Total mass of Mg based material inside tank.
[e] [209] at 573K.
[f] Estimated by proper thermal characterization

3.3.2 Results

Here, the results of numerical simulation performed on macro model were reported. Hydrogen pressure, temperature of metal hydride's bed and reacted fraction data were collected in proper experimental set up and compared with results of numerical simulations performed on macro model, in order to evaluate the goodness of storage tank's modeling.
Desorption case was initially analysed. Experimental procedure involved in the discharge of small aliquot of hydrogen from tank at specific time, t_d (with i, from 1 to 13), decreasing hydrogen pressure in the tank and forcing the desorption process. For simulating experimental procedure, a series of step (rectangle) functions centred on t_d, eq. (3.33), were implemented in the macro model with the aim to simulate experimental procedure.

$$m_{H_2}^{tot} = \sum_{d=1}^{13} m_{H_2}^{d} \delta_{t_d} \tag{3.33}$$

where $m_{H_2}^{d}$ represent the quantity of hydrogen gas removed by the tank, at the time t_d. However, first results showed big discrepancy between temperature and pressure simulated and experimental data. For this reason, assuming that heater's temperature was constant for the overall period of measure, it is possible to suppose that temperature's gaps could be caused by changing in the thermal contact between Mg-pellets and graphite's elements. This can be supported by several factors as change in density between hydride and metal phase transition (pellet's volume decreases for desorption reaction) or crumbling of pellets due to the cycling process. For these reason, a proper time decreasing thermal contact's resistance between graphite's fins and pellet was introduced in the macro model. The value of thermal resistance has been extrapolated at the end of each desorption step, when magnesium and hydrogen system was assumed at pseudo equilibrium conditions and assuming thermal losses constant for overall desorption study.
In fig. 3.11, experimental data obtained by desorption reaction of Mg-based material were compared with results of numerical simulation obtained by macro model. Simulated pressure and reacted fraction values are almost in agreement with experimental data. However, they showed little discrepancies. These are due to several factors as: not proper hydrogen mass subtract to the empty space of tank ($m_{H_2}^{i}$ of eq. (3.33)) or the incorrect estimation of empty tank's volume. Such defects impacted even on the pressure data which were slightly overestimated respect to the experimental ones. Nevertheless, simulated temperature data showed a considerable discrepancy respect to the simulated data. That could be justified by previous cited reasons, as well as a not perfect placement of thermocouple in the pellet. Unfortunately, experimental set up didn't provide any additional thermocouples to check temperature in other point

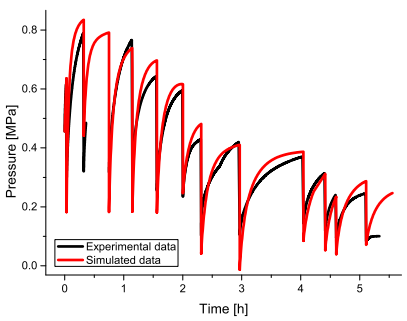

(a) H_2 *Pressure.*

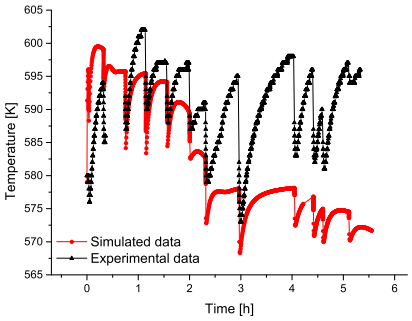

(b) *Temperature.*

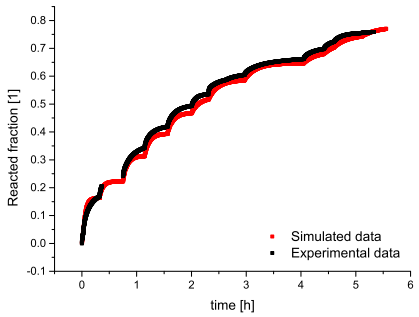

(c) *Reacted fraction.*

Figure 3.11: Numerical simulation performed on desorption reaction of Mg-sandwich tank. Black curve are the experimental data.

of tank.

Finally, absorption case was investigated. Analogously for the desorption study, experimental procedure involved in to introduction of fixed amounts of hydrogen gas in the tank, in order to increase the pressure and to force the absorption reaction of hydrogen on Mg-material. In this case, only three step of adding gas were involved at time t_a. For this reason a proper step function (similar to eq. (3.33)) was implemented in the numerical model.
A constant thermal contact resistance were introduced between graphite's fin and magnesium pellets. Numerical simulation performed on COMSOL, reported data about reacted fraction, pressure and temperate in good agreement with experimental one, as shown in fig. 3.12. Even here, temperature data showed the most relevant deviation respect to experimental one, probably due to incorrect estimation of thermocouple's position. Despite of this, simulated temperature data followed a trend

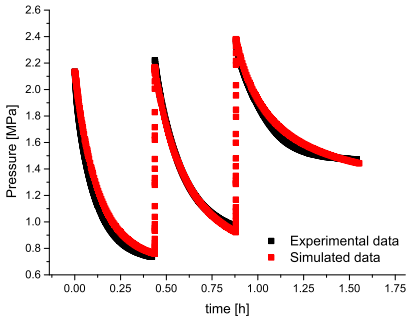

(a) H_2 *Pressure.*

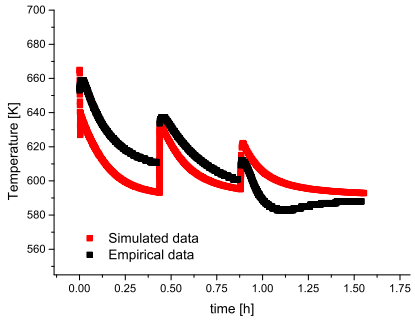

(b) *Temperature.*

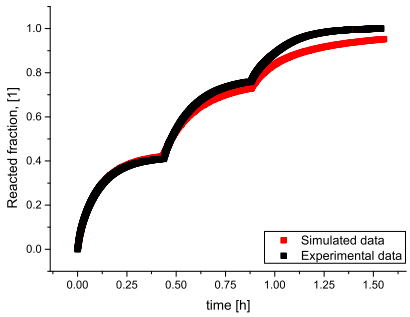

(c) *Reacted fraction.*

Figure 3.12: Numerical simulation performed on absorption reaction of Mg-sandwich tank. Black curve are the experimental data.

very similar to the experimental one (fig. 3.12(b)), supporting the incorrect position of thermocouple as possible reason for data's discrepancy.
At the end, it was possible to claim that numerical simulation results demonstrated the potentialities of macro model, hereby developed, to describe physical parameters in a hydrogen storage tank during hydrogen absorption and desorption reaction. An improvement in the collection of temperature data could be improve reliability of macro model.

3.4 Lumped model

3.4.1 Introduction

Mathematical simulations have a strongly role in the design and optimization of hydrogen storage tank. However, numerical simulations require a well-knowledge about chemical and physical aspects of hydrogen interaction with metal hydrides.

This means to deeply study: mechanisms of reaction, driving force relation, temperature dependence and finally to characterize itself material in order to obtain thermodynamic and kinetics data, useful for numerical simulation. Moreover it is necessary to well-known boundary condition of system, as thermal conductivity of every element, geometrical disposition and dimensioning. So, they can optimize and facilitate the work about the design of tank, but they require the development or application of a suitable and in same case complicated physical model, coupled with a well-expertise, as well as the utilization of powerful software (i.e. COMSOL or FLUENT) [37, 204, 210–213]. Aim of this work is to present a suitable, reliable and simple numerical tool for the development and modeling of high density storage tank with metal hydrides. Model, hereby developed, can describe in first approximation best design for hydrogen storage tank based on metal hydride and in particular it is been utilized to simulated magnesium hydride as active material, but it can be applied on any metal hydride, it is sufficient to introduce correct mathematical formulation of kinetics and suitable thermodynamic data of equilibrium reaction, obtained by micro scale model evaluation. Point of strength of this model is the simplicity, how it is reported in next part of document, mathematical formulation of model is relative more affordable respect to previous one but at the same time fitting very well with results from a more complex model solved by more robust approach and software, as COMSOL. Lumped model is been checked with numerical simulation (FInite Element Method, FEM) performed with a complete physical model ran on ™COMSOL software, developed in previous section of document. In particular, Magnesium hydride is been utilized as example material.

3.4.2 Methods

Lumped model is a further approximation of physical model introduced in the previous section. It means to reduce the description of a generic physical system into discrete entities under fixed assumption, in particular, it introduces constitutive equation (i.e. Darcy's law, analogies between thermal and electrical conductivity/resistance, etc...) assuming material domains like a continuous material, distinguishing domains of single element as pellets or fins. Advantage points of this formulation is the simplicity respect to more complex models, which may includes, complicated PDE's solution. Results of lumped modeling can be utilized only like guidelines for further investigation or as the base on to develop a hydrogen storage tank. Two parameters are introduced to evaluate the performance of a tank: R_{TH} and $R_{KP,}$ which represent thermal and gas diffusion resistance inside tank. It is interesting to note as particular combinations and targets for a tank (flux of hydrogen, hydrogen storage, working temperature, volumetric density, etc.) can be achieved with specific value of such two merit's figures. Such values keep in consideration every possible geometric and design parameter and can be utilized to optimize a specific aspect of tank (heat or

gas diffusion). Limiting some important parameters, as volumetric density, working temperature and exchanged hydrogen flux, it is possible to choose the best or minimal engineering options about the realization of tank (dimensioning of fin, conductive material, geometry, etc) with the specific performance. In this way, it is possible to easily obtain simple output parameters for the developing of a hydrogen storage tank based on magnesium hydride and to dimension it about some input parameters (flux, total capacity, etc.), obviously, knowing parameters of inner materials (thermal conductivity, porosity, etc.). Vice versa, inserting output data (as geometry of tank) it is possible to evaluate the useful working time at a particular flux of hydrogen, as well as final hydrogen pressure inside tank and the goodness of its design.

3.4.3 Mathematical formulation

Here, the theoretical approach for the development of lumped model is reported. Firstly, some important assumptions are introduced:

- Overall tank is approximate as a continuum domains, even distinguishing every inner elements (fins and pellets).
- Model estimates only average or effective value of temperature and pressure inside tank.
- Lumped model considers whole storage tank at stationary state. It means kinetics rate of hydrogen absorption or desorption by HSM coincides with the flow of gas introduced or expelled by tank. This condition is resumed in eq. 3.34.

$$v_{H_2}^{flow} = v_{kin} \tag{3.34}$$

Last one is the core of lumped model. $v_{H_2}^{flow}$ represents the hydrogen release or uptake flow required by tank, while V_{kin} is the proper reaction rate of material, function of pressure and temperature inside tank as well as by the type of stored material and its limited mechanism of reaction. Considering magnesium hydride, and metal hydride in general, kinetics rate is well described by eq.3.1,

$$v_{kin} = f(\theta)D(P)A(T) \tag{3.35}$$

which assumes reactions rate dependent by three terms: reacted fraction (θ), pressure (P) and temperature (T), as described in the first section of this document's chapter, about micro scale model analysis.

About $f(\theta)$, nucleation and growth model has been validated for the description of

hydrogen sorption process on Mg based material. So, f(θ) term is:

$$f(\theta) = n(1-\theta)(-ln(1-\theta)))^{1-1/n} \tag{3.36}$$

where n, JMAK coefficient, assumes n=1 for absorption and n= 3.5 for desorption phenomena.
$D(P_{eq}, P)$ and $A(E_{att}, a_0, T)$ terms include the impact of pressure and temperature on the kinetics performance of hydrogen storage material. However, the type of layout and supporting material used to realize the hydrogen storage tank impact on these terms. In the next sections, these terms are examined.

Temperature modeling

Mathematical representation of $A(T)$ is the Arrhenius relation.

$$A(T) = k_0 e^{-\frac{E_a}{RT_{eff}}} \tag{3.37}$$

Where E_a and k_0 are activation energy of sorption process and the co-factor. Such parameters can be extrapolated by proper kinetics analysis on investigated HSM. The real unknown variable is the temperature which is generally modelled with the robust and reliable three dimensional heat equation ($\frac{\delta T}{\delta t} - a\nabla^2 T = Q_s$, where a is the thermal diffusivity and Q_s is the heat flow, if it is present) and proper starting and boundary conditions. However, the scope of this lumped approach is to strongly simplify the description of heat phenomena in the hydrogen storage tank. For these reason, lumped model summarizes all thermal process that occurs during sorption phenomena in a *effective* temperature T_{eff} and whole heat fluxes pathway in a proper thermal resistance, R_{th}, which considers the layout of tank (design and supporting material).
For a simple geometry as reported in fig. 3.13, (but it is possible to extend this approach on other layouts), model assumes *effective* temperature with follow consistent relation (eq. 3.38):

$$T_H - T_{eff} = \Delta T_{eff} = U_{H_2} R_{TH} \tag{3.38}$$

Where, T_H is the temperature of heater source, while ΔT_{eff} is the difference of temperature between that and T_{eff}. It is function of the heat power required by storing material to release or uptake a known flux of hydrogen, U_{H_2},(easily obtained by enthalpy of reaction, ΔH_{H_2}) as well as thermal resistance of tank.
Goal of lumped model is not to describe or collect temperature data in every point of simulated domains but to estimate average temperature drop in the tank. For this reason an effective value of thermal resistance can be estimate, as representative of goodness of tank layout. R_{th} includes thermal conduction, dimension and layout of el-

ements within storage system, incorporating also thermal contact resistance between interfaces and any components. Representing thermal diffusion as electrical analogy,

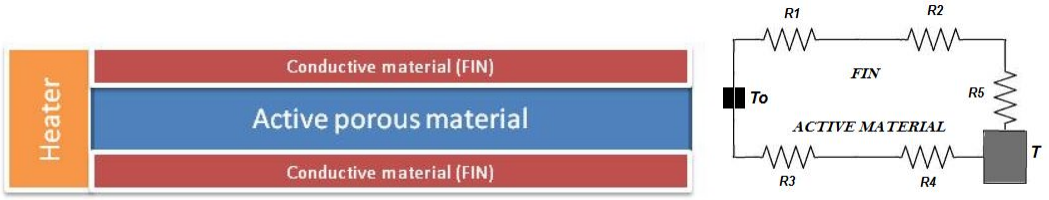

(a) *2D Axial Geometry.* (b) *Equivalent electrical circuit.*

Figure 3.13: (a), 2D axial-symmetrical model of generic inner layer of hydrogen storage tank with cylindrical layout. Stored material is in blue, placed between two high conductive fin (red color). Heater is placed in the middle side of tank. In the (b) figure, the relative electrical analogies for thermal resistance is reported.

it is possible to approximate thermal flux, U_{H_2}, and efficacy temperature drop,ΔT_{eff}, like current flux and differential of voltage through an electrical circuit with suitable thermal resistances as in electrical case. For a simply geometry as showed in fig.3.13 , model calculates R_{th} value as composed by two thermal resistance in parallel, which includes additional thermal resistances in series: first one is thermal diffusion long pellet and second one is long high conductive fins present inside the tank. More specifically, thermal resistance reported in fig. 3.13 are:

- R1, thermal contact resistance between heater and fin,
- R2, thermal conductive resistance long fin,
- R3, thermal contact resistance between fin and active material,
- R4, thermal contact resistance between heater and active material,
- R5, thermal conductive resistance long active material,
- R6 (not sign in fig. 3.13), thermal conductive resistance long active material from fin to the center of pellet (axial direction)
- R7 (not sign in fig. 3.13), thermal conductive resistance long fin material to the surface of pellet (axial direction)

Lumped model considers thermal resistance as formed by contact and conductive resistance inside tank and evaluate them with mathematical formulation reported in tab. 3.11:
Thermal contact is defined by proper empiric surface resistance (γ) and the area (A)

Table 3.11: Contact and conductive resistance mathematical formulation.[214] d_{mean} is estimated as $(r_{pellet} + r_{heater})/4$, which identifies an average lateral surface of pellet.

Thermal resistance	Mathematical formulation
Contact	$R_{cont} = \frac{\gamma}{A}$
Conductive	Axial:$R_{cond} = \frac{\frac{d}{4}}{A\lambda}$
	Radial:$R_{cond} = \frac{ln(\frac{d_{mean}}{d_{heater}})}{2\pi h\lambda}$

involved in thermal exchange, while h is the height of single pellet. Axial conductive resistance of pellet is calculated for cylindrical coordinate at distance equals to a quarter of height of pellet and radius equals to d_{mean} because at this quote, temperature is assumed to be representative of whole material pelleted. So, effective thermal resistance of tank can be expressed as eq.3.39,

$$R_{th} = \frac{1}{\frac{N}{R1+R2+R5+R6+R7} + \frac{N}{R3+R4}} \tag{3.39}$$

N is the number of layer considered into the tank. Consequently, temperature drops can be expressed correlated to required flux of hydrogen, inserting it into eq.3.38:

$$\Delta T = R_{TH} U_{H_2} = R_{TH}\Big(\frac{\overrightarrow{w_{H_2}}}{PM_{H2}}\Delta H_{H_2}\Big) \tag{3.40}$$

ΔH_{H_2} is the enthalpy of the sorption reaction which occurs into tank, while w_{H_2} is the mass flow of hydrogen come out or come in the tank. Finally, estimated temperature inside tank can be assumed to be as $T_{mean} = T_H - \Delta T$, with T_0, constant temperature of surface heater.
Finally, R_{th} term represents an estimation of the thermal resistance of tank, and it can be used as merit's figure to distinguish different investigated layout.

Pressure modeling Mathematical representation of $D(P)$ has to be identify in a proper kinetics analysis. In this case we adopt a general linear normalized relation for absorption case, but it is possible to include a parabolic or other type of mathematical relations,

$$D(P) = P - P_{eq}, \tag{3.41}$$

while for desorption case,

$$D(P) = P_{eq} - P, \tag{3.42}$$

where P_{eq} is the equilibrium pressure of material, estimated by enthalpy and entropy of material through *Van't Hoff* relation, $P_0 exp(\frac{\Delta H}{RT_{eff}} - \frac{\Delta S}{R})$, at T_{eff}, where P_0 is 0.1 MPa. In hydrogen sorption phenomena, pressure is the real driving force of the process of absorption and desorption reaction of metal hydrides. As for temperature, little variation of this value can strongly affect kinetics of material. In metal hydride, a low gas permeability due to too high compression or very low porosity of pellets can raise diffusive resistance phenomena inside itself material. Consequently, an elevate gap between external, P_{ex}, and internal pressure P_{eff} of pellet can strongly impact on the reaction kinetics.
As for temperature, an efficacy pressure value is assumed into the pellet structure. We assumed the value of P_{eff} at d_{mean} distance. Pressure is considered constant long the axial direction of material because gas outlet/inlet is placed on the lateral surface of pellet (right side of fig. 3.13). Aim of the lumped model is to estimate value of pressure drop between external pressure (applied by outside of tank) and such efficacy pressure. For this reason, pressure drop inside pellets is approximated with Darcy's law in porous media. Darcy's expression (eq.3.43) correlates pressure drops to flux intensity of a fluid, similar to the previous electrical case:

$$\overrightarrow{v_{H_2}} = \frac{K_p}{\eta} \nabla P \tag{3.43}$$

where K_p is the gas permeability of pellet (estimated by proper experimental characterization) and η is the viscosity of fluid. Active material is considered as porous matrix and gas diffusion works only long radial direction of pellet, gas diffusion between borders of fin's graphites is not considered. So, pressure resistance (3.44) is obtained by expression of Darcy law for radial flux,

$$(P_{ex} - P_{eff}) = \overrightarrow{v_{H_2}} \cdot R_{kp} = \overrightarrow{v_{H_2}} \cdot \frac{ln\frac{d_{mean}}{r_0} B\eta}{2\pi K_p N h} \tag{3.44}$$

r_0 is the radius of pellet and B is the formation volume factor (represented by the ratio between gas volume in standard and working conditions). Finally, it is possible to estimate a efficacy pressure (eq.3.45) into the material,

$$P_{eff} = P_{ex} + R_{kp}\overrightarrow{v_{H_2}} \tag{3.45}$$

Once to have estimate efficacy values of temperature and pressure inside tank, it is possible to estimate speed of reaction. So, lumped model can evaluate performance and situation of tank at every moment. For instance, it is possible to value final reaction fraction for a tank with a defined inner geometry (R_{th} and R_{kp}) when it achieves a chosen external pressure, and vice versa.

3.4.4 Results

Lumped model has been compared with simulations performed on the same tank's layout by macro model, previously developed in ™Comsol software with FEM approach. Macro model has been already validated in previous part of this document, moreover it is widely claimed as a robust and reliable tool for the modeling and optimization of hydrogen storage tank.[205, 211, 215] Lumped model was compiled on ™EES software an equation-solving program that can numerically solve thousands of coupled non-linear algebraic.

In the next part of document the results of lumped modeling simulation on a certain tank's layout are compared with numerical output of macro modeling obtained by FEM approach (Comsol). EES software hereby used doesn't performs time dependent study on lumped modeling, for this reason, the physical variable as mean temperature, and mean pressure inside and external to the pellet are compared for a specific value of θ. In order to demonstrate the feasibility of lumped modeling as alternative tool for the optimization of tank's design, several simualtion are performed on modified tank's layout, compared with more reliable FEM modeling. In particular, we investigated on the variation of tank's performance, with different radius and height of pellets.

Geometry and boundary condition

Simulated geometry of tank is reported in fig. 3.14. Tank is composed by a series of alternating layer of pellets and high thermal conductivity fin (graphite). Both model (lumped and macro) adopt the same material's and system parameters, reported in tab. 3.10. Tank is considered as composed by cylindrical volume filled by an alternate series of fins and pellet of active material, in this case magnesium hydride addicted with 10% of graphite. In this configuration, heat flux goes from the discs' center to the external side (heater is placed in the middle of tank) from a proper heater element, while hydrogen can diffuse through the lateral face of any pellets (black arrows in fig. 3.14). Hydrogen diffusion in the fins-pellets borders is not considered. Comsol software adopts a reduced geometry, exploiting the symmetry present in the investigated layout. Numerical simulations take in consideration only hydrogen desorption case, assuming no variation in the volume of pellets. Investigation are performed considering a constant hydrogen flow extracted by the tank. We assume that a proper thermostat device is equipped in the system, which maintain center of tank's layout at constant temperature.

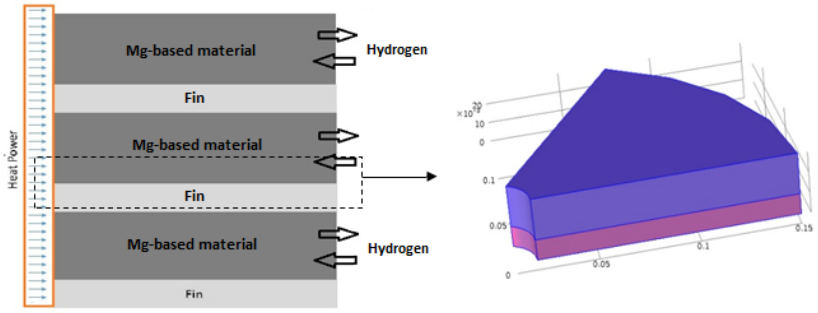

Figure 3.14: Tank layout and geometry used to compare the performance of results of lumped model respect to macro one. Highlighted region is the reduced domain simulated in Comsol software by FEM for symmetry reason.

Comparison of performance

Firstly, tank's layouts with different radius of pellet but constant volume of material (MgH_2)have been investigated.

Fig. fig. 3.15 reported the comparison of: pressure of hydrogen inside tank, (a),

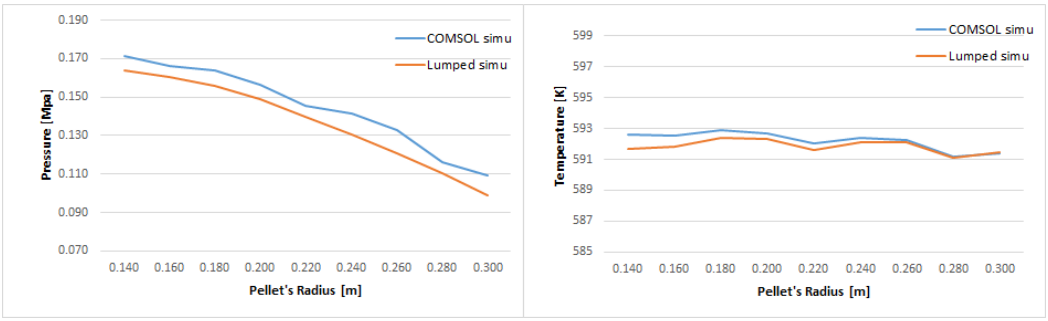

(a) *Mean External pressure.* (b) *Mean Temperature.*

Figure 3.15: Comparison of main physical variable (pressure and temperature) simulated by lumped model on EES solver, and macro model on multiphisics software (FEM approach) for different radius of pellets.

and mean temperature of materials, (b), extrapolated at $\theta = 0.85$ in the last part of sorption phenomena by numerical simulation performed on macro model (Comsol) and Lumped one (EES). Hydrogen flow was fixed at 2.5 g/min of hydrogen, on a total mass of 10 kg of pelleted MgH_2 (7.1 % of gravimetric density), distributed initially in 16 pellet with size of 15 cm of radius and 1.5 cm of height. Heater temperature was imposed at 600 K.

Results of the two modelling were quite similar. Temperature profiles obtained by lumped modeling, (b), was in agreement with macro modeling results performed

with FEM approach. For layout with bigger radius, temperature estimated by two modelling tended to coincide, while for smaller radius's layout, it diverged. This was probably caused by the increment of pellet's radius, which contributed to approach more the assumption of lumped model about efficacy temperature. Indeed, bigger radius-layout meant bigger contact surface between pellet and fin so, with a enhancement of thermal homogeneity in the material's domain. In this condition, the spread of temperature in the pellets was very narrow and the mean value approached the effective one, T_{eff}. Otherwise, smaller radius tended to increase the spread of temperature inside of pellet, shifting away from the assumption of lumped model.
About pressure, it is interesting to note as also lumped model revealed the identical behaviour identified by Macro modeling. As revealed by analysis on R_{th} and R_{kp}

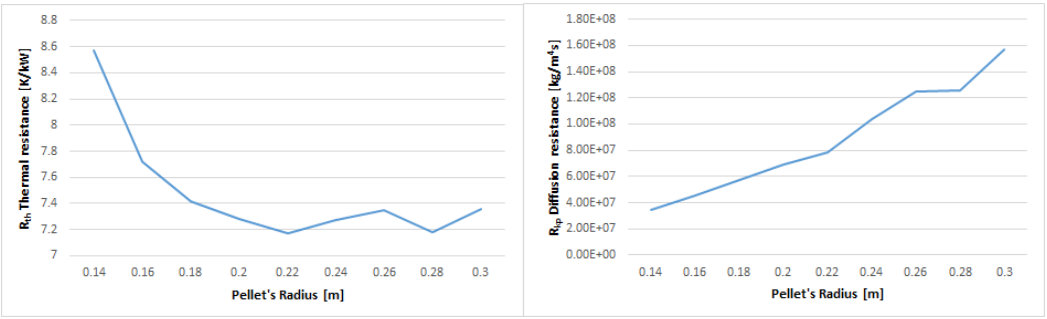

(a) *Estimation of thermal resistance R_{th}.* (b) *Estimation of gas diffusivity resistance R_{kp}.*

Figure 3.16: Thermal and gas diffusion resistance estimated by lumped model for different radius of pellets

terms (fig. 3.16), thermal resistance of tank decreased for layout with bigger radius for the reason exposed before. However for the same logic, gas diffusion resistance increased due to the stretch of gas' path. Consequently, external pressure dropped down, fig. 3.15(a), in order to maintain the constant flow of gas, increasing ΔP term.

Second investigation regarded the impact of pellet's heights on hydrogen storage tank. Some simulation were conducted on the same layout, previously described, changing the height of pellets but maintaining the identical volume of active material.
Fig. 3.17 reported the study conducted on tank layout reported in fig. 3.14 with different pellet's height. Performance of tank can be resumed in the value of external pressure at constant θ. High value of external pressure meant that hydrogen storage system was able to supply a continuous hydrogen flow for more time and so it was more performant. In the investigated case, the increment of pellet's height increased the thermal resistance correlated to the tank's design, reducing the capacity of thermosetting the pellets which iwass not more capable to reach high desorption kinetics

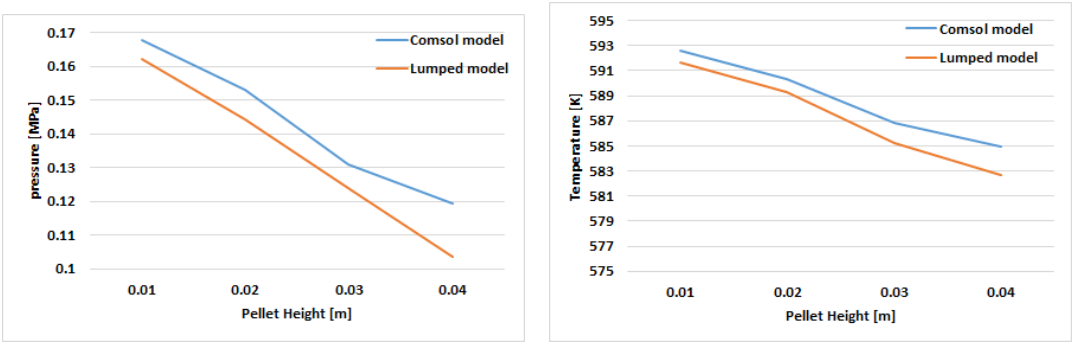

(a) *Mean External pressure.* (b) *Mean Temperature.*

Figure 3.17: Comparison of main physical variable (pressure and temperature) simulated by lumped model on EES solver and macro model on multiphisics software (FEM approach) for different heights of pellets.

and pressure. This can explained the deteriorations of performance for thicker pellet design, resumed in the reduction of external pressure.
In this case, the discrepancies between numerical simulation performed with FEM approach and lumped model (fig. 3.17) were bigger than previous case. This was probably due to the shift away from the assumption of lumped model where mean pressure and temperature were estimated to be constant in axial directions.
Also here, analysis on R_{th} and R_{kp} terms reported in fig.3.18 supports such considerations. Variations of pellet's height had no considerable impacts on gas diffusion

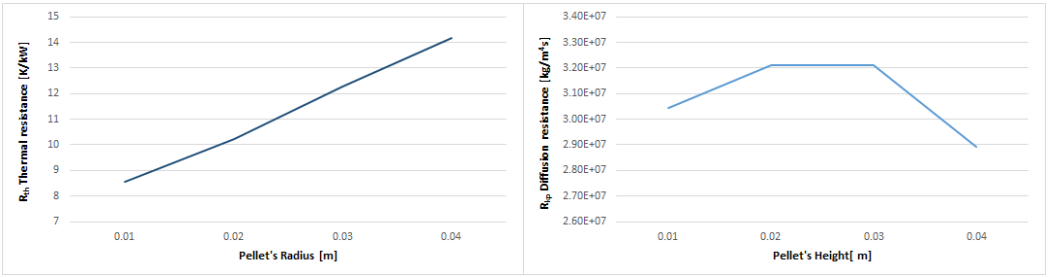

(a) *Estimation of thermal resistance R_{th}.* (b) *Estimation of gas diffusivity resistance R_{kp}.*

Figure 3.18: Thermal and gas diffusion resistance estimated by lumped model for different height of pellets

resistance. Indeed, R_{kp} values was almost constant in the investigated layouts, fig. 3.18(b). On the contrary, R_{th} strongly affected performance of tank when pellet design with higher thick were studied. This can be explained considering the stretching of thermal path caused by increment of thick of pellet, which contributed to a poor thermal diffusion and so, to a considerable lack of performance tank (in term of external

pressure and time working).

It was demonstrate as *lumped model*, hereby developed, is able to describe with a good approximation the results obtained by more complicated but reliable numerical simulations performed by powerful software (as Comsol, Fluent, etc..). Model has been developed to support the realization of hydrogen storage tank, to supply main guidelines for its development and for a preliminary analysis of performance. Moreover, it can be applied on more complex geometry (i.e. with more heater elements), identifying layout's symmetry.

3.5 Conclusion

In this section, it is reported the summary of the physical model to describe the hydrogen storage in generic HSM. The main goal achieved are:

- Novel kinetics model has been developed (Limited NG model), based on the most general nucleation and growth approach, to describe and explain sorption phenomena in HSM. *Limiting growth NG model* were successfully applied to describe absorption phenomena on Mg base material.

- A complete mapping of kinetics mechanism of hydrogen absorption and desorption phenomena were realized in the investigated range of pressure and temperature. Extrapolated kinetics parameters as apparent activation energy agree with literature data, validating the kinetics model here presented.

- A macro model for the description of complete hydrogen storage tank has been realized on the base of micro kinetics modeling developed on Mg-based material. Macro model includes thermal and gas diffusion phenomena in the inner structures of tank (fins and pellets) coupled with sorption kinetics of HSM. Absorption and desorption kinetics reactions were modelled on the base of the results of kinetics analysis performed in the previous section on Mg materials, which includes temperature and pressure dependence of sorption rate. Sorption data on absorption and desorption processes have been compared between a real experimental set up and numerical simulation performed on identical tank's geometry replicated in ™COMSOL software at the same initial conditions. Numerical results are in agreement with experimental data however reporting a strong discrepancies about metal hydride bed's temperature in desorption ans absorption case. This could be probably due to a several factors: firstly a changing in the thermal contact proprieties of magnesium's pellets (properly for desorption process where pellets involves in a volume reduction) and secondly

to a possible incorrect position of temperature's probe in the simulation data.

Macro model, hereby exposed, has been developed and applied within EDEN project. The EDEN project addressed successfully the development of a new storage material with high hydrogen storage capacity, loaded into a specifically designed storage tank managed in real-time and integrated into a complete power conversion system (PCS) for stationary applications and at support of distributed grid level applications.
In this context, macro model was applied for the optimization of hydrogen storage tank's layout, based on Mg material developed within EDEN project. Any inner components of tank's design have been optimized in order to maximize hydrogen sorption rate, reducing temperature gaps between thermostat elements and the active material's pellets, as well as to guarantee a sufficient hydrogen permeability in the porous structure of fins and pellets (fig. 3.19). A proper geometry of tank, including distribution of pellet was optimized by several numerical simulations in order to increase the probability of a one shot-one strike approach for the prototype construction, and to reduce the back-and-forward resource consuming empirical approach.
Hydrogen storage tank were realized within EDEN project based on the design/lay-

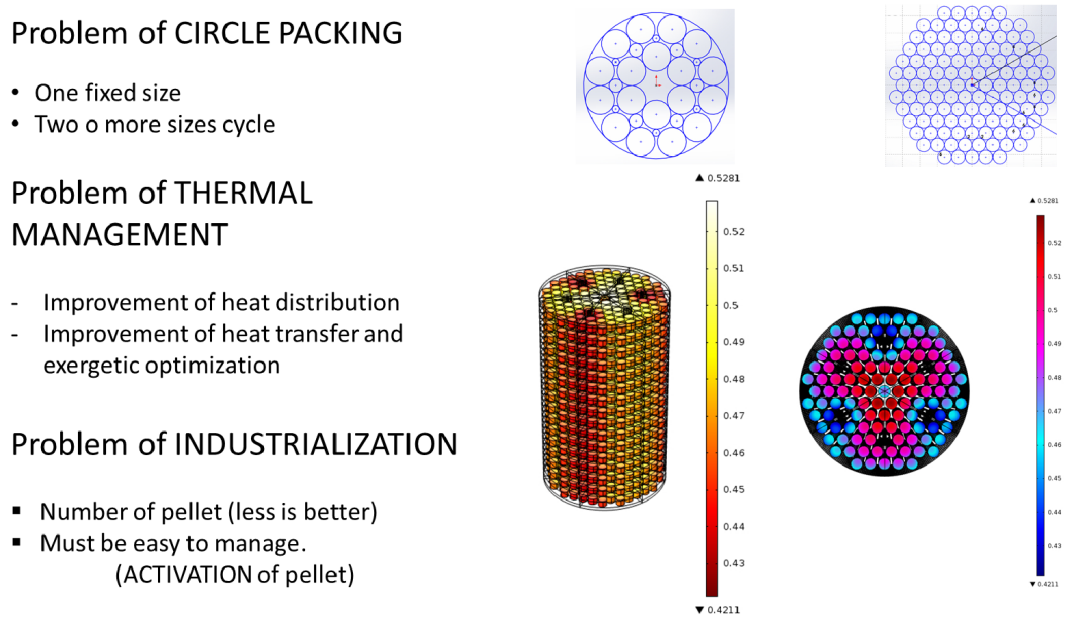

Figure 3.19: Optimization of tank's layout for hydrogen storage application must keep in consideration several issues as thermal and gas diffusion in inner structure of tank, distribution and stacking of pellets.

out identified by numerical optimization. Then, tank was implemented in the PCS's prototype, encountering the needed characteristic of system in terms of working

temperature and hydrogen absorption and desorption rate, and contributing to the successful of the project.

(a) *EDEN's team.*

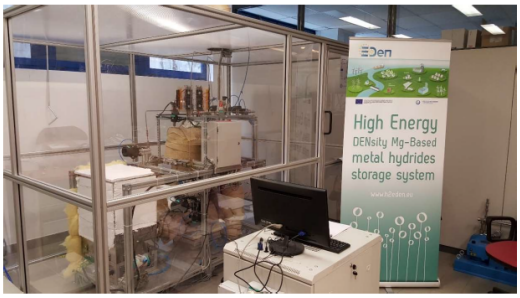

(b) *P2P prototype.*

Figure 3.20: In (a), overall EDEN team with the first prototipe of hydrogen storage tank based on numerical optimizations conducted on macro model hereby presented. In (a), the whole PCS prototype. It is possible to note the reversible solid oxide fuel cell on the left, and the huge version of hydrogen storage tank incorporated in the structrue of prototype.

- Lumped model, hereby developed, was able to describe with a good approximation the results from more complicated and reliable numerical simulations performed by FEM software (as Comsol, Fluent, etc..). Model has been developed to help the realization of hydrogen storage tank, and in particular, to supply main guidelines for its development. Results from lumped tool were compared with previously illustrated macro modelling solved by FEM software (Comsol Multyphysics) with the same parameters, initial constraints and system's geometry. Final output are in agreement with more detailed and reliable results of FEM's numerical simulation. Two macro parameters (R_{th} anf R_{kp}) were identified as merit's figure for a preliminary estimation of tank design's goodness.

4 Novel Mg based material for hydrogen storage application

Abstract

Hydrogen storage applications require reversible material able to absorb and release hydrogen rapidly. In this context, magnesium hydride is considered as one of the possible solutions to successfully store big quantity oh hydrogen in systems with relative high gravimetric and volumetric density. However, the use of MgH_2 has to face many limitations as high thermodynamics stability The consequence is to have high working temperature and a slow kinetic of absorption and desorption. In last years, many researches focus their efforts to improve thermodynamic and kinetic limitations correlated to magnesium hydride. Among them, the introduction of proper metal oxides has revealed a strong catalyst's behaviour, improving kinetic performance of pure magnesium. In this work, it is presented a Mg-based material where Nb_2O_5 catalyst is directly deposited on the powder's surface, approaching two targets: to introduce extremely small amount of expensive catalyst and placed it directly on the surface of magnesium where it is possible to exploit its maximum contribution in terms of reaction kinetic. The improved material has been compared with the no catalysed samples. Catalyst has a great effect on absorption reaction, reducing its apparent activation energy, moreover, the increment of kinetic rate can be also attribute to the physical introduction of catalyst which acts as multiple nucleation seed. The deposition of Nb_2O_5 impact even on the desorption reaction. However, it doesn't change its apparent activation energy. It impacts indeed on desorption phenomena increasing the available nucleation seeds for the growth of transformed phase, such as the absorption case.

4.1 Introduction

Nowadays, magnesium hydride is one the most prominent materials for hydrogen storage application due to the high theoretical gravimetric capacity (7.6 %), volumetric density (110 g/l) as well as the relative cheaper cost[216]. Hydrogen sorption reaction in Mg material involves in a phase transition from ionic MgH_2 lattice to *hcp* metal structure of Mg, and viceversa, with the evolution or absorption of hydrogen gas at characteristic equilibrium pressure, P_{eq}, function of the temperature. There are two main limitations for the industrial and commercial application of Mg-based hydrogen storage system. Firstly, despite of hydrogen-magnesium reaction occurs even at low pressure and temperature condition, it requires elevate temperature (excess of $300^{\cdot}C$) in order to achieve appreciable working pressure (0.1 MPa), due to elevate thermodynamics stability (ΔH = 75 kJ/mol and ΔS=133 J/$(K \cdot mol)$). The second bottleneck regards the slow kinetic of hydriding and dehydriding reaction, which are ascribed to several reasons: the extremely low conductibility of hydride bed when it is incorporated into proper storage tank [118, 120], the low diffusion coefficient for hydrogen into magnesium hydride, the formation of oxide layer on the surface of Mg particles and the low H_2 dissociation rate at magnesium's surface.[217–219].
In the last years, many journal papers have reported several methodology to improve hydrogen sorption kinetic and thermodynamics proprieties of magnesium based material. Principally, we can divide all them in three distinctive approaches: destabilization of Mg-H system, addiction of catalyst and reduction of size of Mg crystal.
Thermodynamics destabilization of H-Mg system aims to introduce in Mg lattice different elements [220, 221], compound or structural defects to form new alloy or solid phases, with the scope to significantly reduce hydrogen bounding enthalpy, or intermediate state leading to multiple-plateau system. Scientific literature reports several study on this topic, where group IV (Si-Ge-Sn [222–224]) and transition elements (Ni-Cu-Co-Fe [222, 225]) are used to form inter-metallic phase and alloys with improved performance. However, the introduction of heavier elements in considerable concentration respect to Mg reduces hydrogen storage capacity of materials.

Secondly, the shrinking of the Mg crystal size is a procedure widelu used to reduce the hydrogen diffusion path in the metal and hydride lattice. Hydrogen atoms diffuse quickly in the grain boundaries and through the defects of the crystal's domain while they diffuse slower in the metal lattice. Here, ball milling is one of the most widely process to obtain material with more favourable kinetic for hydrogen storage application. Magnesium powder is placed in a rotating cylinder or conical mill with a constant flow of inert grinding media. The collisions between the grinding media and the metal cause fracturing particles thus reducing the particle size, creating defects, cracks and fresh surfaces.[34, 226]

Addiction of graphite is another widely approach to increase kinetic and processability of hydrogen storage materials. As reported by Huang et al. [227], graphite improves desorption kinetic due to the interaction graphite-MgH_2. Moreover, the use of carbon additives during HEBM process have many advantages, not only as sorption properties enhancement, but even for heat dissipation and Mg particles covering, with improvement on material cycling.

Last approach regards the improvement of kinetic proprieties introducing proper catalysts, which enhances dramatically the kinetic of the system without affecting substantially the gravimetric capacity of magnesium hydride. Catalyst acts on the surface of the particles, supporting the dissociation of the hydrogen molecules and leaving the atoms to diffuse in the metal lattice during absorption reaction. The addition of transition metal oxides in small quantity (0.5-2 mol%) speeds up the absorption and desorption reaction by several times, as demonstrated by Oelerich et al. [24], Friedrichs et al. [228], Hanada et al. [229], Friedrichs et al. [230]. Nb_2O_5 as catalyst is reported to be superior to all other investigated catalysts for hydrogen sorption.[187, 231] Investigation on the nature of the oxide catalytic role reveals that the catalytic activity is related to a specific propriety of the Nb_2O_5 surface and correlated to the amount of oxygen on the surface of material.[232]

Generally, Nb_2O_5 catalyst is introduced during HEBM process, allowing a intimal penetration of catalyst with the Mg particles for mechanism grinding. Barkhordarian et al. [187], Friedrichs et al. [228], Hanada et al. [229], Friedrichs et al. [230], Barkhordarian et al. [231], Zinsou et al. [233] reported a considerable catalyst's concentration, around 0.05-0.5 % mole or more. At the same way, other works exposed kinetic improvement on Mg thick films with catalyst deposition (in this case pure Nb metal) by means to sputtering techniques [191, 193], with catalyst concentration about 5 %, estimated by EDX technique.

Here, we foresees to bring novelty in catalytic activity in H2 sorption reaction by adding catalyst material directly as a coating onto the surface of the Mg particles, in order to fully exploit the catalyst surface properties. Physical methods for surface modification, applied to powders, include ion beam implantation, arc plasma evaporation, ion beam assisted deposition and magnetron sputtering. Radio-frequency magnetron sputtering has become one of the most widely used techniques for thin film deposition, due to its versatility and ability to produce homogeneous coatings of various materials (conductive, semi-conducting and insulator materials). Moreover, in order to achieve a uniform coating of the powders, the powders must be moved in the chamber to receive the evaporated atoms from the solid source (target) onto

its overall surface. For this reason, a suitable particles motion technique must be considered.

In this context, an innovative hydrogen storage material has been characterized. Material was produced employing high energy ball milling (HEBM-**H**igh **E**nergy **B**all **M**illing) process for magnesium based compounds production and physical vapour deposition (PVD) for catalyst (Nb_2O_5) addition. PVD techniques allows to achieve two target of this work. Firstly, the deposition of an extremely small mass of catalyst on Mg based material and secondly the direct deposition on the surface of active particles where Nb_2O_5 have the biggest impact on the enhancement of kinetic sorption mechanism. In this work, such material is presented and characterized in a range of temperature between 573-633 K and between 0.01-1 MPa of hydrogen pressure. Moreover, a kinetic analysis tents to interpret the kinetic mechanism of sorption reaction and its change with the introduction of catalyst.
In this part of thesis, kinetic performance of Nb_2O_5 sputtered Mg based material is reported. Firstly it is introduced the method followed, including materials used, characterizing instrument and procedures. Finally, kinetic measurements and analysis on investigated materials are shown with a proper discussion about the results.

4.2 Method

4.2.1 Material

Pure Magnesium material was purchased by Sigma Aldrich with 99.9 % purity and analysed exclusively as reference material to compare increasing performance of sputtered Nb_2O_5 procedure. Magnesium based material was produced by *MBN Nanomaterialia* by means to proper patented HEBM process within the European project EDEN (Seventh Framework Programme 2007-2013 for the Fuel Cells and Hydrogen Joint Technology Initiative). Sample includes an relevant amount of graphite (7%), with a theoretical hydrogen storage capacity of 7.1 %. BET analysis reports a surface area of 19.7 m^2/g.
A small aliquot **(53.1 mg)** of milled Mg material has been directly characterized while a second sample (50.6 mg) has been treated in sputtering instrumentation. In the next part of document, samples are indicate as: pure magnesium (Mg), milled graphite-Mg material (Mg-C) and Nb_2O_5 sputtered milled graphite Mg-sample (Mg-Nb).
Catalyst nano-layers deposition onto Mg powders surface were performed by means of RF sputtering. A proper vibrating probe has been developed in order to expose all surface of powder to the sputtering process. The vibrating sample holder is based on the use of a piezoelectric device platform. The piezo-device was directly equipped in the sputtering chamber. The device is controlled by a specific amplifier driven by

a signal generator, which is able to produce different types of wave shapes, different frequencies and amplitudes.
The transfer of magnesium powder under controlled atmosphere is an important step to avoid atmospheric contamination before and after coating and potential self-ignition of magnesium in contact with oxygen. In particular, it takes more importance for thin film deposition and for extremely air-sensitive sample as Mg. For that purpose, a compact vacuum tank was designed and built for the powder protected transfer. The realization of vibrating sample holder, its optimization and the production of sputtered catalyst layer were performed into the facility of FBK by PAM unit.
Nb_2O_5 films were deposited by RF plasma sputtering of a 99.99 % purity niobium pentoxide target. The films were prepared using Argon gas at low pressure. The samples were not externally heated.
The amount of catalyst deposited on the Mg-particles is extremely small. The maximum estimated concentration of catalyst Nb_2O_5 is between 50-100 ppm w/w. This value is an overestimation of deposited catalyst on magnesium sample, because it doesn't consider film's porosity and spherical shape of powder's particles, which negatively impact on deposited layer's growth rate.
Kinetic measurement were performed with Isochoric Differential apparatus (IDA), exposed in the second chapter of this thesis. The high resolution of instrument allows to contemporaneously characterize few tens mg of materials, performing a kinetic characterization at quasi-isobaric condition (± 0.003 MPa).
Mg samples was loaded in a proper sample holder of IDA. Charging procedure was conducted within Argon glow box to avoid air contact with the sample. Mg-samples were degassed overnight at 633 K at 1-5 Pa directly connected to a proper free-oil pump (scroll). Next, sample was activated with 10 fully cycle of hydrogen absorption and desorption at 1 and 0.03 MPa, respectively. Hydrogen gas purity was 99.9999%. kinetic and calibration operations were fully automatized by instrument's software.

4.3 Results

Kinetic measurements were conducted at 633-597-573 K at proper hydrogen pressure for absorption and desorption reaction. Hydrogen storage capacity was estimated by volumetric techniques (reported in chapter 2 of this thesis). It resulted equals to (7.6 ± 0.4) for Mg sample,(7.2 ± 0.4) for Mg-C sample and (7.1 ± 0.4) for Mg-Nb sample. In the next plot, normalized hydrogen sorption values were reported and expressed as reacted fraction θ (from 0 to 1), with an uncertainty of 0.05.
Sorption measure performed at 633 K reported hydrogen evolution during absorption and desorption reaction on Mg based materials. Speaking about absorption, fig. fig. 4.1(a), pure magnesium sample achieved fully saturation state at more than 20000 s, while Mg-C sample approached reacted fraction value of $\theta = 0.98$ at 2100 s and 4900

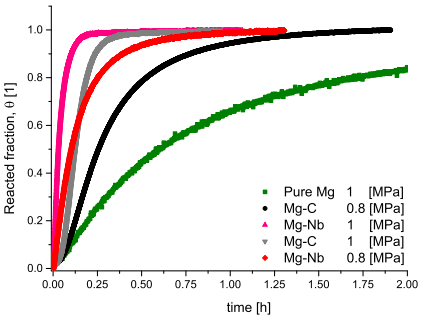

(a) *Absorption at 633 K.*

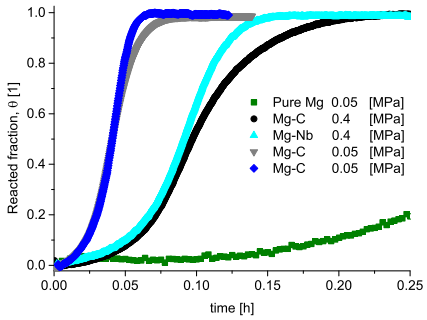

(b) *Desorption at 633 K.*

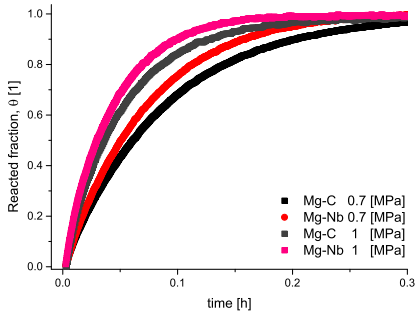

(c) *Absorption at 593 K.*

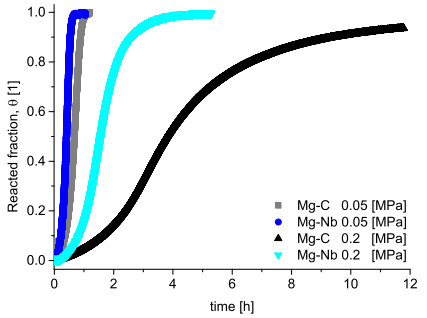

(d) *Desorption at 593 K.*

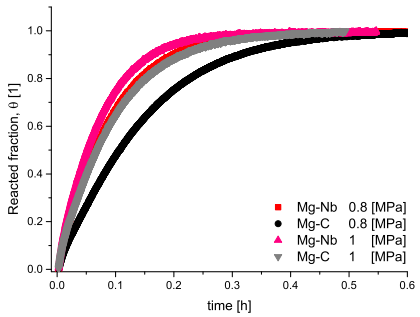

(e) *Absorption at 573 K.*

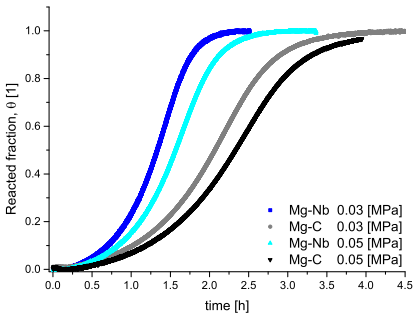

(f) *Desorption at 573 K.*

Figure 4.1: kinetic measurements on Mg, Mg-C and Mg-Nb samples. Study on Mg pure sample is reported only at 633 K for the extremely low kinetic of non-treated material (green curve). In absorption analysis ((a),(c),(e)), Mg-Nb sample are shown red/red-light color, while in desorption analysis ((b),(d),(f)), they are shown in blue/blue-light colors. Measures on Mg-C sample are reported in black/gray curve.

s for measurement performed at 1 and 0.8 MPa, respectively. Sample with sputtered catalyst (Mg-Nb) achieves identical hydriding state at 740 s and 3000 s, demonstrating

superior kinetic performance. Desorption study at the same temperature, fig. 4.1(b), revealed a strongly increment in the hydrogen release rate by milled samples respect to pure Mg. However, catalysed sample showed only slightly improvement on kinetic proprieties compared to no catalysed one. In this case, the pure Mg sample achieves a total conversion of $\theta = 0.98$ in approximately 2200 s, while milled samples in 300 s and 220 s for Mg-C and Mg-Nb samples. Catalysed and no milled materials differed only for the last half part of reaction ($\theta > 0.5$).
At 593 K, in absorption case (fig. 4.1(c)), Mg-C sample approached value of $\theta = 0.98$ at 950 s and 1250 s at 1 and 0.7 MPa of hydrogen pressure, respectively. Catalysed sample absorbed the identical quantity of H_2 in 570 s and 890 s for the same pressure conditions. In this case, the increment of kinetic performance due to the catalyst's layer seemed to be identical for the two measures. In Desorption case (fig. fig. 4.1(d)),the experimental data between Mg-C and Mg-Nb strongly differ edin function of hydrogen pressure applied. At low driving force conditions (0.2 MPa) performance's discrepancy was strongly evident between catalysed (H_2 desorption in 13000 s) and only milled sample which didn't approaches reacted fraction's value of 0.98 in the scale time. However, such gap was dramatically reduced in low pressure measures (high driving force, 0.005 MPa), where Mg-C sample fully completed desorption reaction in 3600 s while catalysed sample in 2200 s.
At 573 K, contribution of catalyst seemed to accelerate both sorption process. Absorption study, fig. 4.1(e), showed an improvement in kinetic rate of catalysed Mg sample. Mg-C sample was fully hydrided in 1300 s and 1800 s at 1 and 0.7 MPa, respectively, while catalysed sample totally reacted in 1000 s and 1200 at the same pressure conditions. Also, in desorption case, fig. 4.1(f), catalyst impact was evident, improving desorption reaction rate for measures performed at 0.03 and 0.05 MPa. In this case, Mg-C sample approached a reacted fraction value of 0.98 in 13000 s and 15600 s at 0.03 and 0.05 MPa. At the same conditions, Mg-Nb desorbed the same amount of H_2 in 7200 and 9200 s.
Considering kinetic measurements, we can confirmed as kinetic sorption was already improved in only milled Mg-C sample compared to the pure Mg sample. However, the introduction of Nb_2O_5 on the particle's surface further busted up sorption reaction, as confirmed in literature [187, 231, 234]. It was interesting to note as catalyst effect for all measures (fig. 4.1) played more relevant role at low driving force conditions, where working pressure was closer to the equilibrium pressure of reaction both for absorption and desorption phenomena.
From a first evaluation, the kinetic mechanism of H_2 sorption reaction seemed to be affected by the presence of catalyst, in particular for the high temperature characterization. Indeed, it was possible to observe a variation in the curve's profile of absorption data between catalysed and non sample at 633 K (fig. 4.1(a)). In this case, Mg-C sample showed a S-shape profile, proper of nucleation and growth kinetic mechanism, however, catalysed sample showed a different monotonic trend (fig. 4.1(a))

more pertinent to a contracting volume or diffusive models.[113]
JKMA model was applied on characterization data of catalysed material. The scope was to evaluate the kinetic sorption mechanism of catalysed materials and possible variation respect to no catalysed sample at different temperature conditions. JMKA model was widely applied to describe hydrogen kinetic sorption oh HSM [113]. JMKA model, known also as Avrami model assumes that hydrogen sorption reaction involves in three different process: nucleation on available site of product phase, growth of nuclei and their impingement. Mathematically, it is formulated as,

$$\theta = 1 - e^{-(kt)^n}, \tag{4.1}$$

where θ is the reacted fraction, t is the time, k is the kinetic parameter while n is JMKA coefficient. Nucleation and growth model theory assumes $n = q + d/m$, which represent: the growth dimensionality of nuclei's growth (d), the type of growth control (m=1, interface, m=2, diffusion) and finally, the type of nucleation process (instantaneous q = 0, linear q=1 or auto-catalyst q>1). The description and fit's procedure of NG model are reported in the previous chapter of this thesis.
The results of JMAK model were reported in tab. 4.1 for all kinetic measures performed on Mg-Nb sample. In Absorption study, nucleation and growth model fitted with very

Table 4.1: Fitting parameters extrapolated by data collected by Mg-Nb sample about JMKA model, eq. (4.1).

	ABSorption				DESorption			
T. [K]	P. [MPa]	n	k[1/s]	Adj. R^2	. [MPa]	n	k[1/s]	Adj. R^2
633	1	1.04	$6.22 \cdot 10^{-3}$	0.9944	0.046	3.97	$6.29 \cdot 10^{-3}$	0.9986
	0.9	1.04	$4.72 \cdot 10^{-3}$	0.9977	0.2	3.95	$5.00 \cdot 10^{-3}$	0.9986
	0.8	0.91	$1.78 \cdot 10^{-3}$	0.9944	0.3	3.04	$4.13 \cdot 10^{-3}$	0.9980
	-	-	-	-	0.4	3.65	$2.79 \cdot 10^{-3}$	0.9983
593	1	0.94	$6.91 \cdot 10^{-3}$	0.9995	0.052	3.78	$6.28 \cdot 10^{-4}$	0.9982
	0.9	0.94	$6.13 \cdot 10^{-3}$	0.9995	0.1	3.79	$4.62 \cdot 10^{-4}$	0.9982
	0.8	1.00	$5.21 \cdot 10^{-3}$	0.9994	0.15	3.62	$3.62 \cdot 10^{-4}$	0.9979
	0.7	1.03	$4.03 \cdot 10^{-3}$	0.9993	0.2	2.66	$1.52 \cdot 10^{-4}$	0.9970
573	1	1.02	$3.82 \cdot 10^{-3}$	0.9992	0.03	3.64	$1.92 \cdot 10^{-4}$	0.9981
	0.8	1.05	$3.05 \cdot 10^{-3}$	0.9995	0.05	3.54	$1.62 \cdot 10^{-4}$	0.9989
553	1	1.00	$1.80 \cdot 10^{-3}$	0.9985	0.03	2.99	$3.63 \cdot 10^{-5}$	0.9990
	0.8	1.07	$1.76 \cdot 10^{-3}$	0.9993	0.05	2.91	$2.71 \cdot 10^{-3}$	0.9983

well with kinetic data (Adj. $R^2 > 0.999$), though to a lesser extent high temperature absorption data (633 K). JMKA coefficient tended approximately to 1 for all absorption measures. This can be interpreted as due to one dimensional growth of superficial nuclei, instantaneously formed on the particle's surface at the begin of reaction.
On the contrary, desorption cases seemed more complex. JKMA coefficients took a

considerable spread of value between 2.66 and 4, identifying a different kinetic mechanism respect to the absorption case, analogously to the study performed on Mg-C sample performed in previous chapter. Generally, high values of JMKA coefficient identified simultaneous processes of nucleation (constant or branching) and multi dimensional growth. Values of n greater than 3 could describe the phenomena of continuous nucleation, where nuclei grow in three dimensional.
However, JMKA coefficients extrapolated by direct fitting could not represent the real mechanism of kinetic sorption, but an average value, as discussed in the chapter 3 about micro modelling of HSM. For this reason, the local n-coefficients of Mg-C and Mg-Nb sample evaluated by eq. 3.24 were compared in fig. 4.2. Even here, local n-terms were expressed in function of proper reacted fraction in order to compare the kinetic mechanism in relation to the progress of the hydriding or de-hydriding reaction. Analysis on local JMKA coefficient revealed as catalyst affects even the kinetic mechanism of reaction. Catalyst's impact was particularity relevant at high temperature where the n-terms (fitted by JMKA model or local n) had the biggest discrepancies, while it presented less or none significant for lower temperature process.
Considering absorption case (fig. 4.2(a)), the local n-terms were completely discordant for the Mg-C and Mg-Nb samples. In no-catalysed sample, the JKMA coefficients quickly achieved n=2, then it approached values equals to n=1 at high reacted fraction. In similar way, catalysed sample approached n=2 for the identical value of reacted fraction, however, n-terms rapidly decreased to 1 respect to Mg-C sample. The initial raising trend of n-terms is not completely understood, it can be due to a incubation process which delays the nuclei's formation, or to an effect of instrumental measurements or data's conditioning. The low temperature measures,fig. 4.2(c) and fig. 4.2(e), showed local JMKA coefficient very similar, with n-terms averagely equals to 1. However, even other kinetic model can be expressed by JMKA coefficient equals to the unit. In particular, shrinking or contraction volume model (CV) assumes identical value at the beginning of reaction.[113]. For this reason, an additional kinetic analysis were performed at 553 K on Mg-Nb sample,fig. 4.2(a) and fig. 4.2(b), to investigate on the prevalence of CV mechanism at the lower temperature.
Even at 553 K, local JMAK coefficient assumes value around 1, identifying the kinetic mechanism of absorption process as the linear growth of a fixed number of superficial nuclei or 3D-contracting volume. Last hypothesis is partially confirmed by fig. 4.3(c). Here, absorption data (θ) obtained at 553-573-593 K and same pressure (1 MPa) are linearised about 3D-shrinking volume model,(3.2), with following relation,

$$1-(1-\theta)^{1/3} = kt \tag{4.2}$$

In this way, absorption measures which followed 3D contracting volume are easily recognised by linear dependence with time. So, the absorption reaction at 553 K can be partially explained by contracting volume mechanism, while kinetic mechanism

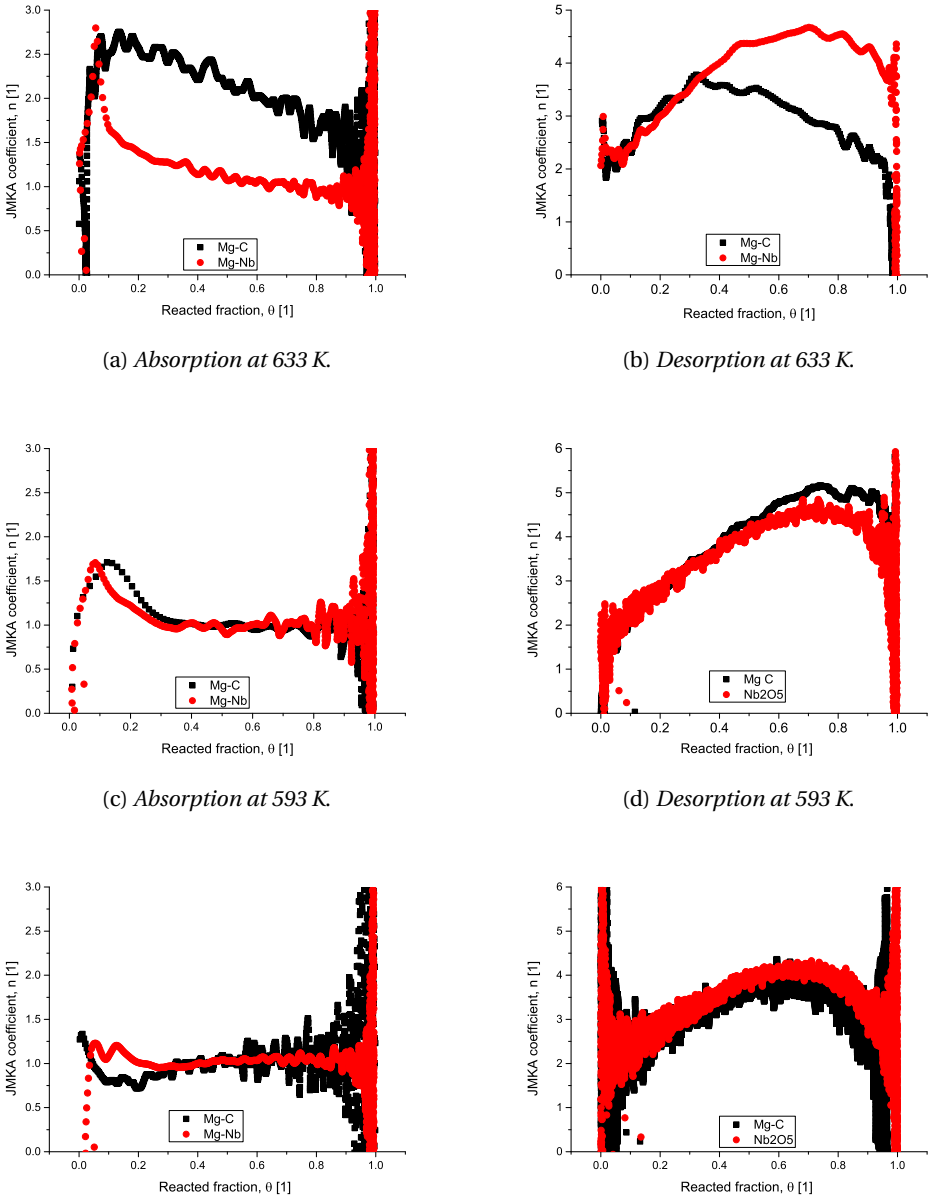

(a) *Absorption at 633 K.*

(b) *Desorption at 633 K.*

(c) *Absorption at 593 K.*

(d) *Desorption at 593 K.*

(e) *Absorption at 573 K.*

(f) *Desorption at 573 K.*

Figure 4.2: In these plots, the investigation on local JMKA coefficient extrapolated by eq. **eq. avrami n local** of absorption measures performed at 1 MPa and at 633 ((a)), 593 ((c)) and 573 K ((e)) and desorption one performed at 33 ((b)), 593 ((d)) and 573 K ((f)) for Mg-C and Mg-Nb sample, are reported.

involved in increasing contribution of 1-dimensional growth of already formed nuclei at higher temperature .
In desorption case (fig. 4.2(b)), Mg-C and Mg-Nb sample manifested the identical

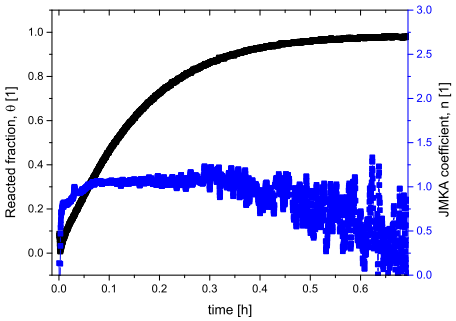

(a) *Absorption at 553 K and 1 MPa.*

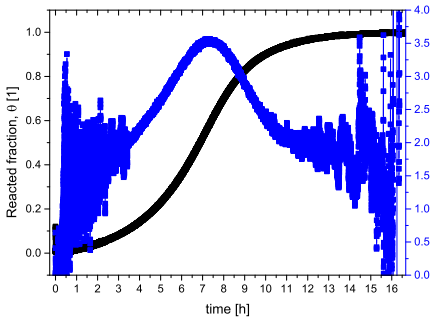

(b) *Desorption at 553 K* and 0.003 MPa.

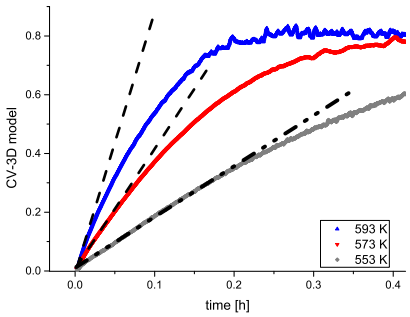

(c) *Linearisation of CV 3D model.*

Figure 4.3: Kinetic characterization performed at 553 K on Mg-Nb. In (a) and (b), absorption and desorption data are reported (black curves) with local JMAK coefficient (blue curves). In (c), comparison of CV-3D model linearisation for kinetic absorption performed at 553-573-593 K at 1 MPa. Black curves are only for eye's guide.

n-terms value up to $\theta = 0.4$. Then, their n-values began to diverges. In Mg-C sample n-terms decreased while in catalysed sample continued to raise up to value of 4.5 and then decreased for higher value of reacted fraction. For low temperature measures, JKMA coefficients were coincident for both catalysed and not sample.

Finally, driving force contribution and apparent energy of activation were extrapolated by experimental data. A proper kinetic analysis was conducted on such data, similar to the procedure followed in chapter 3 for Mg-C sample.
For absorption reaction, kinetic parameter (k) were extrapolated by nucleation and growth model (JMAK equation, 4.1). However, fittings of high temperature characterizations showed a poorer goodness respect to the other one (tab. 4.1). Indeed, they showed a more relevant variation in local n-coefficient during the sorption process (fig. 4.2(a)). For this reason, limited growth models, introduced in the previous section,

were applied on such data.
As reported in fig. 4.4(a), surface limited NG model described very well the absorp-

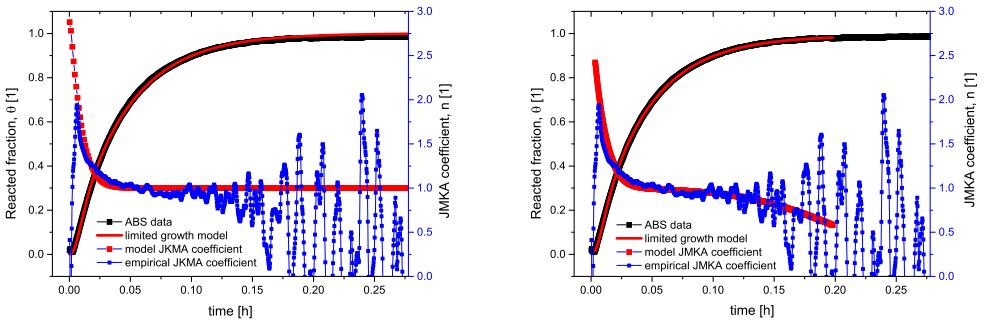

(a) *Surface constraint. (Adj.* $R^2 = 0.9963$*).*

(b) *Surface and radius constraint,(Adj.* $R^2 = 0.9998$*).*

Figure 4.4: Kinetic model applied on high temperature absorption measurement of Mg-Nb sample. In the plot, characterization obtained at 633 K and 1 MPa is reported and modelled by only surface and surface+radius limited growth model. Blue line is the local JMAK extrapolated by experimental data (black). Thick red lines are the local JMAK coefficient extrapolated by fitting data.

tion data at high temperature. So, k-parameters can be extrapolated by such model for HT measures, as demonstrated in previous chapter. It was interesting to note as also limited NG model which includes the spatial constraint relative to the radius of particles, reported in fig. 4.4(b), fitted more comprehensively the absorption reaction also at high value of reacted fraction. This supports the interpretation of hydrogen absorption reaction on Mg proposed by limited growth NG models.
The kinetic parameters (k) were successfully fitted with a parabolic relation, $\sqrt{P} - \sqrt{P_{eq}}$, where P_{eq} is the equilibrium pressure of magnesium, estimated by *Van't Hoff* relation (fig. 4.5). The goodness of data fitting was evaluated by the highest value of R^2 term (>0.995) compared to other driving force relation (reported in tab. 3.3). Next, the pressure-corrected constant rates were plotted in the Arrhenius's plot to extrapolated apparent activation energy's value.
Apparent activation energy for absorption phenomena has been estimated in (76 ± 5) kJ/mole with a temperature independent parameter (k_0) equals to ln(7.1 ± 0.9) [1/s].

For desorption study, parabolic relation ($\sqrt{P_{eq}} - \sqrt{P}$) showed the best data's fitting, fig. 4.6(a). In the same way of absorption analysis, also apparent activation energy for desorption reaction were calculated through Arrhenius's plot, fig. 4.6(b). Apparent activation energy extrapolated by desorption study is (127 ± 1) kJ/mole with k_0 equals to exp(18.7 ± 0.3) [1/s].

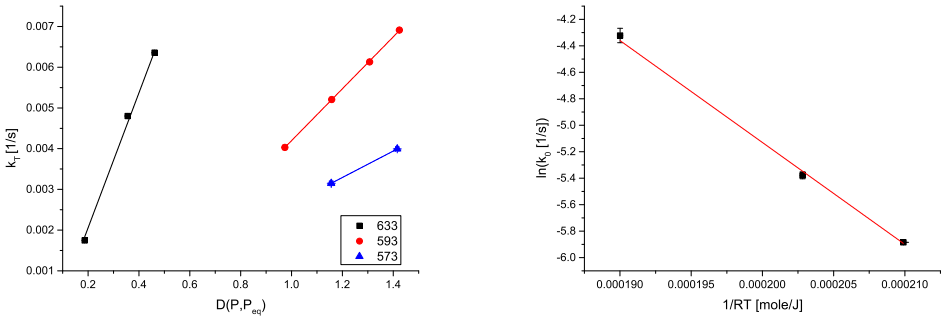

(a) *Driving force contribution.* (b) *Arrhneius plot.*

Figure 4.5: The kinetic analysis on absorption data collected on Mg-Nb sample. In (a) linear regression on pressure data are reported with proper driving force relation. In (b) linear fitting of pressure corrected constant rate are plotted in Arrhenius plot.

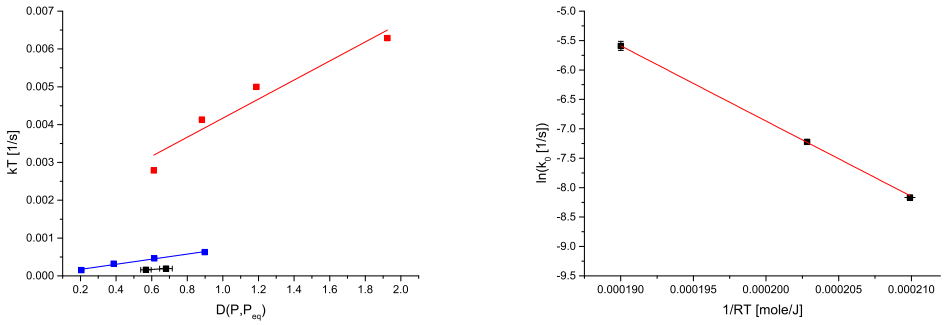

(a) *Driving force contribution.* (b) *Arrhneius plot.*

Figure 4.6: kinetic analysis on desorption data collected on Mg-Nb sample. In (a) linear regression on pressure data are reported with proper driving force relation. In (b) linear fitting of pressure corrected constant rate are plotted in Arrhenius plot.

4.3.1 Discussion

Catalyst improved the performance of hydrogen absorption and desorption reaction on Mg sample, fig. 4.1, but it seemed to act in different way for the two reaction.
In absorption case, the presence of Nb_2O_5 catalysed superficial reaction of dissociation of hydrogen [232], as result, apparent activation energy for catalysed sample (76± 2 [J/mole]) was less than the no catalysed sample (90± 2 [J/mole]). However, this didn't explain the variation of kinetic mechanism for high temperature measurement compared to the Mg-C case. A possible explanation can be correlated to the physical presence of catalyst on the surface of material, that acted as additional nucleation's

seed, increasing the number of available nuclei where phase transition began. This additional nuclei played a relevant role for measures at high temperature where nucleation rate and available nuclei are less than low temperature conditions. [180] The complete covering of powder's surface can be associated at the approaching of JMAK coefficient equals to 1, when reaction proceed only with one dimensional growth (radial direction) to the core of particle. Considering the measures at 633 K, this situation was achieved in Mg-C sample at high reacted fraction's value (more than $\theta > 0.9$), fig. 4.2(a). At the contrary, catalysed sample reached n=1 for θ = 0.4-0.5. So, assuming a isotropic growth velocity, it means that more nuclei were available on the surface respect to no catalysed sample, which contributed to cover all surface in less time.

For desorption case, it was possible to interpret kinetic performance's improvement as caused by a greater number of nucleation site, already available on the surface of particles at the beginning of the reaction. Indeed, apparent activation energy was basically identical for desorption process between Mg-Nb (127± 1 [J/mole]) and Mg-C sample (133 ± 7 [J/mole]), and it can not explain the speeding up of desorption rate. Such effect was particularity evident for low driving force measures (where external hydrogen pressure approached the equilibrium pressure, P_{eq}). In fact, a decrement of driving force increased the nucleation energetic barrier, which thus decreased the nucleation rate as reported by Uchida et al. [156]. But, desorption reaction on catalysed sample can rely on a higher number of nucleation's seed due to the catalyst's layer, which speeded up the reaction.
However, desorption basic mechanism is not so fully understood. The variation of local JMAK coefficients can be partially explained with the raising of a incubation phenomenon but other factors can have considerable impact on desorption mechanism. For this reason, hereby exposed description must be considered as a possible interpretation of sorption phenomena, on the base of acquired data in the considered range of pressure and temperature.

4.4 Conclusion

Kinetic measurements of catalysed magnesium based material, added of graphite and produced by for high energy ball milling, were compared with identical no catalysed sample. PVD techniques were used to deposit a thin layer of catalyst, Nb_2O_5, on the powder's surface in order to achieve two target: reduction of used catalyst mass (50-100 ppm w/w) and surface deposition where catalyst can exploit its maximum effect. Catalysed sample shows clear increment of kinetic performance respect to no catalysed sample both for hydrogen absorption and desorption reaction. Improvement of absorption rate is attributed to the reduction of apparent activation energy

acted by catalyst (76 kJ/mole) and to the increment of the number of available nuclei on the surface of Mg-material probably due to the presence Nb_2O_5's layer. On the contrary, desorption reaction doesn't manifest any variation in apparent activation energy. Its kinetics's improvement can be attributed to the presence of catalyst on the surface of material which behaves as additional nucleation's centres.

5 Conclusion

In this thesis the original results related to experimental and numerical research carried out by the author, aimed at developing a reliable, flexible and validated methodology to investigate the hydrogen sorption characteristic of potential HSM, for different aspects: from the kinetics characterizations of active materials to the macro kinetics modelling of hydrogen storage tank. The thesis is composed by three main chapters. The main outcomes and future prospectives related to each chapter are considered below defined with the $\triangledown$ and $\star$ symbols, respectively.

Chapter 2 presented a novel apparatus to characterize and improve measurement's accuracy of HSM.

- $\triangledown$ A differential volumetric instrument was realized in FBK facility. All the components of apparatus was designed to respond to a wide range of sorption reactions, including small mass of sample materials or limited gas storage capacity. Proper electronic control unit and managing software were developed within the research activates as well as automatizing characterizing procedure as volume calibration and measurements. Theoretical approach was initially validated with proper null measurement.

- $\triangledown$ Differential apparatus was validated for mild experimental condition (293-400 K and hydrogen pressure of 0.001-0.4 MPa) with Palladium as reference material, and at high temperature experimental condition (573-633 K and hydrogen pressure of 0.001-1 MPa) with Magnesium as reference material. Experimental results (enthalpy and entropy of Pd-H and Mg-H reaction) are in good agreement with literature data, confirming the goodness of experimental procedure in the range of pressure and temperature investigated.

- $\triangledown$ Differential layout showed a sensible reduction in the detection of sorbed gas,

respect to classic *Sievert* one, estimated in 10 fold for low pressure (0.1 MPa) measures and 3-fold at mid pressure (1 MPa) conditions. However, the major advantage is ascribed to the reduced incident of temperature fluctuations during sorption characterization also at high working temperature,

▽ The comparison of measure's uncertainties obtained by differential and classic "Sievert" layout highlights as differential design of volumetric instrument fully exploit equipped hardware (pressure and sensor transducers), where the only improvement in accuracy could come from a better estimation of compressibility factor. At the contrary, considering identical expansion and chamber volume's size, classic instrument is limited by the accuracy in calibration procedure and absolute pressure sensors.

⋆ The type of performed characterizations operated by IDA can be potentially extended with additional features. BET analysis and high pressure sorption measurements (typically for the study of physisorption phenomena) will be implemented. Instrument has been already tested for high pressure measures (10 MPa) with proper pressure transducers and sealing, while new cryogenic sample holders are under realization to extended the investigated temperature's range to 77 K.

Chapter 3 reported the development of new kinetics model description of HSM, applied on magnesium based material produced inside EDEN project. This chapter includes the results of: microscopic kinetics modelling of Mg materials, macroscopic kinetics model for hydrogen storage tank based on Mg material and a proposal lumped model for a quick evaluation of design's goodness of storage tank.

▽ Novel kinetics models based on original JMKA theory (nucleation and growth approach) were developed. These models, called limited growth NG model, kept in consideration geometrical limitation to the growth of product's nuclei in the reacting phase of metal-hydride system.

▽ Mg based material produced within European EDEN project has been analysed. A micro kinetics modelling for a wide range of working temperature (573-633 K) and pressure (0.01-1 MPa) was developed for such material, identifying kinetics mechanism of reaction and main kinetics parameter (as the thermodynamics contributions of the pressure and the apparent activation energies) for absorption and desorption reactions.

▽ Hydrogen absorption process on Magnesium sample was identified with a nucleation and growth model in the range of temperature between 633-573 K, while contracting (shrinking) volume mechanism became more relevant for lower

temperature than 573 K. Hydrogen pressure didn't impact on the kinetics mechanism but only on the kinetic rate. The hypothesis suggested in this work include: at low temperature, a greater number of superficial nuclei were instantaneous formed on the surface of magnesium particles, quickly forming a hydride layer which uniformly penetrates into core's particle, as described by shrinking volume model. On the contrary, a less number of superficial nuclei were present at higher temperature, allowing the three-dimensionally growth of few nuclei, only limited by the surface and volume of Mg particles. Absorption kinetics was predicted quite well by limited growth model hereby proposed.

▽ Hydrogen desorption process on Magnesium sample was identify with a nucleation growth model for all investigated temperature. Desorption mechanism involves the growth of nuclei which are continuously formed on the surface and in the bulk of MgH_2 particles. Temperature and pressure affect the JKMA coefficients which take lower values for lower temperature and low driving force, while tend to increase for higher temperature and high driving force.

▽ Macroscopic modelling for hydrogen storage tank was developed on the base of micro kinetics modelling previously reported, including heat and hydrogen diffusion physical model. A dynamic validation of Mg-based tank was performed with ™Comsol software against experimental data obtained by hydrogen storage tank prototype. The measured data were based on absorption and desorption process, involving heat transfer (enthalpy of reactions) and gas diffusion phenomena. The Macro model was able to predict with a relative good accuracy the measured data.

▽ A lumped parameter model has been proposed as quick mathematical tool to preliminary evaluate design's goodness of hydrogen storage tank design. A numerical validation on lumped model's results was carried out against macroscopic model previously described. Lumped model results are in agreement with simulated data. The presented simplified modelling approach allowed to build a reliable simulation tool for predicting the performance of hydrogen storage tank's layout.

⋆ Desorption process on Mg material is not already fully understood. Kinetics micro model hereby proposed were not able to give a possible explanation about variation of local JMKA coefficient during the hydrogen releasing phenomenon. For this reason a further improvement is needed. A suggested route could be the implementation in kinetic model of incubation phenomenon.

⋆ Macro modelling of hydrogen storage tank reported a considerable discrepancy on temperature data between numerical simulation and experimental system. In this context, new experimental measures with multiple thermocouples (possibly

inside graphite's fins and pellet's materials) could give more high quality data for a complete validation of macro modelling.

Chapter 4 reported the kinetics analysis and characterization of novel catalysed magnesium based material.

- ▽ Mg based material catalysed by deposition layer of Nb_2O_5 shows a strong increment in hydrogen sortpion kinetics both for absorption and desorption reaction. This results is particular relevant in the light on the quantity of introduced catalyst,50-100 ppm w/w, obtained by PVD technique.
- ▽ Kinetics analysis reveals as hydrogen absorption reaction on catalysed magnesium material is temperature dependent. It obeys at nucleation and growth model for high temperature, while contribution of contracting volume model appears greater at lower temperature than no-catalysed material. This can be ascribed to a greater number of nucleation site respect to only Mg material. Moreover, catalyst reduces the activation energy of absorption process.
- ▽ Kinetics analysis for hydrogen desorption reaction shows an increment in the kinetic rate. However, activation energy of desorption reaction in catalysed sample is similar to no catalysed one. This support that increment of reaction rate could be ascribed to a greater number of nucleation site.
- ⋆ A further investigation may be necessary to explore the impact of different thickness of deposited catalyst layers. Additional research's activity may regard the sputtering of other different metal oxides on Mg particles to investigate the impact introduced by PVD procedure on HSM.

Model for HSM

Geometrical model Geometrical models are generally known as shrinking models for the characteristic geometric contraction of parent phase to the core of particle. Basically, mathematical relations depends by geometry of crystal: sphere, cylinder, plates, etc, as in fig.1. Taking in consideration spherical particles, geometric approach considers the reacted fraction, θ as eq.1

$$\theta = \frac{\frac{4}{3}n\pi\rho r_0^3 - \frac{4}{3}n\pi\rho[r(t)]^3}{\frac{4}{3}n\pi\rho r_0^3} = \left(1 - \frac{r^3}{r_0^3}\right) \tag{1}$$

where ρ is the density of parent phase, r_0 is the radius of particles while r(t) is the apparent radius at the time t of parent phase during the sorption process and n is the number of particle involved in the sorption phenomenon. If we assume that growth velocity of new phase is constant (k), it is possible to express r(t)=kt, and so substituting in eq:1:

$$\theta = \left(1 - \frac{(kt)^3}{r_0^3}\right) \qquad 1 - (1-\theta)^{1/3} = k_0 t \tag{2}$$

where $k_0 = k/r_0$. Eq.2 represents the mathematical relations for the contracting volume model applied on a 3D spherical particles. Furthermore, we can express the general mathematical form of shrinking model as:

$$1 - (1-\theta)^{1/d} = kt \tag{3}$$

where d depends by geometrical shape of particle and growth process.[113, 134, 235]

Diffusive model In homogeneous kinetics reaction reacting chemical species are readily available for the transformation phase process; on the contrary, in heterogeneous reactions like in investigated solid state material, hydrogen must to permeate the lattice structure of material in order to approach the reaction interface. In some conditions, diffusion transport can limit the sorption kinetics, taking the role of limiting kinetics mechanism.

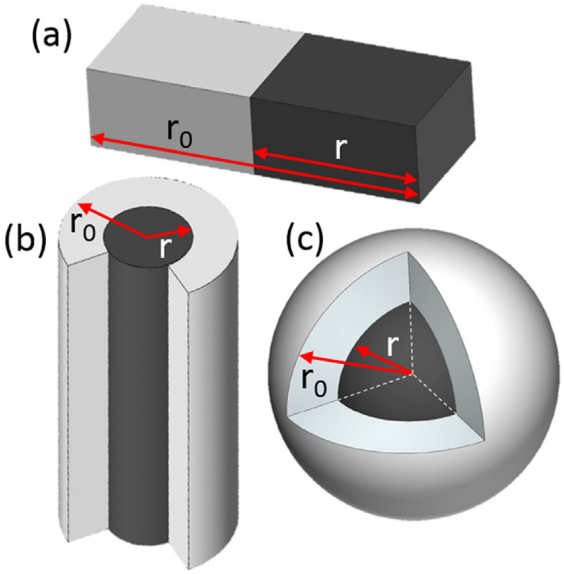

Figure 1: Example of geometrical contraction (*shrinking*) representation for different shape. a)1D b)2D cylindrical c)3D spherical. Image from [113].

In last years, several models have been presented. In this appendix, three of the main are reported.

Jander Model.
Jander model [136] considers diffusion controlled reaction, where growth rate decreases proportionally with the thickness of product layers (*parabolic law*). Mathematical expression derives from the FIck's law:

$$\rho \frac{dr}{dt} = -D\frac{\Delta C}{r_0 - r} \tag{4}$$

where, ΔC is the concentration of hydrogen in the growthing-phase, D id the diffusive coefficient (temperature dependent), r_0 and r are the initial and reduced radius at time t. From Fick's Law is possible to explicit a parabolic relation between reacted fraction and time:

$$r(t)^2 = k_J t \tag{5}$$

with k_J, constant rate that resumes diffusive parameters ($D\Delta C/r_0\rho$).Now, coupling eq. 5 and 2 (for spherical geometry), it is possible to define the Jander eq for spherical particles,

$$[1-(1-\theta)^{1/3}]^2 = k_J t \tag{6}$$

Unfortunately, Jander model introduces two considerable assumption: diffusion interface is constant and volume of HSM is considered identical both for hydride and metal phase.[113, 134, 235]

Ginstling-Brounshtein model [G-B]
In order to keep in consideration the variation of diffusion interface are, GB model [137] elaborates eq.4 for spherical particles in,

$$\rho \frac{dr}{dt} = -D \frac{\Delta C r_o}{(r_o - r) r} \tag{7}$$

Consequently, eq. 7 is elaborated as in the previous case to obtain:

$$1 - \frac{2}{3}\theta - (1-\theta)^{2/3} = k_{GB} t \tag{8}$$

with k_{GB}, constant rate that resumes diffusive parameters ($2D\Delta C / r_0^2 \rho$) Also in this case, variation of particle volume caused by phase transition is not kept in account.

Valensi-Carter model [VC]
Valensi-Carter model [236] introduces the variation of density between hydride and metal form, in a diffusive controlled sorption reaction. VC model for spherical particle is expressed as:

$$\frac{z - [1 + (z-1)\theta]^{2/3} - (z-1)(1-\theta)^{2/3}}{x - 1} = k_{VC} t \tag{9}$$

where z is the density ratio between product phase and the parent one.

The last diffusive model mainly focuses on the interpretation of constant rate extrapolated from the applied diffusive model. Basically, Chou model [111, 141] expresses k-terms as function of proper temperature and pressure contributions:

$$\begin{aligned} k &= k_0 D(T) C(P) \\ D(T) &= D_0 e^{\frac{-\Delta E_D}{RT}} \\ C(P) &= K_p(\sqrt{P} - \sqrt{P_{eq}}) \end{aligned} \tag{10}$$

D(T) is the diffusion coefficient and takes the form of Arrhenius equation, with a proper activation energy for diffusion process.C(P) is the concentration gradient. In most of the diffusive models, it is assumed as constant, and it can be expressed

by Sievert's law, $C = k_p\sqrt{P}$, where P is the pressure of gas-phase while P_{eq} is the equilibrium pressure of hydrogen at a specific temperature. Validation of diffusive methods generally involves to the estimation of diffusivity coefficient, specific for the solid-phase where hydrogen diffuses. Diffusivity coefficient values are reported in several articles (for Mg/MgH_2 material [237–240])

Chemical order model In chemical order model, kinetics rate of hydrogen sorption is function of already reacted fraction. It is possible to distinguish zero, first, second or higher order of reaction, dependent by exponent of reacted fraction in the mathematical relations of model, as reported in tab. 1.

$$\frac{d\theta}{dt} = K(1-\theta)^n \tag{11}$$

Generally, 0-order model is applied to describe chemisorption phenomena. It exclusively depend from available surface.[187]

Table 1: Resuming table with the main chemical order model, derived from eq.11.

Order	Mathematical formulation
0	$\theta = kt$
1	$\theta = 1 - exp(kt)$
2	$\theta = 1 - \frac{1}{kt}$
...	...

Bibliography

[1] Adoption of the paris agreement, 2015.

[2] IEA. Key world energy trends. excerpt from: World energy balances. Technical report, International Energy Agency, 2016.

[3] IEA. Global energy trends: World outlook energy 2015. Technical report, International Energy Agency, 10 November 2015.

[4] Private companies, organization supported by EU commission, and FCH-JU. Commercialization of energy storage in europe. Technical report, European Comission, March 2015.

[5] Körner A. Technology roadmap hydrogen and fuel cells. Technical report, International Energy Agency (IEA), 2015.

[6] U.S. DRIVE Partnership Report. Target explanation document: onboard hydrogen storage for light-duty fuel cell vehicles. Technical report, US Department of Energy, 2015. URL http://energy.gov/sites/prod/files/2015/05/f22/fcto_targets_onboard_hydro_storage_explanation.pdf.

[7] Dr. Darren P. Broom. *Hydrogen Storage Materials: The Characterisation of Their Storage Properties*. Green Energy and Technology. Springer-Verlag London, 1 edition, 2011. doi: 10.1007/978-0-85729-221-6.

[8] Robert A. Varin, Tomasz Czujko, and Zbigniew S. Wronski. *Nanomaterials for Solid State Hydrogen Storage*. Springer US, 2009. URL http://www.ebook.de/de/product/12470413/robert_a_varin_tomasz_czujko_zbigniew_s_wronski_nanomaterials_for_solid_state_hydrogen_storage.html.

[9] E. Mac A. Gray. *Solid-State Hydrogen Storage. Materials and chemistry*, chapter Reliably measuring hydrogen uptake in storage materials, page 600. Woodhead Publishing, 2008. doi: 10.1533/9781845694944.2.174. URL https://www.researchgate.net/publication/279407082_Reliably_measuring_hydrogen_uptake_in_storage_materials.

[10] E. MacA. Gray. Hydrogen storage – status and prospects. *Advances in Applied Ceramics*, 106(1-2): 25–28, feb 2007. doi: 10.1179/174367607x152380.

[11] M.P. de Witt and A. P. C. Faaij. Impact of hydrogen onboard storage technologies on the performance of hydrogen fuelled vehicles: A techno-economic well-to-wheel assessment. *International Journal of Hydrogen Energy*, 32(18):4859–4870, dec 2007. doi: 10.1016/j.ijhydene.2007.07.051.

[12] Fuel Cell Technologies Office. Web site, 2015. URL https://energy.gov/eere/fuelcells/materials-based-hydrogen-storage.

[13] Mc Phy Energy. Web site, 2017. URL http://www.mcphy.com/en/products/solid-hydrogen-storage/.

[14] H_2 Planet. Web site, 2017.

[15] Thomas Graham. On the relation of hydrogen to palladium. *Proceedings of the Royal Society of London*, 17:212–220, 1868-1869.

[16] A. Sieverts. Zur Kenntniss der Okklusion und Diffusion von Gases durch Metalle. *Z. Phys. Chem*, 60:129–201, 1907.

[17] A. Sieverts, G. Zapf, and H. Moritz. Solubility of h_2 , d_2 , and n_2 in fe. *Z. Phys. Chem*, 183:19–37, 1938.

[18] A. Sieverts, E. Jurish, and A. Metz. Solubility of hydrogen in solid alloys of palladium with gold, silver, platinum. *Z. Anorg. Chem.*, 91:1–45, 1915.

[19] M. Avrami. Kinetics of Phase Change. I General Theory. *The Journal of Physical Chemistry*, 7: 1103–1112, 1939.

[20] M. Avrami. Kinetics of Phase Change. II Transformation Time Relations for Random Distribution of Nuclei. *The Journal of Physical Chemistry*, 8:212–224, 1940.

[21] M. Avrami. Granulation, Phase Change, and Microstructure Kinetics of Phase Change.III. *The Journal of Physical Chemistry*, 177, 1941.

[22] George G. Libowitz, Herbert F. Hayes, and Thomas R. P. Gibb. The system zirconium–nickel and hydrogen. *The Journal of Physical Chemistry*, 62(1):76–79, jan 1958. doi: 10.1021/j150559a019.

[23] E Ivanov, I Konstanchuk, A Stepanov, and V Boldyrev. Magnesium mechanical alloys for hydrogen storage. *Journal of the Less Common Metals*, 131(1-2):25–29, mar 1987. doi: 10.1016/0022-5088(87)90497-8.

[24] W. Oelerich, T. Klassen, and R. Bormann. Metal oxides as catalysts for improved hydrogen sorption in nanocrystalline mg-based materials. *Journal of Alloys and Compounds*, 315(1-2): 237–242, feb 2001. doi: 10.1016/s0925-8388(00)01284-6.

[25] K.S. Jung, E.Y. Lee, and K.S. Lee. Catalytic effects of metal oxide on hydrogen absorption of magnesium metal hydride. *Journal of Alloys and Compounds*, 421(1-2):179–184, sep 2006. doi: 10.1016/j.jallcom.2005.09.085.

[26] K.-F. Aguey-Zinsou, T. Nicolaisen, J.R. Ares Fernandez, T. Klassen, and R. Bormann. Effect of nanosized oxides on MgH2 (de)hydriding kinetics. *Journal of Alloys and Compounds*, 434-435: 738–742, may 2007. doi: 10.1016/j.jallcom.2006.08.137.

[27] R. Gupta, F. Agresti, S. Lo Russo, A. Maddalena, P. Palade, and G. Principi. Structure and hydrogen storage properties of MgH2 catalysed with la2o3. *Journal of Alloys and Compounds*, 450(1-2): 310–313, feb 2008. doi: 10.1016/j.jallcom.2006.10.105.

[28] A. C. Dillon, K. M. Jones, T. A. Bekkedahl, C. H. Kiang, D. S. Bethune, and M. J. Heben. Storage of hydrogen in single-walled carbon nanotubes. *Nature*, 386(6623):377–379, mar 1997. doi: 10.1038/386377a0.

[29] Alan Chambers, Colin Park, R. Terry K. Baker, and Nelly M. Rodriguez. Hydrogen storage in graphite nanofibers. *The Journal of Physical Chemistry B*, 102(22):4253–4256, may 1998. doi: 10.1021/jp980114l.

[30] Claudia Zlotea, Pietro Moretto, and Theodore Steriotis. A Round Robin characterisation of the hydrogen sorption properties of a carbon based material. *International Journal of Hydrogen Energy*, 34(7):3044–3057, 2009. ISSN 03603199. doi: 10.1016/j.ijhydene.2009.01.079. URL http://dx.doi.org/10.1016/j.ijhydene.2009.01.079.

[31] Katherine E. Hurst, Philip A. Parilla, Kevin J. O'Neill, and Thomas Gennett. An international multi-laboratory investigation of carbon-based hydrogen sorbent materials. *Applied Physics A*, 122(1), jan 2016. doi: 10.1007/s00339-015-9537-x.

[32] Guang Liu, Yijing Wang, Lifang Jiao, and Huatang Yuan. Understanding the role of few-layer graphene nanosheets in enhancing the hydrogen sorption kinetics of magnesium hydride. *ACS Applied Materials & Interfaces*, 6(14):11038–11046, jul 2014. doi: 10.1021/am502755s.

[33] Yi Jia, Chenghua Sun, Shaohua Shen, Jin Zou, Samuel S. Mao, and Xiangdong Yao. Combination of nanosizing and interfacial effect: Future perspective for designing mg-based nanomaterials for hydrogen storage. *Renewable and Sustainable Energy Reviews*, 44:289–303, apr 2015. doi: 10.1016/j.rser.2014.12.032.

[34] Vincent Bérubé, Gregg Radtke, Mildred Dresselhaus, and Gang Chen. Size effects on the hydrogen storage properties of nanostructured metal hydrides: A review. *International Journal of Energy Research*, 31(6-7):637–663, 2007. doi: 10.1002/er.1284.

[35] F. Feng, M. Geng, and D.O. Northwood. Mathematical model for the plateau region of P–C-isotherms of hydrogen-absorbing alloys using hydrogen reaction kinetics. *Computation Materials Science*, 23:291–299, 2002.

[36] Yuepeng Pang, Dongke Sun, Qinfen Gu, Kuo-Chih Chou, Xunli Wang, and Qian Li. Comprehensive determination of kinetic parameters in solid-state phase transitions: An extended jonhson–mehl–avrami–kolomogorov model with analytical solutions. *Crystal Growth & Design*, 16(4):2404–2415, apr 2016. doi: 10.1021/acs.cgd.6b00187.

[37] A. Chaise, P.deRango, Ph.Marty, and D.Fruchart. Experimental and numerical study of a magnesium hydride tank. *International Journal of Hydrogen Energy*, 2010.

[38] Eden consortium. Web site, 2015. URL http://www.h2eden.eu/. The research leading to these results has received fundingn from the European Union's Seventh Framework Programme (FP7/2007-2013) for the Fuel Cells and Hydrogen Joint Technology Initiative under grant agreement n.303472.

[39] D. P. Broom and M. Hirscher. Irreproducibility in hydrogen storage material research. *Energy Environment Science*, 9:3368–3380, 2016.

[40] James M. Blackman, John W. Patrick, and Colin E. Snape. An accurate volumetric differential pressure method for the determination of hydrogen storage capacity at high pressures in carbon materials. *Carbon*, 44(5):918–927, 2006. ISSN 00086223. doi: 10.1016/j.carbon.2005.10.032.

[41] J. Garche R. Ströbel, P.T. Moseley, L. Jörissen, and G. Wolf. Hydrogen storage by carbon materials. *Journal of Power Sources*, 159:781–801, 2006. doi: 10.1016/j.jpowsour.2006.03.047. URL http://www.sciencedirect.com/science/article/pii/S0378775306005829.

[42] Gary G. Tibbetts, Gregory P. Meisner, and Charles H. Olk. Hydrogen storage capacity of carbon nanotubes, filaments, and vapor-grown fibers. *Carbon*, 39(15):2291–2301, 2001. ISSN 00086223. doi: 10.1016/S0008-6223(01)00051-3.

[43] W. C. Xu, K. Takahashi, Y. Matsuo, Y. Hattori, M. Kumagai, S. Ishiyama, K. Kaneko, and S. Iijima. Investigation of hydrogen storage capacity of various carbon materials. *International Journal of Hydrogen Energy*, 32(13):2504–2512, 2007. ISSN 03603199. doi: 10.1016/j.ijhydene.2006.11.012.

[44] Chao Zhang, XueSheng Lu, and AnZhong Gu. How to accurately determine the uptake of hydrogen in carbonaceous materials. *International Journal of Hydrogen Energy*, 29(12):1271–1276, 2004. ISSN 03603199. doi: 10.1016/j.ijhydene.2003.12.001.

[45] David Langohr, Sandrine Berthon-Fabry, José Gonzalez-Aguilar, Laurent Fulcheri, and Patrick Achard. Development of a volumetric method, experimental test bench for hydrogen storage characterisation. *International Journal of Hydrogen Energy*, 32(12):1846–1854, 2007. ISSN 03603199. doi: 10.1016/j.ijhydene.2006.07.028.

[46] J. Sarada Prasad Dhand V., Kyong Yop Rhee, and Y. Anjaneyulu. Fabrication of high pressure hydrogen adsorption-desorption unit. Adsorption study on flame synthesized carbon nanofibers. *Journal of Industrial and Engineering Chemistry*, 19:944–949, 2013. doi: 10.1016/j.jiec.2012.11.013. URL http://www.sciencedirect.com/science/article/pii/S1226086X12003814.

[47] Broom D. P. and P. Moretto. Accuracy in hydrogen sorption measurements. *Journal of Alloys and Compounds*, 446-447(September 2006):687–691, 2007. ISSN 09258388. doi: 10.1016/j.jallcom.2007.03.022.

[48] D P Broom. *Hydrogen Sorption Measurements*. European Commision and JRC, 2008. ISBN 9789279083457. doi: 10.2790/86100.

[49] Katherine E. Hurst, Philip A. Parilla, Kevin J. O'Neill, and Thomas Gennett. An international multi-laboratory investigation of carbon-based hydrogen sorbent materials. *Appl. Phys. A*, 42 (122), 2016. doi: 10.1007/s00339-015-9537-x. URL http://link.springer.com/article/10.1007/s00339-015-9537-x.

[50] Demirocak D Emre, Sesha S. Srinivasan, Manoj K. Ram, D. Yogi Goswami, and Elias K. Stefanakos. Volumetric hydrogen sorption measurements. Uncertainty error analysis and the importance of thermal equilibration time. *International Journal of Hydrogen Energy*, 38(3):1469–1477, 2013. ISSN 03603199. doi: 10.1016/j.ijhydene.2012.11.013.

[51] R Checchetto, G Trettel, and A Miotello. Sievert-type apparatus for the study of hydrogen storage in solids. *Measurement Science and Technology*, 15(1):127–130, 2004. ISSN 0957-0233. doi: 10.1088/0957-0233/15/1/017. URL http://www.scopus.com/inward/record.url?eid=2-s2.0-0742304792{\protect\T1\textbraceleft}{&}{\protect\T1\textbraceright}partnerID=tZOtx3y1http://www.scopus.com/inward/record.url?eid=2-s2.0-0742304792{&}partnerID=tZOtx3y1.

[52] Cheng H., Deng X., Li S. L., Chen W., Chen D. M., and K. Yang. Design of PC based high pressure hydrogen absorption/desorption apparatus. *International Journal of Hydrogen Energy*, 32(14):3046–3053, 2007. ISSN 03603199. doi: 10.1016/j.ijhydene.2007.01.010.

[53] Wolverton M. J., G. K. Kannarpady, and A. Bhattacharyya. A Temperature Differential Model–Based Sieverts Apparatus. *Instrumentation Science {&} Technology*, 39(2):173–197, 2011. ISSN 1073-9149. doi: 10.1080/10739149.2010.545963. URL http://www.tandfonline.com/doi/abs/10.1080/10739149.2010.545963.

[54] Alfonso Policicchio, Enrico Maccallini, Georgios N. Kalantzopoulos, Ugo Cataldi, Salvatore Abate, Giovanni Desiderio, and Raffaele Giuseppe Agostino. Volumetric apparatus for hydrogen adsorption and diffusion measurements: Sources of systematic error and impact of their experimental resolutions. *Review of Scientific Instruments*, 84(10), 2013. ISSN 00346748. doi: 10.1063/1.4824485.

[55] Lachawiec A. J. A robust volumetric apparatus and a method to measure high pressure hydrogen storage properties of nanostructured materials. *Rev. Sci. Instrum*, 79, 2008.

[56] F. Von Zeppelin, M. Haluska, and M. Hirscher. Thermal desorption spectroscopy as a quantitative tool to determine the hydrogen content in solids. *Thermochimica Acta*, 404:251–258, 2003. doi: 10.1016/S0040-6031(03)00183-7. URL http://www.sciencedirect.com/science/article/pii/S0040603103001837.

[57] Cheng-Si Tsao, Yun Liu, Mingda Li, Yang Zhang, Juscelino B. Leao, Hua-Wen Chang, Ming-Sheng Yu, and Sow-Hsin Chen. Neutron Scattering Methodology for Absolute Measurement of Room-Temperature Hydrogen Storage Capacity and Evidence for Spillover Effect in a Pt-Doped Activated Carbon. *J. Phys. Chem. Lett.*, 1(10):1569–1573, 2010. doi: 10.1021/jz1004472. URL http://pubs.acs.org/doi/abs/10.1021/jz1004472.

[58] D. K. Ross. *Solid-State Hydrogen Storage. Materials and chemistry*, chapter Neutron scattering studies for analysing solid-state hydrogen storage, page 107. Woodhead Publishing, 2008. doi: 10.1533/9781845694944.2.174. URL https://www.researchgate.net/publication/279407082_Reliably_measuring_hydrogen_uptake_in_storage_materials.

[59] International Atomic Energy Agency, editor. *Role of Nuclear based techniques in developement and characterization of materials for hydrogen storage and fuel cells*, number 1676 in 1, Vienna International Centre PO Box 100, A-1400 Vienna, Austria, 2012. URL http://www-pub.iaea.org/books/IAEABooks/8534/Role-of-Nuclear-Based-Techniques-in-Development-and-Characterization-of-Materials-for-Hydrogen-Storage-a ctl00_cphRDBooksHomeMain_FormViewBookDetails_rightsdivdiv.

[60] P. A. Redhead. Thermal Desorption of Gases. *Vacuum*, 1962.

[61] G. Carter. Thermal resolution of desorption energy spectra. *Vacuum*, 12(5), 1962.

[62] P. J. Hatton and B. W. L. Southward. Optimisation of the connection between TA-MS systems together with improved data interpretation for TA-MS applications. *Journal of Thermal Analysis and Calorimetry*, 72(1):83–92, 2003.

[63] Karl J. Gross, K. Russell Carrington, and Philip Parilla. Recommended Best Practices for the Characterization of Storage Properties of Hydrogen Storage Materials. Technical report, National Renewable Energy Laboratory, 2008.

[64] Y Belmabkhout, M Frère, and G De Weireld. High-pressure adsorption measurements. A comparative study of the volumetric and gravimetric methods. *Measurement Science and Technology*, 15(5):848–858, 2004. ISSN 0957-0233. doi: 10.1088/0957-0233/15/5/010.

[65] E. Poirier, R. Chahine, A. Tessier, and T. K. Bose. Gravimetric and volumetric approaches adapted for hydrogen sorption measurements with in situ conditioning on small sorbent samples. *Review of Scientific Instruments*, 76(5), 2005. ISSN 00346748. doi: 10.1063/1.1891647.

[66] Hamid Falahatia and Dominik P.J. Barz. Evaluation of hydrogen sorption models for $AB_5 - type$ metal alloys by employing a gravimetric technique. *Internation journal of hydrogen energy*, 38 (21):8838–8851, 2013.

[67] Hiroyasu Furukawa, Michael A. Miller, and Omar M. Yaghi. Independent verification of the saturation hydrogen uptake in MOF-177 and establishment of a benchmark for hydrogen adsorption in metal–organic frameworks. *J. Mater. Chem.*, 17:3197–3204, 2007.

[68] D.P. Broom. The accuracy of hydrogen sorption measurements on potential storage materials. *International Journal of Hydrogen Energy*, 32:4871 – 4888, 2007.

[69] Isao Suzuki. New apparatus for measuring surface areas as low 0.1 cm^2. *Catalyst Surveys from Japan*, 3:109–118, 1999.

[70] Isao Suzuki. Measurement of 1 cm^2 surface areas by krypton adsorption using an adsorption apparatus with a temperaturecompensated, differential tensimeter of symmetrical design. *Review of Scientific Instruements*, 66:5070–5074, 1995.

[71] C.J. Webb and E.MacA. Gray. The effect of inaccurate volume calibrations on hydrogen uptake measured by the Sieverts method. *Internation journal of hydrogen energy*, 39:2168–2174, 2014.

[72] Blach T. and E. MacA P. Gray. Sieverts apparatus and methodology for accurate determination of hydrogen uptake by light-atom hosts. *Journal of Alloys and Compounds*, 446-447:692–697, 2007. ISSN 09258388. doi: 10.1016/j.jallcom.2006.12.061.

[73] C.J. Webb and E.Mac.A. Gray. Misconceptions in the application of the Sieverts technique. *Internation journal of hydrogen energy*, 38:14281–14283, 2013.

[74] Won Chul Cho, Sang Sup Han, Kyoung Soo Kang, Ki Kwang Bae, Change Hee Kim, Seong Uk Jeong, and Chu Sik Park. Improvement of hydrogen sorption measurement using a Sieverts apparatus with consideration of thermal transpiration. *International Journal of Hydrogen Energy*, 38(14):6241–6248, 2013. ISSN 03603199. doi: 10.1016/j.ijhydene.2012.12.057. URL http://dx.doi.org/10.1016/j.ijhydene.2012.12.057.

[75] C. Yuanzhen, Liu Qing, Yan Yisheng, Cheng Xiaohua, and Liu Yongning. Influence of sample cell physisorption on measurements of hydrogen storage of carbon materials using a Sieverts apparatus. *Carbon*, 48(3):714–720, 2010. ISSN 00086223. doi: 10.1016/j.carbon.2009.10.016. URL http://dx.doi.org/10.1016/j.carbon.2009.10.016.

[76] Voskuilen T., Zheng Yuan, and PourpointTimoth. Development of a Sievert apparatus for characterization of high pressure hydrogen sorption materials. *International Journal of Hydrogen Energy*, 35(19):10387–10395, 2010. ISSN 03603199. doi: 10.1016/j.ijhydene.2010.07.169.

[77] C.J Webb and E. Mac A. Gray. Analysis of the Uncertainties in gas uptake measurements using the Sievert method. *Internation journal of hydrogen energy*, 39:366–375, 2014.

[78] Lachawiec Anthony, Thomas R. J. Di Raimondo, and Ralph T. Yang. A robust volumetric apparatus and method for measuring high pressure hydrogen storage properties of nanostructured materials. *Review of Scientific Instruments*, 79(6), 2008. ISSN 00346748. doi: 10.1063/1.2937820.

[79] Sircar Sarmishtha, Wang Cheng Yu, and Angela D. Lueking. Design of high pressure differential volumetric adsorption measurements with increased accuracy. *Adsorption*, 19(6):1211–1234, 2013. ISSN 09295607. doi: 10.1007/s10450-013-9558-8.

[80] Ali Qajar, Maryam Peer, Ramakrishnan Rajagopalan, and Henry C. Foley. High pressure hydrogen adsorption apparatus: Design and error analysis. *International Journal of Hydrogen Energy*, 37 (11):9123–9136, 2012. ISSN 03603199. doi: 10.1016/j.ijhydene.2012.03.002. URL http://dx.doi.org/10.1016/j.ijhydene.2012.03.002.

[81] John M. Zielinski, Charles G. Coe, Randy J. Nickel, Anthony M. Romeo, Alan C. Cooper, and Guido P. Pez. High pressure sorption isotherms via differential pressure measurements. *Adsorption*, 13(1):1–7, 2007. ISSN 09295607. doi: 10.1007/s10450-007-9005-9.

[82] James M. Blackman, John W. Patrick, Ana Arenillas, Wei Shi, and Colin E. Snape. Activation of carbon nanofibres for hydrogen storage. *Carbon*, 44(8):1376–1385, 2006. ISSN 0008-6223. doi: 10.1016/j.carbon.2005.11.015.

[83] Adam St. John. Development of a Hydrogen Generating Thermal Control for Chemical Hydrogen Storage. Master's thesis, Department of Mining Engineering Queen's University Kingston, Ontario, Canada, 2007.

[84] Darren J. Browning, Mark L. Gerrard, J. Barry Lakeman, Ian M. Mellor, Roger J. Mortimer, and Mark C. Turpin. Studies into the Storage of Hydrogen in Carbon Nanofibers: Proposal of a Possible Reaction Mechanism. *NANO LETTERS*, 2(3):201–205, 2002.

[85] M.O. McLinden E.W. Lemmon and D.G. Friend. *NIST Chemistry WebBook, NIST Standard Reference Database Number 69*, chapter Thermophysical Properties of Fluid Systems. National Institute of Standards and Technology,, 2017.

[86] Parilla P.A. Hydrogen sorbent measurement qualification and characterization. Technical report, DOE Hydrogen and Fuel Cells Program
Annual Merit Review and Peer Evaluation Meeting , p. 12.
National Renewable Energy Technology Laboratory, 2012.

[87] Eric W. Lemmon and Marcia L. Huber. NIST standard reference database 23: reference fluid thermodynamic and transport properties, 2008. URL http://www.nist.gov/srd/nist23.cfm.

[88] D.A. Kouremenos and K.A. Antonopoulos. Compressibility Charts for Gases with Different Acentric Factors and Evaluation of the Redlich-Kwong-Soave Equation of State. *Research in engineering (DE)*, 57(5), 1991.

[89] Eric W. Lemmon, Marcia L. Huber, and Jacob W. Leachman. Revised Standardized Equation for Hydrogen Gas Densities for Fuel Consumption Applications. *Journal of Research of the National Institute of Standards and Technology*, 113(6), 2008.

[90] B. A. Younglove. Thermophysical Properties of Fluids. I. Argon, Ethylene, Parahydrogen, Nitrogen, Nitrogen Trifluoride, and Oxygen, 1985. ISSN 15297845.

[91] Lembeck J. The Calibration of Small Volumetric Glassware. Technical report, NIRST, 1974.

[92] F. D. Manchester, A. San-Martin, and J. M. Pitre. The H-Pd (hydrogen-palladium) System. *Journal of Phase Equilibria*, 15(1):62–83, 1994. ISSN 10549714. doi: 10.1007/BF02667685.

[93] Manchester F.D. and Khatamian D. Mechanisms for activation of intermetallic hydrogen. . *Mater Sci Forum*, 31, 1988.

[94] M.D. Manchester. *Phase Diagrams of Binary Hydrogen Alloys*. ASM INternational, 2000.

[95] Brodowsky E. and Wicke H. The Palladium-Hydrogen System. *Platinum Metals Rev.*, 26(3), 1982.

[96] V. M. Avdjukhina, A. A. Katsnelson, and G. P. Revkevich. Structural Changes and Their kinetics in Hydrogen-Containing Palladium Systems. *P/azinwmMetahh*, 46(4):169–176, 2002.

[97] Andrea Baldi, Tarun C. Narayan, Ai Leen Koh, and Jennifer A. Dionne. In situ detection of hydrogen-induced phase transitions in individual palladium nanocrystals. *NATURE MATERIALS*, 13:1143–1148, 2014.

[98] Linda L. Jewell and Burtron H. Davis. Review of absorption and adsorption in the hydrogen–palladium system. *Applied Catalyst A: General*, 310:1–15, 2006.

[99] R. Lasser and K.H. Klatt. Solubility of hydrogen isotopes in palladium. *PHYSICAL REVIEW 8*, 28 (2), 1983.

[100] E. Wicke, H. Brodowsky, and H. Züchner. *Hydrogen in Metals II:Hydrogen in palladium and palladium alloys*. Springer Berlin Heidelberg, 1978.

[101] Huaiyu Shao, Yuntao Wang, Hairuo Xu, and Xingguo Li. Hydrogen storage properties of magnesium ultrafine particles prepared by hydrogen plasma-metal reaction. *Materials Science and Engineering B*, 110:221–226, 2004.

[102] K. Zeng, T. Klassen, W. Oelerich, and R. Bormann. Critical assessment and thermodynamic modeling of the Mg-H system. *International Journal of Hydrogen Energy*, 24:989–1004, 1999.

[103] J.F. Stampfer, C.E. Holley, and J.F. Suttle. The Magnesium-Hydrogen system. *Journal of Americal Chemical Society*, 85(14):3504–3508, 1960.

[104] A. San-Martin and F.D. Manchester. The h-mg (hydrogen-magnesium) system. *Journal of Phase Equilibria.*, 8(5):431–437, 1987.

[105] B: Vigeholm, J. Kjoller, B. Larsen, and A.S. Pedersen. Formation and decomposition of Magnesium Hydride. *Journal of the Less-Common Metals,*, 89:135–144, 1983.

[106] Tetsu Kiyobayashi, Hiroyuki T Takeshita, Hideaki Tanaka, Nobuhiko Takeichi, Andreas Züttel, Louis Schlapbach, and Nobuhiro Kuriyama. Hydrogen adsorption in carbonaceous materials–How to determine the storage capacity accurately. *Journal of Alloys and Compounds*, 330-332 (November 2015):666–669, 2002. ISSN 09258388. doi: 10.1016/S0925-8388(01)01436-0. URL http://linkinghub.elsevier.com/retrieve/pii/S0925838801014360.

[107] Technical Committee for Flow EURAMET e.V. *Guidelines on the determination of uncertainty in gravimetric volume calibration*. EURAMET cg-19, version 2.1 edition, (03/2012).

[108] Ted B. Flanagan and W.A. Oates. The palladium-Hydrogen system. *Annual Review Material Science*, 21:269–304, 1991.

[109] Borislav Bogdanovic, Klaus Bohmhammel, Babett Christ, Alexander Reiser, Klaus Schlichtea, Ralph Vehlen, and Ulrich Wolf. Thermodynamic investigation of the magnesium–hydrogen system. *Journal of Alloys and Compounds*, 282:84–92, 1999.

[110] M. Lototsky, J.M. Sibanyoni, R.V. Denys, M. Williams, B.G. Pollet, and V.A. Yartys. Magnesium–carbon hydrogen storage hybrid materials produced by reactive ball milling in hydrogen. *Carbon*, 57:146–160, 2013.

[111] Kuo Chih Chou and Kuangdi Xu. A new model for hydriding and dehydriding reactions in intermetallics. *Intermetallics*, 15:767–777, 2007.

[112] E. L. Pang, N. Q. Vo, T. Philippe, and P. W. Voorhees. Modeling interface-controlled phase transformation kinetics in thin films. *Journal of Applied Physics*, 117:175304–1, 2015.

[113] Yuepeng Pang and Qian Li. A review on kinetic models and corresponding analysis methods for hydrogen storage materials. *Internation journal of hydrogen energy*, 30:1–16, 2016.

[114] L. A. Perez-Maqueda, J. M. Criado, and P. E. Sanchez-Jimenez. Combined Kinetic Analysis of Solid-State Reactions: A Powerful Tool for the Simultaneous Determination of Kinetic Parameters and the Kinetic Model without Previous Assumptions on the Reaction Mechanism. *Journal of Physical Chemistry A*, 2006.

[115] Joseph Bloch and Moshe H. Mintz. Kinetics and mechanisms of metal hydrides formation - a review. *Journal of Alloys and Compounds*, 253-254, 1997.

[116] F. Liu, F. Sommer, C. Bos, and E. J. Mittemeijer. Analysis of solid state phase transformation kinetics: models and recipes. *International Materials Reviews*, 52:4, 2007. doi: 10.1179/174328007X160308. 193-212.

[117] Sergey Vyazovkin and Charles A. Wight. Isothermal and nonisothermal kinetics of thermally stimulated reactions of solids. *International Reviews in Physical Chemistry*, 17(3), 1998. doi: http://dx.doi.org/10.1080/014423598230108.

[118] Baptiste Delhomme, Patricia de Rango, Philippe Marty, Maria Bacia, Bartosz Zawilski, Cecile Raufast, Salvatore Miraglia, and Daniel Fruchart a. Large scale magnesium hydride tank coupled with an external heat source. *International journal of hydrogen energy*, 2012.

[119] Baptiste Delhomme, Patricia de Rango, and Philippe Marty. Numerical study of a magnesium hydride tank. *Internation journal of hydrogen energy*, 37:1551–1567, 2012.

[120] S. Garrier, A. Chaise, P. de Rango, P. Marty, B. Delhomme, and D. Fruchart andS. Miraglia. MgH_2 intermediate scale tank tests under various experimental conditions. *International journal of hydrogen energy*, 2011.

[121] P. Marty, J.F. Fourmigue, P. De Rango, D. Fruchart, and J. Charbonnier. Numerical simulation of heat and mass transfer during the absorption of hydrogen in a magnesium hydride. *Energy Conversion and Management*, 47:3632–3643, 2006.

[122] P. Muthikumar and Manvendra M. Umekar. Study of coupled heat and mass transfer during absorption of hydrogen in $MmNi_4 \cdot 6Al_{0.4}$ based hydrogen storage device. *Sadhana*, 34(2): 255–270, 2009.

[123] Maha Bhouri, Jacques Goyette, Bruce J. Hardy, and Donald L. Anton. Honeycomb metallic structure for improving heat exchange in hydrogen storage system. *International Journal of Hydrogen energy*, 36:6723–6738, 2011.

[124] Sarra Wjihi, Houcine Dhaou, Manel Ben Yahia, Salah Knani, Abdelmajid Jemni, and Abdelmottaleb Ben Lamine. Statistical physics modeling of hydrogen desorption from $LaNi_{4.75}Fe_{0.25}$: Stereographic and energetic interpretations. *Physica B*, 479:112–120, 2015.

[125] M. Ben Yahia, S. Knani, H. Dhaou, M.A. Hachicha, A. Jemni, and A. Ben Lamine. Modeling and interpretations by the statistical physics formalism of hydrogen adsorption isotherm on $LaNi_{4.75}Fe_{0.25}$. *Internation journal of hydrogen energy*, 38:11536–11542, 2013.

[126] M.V. Lototskyy. New model of phase equilibria in metal-hydrogensystems: Features and software. *Internation journal of hydrogen energy*, 41:2739–2761, 2016.

[127] Martin Dornheim. *Thermodynamics of Metal Hydrides: Tailoring Reaction Enthalpies of Hydrogen Storage Materials*. Pirajan, 2011. doi: 10.5772/21662.

[128] Y. Mishin and W.J. Boettinger. Thermodynamic model of hydride formation and dissolution in spherical particles. *Acta Materialia*, 58:4968–4977, 2010.

[129] J. R. Larcher. A theoretical formula for the solubility of hydrogen in palladium. *Communicated by R.H.Fowler*, 1937.

[130] Ch. Lexcellent and G. Gondor. Analysis of hydride formation for hydrogen storage: Pressure composition isotherm curves modeling. *Intermetallics*, 15:934–944, 2007.

[131] R.B. Schwarz and A.G. Khachaturyan. Thermodynamics of open two-phase systems with coherent interfaces: Application to metal–hydrogen systems. *Acta Materialia*, 54:313–323, 2006.

[132] F. Askri, M. Ben Salah A. Jemni, and S. Ben Nasrallah. Optimization of hydrogen storage in metal-hydride tanks. *International Journal of Hydrogen Energy*, 34:897–905, 2009.

[133] Michael Brown, D. Dollimore, and A.K. Galwey, editors. *Reactions in the Solid State*. Elsevier Science, 1980.

[134] Khawam A. and Douglas R. Flanagan. Solid-State Kinetic Models: Basics and Mathematical Fundamentals. *J. Phys. Chem. B*, 110(35):17315–17328, 2006. doi: 10.1021/jp062746a.

[135] J. T. Carstensen. Stability of solids and solid dosage forms. *Journal of Pharmaceutical Sciences*, 1974.

[136] Jander W. Reaktionen im festen Zustande bei hoheren Temperaturen. Reaktionsgeschwindigkeiten endotherm verlaufender Umsetzungen. *Z Anorg Allg Chem*, 163:1–30, 1927.

[137] Ginstling A and Brounshtein B. Concerning the diffusion kinetics of reactions in spherical particles. *J Appl Chem USSR*, 23:1327–1338, 1950.

[138] W.A. Johnson and R.F. Mehl. Reaction kinetics in processes of nucleation and growth. *Transactions AIME*, 135:396–415, 1939.

[139] Kolmogorov A.N. On the statistical theory of the crystallization of metals. *Bullettin Academic Scientific USSR Mathematical Service*, 1:379–382, 1937.

[140] A. T. W. Kempen, F. Sommer, and E. J. Mittemeijer. Determination and interpretation of isothermal and non-isothermal transformation kinetics: the effective activation energies in terms of nucleation and growth. *Journal of materials science*, 37:1321–1332, 2002.

[141] Kuo-Chih Chou, Qian Lia, Qin Lina, Li-Jun Jiang, and Kuang-Di Xub. Kinetics of absorption and desorption of hydrogen in alloy powder. *International Journal of Hydrogen Energy*, 30:301 – 309, 2005.

[142] M. Martin, C. Gommel, C. Borkhart, and E. Fromm. Absorption and desorption kinetics of hydrogen storage alloys . *Journal of Alloys and Compounds*, 238:193–201, 1996.

[143] Jing Liu, Xu Zhang, Kuo-Chih Chou Qian Li and, and Kuang-Di Xu. Investigation on kinetics mechanism of hydrogen absorption in the La_2Mg_{17}-based composites. *Internation journal of hydrogen energy*, 34:1951–1957, 2009.

[144] Sweta Shriniwasan, Hiya Goswami, Hung-Yu Tien, Mahesh Tanniru, Fereshteh Ebrahimi, and Sankara Sarma V. Tatiparti. Contributions of multiple phenomena towards hydrogenation: A case of Mg. *Internation journal of hydrogen energy*, 40:13518–13529, 2015.

[145] Jaroslav Sestak and Gunnar Berggren. Study of the kinetics of the mechansim of solid-state reaction at increasing temperature. *Thermochimica Acta*, 3:1–12, 1971.

[146] X.H. An, Y.B. Pan, Q. Luo, X. Zhang, J.Y. Zhang, and Q. Li. Application of a new kinetic model for the hydriding kinetics of $LaNi_5Al_x$ ($0 \leq x \geq 1$). *Journal of Alloys and Compounds*, 506:63–69, 2010.

[147] P. Bracconi. Modeling of the kinetics of chemically controlled double solid-gas reactions. *Solid State Ionics*, 51:261–272, 1992.

[148] Eugen Segal. Rate equations of solid state reactions. Euclidean and fractal models. *Rev. Roum. Chim*, 57:491–493, 2012.

[149] Moshe H. Mintz and Yehuda Zeiri. Hydriding kinetics of powders. *Journal of Alloys and Compounds*, 216:159–175, 1994.

[150] Kazuhiro Nogita, Xuan Q. Tran, Tomokazu Yamamoto, Eishi Tanaka, Stuart D. McDonald, Christopher M. Gourlaya, Kazuhiro Yasuda, and Syo Matsumura. Evidence of the hydrogen release mechanism in bulk MgH_2. *Scientific Reports*, 2015. doi: 10.1038/srep08450.

[151] Chapter 3 kinetic models for solid state reactions. In Michael Brown, D. Dollimore, and A.K. Galwey, editors, *Thermal Decomposition of Ionic Solids*, pages 75–115. Elsevier BV, 1999. doi: 10.1016/s0167-6881(99)80004-4.

[152] E.A. Jagle and E.J. Mittemeijer. The kinetics of grain-boundary nucleated phasetransformations: Simulations and modelling. *Acta Materialia*, 59:5775–5786, 2011.

[153] Sweta Shriniwasan, Hung-Yu Tien, Mahesh Tanniru, Fereshteh Ebrahimi, and Sankara Sarma V. Tatiparti. Transition from interfacial to diffusional growth during hydrogenation of Mg. *Materials Letters*, 161:271–274, 2015.

[154] J.W. CHRISTIAN. The Classical Theory of Nucleation. In *The Theory of Transformations in Metals and Alloys*, pages 422–479. Elsevier BV, 2002. doi: 10.1016/b978-008044019-4/50014-3.

[155] K.B. Gerasimov and E. Yu Ivanov. The mechanism and kinetics of formation and decomposition of magnesium hydride. *Materials Letters*, 3(12):497–499, 1985.

[156] H.T. Uchida, S. Wagner, M. Hamm, J. Kurschner, R. Kirchheim, B. Hjorvarssonb, and A. Pund. Absorption kinetics and hydride formation in magnesium films:Effect of driving force revisited. *Acta Materialia*, 85:279–289, 2015.

[157] Keith J. Laidler. Unconventional applications of the arrhenius law. *Journal of Chemical Education*, 49(5):343, may 1972. doi: 10.1021/ed049p343.

[158] Keith J. Laidler. The development of the Arrhenius equation. *Journal of Chemical Education*, 61 (6):494, jun 1984. doi: 10.1021/ed061p494.

[159] Kissinger H.E. Reaction kinetics in differential thermal analysis. *Anal. Chem*, 29:1702–1706, 1957.

[160] M.J. Starink and A.M. Zahra. An analysis method for nucleation and growth controlled reactions at constant heating rate. *Thermochimica Acta*, 292:159–168, 1997.

[161] Takeo Ozawa. Kinetic analysis by repeated temperature scanning. Part 1. Theory and methods. *Thermochimica Acta*, 356:173–180, 2000.

[162] O. Toft Sorensen J. Rouquerol, editor. *Sample Controlled Thermal Analysis: general Introduction to Sample-Controlled Thermal Analysis (SCTA)*. Springer US, 2003. doi: 10.1007/978-1-4757-3735-6_1.

[163] J. H. Sharp, G. W. Brindley, and B. N. Narahari Achar. Numerical Data for Some Commonly used Solid State Reaction Equations. *Journal of the American Ceramic Society*, 49(7):379–382, 1966.

[164] L.F.Jones, D. Dollimore, and T.Nicklin. Comparison of experimental kinetic decomposition data with master data using a linear plot method. *Thermochimica Acta*, pages 240–245, 1975.

[165] P. Šimon. Isoconversional methods. *Journal of Thermal Analysis and Calorimetry*, 76(1):123–132, 2004. doi: 10.1023/b:jtan.0000027811.80036.6c.

[166] B. Saha, A.K. Maiti, and A.K. Ghoshal. Model-free method for isothermal and non-isothermal decomposition kinetics analysis of PET sample. *Thermochimica Acta*, 444(1):46–52, may 2006. doi: 10.1016/j.tca.2006.02.018.

[167] Joyce D. Sewry and Michael E. Brown. "Model-free" kinetic analysis? *Thermochimica Acta*, 390 (1-2):217–225, jul 2002. doi: 10.1016/s0040-6031(02)00083-7.

[168] J.F. Fernandez and C.R. Snchez. Rate determining step in the absorption and desorption of hydrogen by magnesium. *Journal of Alloys and Compounds*, 340:189–198, 2002.

[169] T. Forde, J.P. Maehlen, M.V. Lototsky V.A.Yartys and, and H. Uchida. Influence of intrinsic hydrogenation/dehydrogenation kinetics on the dynamic behaviour of metal hydrides:A semi-empirical model and its verification. *International Journal of Hydrogen Energy*, 32:1041 – 1049, 2007.

[170] Serge Nyallang Nyamsi, Fusheng Yang, Zhen Wu, Zewei Bao, and Zaoxiao Zhang. Assessment of errors on the kinetic data by entropy generation analysis. *International Journal of Hydrogen Energy*, 37(17):12365–12374, sep 2012. doi: 10.1016/j.ijhydene.2012.05.150.

[171] M. Ron. The normalized pressure dependence method for the evaluation of kinetic rates of metal hydride formation/decomposition. *Journal of Alloys and Compounds*, 283(1-2):178–191, feb 1999. doi: 10.1016/s0925-8388(98)00859-7.

[172] G. Liang, J. Huot, S. Boily, and R. Schulz. Hydrogen desorption kinetics of a mechanically milled MgH_2+5 at.% V nanocomposite. *Journal of Alloys and Compounds*, 305:239–245, 2000.

[173] M. Y. Song and J. Y. LEE. A study of the hydriding kinetics of Mg-(10-20 w/o) $LaNi_5$. *Internation journal of hydrogen energy*, 8(5):363–367, 1983.

[174] Yan-Biao Pan, Yu-Feng Wu, and Qian Li. Modeling and analyzing the hydriding kinetics of Mg–$LaNi_5$ composites by Chou model. *International Journal of Hydrogen Energy*, 36(20):12892–12901, oct 2011. doi: 10.1016/j.ijhydene.2011.06.145.

[175] P. S. Rudman. Hydrogen-diffusion-rate-limited hydriding and dehydriding kinetics. *Journal of Applied Physics*, 50(11):7195–7199, nov 1979. doi: 10.1063/1.325831.

[176] E. D. Snijder, G. F. Versteeg, and W. P. M. van Swaaij. Kinetics of Hydrogen Absorption and Desorptionin $LaNi_{5-x}Al_x$ Slurries. *AIChE Journal*, 39(9):1444–1454, 1993.

[177] M. Miyamoto, K. Yamaji, and Y. Nakata. Reaction kinetics of LaNi5. *Journal of the Less Common Metals*, 89(1):111–116, jan 1983. doi: 10.1016/0022-5088(83)90254-0.

[178] Nobuhiko Takeichi, Yasuhiro Sakaida, Tetsu Kiyobayashi, and Hiroyuki T. Takeshita. Hydrogen Absorption and Desorption Behavior of Magnesium Hydride: Incubation Period and Reaction Mechanism. *MATERIALS TRANSACTIONS*, 55(8):1161–1167, 2014. doi: 10.2320/matertrans.mg201405.

[179] Ki-Joon Jeon, Hoi Ri Moon, Anne M. Ruminski, Bin Jiang, Christian Kisielowski, Rizia Bardhan, and Jeffrey J. Urban. Air-stable magnesium nanocomposites provide rapid and high-capacity hydrogen storage without using heavy-metal catalysts. *Nature materials Letters*, 2011. doi: 10.1038/NMAT2978.

[180] Hung-Yu Tien, Mahesh Tanniru, Chang-Yu Wu, and Fereshteh Ebrahimi. Effect of hydride nucleation rate on the hydrogen capacity of mg. *International Journal of Hydrogen Energy*, 34 (15):6343–6349, aug 2009. doi: 10.1016/j.ijhydene.2009.06.008.

[181] A. Montone, A. Aurora, D. Mirabile Gattia, and M. Vittori Antisari. On the barriers limiting the reaction kinetics between catalysed Mg and hydrogen. *Scripta Materialia*, 63(4):456–459, aug 2010. doi: 10.1016/j.scriptamat.2010.05.003.

[182] M.J. Starink. On the meaning of the impingement parameter in kinetics equation for nucleation and growth reaction. *Journal of Materials Science*, 36:4433–4441, 2001.

[183] Hung-Yu Tien, Mahesh Tanniru, Chang-Yu Wub, and Fereshteh Ebrahimia. Mechanism of hydrogen capacity dependence on the hydrogenation temperature. *Scripta Materialia*, 62: 274–277, 2010.

[184] M. Tanniru, H. Y. Tien, and F. Ebrahimi. Study of the dehydrogenation behavior of magnesium hydride. *Scripta Materialia*, 63:58–60, 2010.

[185] M. Perez, M. Dumont, and D. Acevedo-Reyes. Implementation of classical nucleation and growth theories for precipitation. *Acta Materialia*, 56(9):2119–2132, may 2008. doi: 10.1016/j.actamat.2007.12.050.

[186] Sebastián F. Medina and Manuel Gómez. Nucleation Rate and Number of Precipitates in V and Nb-Microalloyed Steels. *Materials Science Forum*, 783-786:1073–1078, may 2014. doi: 10.4028/www.scientific.net/msf.783-786.1073.

[187] Gagik Barkhordarian, Thomas Klassen, and Rudiger Bormann. Kinetic investigation of the effect of milling time on the hydrogen sorption reaction of magnesium catalyzed with different Nb_2O_5 contents. *Journal of Alloys and Compounds*, 407:249–255, 2006.

[188] A. Revesza and D. Fátay. Hydriding kinetics of ball-milled nanocrystalline MgH_2 powders. *J. Mater. Res.*, 22(11), 2007.

[189] U. Bösenberg, J.W. Kim, D. Gosslar, N. Eigen, T.R. Jensen, J.M. Bellosta von Colbe, Y. Zhou, M. Dahms, D.H. Kim, and R. Günther. Role of additives in LiBH4–MgH2 reactive hydride composites for sorption kinetics. *Acta Materialia*, 58(9):3381–3389, may 2010. doi: 10.1016/j.actamat.2010.02.012.

[190] Moisés Cabo, Sebastiano Garroni, Eva Pellicer, Chiara Milanese, Alessandro Girella, Amedeo Marini, Emma Rossinyol, Santiago Suriñach, and Maria Dolors Baró. Hydrogen sorption performance of MgH2 doped with mesoporous nickel- and cobalt-based oxides. *International Journal of Hydrogen Energy*, 36(9):5400–5410, may 2011. doi: 10.1016/j.ijhydene.2011.02.038.

[191] N. Bazzanella, R. Checchetto, A. Miotello, C. Sada, P. Mazzoldi, and P. Mengucci. Hydrogen kinetics in magnesium hydride: On different catalytic effects of niobium. *Applied Physics Letters*, 89(1):014101, jul 2006. doi: 10.1063/1.2218328.

[192] L. Pasquini, E. Callini, E. Piscopiello, A. Montone, M. Vittori Antisari, and E. Bonetti. Metal-hydride transformation kinetics in mg nanoparticles. *Applied Physics Letters*, 94(4):041918, jan 2009. doi: 10.1063/1.3077186.

[193] Nicola Bazzanella, Riccardo Checchetto, and Antonio Miotello. Catalytic effect on hydrogen desorption in nb-doped microcrystalline MgH2. *Applied Physics Letters*, 85(22):5212–5214, nov 2004. doi: 10.1063/1.1829155.

[194] I. Konstanchuk, K. Gerasimov, and J.-L. Bobet. Cooperative effects at formation and decomposition of magnesium hydride in powders. *Journal of Alloys and Compounds*, 509:S576–S579, sep 2011. doi: 10.1016/j.jallcom.2010.10.120.

[195] J Huot, G Liang, S Boily, A Van Neste, and R Schulz. Structural study and hydrogen sorption kinetics of ball-milled magnesium hydride. *Journal of Alloys and Compounds*, 293-295:495–500, dec 1999. doi: 10.1016/s0925-8388(99)00474-0.

[196] P Wang, A.M Wang, Y.L Wang, H.F Zhang, and Z.Q Hu. Decomposition behavior of MgH2 prepared by reaction ball-milling. *Scripta Materialia*, 43(1):83–87, jun 2000. doi: 10.1016/s1359-6462(00)00370-5.

[197] Lennard Mooij and Bernard Dam. Nucleation and growth mechanisms of nano magnesium hydride from the hydrogen sorption kinetics. *Physical Chemistry Chemical Physics*, 15(27):11501, 2013. doi: 10.1039/c3cp51735g.

[198] Torben R. Jensen, Anders Andreasen, Tejs Vegge, JensW. Andreasen, Kenny Stahl, Allan S. Pedersen, Martin M. Nielsen, Alfons M. Molenbroek, and Flemming Besenbacher. Dehydrogenation kinetics of pure and nickel-doped magnesium hydride investigated by in situ time-resolved powder X-ray diffraction. *International Journal of Hydrogen Energy*, 31(14):2052–2062, nov 2006. doi: 10.1016/j.ijhydene.2006.02.004.

[199] G.Mohan. Performance simulation of metal hydride hydrogen storage device with embedded filters and heat exchanger tuber. *International journal of hydrogen energy*, 2007.

[200] Faouzi Askri, Abdelmajid Jemni, and Sassi Ben Nasrallah. Study of two-dimensional and dynamic heat and mass transfer in a metal–hydrogen reactor. *International journal of hydrogen energy*, 2003.

[201] Jinsheng Xiao, Jijuan Wanga, Daniel Cossement, Pierre Benard, and Richard Chahine. Finite element model for charge and discharge cycle of activated carbon hydrogen storage. *International journal of hydrogen energy*, 2007.

[202] M. Verga, F. Armanasco, C. Guardamagnaa, C. Vallia, A. Bianchin, F. Agrestic, S. Lo Russoand A. Maddalena, and G. Principi. Scaling up effects of mg hydride in a temperature and pressure-controlled hydrogen storage device. *International Journal of Hydrogen Energy*, 2009.

[203] P. Muthukumar, U. Madhavakrishna, and Anupam Dewan. Parametric studies on a metal hydride based hydrogen storage device. *Internation journal of hydrogen energy*, 32:4988–4997, 2007.

[204] Eustathios S. Kikkinides. Design and optimization of hydrogen storage units using advanced solid materials: General mathematical framework and recent developments. *Computers and Chemical Engineering*, 2011.

[205] A. Freni, F. Cipitı, and G. Cacciola. Finite element-based simulation of a metal hydride-based hydrogen storage tank. *Internation journal of hydrogen energy*, 34:8574–8582, 2009.

[206] M. Melnichuk and N. Silin. Guidelines for thermal management design of hydride containers. *Internation journal of hydrogen energy*, 30:1–15, 2012.

[207] Springer-Verlag, editor. *Principles of Heat Transfer in Porous Media.* M.Kaviany, 1991.

[208] MBN-Nanomaterialia. Web site. URL http://www.mbn.it/eng/.

[209] M. W. Chase. *NIST-JANAF Themochemical Tables, Fourth Edition,J. Phys. Chem. Ref. Data, Monograph 9.* American Chemical Society ; Woodbury, N.Y. : American Institute of Physics for the National Institute of Standards and Technology, 1998.

[210] Gustavo A. Lozano, Chakkrit Na Ranong, Jose M. Bellosta von Colbe, Rudiger Bormann, Jobst Hapke, Georg Fieg, Thomas Klassen, and Martin Dornheim. Optimization of hydrogen storage tubular tanks based on light weight hydrides. *International Journal of Hydrogen Energy*, 2012.

[211] Maha Bhouri, Jacques Goyette, Bruce J. Hardy, and Donald L. Anton. Numerical modeling and performance evaluation of multi-tubular sodium alanate hydride finned reactor. *International Journal of Hydrogen Energy*, 2012.

[212] C.A. Chung and Ci-Siang Lin. Prediction of hydrogen desorption performance of mg2ni hydride reactors. *International Journal of Hydrogen Energy*, 2009.

[213] Hui Wang, Ajay K. Prasad, and Suresh G. Advani. Hydrogen storage system based on hydride materials incorporating a helical-coil heat exchanger. *International Journal of Hydrogen Energy*, 2012.

[214] Theodore L. Bergman, Adrienne S. Lavine, Frank P. Incropera, and David P. DeWitt. *Principles of Heat and Mass Transfer.* John Wiley and Sons Ltd, 2012. ISBN 0470646152. URL http://www.ebook.de/de/product/15427361/theodore_l_bergman_adrienne_s_lavine_frank_p_incropera_david_p_dewitt_principles_of_heat_and_mass_transfer.html.

[215] James D Freels. COMSOL Validation Progress on Supercritical Hydrogen Heat Transfer. In *Proceedings of the COMSOL Conference 2007, Boston*, 2007.

[216] Louis Schlapbach and Andreas Züttel. Hydrogen-storage materials for mobile applications. *Nature*, 414(6861):353–358, nov 2001. doi: 10.1038/35104634.

[217] Ming Chen, Xiao-Bao Yang, Jie Cui, Jia-Jun Tang, Li-Yong Gan, Min Zhu, and Yu-Jun Zhao. Stability of transition metals on mg(0001) surfaces and their effects on hydrogen adsorption. *International Journal of Hydrogen Energy*, 37(1):309–317, jan 2012. doi: 10.1016/j.ijhydene.2011.09.065.

[218] I.P. Jain, Chhagan Lal, and Ankur Jain. Hydrogen storage in mg: A most promising material. *International Journal of Hydrogen Energy*, 35(10):5133–5144, may 2010. doi: 10.1016/j.ijhydene.2009.08.088.

[219] M. Dornheim, S. Doppiu, G. Barkhordarian, U. Boesenberg, T. Klassen, O. Gutfleisch, and R. Bormann. Hydrogen storage in magnesium-based hydrides and hydride composites. *Scripta Materialia*, 56(10):841–846, may 2007. doi: 10.1016/j.scriptamat.2007.01.003.

[220] John J. Vajo, Florian Mertens, Channing C. Ahn, Robert C. Bowman, and Brent Fultz. Altering Hydrogen Storage Properties by Hydride Destabilization through Alloy Formation: LiH and MgH_2 destabilized with Si. *The Journal of Physical Chemistry B*, 108(37):13977–13983, sep 2004. doi: 10.1021/jp040060h.

[221] Young Whan Cho, Jae-Hyeok Shim, and Byeong-Joo Lee. Thermal destabilization of binary and complex metal hydrides by chemical reaction: A thermodynamic analysis. *Calphad*, 30(1):65–69, mar 2006. doi: 10.1016/j.calphad.2005.10.002.

[222] R. Janot, F. Cuevas, M. Latroche, and A. Percheron-Guégan. Influence of crystallinity on the structural and hydrogenation properties of mg2x phases (x=ni, si, ge, sn). *Intermetallics*, 14(2):163–169, feb 2006. doi: 10.1016/j.intermet.2005.05.003.

[223] Junxian Zhang, Zhinian Li, Fermin Cuevas, and Michel Latroche. Phase stabilities in the mg–si–h system tuned by mechanochemistry. *The Journal of Physical Chemistry C*, 118(38):21889–21895, sep 2014. doi: 10.1021/jp507624b.

[224] Anna-Lisa Chaudhary, Mark Paskevicius, Drew A. Sheppard, and Craig E. Buckley. Thermodynamic destabilisation of MgH2 and NaMgH3 using group IV elements si, ge or sn. *Journal of Alloys and Compounds*, 623:109–116, feb 2015. doi: 10.1016/j.jallcom.2014.10.086.

[225] E. Callini, L. Pasquini, T.R. Jensen, and E. Bonetti. Hydrogen storage properties of mg–ni nanoparticles. *International Journal of Hydrogen Energy*, 38(27):12207–12212, sep 2013. doi: 10.1016/j.ijhydene.2013.05.139.

[226] D. Mirabile Gattia, A. Montone, and I. Di Sarcina. Improving magnesium based systems for efficient hydrogen storage tanks. *International Journal of Hydrogen Energy*, 41(32):14455–14460, aug 2016. doi: 10.1016/j.ijhydene.2016.03.156.

[227] Z.G. Huang, Z.P. Guo, A. Calka, D. Wexler, and H.K. Liu. Effects of carbon black, graphite and carbon nanotube additives on hydrogen storage properties of magnesium. *Journal of Alloys and Compounds*, 427(1-2):94–100, jan 2007. doi: 10.1016/j.jallcom.2006.03.069.

[228] O. Friedrichs, T. Klassen, J Sanchez Lopez, R. Bormann, and A Fernadez. Hydrogen sorption improvement of nanocrystalline mgh_2 by nb_2o_5 nanoparticles. *Scripta Materialia*, 54(7):1293–1297, apr 2006. doi: 10.1016/j.scriptamat.2005.12.011.

[229] N. Hanada, T. Ichikawa, and H. Fujii. Catalytic effect of ni nano-particle and nb oxide on h-desorption properties in MgH2 prepared by ball milling. *Journal of Alloys and Compounds*, 404-406:716–719, dec 2005. doi: 10.1016/j.jallcom.2004.12.166.

[230] O. Friedrichs, F. Agueyzinsou, J.Fernandez, J.Sanchez Lopez, A. Justo, T. Klassen, R. Bormann, and A. Fernandez. mgh_2 with nb_2o_5 as additive, for hydrogen storage: Chemical, structural and kinetic behavior with heating. *Acta Materialia*, 54(1):105–110, jan 2006. doi: 10.1016/j.actamat.2005.08.024.

[231] Gagik Barkhordarian, Thomas Klassen, and Rüdiger Bormann. Effect of nb2o5 content on hydrogen reaction kinetics of mg. *Journal of Alloys and Compounds*, 364(1-2):242–246, feb 2004. doi: 10.1016/s0925-8388(03)00530-9.

[232] A Borgschulte, J. Rector, B. Dam, R Griessen, and A. Zuttel. The role of niobium oxide as a surface catalyst for hydrogen absorption. *Journal of Catalysis*, 235(2):353–358, oct 2005. doi: 10.1016/j.jcat.2005.08.018.

[233] K Aguey Zinsou, J. R. Ares Fernandez, T Klassen, and R Bormann. Effect of nb2o5 on MgH2 properties during mechanical milling. *International Journal of Hydrogen Energy*, 32(13):2400–2407, sep 2007. doi: 10.1016/j.ijhydene.2006.10.068.

[234] S.T. Sabitu, O. Fagbami, and A.J. Goudy. Kinetics and modeling study of magnesium hydride with various additives at constant pressure thermodynamic driving forces. *Journal of Alloys and Compounds*, 509:S588–S591, sep 2011. doi: 10.1016/j.jallcom.2010.11.174.

[235] A.K. Galwey and M.E. Brown. *Thermal Decomposition of Ionic Solids: Chemical Properties and Reactivities of Ionic Crystalline Phases*. Elsevier, 1st edition, 1999.

[236] Valensi G. Kinetics of the oxidation of metallic spherules and powders. *Compt Rend*, 202:309–312, 1936.

[237] J. Cermak and L. Kral. Hydrogen diffusion in Mg–H and Mg–Ni–H alloys. *Acta Materialia*, 56: 2677–2686, 2008.

[238] H.G. Schimmela, G.J. Kearleya, J. Huotb, and F.M. Muldera. Hydrogen diffusion in magnesium metal (α phase) studied by ab initio computer simulations. *Journal of Alloys and Compounds*, 404:235–237, 2005.

[239] X. Yao, Z.H. Zhu, H.M. Cheng, and G.Q. Lu. Hydrogen diffusion and effect of grain size on hydrogenation kinetics in magnesium hydrides. *J. Mater. Res.*, 23(2):336–340, 2008.

[240] C. Nishimura, M. Komaki, and M. Amano. Hydrogen permeation through magnesium. *Journal of Alloys and Compounds*, 293-295:329–333, 1999.